Title
Microbial Engineering and Process Modeling Toward the Development of Electromicrobial Production Systems

Author
Adams, Jeremy David

Publication Date
2023

Peer reviewed|Thesis/dissertation

Microbial Engineering and Process Modeling Toward the Development of Electromicrobial Production Systems

By

Jeremy David Adams

A dissertation submitted in partial satisfaction of the

requirements for the degree of

Doctor of Philosophy

in

Chemical Engineering

in the

Graduate Division

of the

University of California, Berkeley

Committee in charge:

Professor Douglas S. Clark, Chair
Professor Jay D. Keasling
Professor Adam P. Arkin

Spring 2023

Abstract

Microbial Engineering and Process Modeling Toward the Development of Electromicrobial Production Systems

by

Jeremy David Adams

Doctor of Philosophy in Chemical Engineering

University of California, Berkeley

Professor Douglas S. Clark, Chair

Biochemical engineering has long held potential for large-scale production of fuels, plastics, commodity chemicals, and other products. Biochemical processes hold numerous advantages over traditional petrochemical processes, including their chemical selectivity for complex molecules, low operating temperatures and pressures, ability to self-regenerate biocatalysts, and in particular, their theoretical carbon neutrality. Previous biochemical processes have faced difficulties for widespread industrial chemical production, however, due to their reliance on sugar-based substrates produced through the agricultural sector as well as overall economic considerations.

Electromicrobial production (EMP) processes are next-generation biotechnologies that use electricity or electrochemically generated molecules as energy sources in the place of sugars for microbial product formation. In particular, mediator molecules such as hydrogen gas or formic acid, both of which can be produced electrochemically, can be metabolized by Knallgas bacteria and formatotrophs respectively and can provide the energy required to biochemically convert carbon dioxide to value-added products. Following a description of electromicrobial production and a summary of important previous work on these systems in Chapter 1, in this dissertation I describe work in process modeling and analysis as well as microbial engineering to evaluate and advance electromicrobial technologies.

I describe my analytical work first (Chapters 2 and 3), wherein I use life cycle analysis and techno-economic assessment to evaluate EMP on a systems-level basis. In Chapter 2, I introduce a three-part framework, relying on first principles-based bioreactor modeling, process modeling, and life cycle assessment to examine the potential environmental impacts (namely global warming potential and land use) of three proposed EMP schemes. This framework allows me to compare these proposed EMP systems to each other as well as to a traditional glucose-based bioprocess. This analysis identified environmental hotspots of these EMP processes that should be addressed prior to large-scale deployment and established targets for various metrics such as product yield. In Chapter 3, I take a similar approach to develop a techno-economic model of a hypothetical EMP system that converts air-captured CO_2 to the biofuel n-butanol. I use this model to identify specific economic bottlenecks that currently prevent viability of this specific process and demonstrate what conditions must be met in the path to the marketability of this system.

In the experimental portion of this dissertation (Chapters 4 and 5), I describe efforts in engineering microbial strains with specific functions that can be used in electromicrobial processes, demonstrating the utility of two major strain development techniques: rational genetic engineering and adaptive laboratory evolution. The model Knallgas bacteria *Cupriavidus necator*, one of the primary strains studied in the field of EMP, is the major microbial chassis used in these chapters. In Chapter 4, I address the issue of bioseparations in EMP, focusing on the cell lysis step required to recover intracellular biomolecules. I developed a method to confer susceptibility to osmolysis, or cell lysis in distilled water, to bacteria used for intracellular biomolecule production. This method combines adaptive laboratory evolution to improve a strain's halotolerance and rational knockout of mechanosensitive channel genes to confer this desired phenotype. Variations of this approach led to engineered strains of *C. necator* and *Escherichia coli* that undergo significant cell lysis in distilled water, demonstrating the method's broad applicability. In Chapter 5, I engineer a strain of *C. necator* capable of n-butanol production and use adaptive laboratory evolution to improve the tolerance of *C. necator* to n-butanol. This work establishes a foundation for further engineering, enabling the development of a *C. necator* strain capable of producing the biofuel n-butanol from electrochemically produced substrates with high titers and yields. I then conclude this dissertation in Chapter 6 with a discussion of further academic research that should be pursued in the field of EMP and potential pathways for the real-world use of these systems in industrial settings.

This dissertation combines process modeling and microbial engineering toward the development of electromicrobial production systems, with these two parallel efforts informing each other. This dissertation provides insight on key problems of EMP that must be solved prior to their practical deployment and details examples of how microbial engineering strategies can be used to address those problems. The content of this dissertation can guide research and development of electromicrobial technologies, from laboratory research to industrial adoption.

Table of Contents

Acknowledgements

Throughout the course of this dissertation, you will see me use the first-person pronoun “I” in relation to the work described. This is the convention of dissertations, to display a level of ownership of the contents of my doctoral work. In truth, this work could not have taken place without the contributions of a vast number of people. Although scientists are often incentivized to be territorial over their work, science is inherently collaborative. There are of course those who contributed directly to the work described here, either by aiding in the experimental process or through the exchange of ideas. These are the people traditionally given credit in scientific publishing, through co-authorship or acknowledgement, and those with direct contributions to the content of this dissertation will be named specifically at the end of each chapter. However, the project of science requires the work of many who are not usually named in publications.

This work could not have been possible without many other workers, from the administrators who make sure I have the resources I need to accomplish the work, to those who deliver our gas cylinders and manage our warehouses, to the public bus drivers who get me to lab every day, to those who made the several hundred burritos that got me through the long days of my Ph.D. It also could not have been possible without the countless people who have put me in a position to do the work I describe here. From my family and friends, to the public school system that educated me, to the community that I grew up with, I would not be in the position to pursue a Ph.D. without a supportive social network.

Science is a social endeavor. It could not be done without a vast network of people throughout our society. It is the duty of scientists to recognize this, and therefore ensure that the benefits of science are shared equitably and broadly throughout the society that allowed it to happen.

I would like to thank a number of people, therefore, who in one way or another contributed to this dissertation. I will start with the most direct contributors first. I would like to thank my advisor Prof. Doug Clark for giving me the opportunity to work on this research, sharing his knowledge of the field of biochemical engineering, allowing me the intellectual freedom to pursue research directions that I found most interesting, and for teaching me when to use “that” and when to use “which”. I would also like to thank my closest collaborator Dr. Anthony Abel for introducing me to this type of research, for his many contributions to the content of this dissertation, and for the countless discussions and thought experiments regarding electromicrobial production. The opportunity to work nearly every day with a brilliant collaborator and close friend was a highlight of my Ph.D. I would also like to thank the many other great scientists that I’ve gotten to work with throughout my Ph.D., including Joachim Justad Røise, Hesong Han, Jake Hilzinger, Kyle Sander, Dawei Xu, Stefeno Cestellos-Blanco, Hee-Jeong Cha, Josh Hubbard, Hye Jin Jo, Jinhyun Kim, Tianqiong Ma, Craig Criddle, Adam Arkin, and everyone else in the Murthy Lab, the Clark Lab, the Center for the Utilization of Biological Engineering in Space (CUBES), the ARPA-E DAC-EMP Project, and the broader UC Berkeley Chemical Engineering Department. I also am grateful for the undergraduate students I’ve gotten to work with, David Lee, Chloe Li, and Ryan Liang. My Ph.D. could also not have been done without the administrative support from Christine Balolong and Carlet Altamirano.

I would also not be in the position I am without numerous mentors and educators prior to my Ph.D. I am particularly grateful to Prof. Brent Nannenga, Dr. David Taylor, and Prof. Jenny Dyck Brian at Arizona State University for their role in my scientific education.

I am also thankful for the friends I made before my Ph.D. that have supported me despite the distance, including Joseph Struble, Taylor Sackson, Taylor Schwenn, and Andra Yung. I am deeply grateful to Katie Leavitt for her years of support and friendship.

The undeniably best aspect of my Ph.D. has been the amazing people I've had the chance to meet. I'm thankful for the chance to organize with Helen Bergstrom, Adrian Davey, Anthony Abel, Josh Hubbard, Natalie Lefton, Hailey Boyer, Pedro Guimaraes Martins, Abraham Martinez and others throughout my time at Berkeley, and am grateful for their commitment to a vision of equity in higher education.

I thank Bridgette Lafaye, Anthony Abel, Helen Bergstrom, Katie Engler, Angelo Bonzanini, Julie Fornaciari, Sarah Yang, David Brown, Lorena Grundy, Adam Uliana, and the rest of the 2017 Chemical Engineering Cohort and broader CBE community for their friendship throughout the Ph.D. experience. It's been an immense pleasure to struggle through this part of my life with you all, and I will always be grateful for your roles in my life. Special thanks also for the owners of El Talpense Mexican Restaurant who played a very important role in getting me through the Ph.D.

And I would like to especially thank Pauline Harris. The final year of my Ph.D. would have been much less enjoyable without your constant presence. For being the person who reminds me to take breaks, to laugh, to enjoy things, and for being the person always there for me when things are hard, I will always be thankful. I am also thankful to always have someone I can go to for writing and grammar advice.

And lastly none of this would be remotely possible without my family. I would like to thank all of my grandparents, aunts, uncles, and cousins for supporting me throughout my entire life. I'm deeply thankful for my brother Josh Adams and sister Ashleigh Adams-Covell for always being there for me, as well as my sisters-in-law Linsey LeVan and Christine Adams-Covell for making my family even more complete. My niece and nephews, Dakota, Micah, and Noah have brought me so much happiness through the grueling slog of the Ph.D. And finally, I am unendingly thankful for my parents, Kevin and Bridget Adams, for being there for every high and low of my academic career. I could not imagine completing a Ph.D. without them. Many people think they were born with the best parents; I am likely not unique in that regard. But someone has to be right, and I have good reason to believe that that person is me.

Thank you to everyone for shaping my life, and by extension, shaping the work described in this dissertation.

Chapter 1: Electromicrobial Production

1.1 Biochemical Engineering

The field of biochemical engineering—that is, the development of processes in which living cells (or their components) catalyze the conversion of low-value feedstocks into value-added products—has played an important role in human history and holds significant promise toward addressing many global challenges in the coming century. Microorganisms have been employed to carry out desirable chemical transformations for millennia, as the use of yeast to ferment sugar into ethanol for the production of beverages such as beer, wine, and mead has existed in many societies for at least six thousand years.[1]

The development of the field of microbiology in the 19th century substantially advanced the field of biochemical engineering,[2] as fundamental knowledge of microorganisms was translated toward the development of bioprocesses. For example, the acetone-butanol-ethanol fermentation (commonly referred to as ABE fermentation) relying on *Clostridium* sp. was an important source of the commodity chemical acetone.[3,4] However, these bioprocesses fell out of favor due to the growing petrochemical industry beginning in the 1950's. The discovery of penicillin in the fungus *Penicillium rubens* in 1928 and its subsequent mass production two decades later also demonstrated the power of biochemical engineering in the field of human health.[5]

The ability to develop novel bioprocesses was accelerated with the advent of recombinant DNA technologies beginning in the 1970's,[6] which allowed researchers to engineer microorganisms with non-native genes and therefore synthesize bioproducts of interest. The production of human insulin, the first recombinant protein, in *Escherichia coli* and *Saccharomyces cerevisiae*, not only significantly advanced medicine but demonstrated that genetically engineered microbes could serve as biocatalysts for important biomolecules produced in biochemical processes.[7] The growing fields of synthetic biology and metabolic engineering, especially since the early 2000's, have further increased the types of molecules that can be produced in biochemical processes. Rather than introducing single genes to produce proteins, engineering entire metabolic pathways allowed the production of numerous small-molecule products for various applications, including drugs, biofuels, dyes, biopolymers, and other value-added compounds.[8–12]

Whole-cell biocatalysis provides many advantages compared to traditional chemical processing. Biochemical processes in general can catalyze chemical transformations at ambient temperatures and pressures, much lower than those required in conventional chemical processes. Catalysts used in microbial processes (*i.e.*, microbial cells themselves) can also be easily regenerated through cell growth. In addition, biocatalysis, which ultimately relies on the catalytic activity of one or more (or sometimes significantly more)[13] enzymes, provides better selectivity compared to chemical synthesis, especially for complex molecules with multiple chiral centers such as many important pharmaceuticals.[14] Indeed some molecules, such as proteins, are sufficiently large and complex that there are currently no practical alternatives to biological synthesis (except for peptides only a few dozen amino acids in length).[15,16]

Biochemical production of smaller and less complex molecules also holds many advantages over traditional chemical processing. Despite having been largely supplanted by the petrochemical industry to produce fuels, plastics, and commodity chemicals, biochemical engineering holds

many benefits for the large-scale production of these compounds due to the existential threat the fossil economy poses to our socio-ecological system.[17*] In principle, microbial processes can produce these commodity compounds in a carbon-neutral manner, due to their use of non-fossil feedstocks. Ethanol fermentation has received interest over the past decades as a potential replacement for, or additive to, gasoline.[18] Other alcohols, such as propanol and butanol, have been biosynthesized as possible replacements for fossil fuels.[19,20] Bioplastics, which often have the added benefit of possessing some degree of biodegradability, can be produced through biochemical processing.[21] Renewable substrates can either be biologically converted to a full-length polymer, as is the case for polyhydroxyalkanoates, or to monomers which can be chemically synthesized into full-length polymers such as polylactic acid. An array of other low-value commodity compounds that have historically been manufactured from fossil feedstocks have been produced biologically, such as adipic acid and 1,4-butanediol.[22–24]

Approaches to microbial bioproduction can be classified into distinct generations based on the energy source that is used by the microorganism to produce the desired product. First generation biofuels, for example, include fuels such as ethanol that are produced from the fermentation of sugars derived from edible biomass such as corn and sugarcane.[25] More broadly, first generation bioproduction can encompass other products made using crop-derived sugars as substrates, such as the bioplastic polylactic acid or the industrial solvent acetone.[3,26] Most commercial efforts at utilizing microbes for bioproduction to date have relied on first generation technologies.[27] While promising in their ability to shift production of chemicals away from the petrochemical industry, these systems still have major drawbacks that stem from the need to first produce the feedstock crop. Associated CO_2 emissions from fertilizer production, N_2O emissions due to fertilizer application, and land use changes required to farm the feedstock crops all cause concern over the environmental sustainability of first generation bioprocesses, with some estimates putting the greenhouse gas footprint of first generation biofuels comparable to those of their petroleum-based competitors.[28–30] Moreover, production of crops as feedstocks in bioprocesses would compete with the food supply in what has been dubbed the "food versus fuel" debate.[31]

In response to these concerns, a second generation of bioproduction has been pursued, greatly expanding the range of usable plant-based feedstocks by valorizing non-edible lignocellulosic biomass. Lignocellulosic feedstocks, including waste biomass (*e.g.*, corn stover) or energy crops (*e.g.*, switchgrass, elephant grass), are cheap, abundant, and do not compete with the food supply.[32,33] A drawback of this generation is that lignocellulose is much more difficult to convert to simple sugars compared to starchy crops like corn. Although significant effort has been made in developing effective pretreatment methods,[33] the required conversion of lignocellulose to fermentable sugars has often been too costly for an economically competitive process.[34]

In the third generation of bioproduction, heterotrophs could be replaced by photoautotrophic microbes, obviating the need for plant-based feedstocks altogether.[25] Microalgae and cyanobacteria utilize carbon dioxide as a carbon source and light as an energy source to produce cellular biomass, which can then be used to produce fuels by extracting the lipids to convert to

[*] I should note that technological advancement and innovation on its own is woefully insufficient to address the severity of the climate crisis, which would require substantial socio-political change to avoid the most catastrophic consequences.[229] A complete detailing of these socio-economic and political factors, despite their obvious importance, is far outside the scope of this technical manuscript.

biodiesel or converting the biomass to biocrude by hydrothermal liquefaction.[35,36] Moreover, microorganisms such as cyanobacteria could be genetically engineered to produce various other compounds of interest.[37,38] While these microbes can grow faster and utilize light energy more efficiently than terrestrial plants, cyanobacteria and microalgae grow much slower than other industrial microbial strains, and photosynthesis remains a fairly inefficient method of transferring solar energy.[39,40]

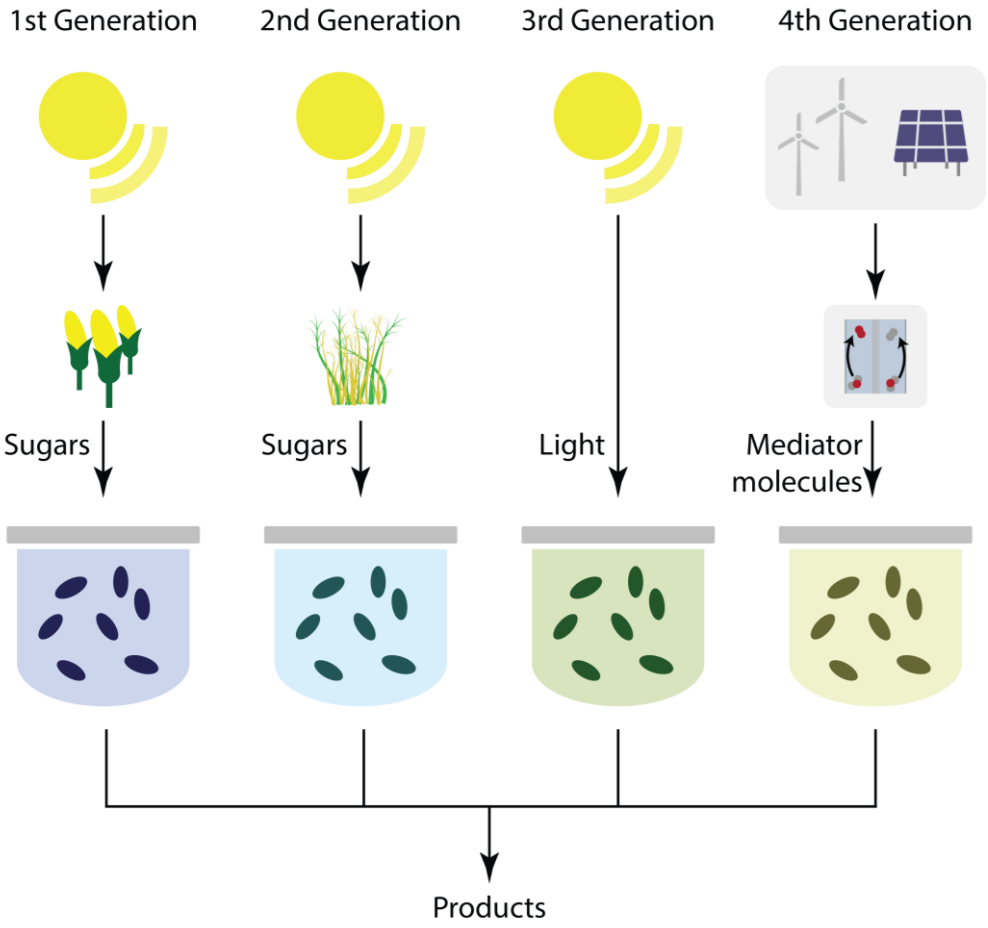

Figure 1.1. The four generations of bioproduction. Categorization of microbial bioproduction strategies developed this far, based on the energy source utilized by the microorganism. First generation bioproduction relies on crop-derived sugars (*e.g.*, from corn, sugarcane). Second generation bioproduction uses sugars derived from lignocellulosic biomass. Third generation bioproduction uses photoautotrophic microbes that use light and CO_2 as energy and carbon sources, respectively. Fourth generation, or electromicrobial production, processes use electricity or electrochemically generated mediator molecules as energy sources.

1.2 Electromicrobial Production: A Fourth-Generation Bioprocess

Seeking to build on previous generations of bioprocessing as well as address some of the shortcomings of those approaches, researchers have pursued electromicrobial production (EMP),

which can be described as a fourth generation of bioprocessing.[41,42†] EMP uses a combination of electrochemical and biological processes that together convert carbon dioxide (CO_2) to value-added products using electricity as an energy source. To qualify as an EMP system under the definition used in this work, a process must meet three major criteria: 1) CO_2 is the primary carbon source for the process; 2) microbial biocatalysts are used to produce the final product of interest; and 3) the energy required to drive the conversion ultimately comes from electricity.

I use the term electromicrobial production[43] in a manner that is broader than the related term microbial electrosynthesis (MES). The latter term is often used to refer to systems in which microorganisms catalyze electrochemical reactions on the surface of an electrode, usually involving some form of extracellular electron transfer (EET).[44] EMP, on the other hand, also includes systems in which energy is transferred to microbes through electrochemically generated mediator molecules. Therefore, EMP systems can be divided into two major categories: direct EMP systems (dEMP) where reducing power is delivered to cells directly by electrons via electron conduit proteins, and mediated EMP systems (mEMP) where reducing power is delivered by a mediator molecule. Common mediator molecules include hydrogen gas, formic acid, carbon monoxide, methane, and methanol.[43]

While direct electron-mediated EMP systems are incredibly interesting and provide a substantial wealth of information in understanding electron transfer mechanisms in microorganisms, mediated EMP systems provide many advantages for industrial-scale bioproduction. The metabolism of substrates such as hydrogen or formate is more well-characterized than direct electron transport mechanisms. At the current date, electrochemical systems such as the electrolysis of water can operate at much higher current densities than integrated bioelectrochemical systems, suggesting that mediated EMP systems possess a higher technological readiness. Mediated EMP systems will be the focus of this dissertation.

In one of the best-studied cases of mediated EMP, hydrogen gas derived from the electrolysis of water, as well as CO_2 and O_2, are converted to value-added products by a Knallgas (aerobic hydrogen-oxidizing) bacterium such as *Cupriavidus necator*[45,46]. Alternatively, carbon dioxide may be electrochemically reduced to formic acid, which can be upgraded by a formatotrophic organism (such as the native formatotroph *C. necator*[47] or an engineered formatotrophic strain of *E. coli*[48]) to the desired product. Most formatotrophic organisms oxidize formic acid to CO_2 to produce NADH which provides the reducing power to fix CO_2 via the Calvin Cycle. However, microbes can also be engineered to contain the reductive glycine pathway, a synthetic carbon fixation pathway.[48] Due to their reliance on oxidative phosphorylation to produce the ATP required to fix carbon dioxide, both Knallgas bacteria and formatotrophs require oxygen or an equivalent electron acceptor.

Acetogens possessing the Wood-Ljungdahl pathway can grow on a CO_2/H_2 gas mixture, formic acid, or carbon monoxide, energy sources which can be produced electrochemically.[49,50] These bacteria enjoy the highest energetic efficiency of carbon fixation among the strains of interest in

† The categorization of bioproduction strategies into generations as I do here is of course open to interpretation, and others have described other classification schemes. For instance, some have described genetically engineered microalgae as a fourth generation of bioproduction.[230] However, I find it more useful to categorize these generations of bioproduction based on the energy source provided to bacteria (crop-derived sugars, lignocellulose-derived sugars, light, and electricity), and would hence include the use genetically engineered microalgae as a subset of third-generation bioproduction.

EMP systems and can be used in the bioproduction of various molecules.[43] Two-step electromicrobial production systems relying on acetogens have also been explored. In these, C_1 substrates are first converted to acetate, which can then be biocatalytically upgraded by an acetotrophic microbe to the desired end product.[51,52] Methane and methanol, meanwhile, can be used as carbon and energy sources for methylotrophic bacteria.[53] Both substrates can be generated electrochemically, although the energetic efficiency with current technologies is low.[54] These compounds can also be produced in thermochemical processes using H_2/CO_2 (Sabatier process) or H_2/CO (methanol synthesis), although the extra processing required to produce these substrates would be a disadvantage. In principle, carbon dioxide can be converted to C_2 compounds such as ethanol and acetate electrochemically, which can, in turn, serve as a substrate for microbial growth. However, due to the low energy efficiencies of the electrosynthesis component, these systems have not been significantly pursued.[43,54] As such, mediator molecules such as hydrogen gas, formic acid, and carbon monoxide are often viewed as the most promising microbial energy sources in EMP systems.[43]

1.3 State of the Field and Future Promise

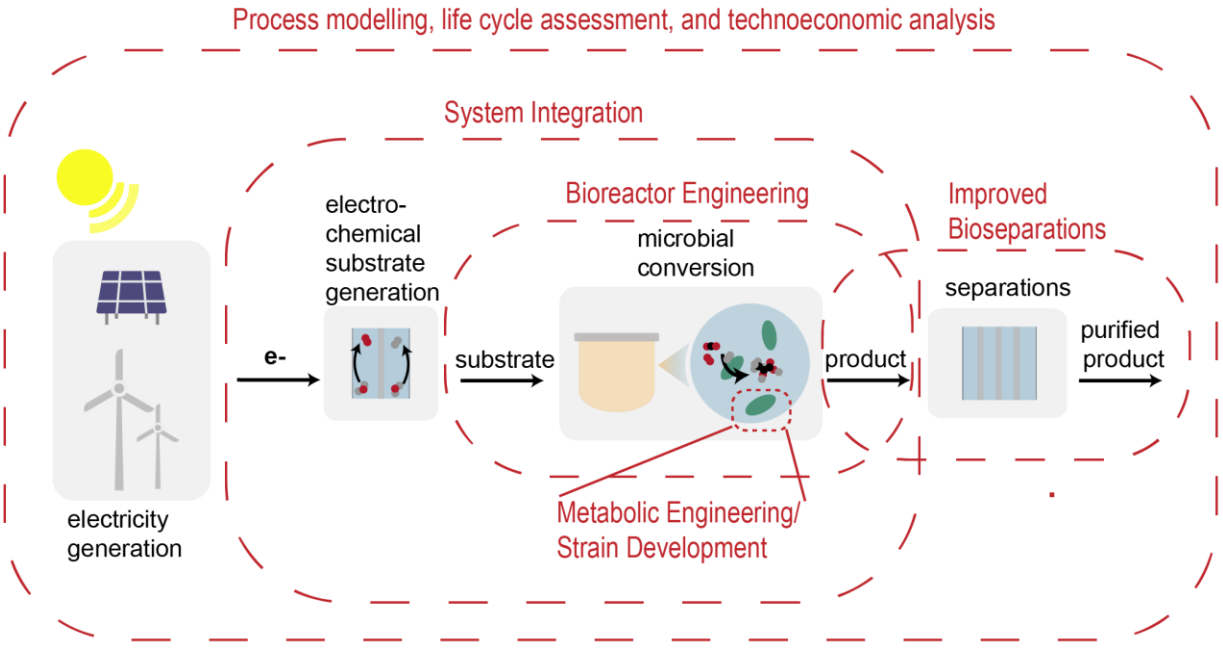

Figure 1.2. Schematic overview of electromicrobial production systems and areas of active research.

The promising benefits described previously have prompted academics (and some in industry) to pursue the research and development of EMP systems. Work on these systems has spanned various scales, and I therefore categorize the work done in developing this field into four major areas: microbial engineering, bioprocess engineering, systems-level analysis, and industrial adoption.

Microbial engineering for EMP processes

The bulk of the research progress toward the development of EMP systems has involved engineering microbes that can convert an electrochemically generated substrate into a product of

interest, aided by improvements in metabolic engineering and synthetic biology, in particular the expansion of genetic toolkits for non-conventional microorganisms. Developing whole-cell biocatalysts that can generate a diverse spectrum of value-added products has been a particular interest of the field in an attempt to demonstrate the breadth of EMP's potential. For some applications, strains exist in nature that can metabolize an electrochemically generated substrate and generate a value-added product of interest in high yield (*e.g.*, acetic acid and ethanol in acetogens or polyhydroxybutyrate in many bacteria). However, these examples are limited, and most products will involve some degree of metabolic engineering to produce in an EMP system.

Two major approaches have been pursued toward this end. In one strategy, microorganisms that can natively metabolize substrates of interest (*e.g.*, hydrogen gas or formate) are metabolically engineered to produce various compounds. In this category, the Knallgas bacteria *Cupriavidus necator* and various acetogens (especially in the *Clostridium* genus) have been prevalent chassis. As the genetic tools for these microbes are fairly underdeveloped compared to more common hosts such as *E. coli*, efforts have been made to develop expression vectors,[55,56] promoter libraries,[57] and CRISPR-based recombination methods[58,59] for use in these strains.

A second strategy that has been pursued is to engineer non-native metabolisms into strains with a larger set of genetic tools. Notably, the synthetic reductive glycine pathway, which can metabolize formic acid more efficiently than the Calvin cycle, has been engineered in *E. coli*, enabling formatotrophic growth and commodity chemical production.[48,60] This approach can leverage the vast amount of engineering work already done in *E. coli* to engineer microbes for electromicrobial production. A (non-exhaustive) selection of promising work toward developing biocatalysts capable of producing a broad range of different products is shown in Table 1.1.

Table 1.1. Examples of EMP products demonstrated in the literature

Product	Substrate	Strain	Yield	Selectivity	Reference
PHB	$H_2/CO_2/O_2$	*Cupriavidus necator*	-	74% [a]	[61]
Sucrose	$H_2/CO_2/O_2$	*Cupriavidus necator*	-	11% [a]	[62]
Isopropanol	$H_2/CO_2/O_2$	*Cupriavidus necator*	31% [b]	-	[63]
Heptadecene	$H_2/CO_2/O_2$	*Cupriavidus necator*	-	0.1% [a]	[64]
Acetoin	$H_2/CO_2/O_2$	*Cupriavidus necator*	67% [c]	-	[65]
Isobutanol	Formate/O_2	*Cupriavidus necator*	-	33% [a]	[66]
L-lactate	Formate/O_2	*Escherichia coli*	10% [d]	-	[60]
Acetic acid	$H_2/CO/CO_2$	*Acetobacterium woodii*		94% [a]	[67]
Acetone	$H_2/CO/CO_2$	*Clostridium autoethanogeum*		90% [e]	[68]
PHB	Acetate (produced from H_2/CO_2)	*Sporomusa ovata/ Cupriavidus basilensis*	11% [f]		[69]

[a] Selectivity reported on a carbon-mole basis (moles of carbon in product to total carbon fixed).
[b] Yield on energetic basis, includes energy of hydrogen generation step.
[c] Yield as a percentage of the maximum stoichiometric yield of acetoin on hydrogen in a Knallgas bacterium employing the Calvin Cycle, calculated from molar yield reported in paper (see Chapter 2 Methods).
[d] Yield as a percentage of the maximum theoretical yield.
[e] Selectivity reported on an energetic basis (energy embodied in product of interest compared to all other byproducts).
[f] Yield reported on a carbon-mole basis (moles of carbon in product per mole of carbon in substrate).

While productivity and titer are interesting metrics often reported in these papers, values related to yield (either the absolute g/g yield or a percentage of the maximum yield) or selectivity are much more relevant when considering the actual applications of these systems. Laboratory experiments, especially when using gaseous substrates such as hydrogen, are often done on small batch scales with relatively low pressure due to safety concerns.[62] These conditions will naturally limit the titer (due to a low substrate concentration) and productivity (due to low gas-liquid mass transfer) compared to that which could be achieved in an industrial fermenter. While yields and selectivities may change slightly during scale-up as bioreactor conditions change, these data from bench-scale experiments are much more indicative of the actual performance of the microbe.

Bioprocess engineering of EMP processes

Bioprocess engineering is another major component of the research required for the eventual industrial adoption of EMP systems. Even if microbes capable of the desired biochemical transformations are isolated or engineered, systems must be constructed that can efficiently deliver electrochemically generated substrates to the microbe while maximizing volumetric productivity and minimizing waste. Tanaka and Ishizaki performed much of the early work in developing bioreactor engineering strategies for producing PHB from hydrogen, oxygen, and carbon dioxide.[45,70,71] These authors demonstrated that strategies such as maximizing liquid-gas mass transfer, reducing oxygen concentration in the feed, and recycling the gas led to systems with high PHB productivity, reduced combustion risks, and high utilization rates of the substrate. While noting that industrial scale-up would likely lead to some reduction in performance, they operated a gas fermenter system with a cell density above 90 g/L and a maximum PHB productivity of around 5 g/L/h, rivaling that of more traditional heterotrophic fermentation systems.[71]

Similar work has been carried out for acetogen- and formatotroph-based systems. Groher and Weuster-Botz studied the performance of various acetogens in a stirred-tank bioreactor with continuous provision of H_2 and CO_2 while Kantzow *et al.* demonstrated that the use of a submerged membrane in the reactor could significantly improve the acetate productivity (~6 g/L/h) in a similar process.[67,72] Grunwald *et al.* used pH-controlled continuous and fed batch systems to study the kinetics of formatotrophic growth of *C. necator*, as well as the effect of substrate toxicity on the yield of biomass.[47] The continuous system developed enabled higher biomass titers (~10 g/L) than had been achieved in previous systems.

Much of the recent work in engineering for electromicrobial production has entailed developing systems in which the electrochemical and biochemical components of these systems have been integrated in a single module. Li *et al.*, for instance, created a bioelectrochemical reactor integrating an electrocatalyst that reduces CO_2 to formate and a biocatalyst (*Cupriavidus necator*) that converts formate to alcohols.[66] Liu *et al*. constructed a similar hybrid system consisting of a water splitting electrochemical component and the Knallgas bacteria *Cupriavidus necator* to convert CO_2, H_2O, and electricity to various fusel alcohols in a single self-contained module with energy conversion efficiencies much higher than can be achieved by photosynthetic organisms.[63] Liu *et al.* (same lead author with a different research group some years earlier) developed a nanowire-bacteria hybrid system composed of a photoactive semiconductor and the acetogen *Sporomusa ovata* that enabled the conversion of water and carbon dioxide to acetic acid.[51] This study also demonstrated that the acetic acid produced in the system could then be biologically upgraded to various value-added products such as PHB, n-butanol, and isoprenoids using

engineered *E. coli* strains, expanding the possible product spectrum that can be generated using this strategy.

Systems-level analysis of potential EMP processes

Most of the experimental work toward the development of EMP systems described until now has taken place on a relatively small scale, much smaller than would be required for industrial adoption of EMP systems. Therefore, it's been difficult to directly assess the performance and impact of these systems on an industrial scale. To that end, efforts in modelling and analyzing EMP systems on a systems level have been carried out to predict performance metrics including productivity, energy/resource demand, costs, and environmental impacts.

Mozumder *et al.* created a bioreactor model to describe the conversion of CO_2 to PHB in Knallgas bacteria that accounted for not only microbial growth and product formation kinetics, but also explicitly described liquid-gas mass transfer of substrates into the reactor, as well as effects of nitrogen and oxygen availability on the selectivity of PHB over biomass formation.[73] A similar type of biochemical reactor model was developed to describe a system that converted synthesis gas to acetate and ethanol using acetogenic bacteria.[74] Merasz *et al*. developed a model describing the kinetics of biological conversion of methane to bioplastics using Type II methanotrophs, and validated the predictive ability of the model against datasets in the literature.[53] Models of integrated bioelectrochemical reactors that convert carbon dioxide to multi-carbon products, either through direct electron transfer or mediated through in-situ generated formate, have also been detailed in the literature.[75,76]

Modelling and analysis of these systems enables direct comparison of the various forms of EMP (both direct and mediated) to each other. For example, Claassens *et al.* performed an extensive analysis comparing various routes of electromicrobial production by considering energetic efficiencies of electrochemical production of various substrates, rates and efficiencies of microbial conversion of those substrates through different metabolic pathways, and the physicochemical properties (*e.g.*, solubility, mass transfer coefficient) of the substrates themselves.[43] In this paper, the authors made the case that separating the electrochemical and biochemical modules of an EMP system will lead to better overall system performance, due to incompatibilities of pH, temperature, and ionic strength between the two components, a consideration that was also demonstrated quantitatively by the physics-based modelling carried out by Abel *et al.*[77] Salimijazi *et al.* took a thermodynamics-based approach to model both direct and H_2-mediated EMP systems on both the metabolic and reactor scales, and predicted maximum efficiencies these systems can achieve for the conversion of CO_2 to biofuels.[78]

Process modeling and analysis has also been used to evaluate the claims of environmental benefits that proponents of EMP have asserted. Leger *et al.*, for instance, devised a model to study the energy and land occupation footprints in the electromicrobial production of single-celled protein, demonstrating its superiority over land-intensive crop-based systems.[79] While many of the insights of this analysis can be generalized for other EMP systems, the direct results are limited to the simplest possible product of EMP (*i.e.*, raw cellular biomass). Given the breadth of possible substrates that can be utilized, microbes that can be employed, and products that can be generated through EMP, tools that predict environmental benefits and impacts of an array of possible EMP systems are desirable. Meanwhile, while back-of-the-envelope calculations regarding the cost of EMP have accompanied some of the modeling endeavors described here,[43] thorough techno-economic assessments that can predict economic feasibility and identify bottlenecks are still

needed. Frameworks that can piece together physics-based bioreactor models, process models including electrochemical components, and analyses that can output metrics of interest including energy requirements, economic viability, and environmental impacts would be beneficial to understand the potential of EMP, guide laboratory research directions, and ultimately aid the design of scaled-up systems.

Early efforts toward commercialization of EMP

Over the past several years, multiple companies have emerged that seek to commercialize electromicrobial technologies. U.S.-based company Air Protein and Finnish company Solar Foods both utilize hydrogen-oxidizing bacteria to produce cellular protein as a substitute for plant and animal sources.[80,81] Circe Biosciences meanwhile employs a similar strategy to produce tailored fats from hydrogen and carbon dioxide.[82] Each of these companies promote their processes as enabling food production fully independent of the agricultural sector, one of the key advantages of electromicrobial production.

Arguably, the venture that has made the largest impact in this space commercially has been Lanzatech. Lanzatech has, since its pilot-scale demonstration in 2008, pioneered gas fermentation technology using acetogens operating at an industrial scale.[83] While Lanzatech has focused on converting CO-rich waste industrial gases to ethanol,[84] their platform can easily be adapted to utilize carbon dioxide and electrolytically generated hydrogen as substrates, enabling electromicrobial production. In addition to ethanol (as a platform for jet fuel and other higher-value products)[85], Lanzatech has shown interest in employing synthetic biology and metabolic engineering approaches toward optimizing acetogens to produce various other commodity chemical products such as acetone and isopropanol.[68] Given the overall interest in EMP, it is likely that several more startups will emerge in the coming years leveraging this technology for various applications.

Realizing the potential of electromicrobial production

A circular bio-based carbon economy has the potential to replace the current extractive, unidirectional fossil-based economy for the production of many goods. Yet, bioprocessing in general has not yet reached this potential due to a combination of economic factors and environmental concerns of traditional bioprocesses. The development of industrial electromicrobial production systems for a variety of liquid fuels, bioplastics, commodity chemicals, and perhaps even specialty chemicals and protein products provides an alternative to fossil-based production, traditional bioproduction, and fully abiotic electrochemical production of these goods.

Both technological and broader developments, many in the last ten years, have created an environment beneficial for the adoption of industrial EMP systems. Expansion of genetic toolkits and metabolic engineering techniques has enabled EMP-relevant strains to be engineered with relative ease. Basic research on carbon fixation metabolisms and the creation of synthetic carbon fixation pathways enable multiple routes for conversion of CO_2 to value-added molecules. Novel prototypical EMP systems have been pursued by various groups. Meanwhile, the price of clean solar energy has fallen dramatically in recent years, a trend expected to continue and allow the electrification of many aspects of industry. Electrochemical technologies that can enable EMP, especially electrolysis of water to generate hydrogen, have concurrently become much more mature, energy-efficient, and inexpensive.

Still, much work remains to be done to realize the revolutionary potential of EMP. To achieve production rates competitive with traditional biosystems, reactor engineering strategies must be developed and employed at scale to efficiently (and safely) deliver the electrochemically generated substrate to the microbe while maintaining physiologically appropriate environmental conditions. Moreover, most academic literature on EMP has not addressed the question of bioseparations, which is a critical and costly component of bioprocesses. Ideal separation processes downstream of EMP systems will be cheap and require minimal energy.

Early commercialization efforts have tended to focus on products native to the microbial host of interest (*e.g.*, acetic acid, ethanol, polyhydroxybutyrate, cell biomass) that are naturally produced in high yields. The impressive number of non-native molecules produced from EMP-relevant substrates still pales in comparison to the product spectrum demonstrated in traditional heterotrophic processes, limiting the scope of current EMP systems. The vast toolkit of synthetic biology developed in recent decades, combined with that of biochemical engineering, should be used to develop techniques to maximize conversion of a given substrate to the non-native product of interest.

EMP provides an alternative to traditional bioprocessing by replacing carbohydrates, the primary energy source driving bioconversion, with electricity. Literally and figuratively, electromicrobial production provides an opportunity to electrify biotechnology. While early efforts of commercializing EMP are ongoing, academic research in the field is steadily advancing in broadening the application-space of the technology. Addressing the areas and answering some of the open questions posed throughout this section will allow these efforts to continue to move forward. I hope that the work in this dissertation provides a modest step forward in addressing some of these outstanding areas.

1.4 Structure of this Dissertation

The work detailed in this dissertation is aimed at addressing several of the areas outlined in the previous section and seeks to move the needle toward the industrial deployment of electromicrobial production systems. Due to the advantages described previously in the introduction, I focus my efforts on mediated electromicrobial systems. The work can roughly be divided into two sections: process-scale analysis of EMP systems (Chapters 2 and 3), and microbial engineering for EMP systems (Chapters 4 and 5). In Chapter 2, I develop a tripartite framework relying on physics-based bioreactor modeling, process modeling, and life cycle impact assessment to evaluate the potential environmental benefits/impacts of scaled-up EMP systems, comparing three candidate EMP systems to each other and to a more traditional glucose-based bioprocess. In Chapter 3, I develop a techno-economic model of a specific acetate-mediated EMP system that converts air-captured CO_2 to the alternative biofuel n-butanol and assess the economic viability of EMP for a specific application as well as identify the economic bottlenecks that are the most important. A theme of both chapters is the utility of integrated analytical frameworks in directing future research directions for the field.

Chapters 4 and 5 both contain work in microbial engineering of the bacteria *Cupriavidus necator* for two different applications. These two chapters rely on two primary methods of microbial engineering: adaptive laboratory evolution and rational genetic engineering. In Chapter 4, I develop two parallel and compatible methods to make bacteria susceptible to osmolysis (lysis in

distilled water), a characteristic that can be exploited for the purification of intracellular biomolecules. *C. necator*, due to its use in EMP systems, serves as the prototypical strain in this study, while *E. coli* serves as a secondary strain to validate the broader applicability of these strategies. In Chapter 5, I describe work in engineering a strain of *C. necator* to convert acetate into the biofuel n-butanol, paralleling the analytical work described in Chapter 3. I conclude in Chapter 6 by summarizing the key findings in this dissertation, describing the common themes tying the work together, and discussing the prospects moving toward the development of electromicrobial production systems.

Chapter 2: Process Modelling and Comparative Life Cycle Assessment of Electromicrobial Production Systems[‡]

2.1 Abstract

Electromicrobial production (EMP) processes, in which electricity or electrochemically derived mediator molecules serve as energy sources to drive biochemical processes, represent an attractive strategy for the conversion of CO_2 into carbon-based products. However, these systems have yet to be employed on an industrial scale, limiting our understanding of their potential performance and environmental benefits/impacts. In this chapter, I describe the development and application of a comprehensive framework to analyze EMP systems relying on reactor, process, and life cycle impact models. This framework is used to analyze three proposed EMP systems relying on formate, H_2, and acetate as intermediate molecules, each producing three hypothetical products: biomass, lactic acid, and industrial enzymes. Physics-based bioreactor models predict that EMP systems can achieve productivities up to 0.65 g/L/h for biomass production and 0.42 g/L/h for the production of lactic acid. Process models revealed that substrate generation was by far the largest energy demand of the EMP systems, followed by carbon capture and ammonia production, while energy required for gas-liquid mass transfer and fluid mixing accounted for only a small fraction of the systems' energy footprints. Life cycle impact model results demonstrated that EMP systems can achieve a smaller carbon footprint than traditional bioprocessing strategies if the electric grid providing electricity to the EMP system is composed of at least 90% renewable energy sources. For each of the three products considered, the H_2-mediated Knallgas bacteria system achieves the lowest overall global warming potential, indicating that this EMP strategy may be best-suited for industrial efforts based on current technology. EMP systems also would use ~95% less land compared to traditional bioprocesses. I also identify environmental hotspots and process limitations that are key targets for future engineering and research efforts for each EMP system. This analysis demonstrates the utility of an integrated assessment framework and should help guide the design of working, scalable, and sustainable electromicrobial production systems.

2.2 Introduction

Ongoing and worsening ecological and humanitarian crises caused by anthropogenic climate change have precipitated efforts to transition away from fossil fuel-based commodity chemical production. Whole-cell biocatalysis provides a theoretically carbon neutral method of producing value-added products if all of the required carbon is originally fixed from atmospheric carbon dioxide (CO_2). Many petroleum-based products including fuels, plastics, and commodity chemicals can be produced biologically.[21,24,86] Moreover, some products, such as proteins, can only be produced biologically and have wide-ranging applications including in food production, chemical sensing, and as therapeutics.[87–89] Traditional bioprocesses rely on heterotrophic microbes that require exogenous sources of carbon and energy (Fig. 2.1).

[‡] This chapter has been adapted from an article that was originally published in *Energy and Environmental Science* and has been included with the permission from the co-authors.[231]

Glucose from corn starch and sucrose from sugarcane are currently the most common feedstocks in bioprocessing. These biochemical processes rely on extensive agricultural production and therefore compete with the food supply and require land use changes that have significant negative impacts on the environment. Moreover, the high carbon footprint associated with fertilizer production and application, especially when growing corn as a feedstock, causes traditional bioprocesses to have a relatively high carbon footprint. To alleviate some of these challenges, researchers have proposed cyanobacteria and algae as alternative microorganisms to be used in bioprocessing, and have demonstrated photosynthetic production of fuels, plastics, and pharmaceuticals.[90] However, these systems are still limited by slow growth rates and the relatively inefficient energy conversion of photosynthesis.[39] To overcome these shortcomings, and with the expectation of cheaper and cleaner electricity in the intermediate future, various electromicrobial production (EMP) processes have been proposed and demonstrated (Fig. 2.1).

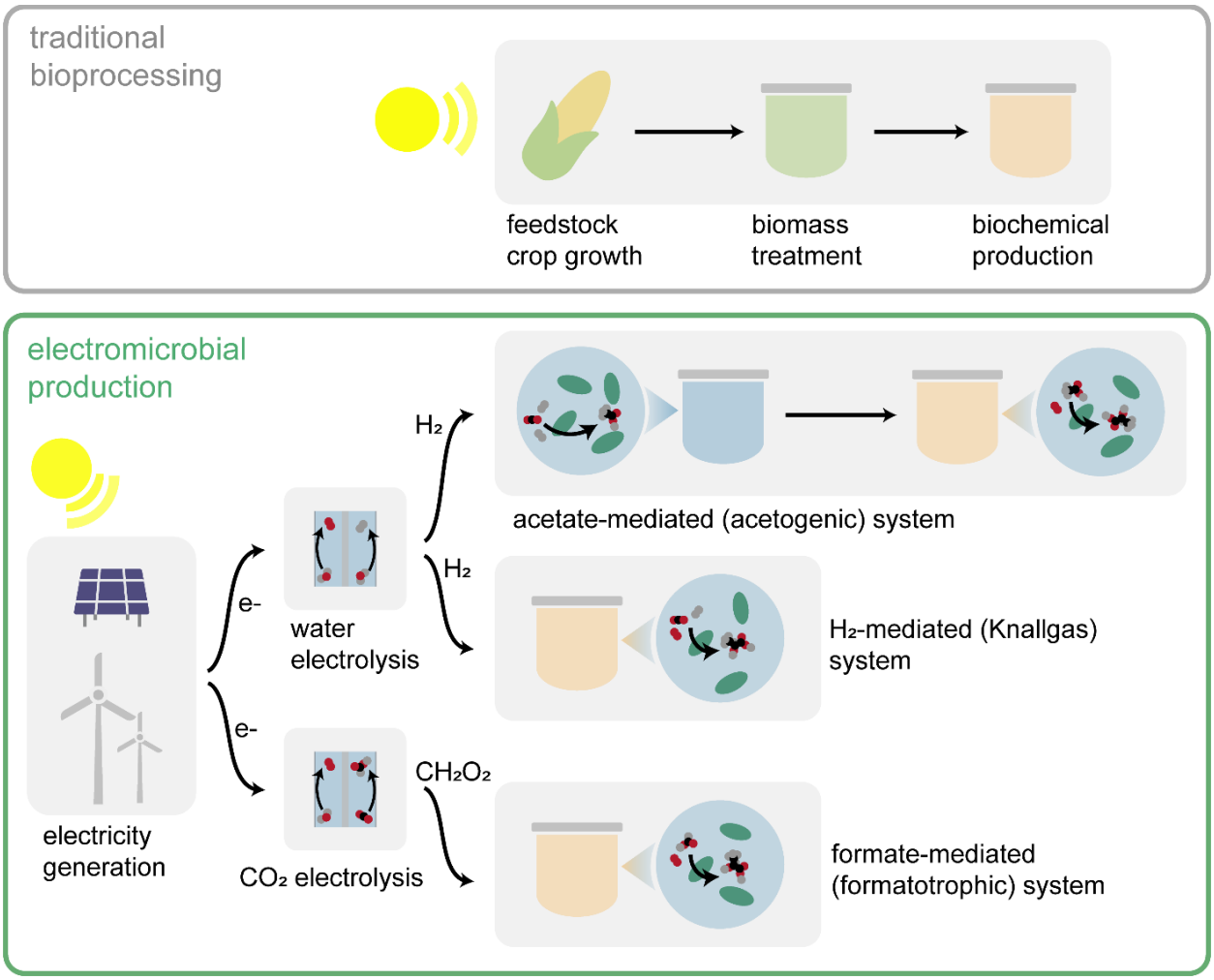

Figure 2.1. Overview of traditional bioprocessing and electromicrobial production. Traditional bioprocessing relies on feedstock crop growth, pretreatment of the resulting biomass (typically enzymatic or chemical), and subsequent biochemical production using crop-derived sugars as the feedstock. Electromicrobial production uses electricity (ideally renewable) to produce energy substrates (*e.g.,* H_2) for biochemical production from CO_2.

Although nomenclature for bioelectrochemical systems varies in the literature, I define EMP processes as any process that converts CO_2 into a value-added product (*i.e.*, contains some form of primary production), uses electricity as the primary source of energy driving that transformation, and uses microbes to produce the final product. Perhaps most notable are systems based on Knallgas (aerobic hydrogen-oxidizing) bacteria, such as *Cupriavidus necator*, which use molecular hydrogen (H_2), produced by the electrolysis of water, to fix CO_2. *C. necator* has historically been studied for production of its natively-produced polymer polyhydroxybutyrate (PHB)[45] and of biomass for use as a single cell protein.[46] More recently, *C. necator* has been engineered to produce other carbonaceous products including fuels and commodity chemicals.[64,65,91] As an alternative, formatotrophic microorganisms have been employed, in which formic acid produced from the electrochemical reduction of CO_2 is used as an energy source or assimilated by microbes to produce value-added products.[66,75,92] Naturally formatotrophic microbes such as *C. necator* have been studied for this purpose,[47] as have organisms engineered to express formate-assimilating pathways.[48] Two-step systems have also been developed based on bio-acetate as an intermediary molecule, in which CO_2 and H_2 are consumed by the acetogen *Sporomusa ovata* to produce acetate, which is then converted by a heterotroph such as *Escherichia coli* to produce various value-added products.[51,69] Other EMP strategies are possible; however, the three EMP systems described here are well-represented in the literature and have been employed for a wide variety of products through genetic engineering.

To date, research efforts have focused primarily on studying the fundamental metabolisms that permit EMP processes or on engineering metabolic pathways to enable production of specific products in relevant microbial chassis. Despite these successful bench-scale demonstrations, progress toward scaled and integrated processes has remained limited. Moreover, rigorous calculations of productivity and efficiency limits that can enable comparisons among EMP processes have been elusive, in part due to significantly different operating conditions across laboratories. Physics-based models that capture relevant phenomena (microbial growth, production and consumption of species, acid/base reactions, gas/liquid mass transfer, *etc.*) can enable like-to-like comparisons across EMP processes. Additionally, such models are necessary to quantify design and operation strategies that optimize performance and to identify process parameters that limit productivity and efficiency.

To that end, several computational analyses of EMP processes have been developed. Claassens *et al.* developed a data-driven analysis to calculate metabolic efficiencies and to quantify the specific growth rates of organisms relying on H_2, formate, acetate, and other substrates for biomass formation.[43] Salimijazi *et al.* developed thermodynamic models of metabolism in a variety of EMP systems based on direct electron transfer or H_2-mediated growth.[78] They used their model to calculate the limiting efficiency of these EMP systems and the relative area necessary for photovoltaic cells and bioreactors. Recently, Leger *et al.* compared biomass production efficiency for photovoltaics-driven EMP using H_2, formate, and methanol as mediator molecules.[79] Their analysis included quantification of biomass yields and energy demands for supporting processes such as carbon capture and electrolysis. They demonstrated that EMP-based biomass production could use sunlight more efficiently than crop growth. Because these analyses focused on quantifying metabolic limits to energy efficiency, their analyses did not consider other factors that may induce upper-bounds on the productivity or practical efficiency, including gas-liquid mass transfer, pH control, and salinity effects.

EMP systems also rely on subprocesses, such as electrocatalysis and carbon capture, that are outside the purview of most literature that focuses on the microbial and biochemical reaction engineering components of these processes. While metabolic efficiencies, productivities, and yields of these systems may be compared, these analyses do not consider differences in electrocatalytic efficiencies and productivities that affect the viability of the process as a whole. Hence, development of end-to-end process models that rely on the material and energy balances quantified in individual reactor models is necessary for a comprehensive analysis of the relative merits of EMP process options.

Life cycle assessment (LCA) is a tool for quantifying the environmental impact of products and processes across their entire life cycle in relevant categories including greenhouse gas emissions, human and environmental health effects, and resource depletion. LCAs, which follow the standards set by ISO 14040 and 14044,[93,94] aggregate and analyze material and energy flows as well as emissions from every step in the supply chain within a given system boundary and quantify the impact of a process in the desired impact categories. LCAs aid in decision-making in process design as they can be used to evaluate the environmental impacts of multiple alternatives and inform strategies to lower their footprints. Life cycle assessment has been critical in evaluating the environmental tradeoffs of biochemical production strategies, particularly in the development of biofuels.[28,90,95] Because EMP systems have been proposed as more sustainable alternatives to traditional bioprocesses, conducting LCAs on these systems is a crucial tool in assessing these claims. Principles of life cycle assessment have been applied to analyze EMP systems to date. For example, Nangle *et al.* included land use calculations in addition to demonstrating lithoautotrophic production of novel chemicals.[62] Leger *et al.* produced a comprehensive analysis of energy and land occupation footprints in the electromicrobial production of single-celled protein (SCP),[79] expanding on similar assessments of SCP production.[96,97] However, comprehensive life cycle assessments which simultaneously consider various EMP pathways, products, and impact categories to develop broad insights to the field, are still needed.

Here, I present a detailed LCA of three major EMP process options relying respectively on acetate, H_2, and formate/ic acid as mediator molecules and compare their impacts to a traditional bioprocessing scheme relying on corn-derived glucose (Fig. 2.1). Biomass, enzymes, and lactic acid are chosen as examples to represent the breadth of products that can be manufactured by EMP systems. Biomass is useful as a reference product to assess energy demands solely to grow the bacteria. Enzymes are useful representatives of low yield, high value biomacromolecules while lactic acid is a good example of a low-value, high yield commodity chemical. Two-phase bioreactor models are developed that describe microbial growth and product formation, acid/base reactions, gas/liquid mass transfer, gas and liquid phase flow, and active pH control. The models are used to evaluate the effects of reactor parameters and operating conditions on critical performance metrics including productivity, titer, and material and energy efficiency, and are coupled to process models that present a complete picture of material and energy demands for the EMP processes. This analysis demonstrates the utility of integrating reactor, process, and life cycle impact models for comprehensively evaluating biotechnological processes. Together, the presented models, methodology, and analysis provide a framework for analyzing EMP systems that can help enable working, scalable, and sustainable electromicrobial production processes.

2.3 Analytical and Computational Methods

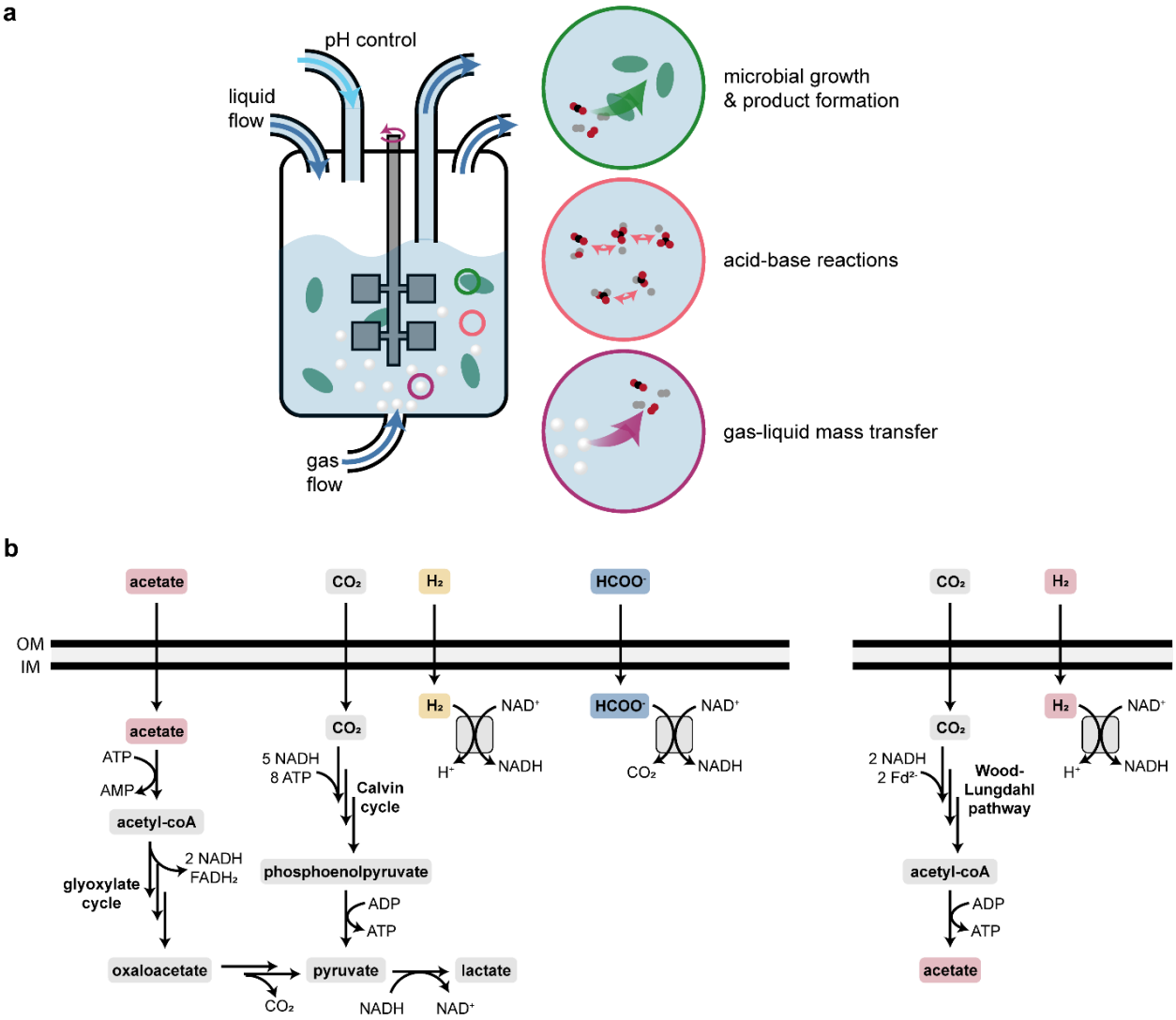

Figure 2.2. Overview of reactor model and metabolic pathways. (**a**) Bioreactor scheme. Gas and liquid media (dark blue arrows) are fed to and extracted from a two-phase, well-mixed bioreactor. The model considers gas-liquid mass transfer (purple), acid-base reactions (pink), microbial growth and product formation (green), and pH control (light blue). (**b**) Metabolic pathway map showing acetate assimilation and H_2 and formate oxidation coupled to lactate production (left), and acetate production in acetogenic microbes (right). Colors correspond to the three processes evaluated (red: acetate-mediated; yellow: H_2-mediated; blue: formate-mediated).

System overview and governing equations

All bioreactor models (Fig. 2.2a) assume well-mixed gas and liquid phases that are exchanged at fixed liquid- and gas-phase dilution rates. In the liquid phase, components include dissolved CO_2, dissolved H_2, dissolved O_2, bicarbonate anions (HCO_3^-), carbonate anions (CO_3^{2-}), protons (H^+), hydroxide anions (OH^-), sodium cations (Na^+), chloride anions (Cl^-), formic acid ($HCOOH$), formate ($HCOO^-$), acetic acid ($H_3C_2O_2H$), acetate anions ($H_3C_2O_2^-$), lactic acid ($H_5C_3O_3H$), lactate anions ($H_5C_3O_3^-$), enzyme (E), and microbes (X). In the gas phase, CO_2, H_2, and O_2 are considered.

Ammonium/a species are not explicitly accounted for in the reactor model (although will be considered in the process modeling stage).

The well-mixed phases are assumed to have sufficient convective mixing such that no concentration gradients are formed. Such an open, well-mixed system must satisfy mass conservation, given generally for the liquid phase as:

$$\frac{dc_i}{dt} = R_{\mathrm{X},i} + R_{\mathrm{A-B},i} + R_{\mathrm{LF},i} + R_{\mathrm{G-L},i} + R_{\mathrm{pH},i} \tag{2-1}$$

and for the gas phase as:

$$\frac{dp_i}{dt} = RT(R_{\mathrm{GF},i} - R_{\mathrm{G-L},i}) \tag{2-2}$$

where c_i is the concentration, p_i is the partial pressure, R_i is the net volumetric rate of formation and consumption due to microbial growth (X), acid/base reactions (A–B), liquid or gas flow (LF/GF), gas-liquid mass transfer (G–L), and pH control (pH) for species i (Fig. 2.2a). The operating temperature is given by T, and R is the gas constant. Note that the gas phase species are assumed to follow ideal behavior and that the liquid and gas volumes in the reactor are equal.

Microbial growth and product formation

Microbial growth occurs in the well-mixed liquid phase and is responsible for the production of more cells and the consumption or production of several chemical species (Fig. 2.2a). These reactions are compiled in $R_{\mathrm{X},i}$. The model assumes that the kinetics of carbon fixation (or acetate uptake, in the case of acetotrophic growth) represent the upper bound on the biomass and product formation rates because all carbon-containing molecules produced by the cell are derived from the carbon-fixing metabolism. Hence, the combined rate of biomass and product (lactate or enzyme) formation (moles carbon per volume per time) is dependent on the molar biomass carbon concentration (c_{X}) and the specific growth rate (μ). For lactate, this results in:

$$R_{\mathrm{X,X}} + 3R_{\mathrm{X,L}} = \mu c_{\mathrm{X}} \tag{2-3}$$

where the factor of 3 precedes $R_{\mathrm{X,L}}$ because lactate is a 3-carbon molecule. For the enzyme, the analogous equation is given by:

$$R_{\mathrm{X,X}} + R_{\mathrm{X,E}} = \mu c_{\mathrm{X}} \tag{2-4}$$

I define the fraction of carbon diverted to biomass as:

$$\begin{aligned} x &= \frac{1}{1+3\zeta} \ \text{(lactate)} \\ x &= \frac{1}{1+\zeta} \ \text{(enzyme)} \end{aligned} \tag{2-5}$$

where ζ is the stoichiometric ratio of products to cells in, for example, the generic equation given by:

$$\sum_i \alpha_i \mathrm{S}_i = \mathrm{X} + \zeta \mathrm{P} \tag{2-6}$$

where S is a generic substrate, P is a generic product, and α_i is the stochiometric coefficient of substrate i. I assume x is an engineerable parameter (*e.g.*, by tuning the expression levels of different enzymes) and calculate ζ according to:

$$\begin{aligned} \zeta &= \frac{1-x}{3x} \text{ (lactate)} \\ \zeta &= \frac{1-x}{x} \text{ (enzyme)} \end{aligned} \tag{2-7}$$

Hence, the biomass growth rate ($R_{\mathrm{X,X}}$) and product formation rate ($R_{\mathrm{X,L}}$, $R_{\mathrm{X,E}}$) are given by:

$$\begin{aligned} R_{\mathrm{X,X}} &= x\mu c_{\mathrm{X}} \\ R_{\mathrm{X,L/E}} &= \zeta x\mu c_{\mathrm{X}} \end{aligned} \tag{2-8}$$

and consumption or production of other molecules (*e.g.*, O_2, H_2, CO_2, *etc.*) is written as:

$$R_{\mathrm{X},i} = \alpha_{\mathrm{X},i} R_{\mathrm{X,X}} + \alpha_{\mathrm{L/E},i} R_{\mathrm{X,L/E}} \tag{2-9}$$

where $\alpha_i < 0$ if the species is consumed in the reaction following standard convention.[98]

Microbial growth kinetics are defined using the Monod model with dependencies on each potentially growth-limiting substrate. The equations for aerobic formatotrophic (F), aerobic hydrogenotrophic (H_2), anaerobic acetogenic (A), and aerobic acetotrophic growth (Ac) are given as:

$$\mu_{\mathrm{F}} = \mu_{\mathrm{max,F}} \left(\frac{c_{\mathrm{F}}}{K_{\mathrm{F}} + c_{\mathrm{F}}}\right)\left(\frac{c_{\mathrm{O_2}}}{K_{\mathrm{O_2}} + c_{\mathrm{O_2}}}\right) \tag{2-10}$$

$$\mu_{\mathrm{H_2}} = \mu_{\mathrm{max,H_2}} \left(\frac{c_{\mathrm{H_2}}}{K_{\mathrm{H_2}} + c_{\mathrm{H_2}}}\right)\left(\frac{c_{\mathrm{O_2}}}{K_{\mathrm{O_2}} + c_{\mathrm{O_2}}}\right)\left(\frac{c_{\mathrm{CO_2}}}{K_{\mathrm{CO_2}} + c_{\mathrm{CO_2}}}\right) \tag{2-11}$$

$$\mu_{\mathrm{A}} = \mu_{\mathrm{max,A}} \left(\frac{c_{\mathrm{H_2}}}{K_{\mathrm{H_2}} + c_{\mathrm{H_2}}}\right)\left(\frac{c_{\mathrm{CO_2}}}{K_{\mathrm{CO_2}} + c_{\mathrm{CO_2}}}\right) \tag{2-12}$$

$$\mu_{\mathrm{Ac}} = \mu_{\mathrm{max,Ac}} \left(\frac{c_{\mathrm{Ac}}}{K_{\mathrm{Ac}} + c_{\mathrm{Ac}} + \frac{c_{\mathrm{Ac}}^2}{K_{\mathrm{I,Ac}}}}\right)\left(\frac{c_{\mathrm{O_2}}}{K_{\mathrm{O_2}} + c_{\mathrm{O_2}}}\right) \tag{2-13}$$

where $\mu_{\max}$ is the maximum specific growth rate of the organism when all fixed carbon is diverted to biomass and K_i is the Monod constant for substrate i. Note that acetotrophic growth includes an Andrews/Haldane inhibition term ($K_{\mathrm{I,Ac}}$) to account for growth defects associated with high acetate concentrations reported previously.[99]

Biomass and product yield

A combination of experimental values and stoichiometric and energetic calculations are used to determine the yields of biomass and products on different carbon and energy sources (Fig. 2.2b). In all cases, enzyme yield ($Y'_{\mathrm{E}/i}$) and biomass yield ($Y'_{\mathrm{X}/i}$) are assumed to be equivalent and enzymes are assumed to have approximately the same chemical composition as biomass.

Formatotrophic (aerobic) growth

For formatotrophic growth with O_2 as the terminal electron acceptor and formate as the energy and carbon source (note that formate is completely oxidized and CO_2 is fixed via the Calvin cycle in *C. necator*), the biomass reaction is written as:

$$\begin{aligned}\alpha_{\mathrm{X,F}}\mathrm{HCOO^-} + \alpha_{\mathrm{X,F}}\mathrm{H^+} + \beta_{\mathrm{X,F}}\mathrm{NH_3} + \gamma_{\mathrm{X,F}}\mathrm{O_2} \\ \rightarrow \mathrm{CH_{1.77}O_{0.49}N_{0.24}} + \kappa_{\mathrm{X,F}}\mathrm{CO_2} + \epsilon_{\mathrm{X,F}}\mathrm{H_2O}\end{aligned} \tag{2-14}$$

where $\mathrm{CH_{1.77}O_{0.49}N_{0.24}}$ represents cell mass (molar mass ~25 g mol^{-1}). The stoichiometry gives:

$$\begin{gathered}\alpha_{\mathrm{X,F}} = \frac{1}{Y'_{\mathrm{X/F}}} \\ \beta_{\mathrm{X,F}} = 0.24 \\ \gamma_{\mathrm{X,F}} = \frac{1}{2}\left(0.49 + 2\kappa_{\mathrm{X,F}} + \epsilon_{\mathrm{X,F}} - 2\alpha_{\mathrm{X,F}}\right) \\ \kappa_{\mathrm{X,F}} = \alpha_{\mathrm{X,F}} - 1 \\ \epsilon_{\mathrm{X,F}} = \frac{1}{2}\left(2\alpha_{\mathrm{X,F}} + 3\beta_{\mathrm{X,F}} - 1.77\right)\end{gathered} \tag{2-15}$$

where $Y'_{\mathrm{X/F}}$ is the molar yield of biomass on formate, which is defined according to a previously described empirical relationship:[47,75]

$$Y'_{\mathrm{X/F}} = Y'_{\mathrm{X/F,max}}\left(1 - \frac{c_{\mathrm{F}} + c_{\mathrm{FA}}}{\theta_{\mathrm{F}}}\right) \tag{2-16}$$

where θ_{F} is a fitting parameter that represents the maximum formate/ic acid concentration at which cells can grow.

The lactate formation reaction is written as:

$$\begin{aligned}\alpha_{\mathrm{L,F}}\mathrm{HCOO^-} + (\alpha_{\mathrm{L,F}} - 1)\mathrm{H^+} + \beta_{\mathrm{L,F}}\mathrm{NH_3} + \gamma_{\mathrm{L,F}}\mathrm{O_2} \\ \rightarrow \mathrm{C_3H_5O_3^-} + \kappa_{\mathrm{L,F}}\mathrm{CO_2} + \epsilon_{\mathrm{L,F}}\mathrm{H_2O}\end{aligned} \tag{2-17}$$

Relying on stoichiometry, parameters are written as:

$$\begin{gathered}\alpha_{\mathrm{L,F}} = \frac{1}{Y'_{\mathrm{L/F}}} \\ \beta_{\mathrm{L,F}} = 0 \\ \gamma_{\mathrm{L,F}} = \frac{\alpha_{\mathrm{L,F}}}{2} - 3 \\ \kappa_{\mathrm{L,F}} = \alpha_{\mathrm{L,F}} - 3 \\ \epsilon_{\mathrm{L,F}} = \alpha_{\mathrm{L,F}} - 3\end{gathered} \tag{2-18}$$

where $Y'_{\mathrm{L/F}}$ is the molar yield of lactate on formate. To determine this value, the stoichiometry and energetics of carbon fixation via the Calvin cycle to lactate are considered as follows.

Microbes support energy carrier (NADH and ATP) regeneration by using NAD^+-dependent formate dehydrogenases to catalyze the reaction:

$$\mathrm{HCOO^-} + \mathrm{NAD^+} \rightarrow \mathrm{CO_2} + \mathrm{NADH} \tag{2-19}$$

NADH is then used to regenerate ATP following aerobic respiration (oxidative phosphorylation):

$$\mathrm{NADH} + \mathrm{H^+} + \frac{1}{2}\mathrm{O_2} + \left(\frac{\mathrm{P}}{\mathrm{O}}\right)(\mathrm{ADP} + \mathrm{P_i}) \rightarrow \mathrm{NAD^+} + \mathrm{H_2O} + \left(\frac{\mathrm{P}}{\mathrm{O}}\right)\mathrm{ATP} \tag{2-20}$$

where $\mathrm{P/O}$ is the oxidative phosphorylation ratio (typically 2–3). When using the Calvin cycle to fix CO_2, seven ATP and five NADH are consumed to fix three CO_2 molecules into one pyruvate molecule:

$$3\mathrm{CO_2} + 5\mathrm{NADH} + 7\mathrm{ATP} + 4\mathrm{H^+} \rightarrow \mathrm{C_3H_3O_3^-} + 5\mathrm{NAD^+} + 7(\mathrm{ADP} + \mathrm{P_i}) + 3\mathrm{H_2O} \tag{2-21}$$

Pyruvate is then converted to lactate via lactate dehydrogenase according to:

$$\mathrm{C_3H_3O_3^-} + \mathrm{NADH} + \mathrm{H^+} \rightarrow \mathrm{C_3H_5O_3^-} + \mathrm{NAD^+} \tag{2-22}$$

The resulting overall reaction for lactate production (using a $\mathrm{P/O}$ ratio of 2.5) is given by:

$$8.8\mathrm{HCOO^-} + 7.8\mathrm{H^+} + 1.4\mathrm{O_2} \rightarrow \mathrm{C_3H_5O_3^-} + 5.8\mathrm{CO_2} + 5.8\mathrm{H_2O} \tag{2-23}$$

Hence, the maximum theoretical molar yield of lactate on formate is ~0.11 mol mol^{-1}. Because the molar cell yield ($Y'_{X,F}$) is influenced by the formate concentration due to a variety of toxicity effects in *C. necator*, this dependency is included for lactate as well:

$$Y'_{\mathrm{L/F}} = Y'_{\mathrm{L/F,max}}\left(1 - \frac{c_\mathrm{F} + c_\mathrm{FA}}{\theta_\mathrm{F}}\right) \tag{2-24}$$

Hydrogenotrophic aerobic (Knallgas) growth

I use the same formulation as that for formatotrophy to describe biomass growth and product formation, but modify the stoichiometry to account for the different energy source. The biomass equation is written as:

$$\alpha_{\mathrm{X,H}}\mathrm{H_2} + \beta_{\mathrm{X,H}}\mathrm{NH_3} + \gamma_{\mathrm{X,H}}\mathrm{O_2} + \kappa_{\mathrm{X,H}}\mathrm{CO_2} \rightarrow \mathrm{CH_{1.77}O_{0.49}N_{0.24}} + \epsilon_{\mathrm{X,H}}\mathrm{H_2O} \tag{2-25}$$

resulting in the stoichiometric relationships given by:

$$\begin{aligned} \alpha_{\mathrm{X,H}} &= \frac{1}{Y'_{\mathrm{X/H}}} \\ \beta_{\mathrm{X,H}} &= 0.24 \\ \gamma_{\mathrm{X,H}} &= \frac{1}{2}\left(0.49 + \epsilon_{\mathrm{X,H}} - 2\kappa_{\mathrm{X,H}}\right) \\ \kappa_{\mathrm{X,H}} &= 1 \\ \epsilon_{\mathrm{X,H}} &= \frac{1}{2}\left(2\alpha_{\mathrm{X,H}} + 3\beta_{\mathrm{X,H}} - 1.77\right) \end{aligned} \tag{2-26}$$

The lactic acid production reaction is written as:

$$\alpha_{\mathrm{L,H}}\mathrm{H_2} + \beta_{\mathrm{L,H}}\mathrm{NH_3} + \gamma_{\mathrm{L,H}}\mathrm{O_2} + \kappa_{\mathrm{L,H}}\mathrm{CO_2} \rightarrow \mathrm{C_3H_6O_3} + \epsilon_{\mathrm{L,H}}\mathrm{H_2O} \tag{2-27}$$

with stoichiometry given by:

$$\begin{aligned} \alpha_{\mathrm{L,H}} &= \frac{1}{Y'_{\mathrm{L,H}}} \\ \beta_{\mathrm{L,H}} &= 0 \\ \gamma_{\mathrm{L,H}} &= \frac{\alpha_{\mathrm{L,H}}}{2} - 3 \\ \kappa_{\mathrm{L,H}} &= 3 \\ \epsilon_{\mathrm{L,H}} &= \alpha_{\mathrm{L,H}} - 3 \end{aligned} \tag{2-28}$$

The lactic acid production yield on H_2 ($Y'_{\mathrm{L/H}}$) following the same method as for formate, is:

$$8.8\mathrm{H_2} + 3\mathrm{CO_2} + 1.4\mathrm{O_2} \rightarrow \mathrm{C_3H_6O_3} + 5.8\mathrm{H_2O} \tag{2-29}$$

The theoretical molar yield of lactate on H_2 and formate is equivalent because H_2 and formate oxidation both result in the reduction of one molecule of NAD^+ to NADH (Fig. 2.2b).

Acetogenic (anaerobic) growth

Acetogenic growth relies on the energy derived from acetate generation to drive biomass formation. Following Fast and Papoutsakis,[100] H_2 oxidation drives acetyl-CoA formation from CO_2 given by:

$$\begin{aligned} 4\mathrm{H_2} + 2\mathrm{CO_2} + (1-n)\mathrm{ATP} + \mathrm{HSCoA} \\ \rightarrow \mathrm{C_2H_3OSCoA} + 3\mathrm{H_2O} + (1-n)(\mathrm{ADP} + \mathrm{P_i}) \end{aligned} \tag{2-30}$$

where n is the ATP conservation coefficient, representing ATP regeneration driven by the conservation of energy from proton or sodium gradients.[100,101] A simple equation for biomass formation from acetyl-CoA is also derived by Fast and Papoutsakis,[100] written as:

$$0.5\mathrm{C_2H_3OSCoA} + 4\mathrm{ATP} + \frac{\Delta\gamma}{2}\mathrm{NADH} \rightarrow \mathrm{CH_{1.77}O_{0.49}N_{0.24}} \tag{2-31}$$

where $\Delta\gamma$ is the difference in the degree of reduction between acetyl-CoA ($\gamma = 4$) and biomass ($\gamma = 4.07$). This equation, as written, is neither atomically nor charge balanced, so it should be taken to only represent the energy carrier demand of biomass formation. To generate the necessary energy, acetyl-CoA can be oxidized to acetic acid, resulting in the generation of an ATP:

$$\mathrm{C_2H_3OSCoA} + (\mathrm{ADP} + \mathrm{P_i}) + \mathrm{H_2O} \rightarrow \mathrm{C_2H_4O_2} + \mathrm{HSCoA} + \mathrm{ATP} \tag{2-32}$$

A linear combination of these equations to balance ATP results in:

$$\begin{aligned} \frac{18}{n}\mathrm{H_2} + \frac{9}{n}\mathrm{CO_2} + \frac{\Delta\gamma}{2}\mathrm{NADH} \\ \rightarrow \mathrm{CH_{1.77}O_{0.49}N_{0.24}} + \left(\frac{4.5}{n} - \frac{1}{2}\right)\mathrm{C_2H_4O_2} + \left(\frac{9}{n} - 1\right)\mathrm{H_2O} \end{aligned} \tag{2-33}$$

NADH is readily generated by the oxidation of H_2 using hydrogenases, and the nitrogen content in biomass can be supplied by ammonia. Hence, a balanced overall acetogenic growth equation is given by:

$$\left(\frac{18}{n}+\frac{\Delta\gamma}{2}\right)\mathrm{H_2}+\frac{9}{n}\mathrm{CO_2}+0.24\mathrm{NH_3} \rightarrow C\mathrm{H_{1.77}O_{0.49}N_{0.24}}+\left(\frac{4.5}{n}-\frac{1}{2}\right)\mathrm{C_2H_4O_2}+\left(\frac{9}{n}+(1-b)\right)\mathrm{H_2O} \tag{2-34}$$

where b is the oxygen content in the biomass equation (0.49 in this case).

Acetotrophic (aerobic) growth

The biomass equation is written as:

$$\alpha_{\mathrm{X,A}}\mathrm{C_2H_3O_2^-}+\alpha_{\mathrm{X,A}}\mathrm{H^+}+\beta_{\mathrm{X,A}}\mathrm{NH_3}+\gamma_{\mathrm{X,A}}\mathrm{O_2} \rightarrow \mathrm{CH_{1.77}O_{0.49}N_{0.24}}+\kappa_{\mathrm{X,A}}\mathrm{CO_2}+\epsilon_{\mathrm{X,A}}\mathrm{H_2O} \tag{2-35}$$

with stoichiometry given by:

$$\begin{gathered}\alpha_{\mathrm{X,A}}=\frac{1}{Y'_{\mathrm{X/A}}}\\ \beta_{\mathrm{X,A}}=0.24\\ \gamma_{\mathrm{X,A}}=\frac{1}{2}\left(0.49+2\kappa_{\mathrm{X,A}}+\epsilon_{\mathrm{X,A}}-2\alpha_{\mathrm{X,A}}\right)\\ \kappa_{\mathrm{X,A}}=2\alpha_{\mathrm{X,A}}-1\\ \epsilon_{\mathrm{X,H}}=\frac{1}{2}\left(4\alpha_{\mathrm{X,A}}+3\beta_{\mathrm{X,A}}-1.77\right)\end{gathered} \tag{2-36}$$

The lactate-forming reaction is written similarly:

$$\alpha_{\mathrm{L,A}}\mathrm{C_2H_3O_2^-}+\left(\alpha_{\mathrm{L,A}}-1\right)\mathrm{H^+}+\beta_{\mathrm{L,A}}\mathrm{NH_3}+\gamma_{\mathrm{L,A}}\mathrm{O_2} \rightarrow \mathrm{C_3H_5O_3^-}+\kappa_{\mathrm{L,A}}\mathrm{CO_2}+\epsilon_{L,\mathrm{A}}\mathrm{H_2O} \tag{2-37}$$

resulting in stoichiometry given by:

$$\begin{gathered}\alpha_{\mathrm{L,A}}=\frac{1}{Y'_{\mathrm{L/A}}}\\ \beta_{\mathrm{L,A}}=0\\ \gamma_{\mathrm{L,A}}=2\alpha_{\mathrm{L,A}}-3\\ \kappa_{\mathrm{L,A}}=2\alpha_{\mathrm{L,A}}-3\\ \epsilon_{\mathrm{L,H}}=2\alpha_{\mathrm{L,A}}-3\end{gathered} \tag{2-38}$$

The yield of lactate on acetate ($Y'_{\mathrm{L/A}}$), is determined following the stoichiometry and energetics of acetate assimilation and oxidation through the glyoxylate shunt (Fig. 2.2b). Acetate is first activated to acetyl-CoA according to:

$$C_2H_3O_2^- + 2ATP + HSCoA + H^+ \rightarrow C_2H_3OSCoA + 2(ADP + P_i) + H_2O \quad (2\text{-}39)$$

Acetyl-CoA is passed through the glyoxylate shunt to produce oxaloacetate and regenerate energy carriers, resulting in the net reaction given by:

$$2C_2H_3OSCoA + 3H_2O + 2NAD^+ + FAD \rightarrow C_4H_3O_5^- + 3H^+ + 2NADH + FADH_2 + 2HSCoA \quad (2\text{-}40)$$

Oxaloacetate is then converted to lactate via phosphoenolpyruvate and pyruvate with the net reaction:

$$C_4H_3O_5^- + NADH + H^+ \rightarrow C_3H_5O_3^- + CO_2 + NAD^+ \quad (2\text{-}41)$$

Using the P/O ratio of 2.5 for NADH (as above) and 1.5 for $FADH_2$, the resulting net reaction for acetate conversion to lactate is given as:

$$2C_2H_3O_2^- + O_2 + H^+ \rightarrow C_3H_5O_3^- + CO_2 + H_2O \quad (2\text{-}42)$$

Hence, the theoretical molar yield of lactate on acetate ($Y'_{L/A}$) of 0.5 mol mol^{-1}.

Growth rate dependence on pH and salinity

A simple model to describe the effects of pH and salinity on microbial growth is used:

$$\mu_{max} = \mu_{opt}\rho(pH)\nu(c_{Na}) \quad (2\text{-}43)$$

where μ_{opt} is the specific growth rate at optimal conditions and $\rho(pH)$ and $\nu(c_{Na})$ are functions describing the impacts of pH and Na^+ concentration on the growth rate.

Following Rosso *et al.*,[102] $\rho(pH)$ is written as:

$$\rho(pH) = \begin{cases} 0 & pH < pH_{min} \\ f(pH) & pH_{min} \leq pH \leq pH_{max} \\ 0 & pH > pH_{max} \end{cases} \quad (2\text{-}44)$$

Here, $pH_{min/max}$ is the range of pH over which microbial growth is observed, and the function $f(pH)$ is:

$$f(pH) = \frac{(pH - pH_{min})(pH - pH_{max})}{(pH - pH_{min})(pH - pH_{max}) - (pH - pH_{opt})^2} \quad (2\text{-}45)$$

where pH_{opt} is the optimal pH for growth.

Microbial growth is strongly dependent on the salinity of the medium. In an effort to adapt *E. coli* to high salt concentrations necessary for high lactic acid titers, Wu *et al.* demonstrated that the effect is determined primarily by the Na^+ concentration, and that the maximum growth rate decreases approximately linearly with increasing Na^+ concentration.[103] Data from Wu *et al.* are used to fit this dependence according to:

$$\nu(c_{Na}) = \begin{cases} 1 & c_{Na} < c_{Na,min} \\ f(c_{Na}) & c_{Na,min} < c_{Na} < c_{Na,max} \\ 0 & c_{Na} > c_{Na,max} \end{cases} \quad (2\text{-}46)$$

where $c_{\mathrm{Na,min/max}}$ is the range of Na^+ concentration over which growth is impacted, and the function $f(c_{\mathrm{Na}})$ is given by:

$$f(c_{\mathrm{Na}}) = 1 - \frac{c_{\mathrm{Na}}}{c_{\mathrm{Na,max}} - c_{\mathrm{Na,min}}} \tag{2-47}$$

To ensure a fair comparison across processes, it is assumed that the Na^+ concentration has the same impact on each organism.

Acid/base reactions

The acid/base bicarbonate/carbonate, formic acid/formate, acetic acid/acetate, lactic acid/lactate, and water dissociation reactions shown below occur in the liquid phase (Fig. 2.2a) and are treated as kinetic expressions without assuming equilibrium:

$$\mathrm{CO_{2(aq)}} + \mathrm{H_2O} \overset{k_{+1},k_{-1}}{\Longleftrightarrow} \mathrm{H^+} + \mathrm{HCO_3^-} \qquad K_1 \tag{2-48}$$

$$\mathrm{HCO_3^-} \overset{k_{+2},k_{-2}}{\Longleftrightarrow} \mathrm{H^+} + \mathrm{CO_3^{2-}} \qquad K_2 \tag{2-49}$$

$$\mathrm{CO_{2(aq)}} + \mathrm{OH^-} \overset{k_{+3},k_{-3}}{\Longleftrightarrow} \mathrm{HCO_3^-} \qquad K_3 = K_1/K_{\mathrm{W}} \tag{2-50}$$

$$\mathrm{HCO_3^-} + \mathrm{OH^-} \overset{k_{+4},k_{-4}}{\Longleftrightarrow} \mathrm{CO_3^{2-}} + \mathrm{H_2O} \qquad K_4 = K_2/K_{\mathrm{W}} \tag{2-51}$$

$$\mathrm{HCOOH} \overset{k_{+5},k_{-5}}{\Longleftrightarrow} \mathrm{H^+} + \mathrm{HCOO^-} \qquad K_5 \tag{2-52}$$

$$\mathrm{H_3C_2OOH} \overset{k_{+6},k_{-6}}{\Longleftrightarrow} \mathrm{H^+} + \mathrm{H_3C_2OO^-} \qquad K_6 \tag{2-53}$$

$$\mathrm{H_5C_3O_2OH} \overset{k_{+7},k_{-7}}{\Longleftrightarrow} \mathrm{H^+} + \mathrm{H_5C_3O_2O^-} \qquad K_7 \tag{2-54}$$

$$\mathrm{H_2O} \overset{k_{+w},k_{-w}}{\Longleftrightarrow} \mathrm{H^+} + \mathrm{OH^-} \qquad K_{\mathrm{W}} \tag{2-55}$$

where k_{+n} and k_{-n} are the forward and reverse rate constants, respectively, and K_n is the equilibrium constant for the nth reaction. For formic acid, acetic acid, lactic acid, and water, K_n is calculated from the van't Hoff equation using the change of entropy, ΔS_n, and the heat of reaction, ΔH_n, given by:

$$K_n = \exp\left(\frac{\Delta S_n}{R}\right)\exp\left(-\frac{\Delta H_n}{RT}\right) \tag{2-56}$$

For CO_2/HCO_3^- and HCO_3^-/CO_3^{2-} equilibria, K_n is determined using the empirical relationships compiled by W.G. Mook that account for salinity-induced impacts on the equilibrium constant:[104]

$$pK_1 = \frac{3670.7}{T} - 62.008 + 9.7944\ln(T) - 0.0118S + 0.000116S^2 \tag{2-57}$$

$$pK_2 = \frac{1394.7}{T} + 4.777 - 0.0184S + 0.000118S^2 \tag{2-58}$$

where S is the medium salinity (in units g/kg water).

Source and sink terms resulting from these reactions are compiled in $R_{\mathrm{A-B},i}$, written as:

$$R_{\mathrm{A-B},i} = \sum_i \nu_i \left(k_{+n} \prod_{\nu_i<0} c_i - k_{-n} \prod_{\nu_i>0} c_i \right) \tag{2-59}$$

where ν_i is the stoichiometric coefficient of species i for the nth reaction and reverse rate constants (k_{-n}) are calculated from:

$$k_{-n} = \frac{k_{+n}}{K_n} \tag{2-60}$$

Liquid and gas flow

Liquid media is fed to and extracted from the well-mixed liquid phase at a constant dilution rate (Fig. 2.2a), resulting in a feed term written as:

$$R_{\mathrm{LF},i} = D_{\mathrm{liq}}\left(c_{\mathrm{f},i} - c_i\right) \tag{2-61}$$

where D_{liq} is the liquid dilution rate (defined as the inverse space time, or volumetric flow rate divided by reactor volume). The feed stream is assumed to be free of microbes. A feed term for the gas phase is similarly defined as:

$$R_{\mathrm{GF},i} = \frac{D_{\mathrm{gas}}}{RT}\left(p_{\mathrm{f},i} - p_i\right) \tag{2-62}$$

where D_{gas} is the gas dilution rate.

Gas-liquid mass transfer

Gas fed to the reactor results in mass transfer to the liquid phase according to:

$$R_{\mathrm{G-L},i} = k_{\mathrm{L}} a_i (\beta_i p_i - c_i) \tag{2-63}$$

where $k_{\mathrm{L}} a_i$ is the volumetric mass-transfer coefficient on the liquid side of the gas/liquid interface, and β_i is the Bunsen solubility coefficient (Fig. 2.2a). The volumetric gas/liquid mass transfer coefficient (for oxygen) can be calculated using the correlation developed by Vasconcelos *et al.* for stirred tank reactors with a height that is twice the diameter:

$$k_{\mathrm{L}} a_{\mathrm{O}_2} = 22.3 (P_{\mathrm{G}})^{0.66} (u_{\mathrm{G}})^{0.51} \tag{2-64}$$

where P_{G} is the specific power input (in units W m^{-3}) and u_{G} is the superficial gas velocity (in units m s^{-1}), which is related to the gas phase dilution rate using:

$$u_{\mathrm{G}} = \frac{D_{\mathrm{gas}}}{A_{\mathrm{S}}} \tag{2-65}$$

where A_{S} is the surface area per reactor volume of the sparging holes. A value of 5.6 m^{-1} is assumed to make a gas dilution rate of 100 hr^{-1} correspond to a superficial gas velocity of 0.05 m s^{-1}, and the correlation above is used to determine the power demand necessary to achieve a given gas/liquid mass transfer rate.

To calculate the $k_{\mathrm{L}} a$ value for CO_2 and H_2, the $k_{\mathrm{L}} a$ for oxygen under equivalent calculations is calculated, and is then adjusted by the following relationship:

$$k_{\mathrm{L}}a_{i\neq \mathrm{O}_2} = \sqrt{\frac{D_i}{D_{\mathrm{O}_2}}}k_{\mathrm{L}}a_{\mathrm{O}_2} \tag{2-66}$$

where D_i is the diffusivity of species i following Meraz *et al.* to account for differences in the mass transfer coefficient (k_{L}).[105]

The equilibrium solubility of CO_2, O_2, and H_2 are calculated according to the empirical relationship for the Bunsen solubility coefficient (β):

$$\ln\beta = A_1 + A_2\left(\frac{100}{T}\right) + A_3\ln\left(\frac{T}{100}\right) + S\left[B_1 + B_2\left(\frac{T}{100}\right) + B_3\left(\frac{T}{100}\right)^2\right] \tag{2-67}$$

where A_n and B_n are fitting parameters and S is the medium salinity (in units g kg^{-1} water).

pH control

A feedback control loop is included in the reactor to maintain an optimal pH for microbial growth by adding 1 M hydrochloric acid or 1 M sodium hydroxide solutions where appropriate (Fig. 2.2a). The manipulated flow rate variable (units hr^{-1}) is defined as:

$$r_{\mathrm{M}} = 0 + K_{\mathrm{C}}\left(E + \frac{1}{\tau}\int Edt\right) \tag{2-68}$$

where K_{C} is the controller gain, E is the error, and τ is the controller reset time. The error (E) is defined according to:

$$E = \mathrm{pH}^{\mathrm{set}} - \mathrm{pH} \tag{2-69}$$

where $\mathrm{pH}^{\mathrm{set}}$ is equivalent to $\mathrm{pH}_{\mathrm{opt}}$. The resulting pH control flow is given by:

$$R_{\mathrm{pH},i} = r_{\mathrm{M}}c_{\mathrm{pH},i} \tag{2-70}$$

where $c_{\mathrm{pH},i}$ is 1 M for H^+/Cl^- (acid addition) or 1 M for OH^-/Na^+ (base addition).

Reactor model analysis

A normalized dilution rate (δ) is defined as:

$$\delta = \frac{D_{\mathrm{liq}}}{x\mu_{\max}} \tag{2-71}$$

to account for the fact that the maximum growth rate is reduced by diversion of carbon to the product. The reactor productivity can then be calculated as:

$$\dot{m}_{j,n} = Z_j\delta_{j,n}x_j\mu_{\max,n}c_j \tag{2-72}$$

where Z_j is the molar mass of product j and the subscript n refers to a particular process. For the acetogenic system, full-system productivity is calculated, accounting for flow through both reactors using:

$$\dot{m}_{j,\mathrm{AA}} = \frac{\dot{m}_{j,\mathrm{Ac}}}{1 + \frac{\delta_{j,\mathrm{Ac}} x_j \mu_{\max,\mathrm{Ac}}}{\delta_{\mathrm{A}} \mu_{\max,\mathrm{A}}}} \tag{2-73}$$

where the subscripts "Ac" and "A" refer to the acetotrophic and acetogenic reactors, respectively, and the subscript "AA" refers to the full acetate-mediated system.

The energy efficiency of each reactor system can be calculated as:

$$\eta_{\mathrm{E},j,n} = \frac{P_{\mathrm{C},j,n}}{P_{\mathrm{C},n} + P_{\mathrm{G},j,n} + P_{\mathrm{th},j,n}} \tag{2-74}$$

where P_{C} is power embodied in the formation of product j or the substrate in process n, P_{G} is the power demand from mixing and gas/liquid mass transfer (calculated using Eqn. 2-64), and P_{th} is the power necessary to heat the liquid feed from room temperature to the operating temperature. I define the power of formation of a chemical species as the Gibbs free energy change per volume per time associated with the complete combustion of the chemical species following Claassens *et al.*[43]:

$$P_{\mathrm{C},i,n} = \left| R_{\mathrm{LF},i,n} \Delta_{\mathrm{r}} G_i^0 \right| \tag{2-75}$$

for liquid-phase species and

$$P_{\mathrm{C},i,n} = \left| R_{\mathrm{GF},i,n} \Delta_{\mathrm{r}} G_i^0 \right| \tag{2-76}$$

for gas-phase species. I note that these formulations mean that I have assumed residual substrate can be perfectly recycled and therefore represent upper bounds on the efficiency of the systems. The power necessary to heat the liquid feed, P_{th}, is given by:

$$P_{\mathrm{th},j,n} = \frac{\delta_{j,n} x_j \mu_{\max,n} C_{\mathrm{P,W}} \rho_{\mathrm{W}} (T - T_0)}{\mathrm{COP}} \tag{2-77}$$

where $C_{\mathrm{P,W}}$ and ρ_{W} are the heat capacity and density of water, respectively, and COP is the coefficient of performance of the heat transfer unit.

In the formate-mediated system, the productivity of lactic acid is enhanced by concentrating the formate/ic acid effluent from the CO_2 electrolysis system (see Results and Discussion). The power demand associated with this:

$$P_{\mathrm{conc,LLA,F}} = \frac{\delta_{\mathrm{LLA,F}} x_{\mathrm{LLA}} \mu_{\max,\mathrm{F}} c_{\mathrm{FFA,f}} RT}{\eta_{\mathrm{ED,F}}} \ln\left(\frac{c_{\mathrm{FFA,f}}}{c_{\mathrm{FFA,eff}}}\right) \tag{2-78}$$

where $c_{\mathrm{FFA,f}}$ is the total concentration of formate and formic acid in the feed stream for the system, $\eta_{\mathrm{ED,F}}$ is the energy efficiency of the electrodialysis system concentrating formate/ic acid, and $c_{\mathrm{FFA,eff}}$ is the total concentration of formate/ic acid in the effluent stream of the CO_2 electrolyzer. This power demand is then included in the reactor efficiency calculation (Eqn. 2-74).

CO_2 demand

For each reactor, it is assumed that all fed CO_2 (in the gas phase) that is not transferred to the liquid phase is recycled perfectly such that the net CO_2 demand for the reactor producing product j is given directly by the net gas phase CO_2 feed rate:

$$\dot{n}_{\mathrm{CO_2},j,n} = R_{\mathrm{GF,CO_2},j,n} \tag{2-79}$$

This balance accounts for the fact that CO_2 is generated by microbes oxidizing formate (in the formate-mediated system) and acetate (in the acetate-mediated system). In these reactors, $\dot{n}_{\mathrm{CO_2}} < 0$ because CO_2 is generated. In the formate-mediated system, CO_2 is consumed to produce formate by the CO_2 electrolyzer. Hence, the full-system net consumption of CO_2 is given by:

$$\dot{N}_{\mathrm{CO_2},j,\mathrm{F}} = R_{\mathrm{LF,FFA},j,\mathrm{F}} + \dot{n}_{\mathrm{CO_2},j,\mathrm{F}} \tag{2-80}$$

where $R_{\mathrm{LF,FFF},j,\mathrm{F}}$ is the liquid-phase net feed rate of formate/ic acid (which is produced on a 1:1 molar basis from CO_2 in the upstream electrolyzer). In the acetate-mediated system, CO_2 is consumed in the acetogenic reactor and consumed in the acetotrophic reactor. Hence, the full-system net consumption of CO_2 is written as:

$$\dot{N}_{\mathrm{CO_2},j,\mathrm{AA}} = R_{\mathrm{GF,CO_2},j,\mathrm{Ac}} + \left(\frac{\delta_{j,\mathrm{Ac}} x_j \mu_{\mathrm{max,Ac}}}{\delta_{\mathrm{A}} \mu_{\mathrm{max,A}}}\right) R_{\mathrm{GF,CO_2,A}} \tag{2-81}$$

where the subscript "AA" refers to the full acetate-mediated system.

Reactor model implementation

All equations are solved using the MUMPS general solver in COMSOL Multiphysics 5.4. Model parameters are listed in Table A.1, Appendix A.

Life cycle analysis goal and scope definition

This life cycle assessment was carried out according to the standards in ISO 14044.[93] The open source life cycle assessment software openLCA version 1.10.3 (https://www.openlca.org/)[106] was used to aggregate life cycle inventory data and apply impact assessment methods. The Product Environmental Footprints Dataset[107] was used to obtain most background life cycle inventories while others were aggregated from literature as needed. Unless otherwise stated, the analysis was made indifferent to the exact location of the process. MATLAB was used to develop an impact model sensitive to changes of various variables and parameters studied.

The primary goal of this LCA is to predict the performance of three electromicrobial production systems (labelled as the Knallgas bacteria-based system, the formatotrophic system, and the acetogenic system) with regard to two sustainability metrics: global warming potential and land occupation. The LCA compares these systems to each other as well as to a traditional bioprocess using corn-derived glucose as a feedstock for a heterotrophic bacterium. A secondary goal of this analysis is to determine the specific limitations, bottlenecks, and environmental hotspots of each proposed EMP system. The final goal of this analysis is to integrate the life cycle impact model with the bioreactor models developed to create a tool enabling the eco-design of EMP processes.

Functional unit and system boundaries

The production of three products is considered: biomass, industrial enzymes, and lactic acid. The life cycle impact analysis ends at the production of each product in unprocessed form. Downstream processing is not considered, as the processing of a given product would be identical for each system studied. For the production of biomass, the functional unit is 1 kg biomass. For industrial enzyme production, the functional unit is 1 kg of enzyme unpurified from the cell pellet. For lactic acid, the functional unit is 1 kg of lactic acid at a concentration of 100 g/L.[108] Despite not

considering end of life processing of the products, biogenic carbon is not considered as sequestered carbon, and all biogenic carbon is assumed to decompose to carbon dioxide.

Process modelling and life cycle inventory

Material and energy requirements for the process are obtained from the results of the EMP reactor models and are sub-divided into the following categories: electricity generation for the EMP system; carbon dioxide direct air capture; ammonia production; other required nutrients and pH control agents; electrolyzer materials; electrodialysis materials; and plant and bioreactor construction. In addition, a (corn-derived) glucose-fed *E. coli* process is modelled, in which glucose production is added as a process category. Carbon dioxide flows are explicitly considered in the EMP models (see Eqn. 2-79:81). For all other non-substrate nutrient requirements, the medium is assumed to be recycled such that 95% of input materials are consumed by cells in the bioreactor (*i.e.*, the nutrient utilization ratio is 0.95). I assume a C:P ratio of 50:1 and base calcium, magnesium, and sulfur requirements on the elemental composition of *E. coli*.[109]

I assume each major process in the system draws electricity from a grid composed of coal, natural gas, hydropower, nuclear, photovoltaic, and wind-derived energy. The composition of the grid is treated as a variable in the impact assessment model. The life cycle inventories of these six electricity sources are obtained from the Product Environmental Footprints (PEF) dataset. Direct air capture of carbon dioxide via temperature-vacuum swing adsorption is modelled based on Duetz and Bardow's analysis of industrial-scale plants operated by Climeworks.[110] Two possible routes for ammonia synthesis are considered, both involving the Haber-Bosch process. In one route, hydrogen for ammonia synthesis is obtained from steam methane reforming (SMR). In an alternative route, hydrogen is obtained from electrolysis of water drawing electricity from the grid (green ammonia). In both cases, the energy requirements and life cycle impacts are adapted from Singh *et al.*[111] A mix of ammonium phosphate (from phosphoric acid) and ammonium chloride (from hydrochloric acid) is supplied to the bioreactor to maintain the assumed C:N:P ratio. Life cycle inventories for phosphoric acid, magnesium sulfate, and calcium chloride are obtained from the PEF dataset. The pH is controlled in the bioreactor by addition of hydrochloric acid and sodium hydroxide, which are obtained through the chlor-alkali process and rely on electricity from the grid. Energy requirements and life cycle impacts are derived from Garcia-Herrero *et al.*[112]

Power demand for electrolytic H_2 production in the Knallgas system is given by:

$$P_{\mathrm{E},j,\mathrm{H}} = \frac{V_{\mathrm{H_2}} n_{\mathrm{H_2}} F}{\eta_{\mathrm{F,H_2}}} R_{\mathrm{GF,H_2},j,\mathrm{H}} \tag{2-82}$$

where $V_{\mathrm{H_2}}$ is the operating voltage of the electrolyzer, $n_{\mathrm{H_2}}$ is the stoichiometric ratio of electrons to product, F is Faraday's constant, and $\eta_{\mathrm{F,H_2}}$ is the Faradaic efficiency of the electrolyzer producing H_2. Power demand for formate production in the formatotrophic system is calculated similarly, resulting in:

$$P_{\mathrm{E},j,\mathrm{F}} = \frac{V_{\mathrm{F}} n_{\mathrm{F}} F}{\eta_{\mathrm{F,F}}} R_{\mathrm{LF,FFA},j,\mathrm{F}} \tag{2-83}$$

Power demand for H_2 production in the acetate-mediated system is calculated using:

$$P_{\mathrm{E},j,\mathrm{AA}} = \frac{V_{\mathrm{H_2}} n_{\mathrm{H_2}} F}{\eta_{\mathrm{H_2}}} \left(\frac{\delta_{j,\mathrm{Ac}} x_j \mu_{\mathrm{max,Ac}}}{\delta_{\mathrm{A}} \mu_{\mathrm{max,A}}} \right) R_{\mathrm{GF,H_2,A}} \tag{2-84}$$

to account for the two-step conversion of H_2 into products with acetate as the intermediate. Electrolyzer material requirements are adapted from previous literature[113–115] and the life cycle inventories associated with each component are obtained from the PEF database. The lifetime of the electrolyzers is assumed to be three years.

Because none of the processes achieve a lactic acid titer of 100 g/L, the power demand necessary to concentrate lactate using an electrodialysis system is modeled, using data from Hábová *et al.*,[116] to fit an empirical relationship (see Supplementary Note A.5, Appendix A) between the lactate titer fed to the electrodialysis system and the energy demand for separation and concentration, resulting in:

$$P_{\mathrm{conc,LLA,n}} = \dot{m}_{\mathrm{LLA},n} \left(a_{\mathrm{ED}} - b_{\mathrm{ED}} c_{\mathrm{LLA},n} \right) \tag{2-85}$$

where a_{ED} and b_{ED} are fitting parameters. To determine material demands of electrodialysis, an empirical equation (see Supplementary Note A.5, Appendix A) of the form is used to relate the rate of lactic acid flux ($\Gamma_{\mathrm{LLA},n}$) through the membrane to the titer of lactic acid effluent from the reactor:

$$\Gamma_{\mathrm{LLA},n} = \Gamma_{\mathrm{max}} \left(\frac{c_{\mathrm{LLA},n}}{\kappa_{\mathrm{M}} + c_{\mathrm{LLA},n}} \right) \tag{2-86}$$

Here, both Γ_{max} and κ_{M} are fitting parameters meant to represent the maximum rate of lactic acid flux and the concentration at half the maximum rate, respectively. Using this calculated flux, an assumed lifetime (t_{M}) of three years, and an assumed diluate concentration ($c_{\mathrm{LLA,d}}$) of 1 g/L, the membrane material requirements are given by:

$$M_{\mathrm{M,LLA},n} = \left(\frac{\delta_{\mathrm{LLA},n} x_{\mathrm{LLA}} \mu_{\mathrm{max},n} \left(c_{\mathrm{LLA},n} - c_{\mathrm{LLA,d}} \right) d_{\mathrm{M}} \rho_{\mathrm{M}}}{\Gamma_{\mathrm{LLA},n}} \right) \left(\frac{1}{t_{\mathrm{M}} \dot{m}_{\mathrm{LLA},n}} \right) \tag{2-87}$$

The same calculations are used to determine the material demands for concentrating the formate feed stream in the formate-mediated system in the case of lactic acid production, and the life cycle inventory associated with the electrodialysis membrane (Nafion 324 is used as a stand-in) is obtained from the Stropnik *et. al*.[117]

The process productivities obtained from the reactor models are used to determine the total bioreactor volumes required to produce the functional unit of a given product. Stainless steel bioreactors are used, with material requirements calculated based on the design of Mobius Bioreactors from EMD Millipore. The impacts of the bioreactor and the plant facility are due primarily to producing the required construction materials—stainless steel for the bioreactor and concrete and steel for the plant, assuming a constant amount of concrete and steel per square meter of facility area.[118] The area of facility space required per aggregate volume of the bioreactors is based on the Natureworks lactic acid production facility in Blair, NE. Steel, stainless steel, and concrete life cycle inventories are all obtained from the PEF database. I assume a reactor lifetime of eight years and a plant lifetime of thirty years.

Glucose for the heterotrophic process is obtained from the hydrolysis of corn starch, and life cycle inventories of glucose production are obtained from the PEF dataset. Ammonia requirements for

corn production are obtained from Ma *et al*.[119] and the life cycle inventories for glucose production are adjusted to account for reduced carbon emissions in the case of green ammonia production.

Life cycle impact assessment (LCIA)

Global warming potentials were calculated according to the 2013 IPCC model for 100-year global warming potential and are expressed in kilograms of CO_2-equivalents [kg CO_2-e].[120] The land use footprint is calculated using the ReCiPe (H) 2016 method, which weights the impact of various types of land use by their impact on biodiversity.[121] The units of land use are expressed as m^2·year crop equivalents, representing the weighted land use needed to produce a given functional unit of product per year.

Sensitivity analysis

All parameters used in the development of the bioreactor models and life cycle analysis (*e.g.*, growth rates, reactor lifetimes, solar electricity GWP) other than physical properties (molecular weights, heat capacities, *etc.*) were independently altered by +/-30% and the global warming potential of each process was recalculated. The ratio of the global warming potential of each EMP process (formatotrophic, Knallgas, and acetogenic) and the global warming potential of the heterotrophic process in each scenario was taken to be the metric of interest to evaluate the sensitivity of each parameter. The parameters that caused the largest deviation of this ratio from the equivalent ratio for the base case value of all parameters were taken to be the most critical parameters in the study (a 10% deviation of this ratio from the base case value was used as a cutoff).

2.4 Results and Discussion

Reactor models reveal trade-offs in productivity and efficiency across processes

Trends in the productivity (Fig. 2.3a-c), titer (Fig. 2.3d-f), and efficiency (Fig. 2.3g-i) of the three EMP processes producing biomass, enzyme, and lactic acid are identified. The productivity, titer, and efficiency of biomass and enzyme production for each system have nearly identical dynamics. Because formate is fed in the liquid phase, the formatotrophic system follows the standard trend of initially increasing productivity as a function of the dilution rate, followed by a rapid decline as cell washout occurs (Fig. 2.3a, b). Complete washout (*i.e.*, a productivity and titer of ~0) occurs well before the dilution rate exceeds the maximum growth rate (at a normalized dilution rate of 1). This is due to the limitation on productivity imposed by O_2 gas-liquid mass transfer. As the dilution rate increases, the formate feed rate exceeds the consumption rate limit imposed by O_2 mass transfer, causing toxic build-up of formate in the reactor. Formate build-up prevents cell growth, which results in cell washout. Mass transfer limit-induced washout dynamics are also observed in the acetogenic system (Fig. 2.3a, b; d, e), although the behavior for acetate is slightly different from that for the formate case due to the different strategies for modeling acetate and formate toxicity. The productivity of biomass (Fig. 2.3a) and enzymes (Fig. 2.3b) in the H_2 mediated system does not follow the typical trend because all substrates necessary for growth are fed via the gas phase. Hence, productivity is only slightly dependent on the liquid phase dilution rate until washout begins to occur at a normalized dilution rate of ~0.85 (Fig. 2.3a, b). Instead, for the H_2-mediated system, product titer is controlled by the liquid dilution rate, enabling a wide range of

achievable product titers (Fig. 2.3d, e). For each system, the optimal efficiency occurs at the same dilution rate at which the productivity is maximized.

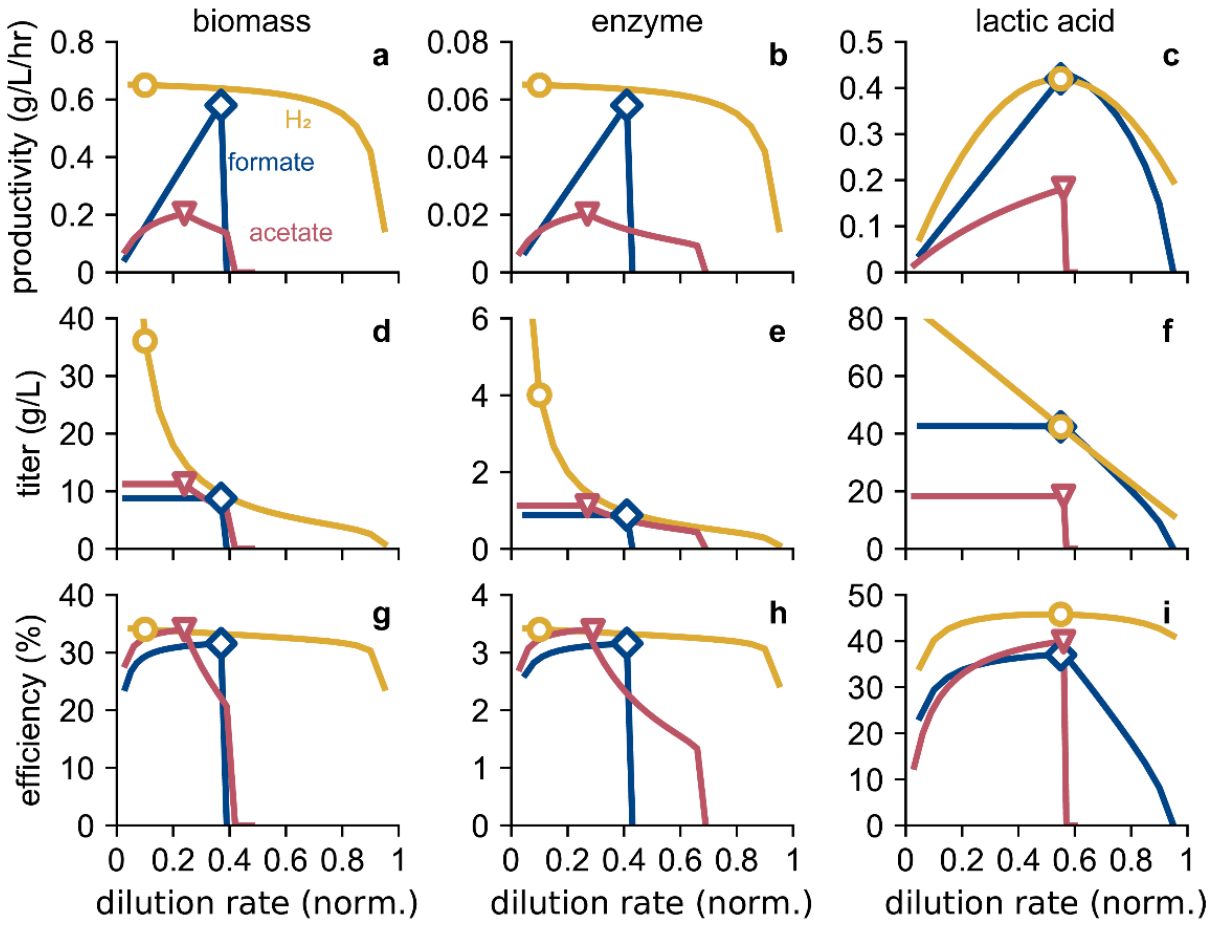

Figure 2.3. EMP reactor performance. Productivity (**a**, **b**, **c**), titer (**d**, **e**, **f**), and energy efficiency (**g**, **h**, **i**) as a function of normalized dilution rate (δ) for the three EMP systems producing biomass (**a**, **d**, **g**), enzyme (**b**, **e**, **h**), and lactic acid (**c**, **f**, **i**). Base case conditions (see Table 2.1) are indicated by blue diamonds (formate-mediated), yellow circles (H_2-mediated), and red triangles (acetate-mediated). The color scheme in all panels follows that in (**a**).[§]

In each system, lactic acid production is significantly influenced by the toxicity induced by high salinity (Fig. 2.3c, f, i). In the formatotrophic system, the productivity initially increases as the dilution rate increases, reaching a maximum at a normalized dilution rate of 0.55 (Fig. 2.3c). In contrast to biomass and enzyme production, this maximum is not due to the gas-liquid mass transfer limit of O_2. Instead, lactic acid production (resulting in a lactic acid titer of ~42 g/L, Fig. 2.3f), requires pH control to maintain an optimal pH for microbial growth. This results in a high Na^+ concentration due to NaOH addition, reducing the maximum growth rate of cells (Eqn. 2-46 and 2-47). In this case, the lactic acid titer of ~42 g/L reduces the growth rate to ~56% of its maximum value, causing cell washout to begin to occur at a normalized dilution rate of ~0.56 (Fig.

[§] I would like to thank Dr. Paul Tol (Netherlands Institute for Space Research, SRON) for a helpful reference on accessible color schemes (https://personal.sron.nl/Bpault/), which aided in the design of most figures shown in this dissertation.

2.3c, f). Cell washout also reduces the titer of lactic acid (Fig. 2.3f). These effects, in addition to the incomplete utilization of the formate feed as cell washout occurs, combine to reduce the efficiency of formatotrophic lactic acid production as the normalized dilution rate exceeds ~0.56 (Fig. 2.3i).

In the acetate-mediated system, the toxicity effect of high salinity also causes cell washout near ~56% of the maximum growth rate (Fig. 2.3c, f). The decline in productivity, titer, and efficiency is much more rapid than in the formatotrophic case. This is because the Na^+ concentration in the feed stream is much higher than in the formate case. Acetic acid production in the upstream reactor requires NaOH addition to maintain a neutral pH for acetogenesis, so the acetotrophic reactor cannot avoid a high Na^+ concentration by reducing the lactic acid titer. Hence, even though the acetotrophic reactor requires acid addition to maintain a near-neutral pH (resulting in no additional Na^+ supplied to the reactor), the residual Na^+ fed from the acetogenic reactor is sufficient to result in cell washout above a normalized dilution rate of ~0.56.

In the H_2-mediated system, Na^+ toxicity limits the productivity and titer of lactic acid, although this limitation occurs at lower dilution rates ($\delta < 0.55$) rather than high dilution rates. This effect is because the lactic acid titer (and therefore, the Na^+ concentration) increases as the dilution rate decreases (Fig. 2.3f), which in turn is a result of the fact that all substrates for growth and lactic acid formation (H_2, CO_2, O_2) are fed via the gas phase (similar to the biomass and enzyme production cases).

The efficiency of lactic acid production, in addition to that of biomass and enzyme production, is optimized at the maximum productivity. Base-case operating conditions that maximize the productivity for each system are selected (Table 2.1). A minimum normalized dilution rate of 0.1 was arbitrarily set for the H_2-mediated system producing biomass and enzymes because it has a wide dilution rate range at which the productivity is roughly equal. In the acetate-mediated system, the dilution rate in the acetogenic reactor that maximizes the full-system productivity was chosen as the base case. For lactic acid production in the formate-mediated system, a concentrated (5.1 M) formate feed stream maximizes the productivity (see Supplementary Note A.1).

Considering biomass first, the achievable productivity is highest for the H_2-mediated system at ~0.65 g/L/h, ~11% and ~225% higher than the productivities of the formatotrophic and acetogenic systems, respectively (Fig. 2.3a). The former difference is due to the ~13% higher biomass yield on O_2 with H_2 as the energy substrate than with formate and the fact that the H_2 gas/liquid mass transfer limit is slightly lower than the O_2-imposed limit. The acetogenic system, in contrast, is primarily limited by the acetate production rate of the acetogen, which grows ~4-fold slower than Knallgas and formatotrophic bacteria.

The Knallgas system also achieves the highest biomass titer (~36 g/L vs. ~8.8 g/L and ~11 g/L) because the titer is fully controllable by the liquid-phase dilution rate for this system (Fig. 2.3d). These trends also hold for the enzyme production case, although the productivity, titer, and efficiency are all ~10-fold lower than for biomass because only 10% of the fixed carbon is diverted to enzyme production (Fig. 2.3b, e). For biomass formation, the maximum efficiency of each EMP process is remarkably similar (~32-34% for biomass production, Fig. 2.3g). These efficiencies are dominated by the metabolic efficiency, defined as the ratio of energy embodied in the product to energy embodied in the main substrate. That these efficiencies are nearly equal is surprising given the remarkably different metabolic strategies for biomass production.

Table 2.1. Base case operating parameters

Parameter		Value			
Parameter Description	**Variable**	**Formatotrophic**	**Knallgas**	**Acetogenic**	**Units**
Biomass					
Normalized Dilution Rate (Liquid Phase)	δ	0.37	0.1	0.55 (*S. ovata*) 0.24 (*E. coli*)	--
H_2 Feed Pressure	P_{H_2}	--	1	1 (*S. ovata*) -- (*E. coli*)	atm
O_2 Feed Pressure	P_{O_2}	0.21	0.21	-- (*S. ovata*) 0.21 (*E. coli*)	atm
Formate Feed Concentration	$c_{FFA,f}$	2.08	--	--	M
Titer	c_X	8.8	36.1	11.25	g L^{-1}
Productivity	$\dot{m}_X$	0.585	0.65	0.20	g L^{-1} h^{-1}
Efficiency	η_X	31.6	34.0	34.0	%
Enzyme					
Normalized Dilution Rate (Liquid Phase)	δ	0.41	0.1	0.55 (*S. ovata*) 0.27 (*E. coli*)	--
H_2 Feed Pressure	P_{H_2}	--	1	1 (*S. ovata*) -- (*E. coli*)	atm
O_2 Feed Pressure	P_{O_2}	0.21	0.21	-- (*S. ovata*) 0.21 (*E. coli*)	atm
Formate Feed Concentration	$c_{FFA,f}$	2.08	--	--	M
Carbon Fraction To Biomass	x	0.9	0.9	-- (*S. ovata*) 0.9 (*E. coli*)	--
Titer	c_E	0.88	4.0	1.1	g L^{-1}
Productivity	$\dot{m}_E$	0.058	0.065	0.020	g L^{-1} h^{-1}
Efficiency	η_E	3.16	3.40	3.38	%
Lactic Acid					
Normalized Dilution Rate (Liquid Phase)	δ	0.55	0.55	0.55 (*S. ovata*) 0.56 (*E. coli*)	--
H_2 Feed Pressure	P_{H_2}	--	1	1 (*S. ovata*) -- (*E. coli*)	atm
O_2 Feed Pressure	P_{O_2}	0.21	0.21	-- (*S. ovata*) 0.21 (*E. coli*)	atm
Formate Feed Concentration	$c_{FFA,f}$	5.1	--	--	M
Carbon Fraction To Biomass	x	0.1	0.1	-- (*S. ovata*) 0.1 (*E. coli*)	--
Titer	c_{LLA}	42.4	42.4	18.3	g L^{-1}
Productivity	$\dot{m}_{LLA}$	0.42	0.42	0.18	g L^{-1} h^{-1}
Efficiency	η_{LLA}	37.0	45.8	39.9	%

In contrast to the case for biomass and enzyme formation, the formate-mediated and H_2-mediated lactic acid productivity is equal at ~0.42 g/L/h, ~130% higher than the acetogenic system (Fig. 2.3c). Each system is limited by the Na^+ concentration-induced toxicity; in the acetate-mediated system, each of the two bioreactors experience this limitation, which is responsible for the substantially lower productivity. The H_2-mediated system achieves the highest efficiency of the three EMP options; the efficiency of the formate-mediated system is hindered by the requirement that the formate effluent from the CO_2 electrolyzer must be concentrated by a factor of ~2.5 to achieve high productivity (see Supplementary Note A.1).

Several initial conclusions can be drawn from this analysis. First, both the Knallgas and formatotrophic systems can achieve higher productivities than the acetogenic system. The acetogen-based system does maintain advantages not captured in this analysis, including that a wider range of industrial microorganisms (*e.g.*, *E. coli*, *Bacillus licheniformis*, and some oleaginous yeasts) grow naturally on acetate, but bioengineering efforts could obviate this advantage in the future. Second, the solubility advantage of formate as a growth substrate is only relevant in cases where the O_2 gas-liquid mass transport is a less stringent limit on productivity than H_2 transport. This depends both on the ratio of H_2 to O_2 in the gas phase and the ratio of H_2 to O_2 consumed per unit of product. In the production cases explored here, the formatotrophic system never achieves a higher productivity than the Knallgas system. In the biomass and enzyme production cases, the O_2 mass transport limit is rate-determining. In principle, the formatotrophic system could achieve a higher lactic acid productivity than the Knallgas system, but salinity effects prevent this (Fig. 2.3c). Third, the necessity of concentrating formate from the effluent of a CO_2 electrolyzer to achieve high formatotrophic productivity when O_2 gas liquid mass transfer is not rate-limiting represents a non-negligible energy penalty, reducing energy efficiency (Fig. 2.3i). Improvements in CO_2 electrolysis reactor operation may overcome this challenge, as discussed later.

Another aspect not directly quantified in the model is safety. The gas mixture fed to the Knallgas system under base-case operation is flammable.[122] A nonflammable gas mixture would either require significantly less air (~0.27 atm vs. the assumed 1 atm), reducing productivity by decreasing O_2 solubility, or significantly more H_2 (~3.62 atm vs. the assumed 1 atm), increasing safety concerns associated with pressurized gases and likely increasing reactor and control systems complexity.

These results indicate trade-offs in productivity, titer, and efficiency such that reactor models alone cannot identify a clearly best EMP strategy. Moreover, upstream processes including energy substrate generation (via either water of CO_2 electrolysis), CO_2 capture, ammonia production, NaOH and HCl production for pH control, and other considerations, require explicit attention as important drivers of material and energy demand for EMP processes. I therefore developed a complete process model (diagrammed in Fig. 2.4) for the EMP processes to understand material and energy flows for the full system.

Energy requirements for EMP Processes

In the EMP process model (see methods), there are five major energy demands: electrosynthesis of mediator molecules (H_2 or formic acid), bioreactor energy demands (heating, gas-liquid mass transfer, etc.), direct air capture of carbon dioxide, green ammonia production, and production of NaOH and HCl for pH control through electrolysis of NaCl and water. The material and energy

flows for each of the three systems are summarized in Table 2.2, with process power demands broken down by subcategory in Table A.2 in Appendix A.

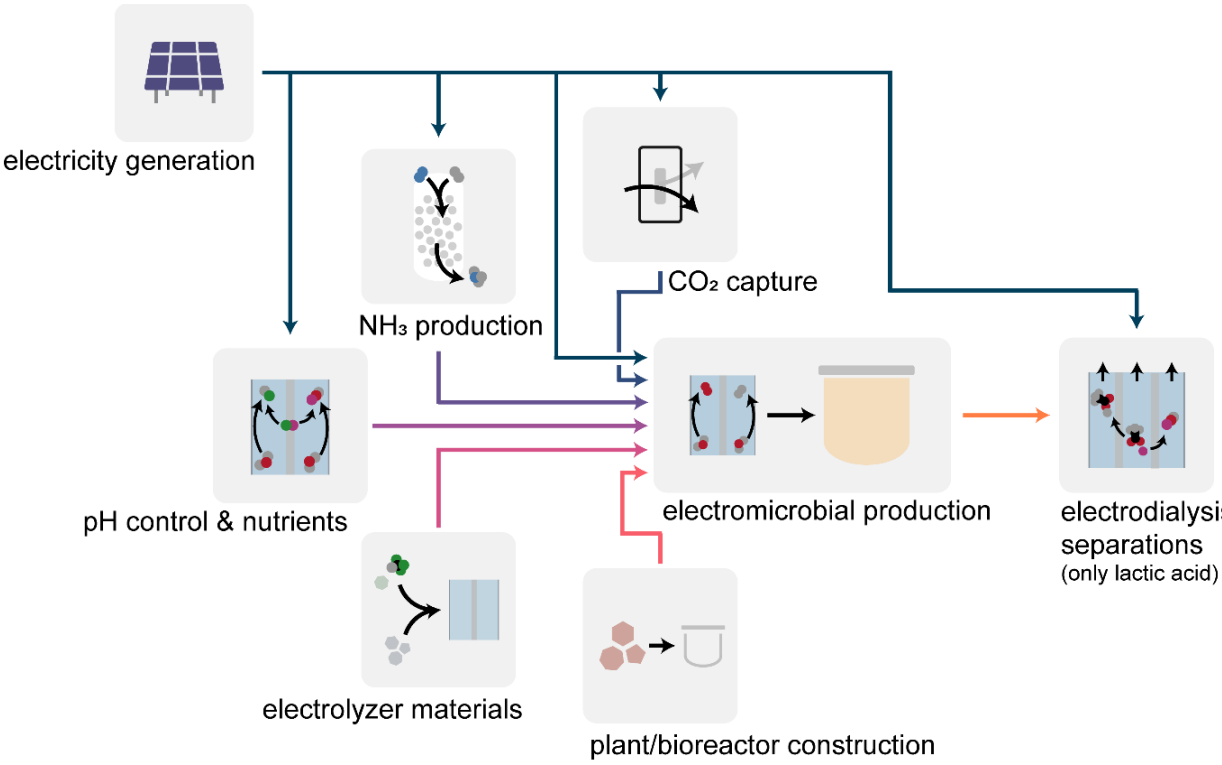

Figure 2.4. Schematic representation of the EMP system. Grid electricity (midnight blue) supplies electricity to the EMP reactors and supporting processes, including direct air capture of CO_2 (blue), ammonia production via the Haber-Bosch process (royal purple), the chlor-alkali process producing pH control agents (purple), and downstream electrodialysis-based separations for lactic acid (orange). Mining and production of electrolyzer materials (magenta) and materials for reactor and plant construction (bright pink) are also considered within the impact model.

In all cases, electrolysis to produce H_2 or formate contributes the majority of the energy demand of each system over the entire process. Even though the acetogenic EMP system has the lowest energy requirements when considering only electrolysis and bioreactor operation (Table 2.2), the Knallgas bacteria system has the overall lowest energy demand of the three systems when considering the entire electromicrobial production process. This is caused by a combination of lower CO_2 and NH_3 consumption, and the lack of required pH control in the Knallgas bacteria system. The increased carbon and nitrogen requirements of the acetogenic process stem from the "wasteful" production of *S. ovata* biomass (Eqn. 2-33).

The Knallgas bacteria system requires no pH control (see Eqn. 68-70) because conversion of H_2 and CO_2 to biomass involves no net consumption or generation of protons (Eqn. 2-25). The formatotrophic system requires only a relatively small amount of NaOH to balance the pH due to the formic acid feed (Eqn. 2-14). The model predicts the acetogenic system requires substantial pH control (Eqn. 2-33 and 2-35), as conversion of CO_2 into acetate lowers the pH of the *S. ovata* medium (requiring addition of basic solution) while conversion of acetate to biomass raises the pH of the heterotroph reactor (requiring addition of acidic solution). Owing to the substantial amount

of electricity required by the chlor-alkali process to produce NaOH and HCl, pH control accounts for 12.4% of the total electricity required by the acetogenic EMP process (Table 2.2).

Table 2.2. Energy and material demand for biomass production

Process Demand	*Formatotrophic*	*Knallgas*	*Acetogenic*	*Theoretical* [a]	Units
total process electricity	**54.3**	**28.4**	**32.0**	**6.55**	**kWh/kg CDW**
electrolysis & bioreactor electricity	48.0	23.2	21.5	5.32	kWh/kg CDW
CO_2	2.09	1.76	2.08	1.76	kg CO_2/kg CDW
NH_3	0.179	0.179	0.201	0.17	kg NH_3/kg CDW
total NaOH and HCl	0.30	0	3.23	0	kg/kg CDW

[a] Theoretical energy and material demand calculations can be found in Supplementary Note A.6.

Direct air capture (DAC), despite being a relatively immature technology industrially, only accounts for (at most) 12.5% of the total energy use of the EMP systems given current industrial DAC data (Table A.2, Appendix A). Improvements to the direct air capture process or utilizing carbon from a different source with lower energy requirements are therefore unlikely to substantially alter the results of this analysis.

Global warming potential of EMP processes

The global warming impacts of all components shown in Figure 2.4 were calculated as outlined in the methods section for each of the three EMP systems and the traditional glucose-fed process. For the case of a wind-powered process, the global warming potential broken down by process categories is shown in Figure 2.5. It should be noted that other means of clean electricity production (such as thin-film photovoltaics and hydropower) have roughly equivalent life cycle emissions per kWh produced, and therefore would lead to similar results. To study general trends regarding the potential of each process alternative, 1 kg of biomass is chosen as the product and functional unit as a baseline comparison.

The impact model shows that all three proposed EMP systems have the potential to have a lower global warming potential than that of the corn-based glucose-fed bioprocess, given a clean electricity source. This analysis indicates the Knallgas bacteria system has a lower overall global warming potential (0.68 kg CO_2-eq./kg biomass) than both the formatotrophic system and acetogenic system (1.16 and 1.35 kg CO_2-eq./kg biomass respectively). The reduction in greenhouse gas emissions associated with electromicrobial production compared to the heterotrophic system stems from the low emissions of the individual components of the EMP systems when drawing energy from a low-impact energy grid. The high-impact agricultural

production of corn and other crops as feedstocks in bioprocesses contributes the largest share of the global warming potential of these systems. While the carbon emissions associated with fertilizer production can be reduced with increased clean energy (as calculated in the impact model), the large amount of nitrous oxide emissions due to fertilizer application will not be affected by this change, leading to a relatively large global warming potential of traditional bioprocesses. Therefore, in a clean-electricity dominated scenario, the Knallgas bacteria-based EMP system will have a GWP 64% lower than a glucose-fed process (Fig. 2.5).

Although both rely on the same microorganism in the model (*C. necator*), the formate-mediated electromicrobial system will have a larger global warming potential than a hydrogen-mediated system. CO_2 electrolysis to formate occurs at lower current densities (140 mA/cm^2 vs. 1 A/cm^2) and with higher overpotentials (>2 V vs. ~0.8 V) compared to water electrolysis, resulting in an increased carbon footprint due to an increased demand for electrolyzer materials (*e.g.*, Ir, Pt, Nafion) and increased energy consumption. I further describe the effects of potential improvements to this system in the later section titled "LCA as an ecodesign tool: engineering targets for formate electrolysis".

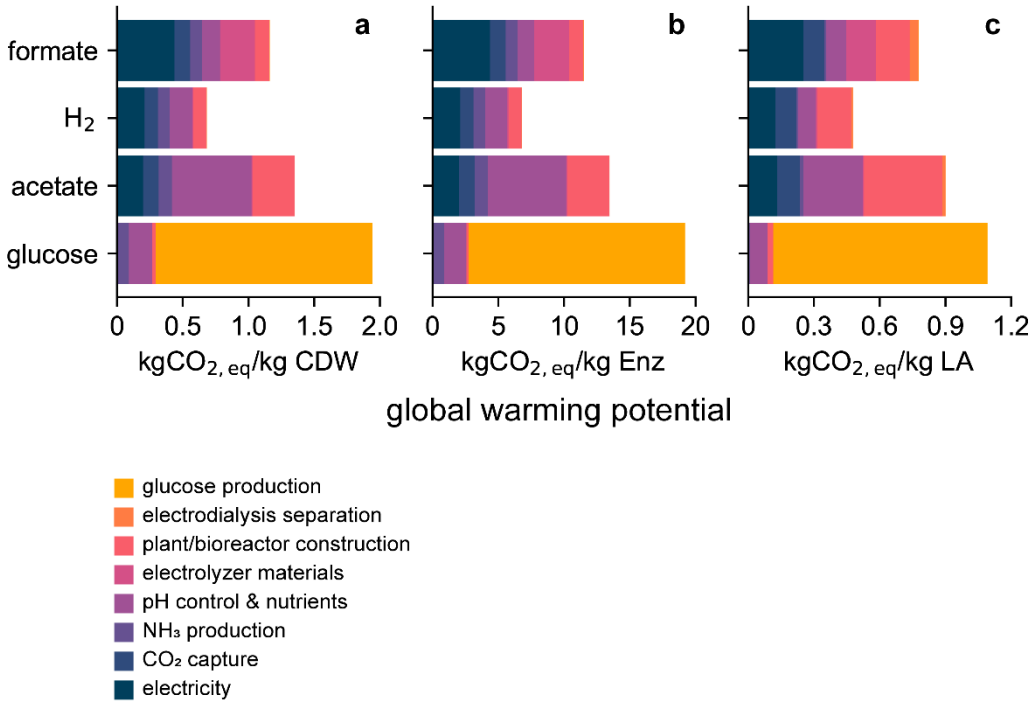

Figure 2.5. Global warming potential of EMP and traditional bioprocesses. Global warming potential for the three EMP systems and traditional heterotrophic system producing (**a**) biomass, (**b**) enzymes, and (**c**) lactic acid, broken down by process category. Data shown here assume base-case conditions as described in Table 2.1.

The greatest environmental hotspot of the acetogen-based system compared to the others is due to the production of NaOH and HCl for pH control (Fig. 2.5). The chlor-alkali process that produces NaOH and HCl is an energy-intensive electrolytic process, and therefore contributes a substantial carbon footprint. Even when running the chlor-alkali process with clean electricity, NaCl production and other processing steps still contribute to the carbon footprint of pH control.[112] However, there are a couple options to help alleviate this constraint. For example, engineering the

acetogen-based process to take place in a single reactor could address the problem of pH control because the combined biochemical reactions result in no net generation or consumption of protons. The key impediment to this solution is the strict oxygen sensitivity of acetogens such as *S. ovata*[123] and the requirement for oxygen in assimilation of acetate as a sole carbon source.[124] However, for certain applications, this may be achievable. *S. ovata* has recently been evolved to tolerate low concentrations of oxygen.[125] If paired with a heterotroph producing a product traditionally produced by fermentation such as butanol,[126] microaerobic conditions would be suitable to achieve high yields. Therefore, the aeration conditions of the two organisms could be similar enough to warrant their co-culture in a single reactor.

Further transitions to a clean energy grid will likely reduce the carbon footprint of EMP processes due to a combination of effects too granular to be captured in the model. The life cycle carbon footprint of solar energy production, for example, will likely fall as silicon production and purification processes begin to use cleaner energy. Emissions due to transportation along the supply chain will likely fall due to increased use of electric vehicles. As such changes continue to occur, it is in principle feasible for electromicrobial production processes to achieve full carbon neutrality. The carbon footprint of glucose-based bioprocesses, however, is unlikely to achieve full carbon neutrality. Cleaner methods of fertilizer production and electrified processes for farming machinery and glucose processing will indeed lower the carbon footprint of conventional bioprocesses. However, the primary source of greenhouse gas emissions in corn production is due to the application of fertilizers, as nitrogenous fertilizers are partially degraded to nitrous oxide, a greenhouse gas with 298-fold higher global warming potential than of CO_2.[119,120] Further transitions to a clean electric grid and electrified processing, then, are more likely to decrease the global warming potential of EMP processes than that of heterotroph-based processes.

The life cycle impact analysis is extended to the other two products modelled, industrial enzymes and lactic acid (Fig. 2.5b,c). In the case of an industrial enzyme as the product of interest, the trends largely follow that of biomass (Fig. 2.5b). Assuming the industrial enzyme product is intracellular, effects of titer do not impact the energy demand as low-energy separation methods (*e.g.*, settling, filtering) are possible. Therefore, similar trends for GWP in enzyme and biomass production, scaled due to the relative yields of each, are expected. In the case of lactic acid production, the trends between EMP systems are similar to those of biomass production, with Knallgas bacteria-based production of lactic acid exhibiting the lowest global warming potential of the systems studied. The lactic acid effluent must be concentrated (modeled as an electrodialysis process, see Methods) in all three EMP systems studied in order to achieve the desired 100 g/L titer. However, due to the relatively low material and energy demands of the electrodialysis process, this does not significantly impact the global warming potential (Fig. 2.5c).

I have also calculated a cradle-to-grave life cycle global warming potential of polylactic acid (PLA) made from lactic acid in each of these processes (Fig. A.3, Appendix A), assuming the PLA is composted at the end-of-life. PLA made from EMP-generated lactic acid will have lower life-cycle greenhouse gas emissions compared to petroleum-based plastics such as polystyrene (PS) and polyethylene terephthalate (PET), assuming a sufficiently high yield (see Supplementary Note A.3, Appendix A).

Importantly, the data shown in Fig. 2.5 assume 90% of the fixed carbon is converted to lactic acid (see Table 2.1), which matches the yield commonly achieved by lactic acid fermentation from glucose.[127] This high yield of lactic acid, achievable due to the high yield of fermentation products

during anaerobic growth, may not be achievable in EMP systems. All three EMP systems considered (based on hydrogen-oxidizing, formatotrophic, or acetotrophic metabolism) require respiration, suggesting that high yields of lactic acid may be difficult to achieve. I expand on the effect product yield has on the viability of EMP systems in the following section.

Effect of electric grid on global warming potential of EMP systems

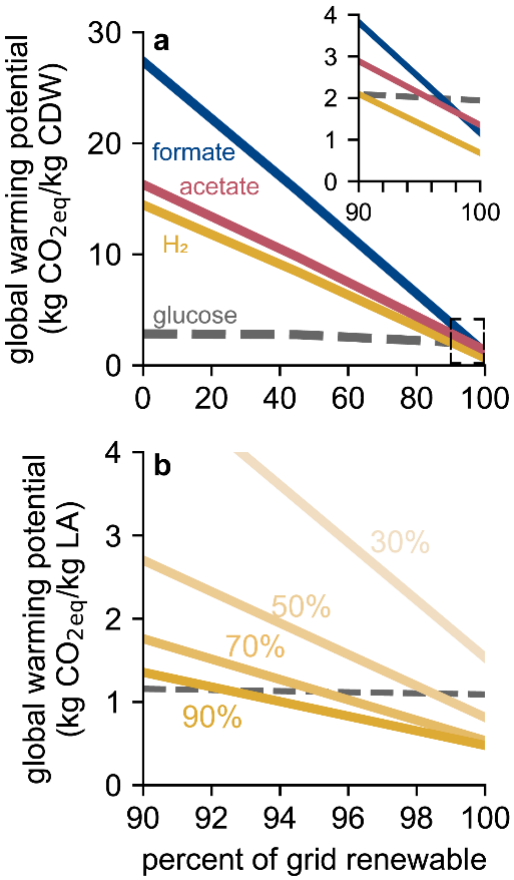

Figure 2.6. Effect of electricity grid on global warming potential. (**a**) Global warming potential for the production of biomass for the formate- (blue), acetate- (red), H_2- (Knallgas, yellow), and glucose-fed (traditional bioprocessing, dashed gray) systems drawing electricity from a grid composed of variable fractions of wind power (renewable) and natural gas (non-renewable). Inset shows the >90% renewables region bounded by the dashed box. (**b**) Global warming potential for the production of lactic acid in the H_2-fed (Knallgas) system (yellow) as a function of electricity grid compositions for variable carbon efficiencies (fraction of fixed carbon diverted to lactic acid) as well as global warming potential for the traditional glucose fermentation of lactic acid (dashed gray).

Due to the high electricity demand of each system, the dominant factor affecting the environmental sustainability of electromicrobial production systems is the source of energy. I therefore studied how the electricity grid composition affects the global warming potential associated with each system (Fig 2.6a). Although the impact model can input an electric grid composition comprising several sources (coal, natural gas, hydropower, nuclear, photovoltaic, and wind), to simplify the results an electric grid comprised of some combination of wind power and natural gas is considered, defining the fraction of electricity derived from wind power as the "percent of grid renewable." It should be noted that the electric grid composition of the United States (as of 2019) has a global warming potential of about 450 g CO_2/kWh, roughly equivalent to a grid that is based 100% on natural gas.[128] As shown in Figure 2.6a, even the Knallgas bacteria system, which has the lowest GWP of the three schemes, will not have a lower GWP than a traditional glucose-based system unless over 90% of the electric grid comes from renewable resources. These "breakeven" values are 95% and 97% renewable electricity for the acetogenic and formatotrophic system, respectively.

Figure 2.6b shows similar breakeven curves for the production of lactic acid in a Knallgas bacteria-based system at a range of carbon efficiencies (defined as the fraction of fed or fixed carbon diverted to lactic acid). The carbon efficiency of product formation will play a large role in its global warming potential. At 90% carbon efficiency, lactic acid production in a hydrogen-fed system will attain environmental viability if at least 90% of the electric grid is composed of renewable resources. At lower carbon efficiencies, stricter requirements of the grid are necessary to achieve a lower GWP than traditional glucose-fed processes. At 30%, production of lactic acid through EMP will result in higher greenhouse gas emissions than the glucose-fed process (Fig. 2.6b) regardless of the electricity source. This result highlights the importance of maximizing the product yield as electromicrobial systems are developed and establishes a target yield of at least 50% of the theoretical maximum. Lactic acid production using formate as a substrate has been demonstrated in the literature, with a yield roughly 10% of the theoretical maximum.[60] While this is an important proof of principle, further work in improving the yield will be required for the process to be environmentally sustainable.

Land use of EMP processes

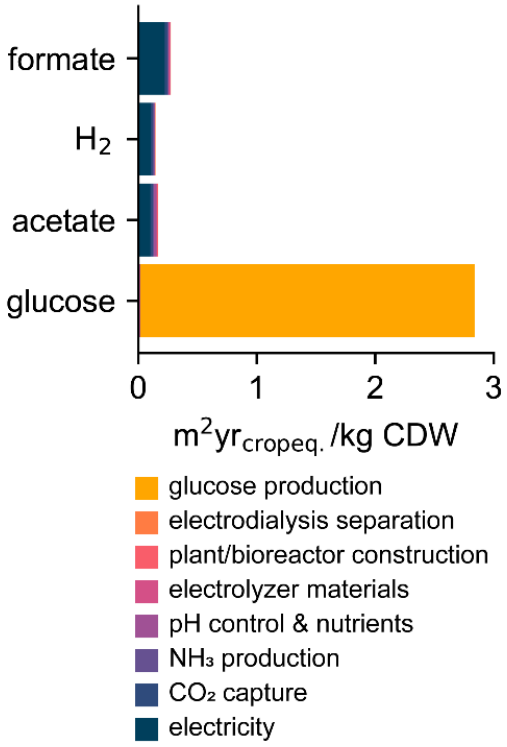

Figure 2.7. Land occupation footprints of EMP and traditional bioprocesses. Land occupation footprint as calculated by ReCiPe 2016 (H) midpoint method for the three EMP systems and traditional heterotrophic system for the production of biomass, broken down by process category.

This impact assessment demonstrates a significantly lower land use of EMP systems compared to traditional bioprocesses, even when using solar energy, the electricity generation method with the largest land occupation footprint (Fig. 2.7). This result is expected as EMP processes have been proposed in part to alleviate the "food vs. fuel debate" that stems from the high agricultural land use of traditional bioprocesses and biofuels. The dominant factor determining the land occupation of EMP systems is the land used by solar panels required for electricity production, including electricity production for electrolysis, ammonia production, and HCl/NaOH production. Therefore, the land occupation impacts follow the same trends of total electricity use in Table 2.2. The weighted land occupation footprint of the Knallgas bacteria system is 0.15 $m^2 \cdot yr$ crop-eq./kg

compared to 2.84 m^2·yr crop-eq./kg for a glucose-fed system, representing a 95% reduction in land use. The improved energetic efficiencies of lithoautrotrophic carbon fixation compared to photosynthetic carbon fixation is the primary driver of this disparity.

The land occupation footprint described by the ReCiPe 2016 midpoint method used here weights different types of land use according to their impact on the environment. Solar panels may be deployed in many environments, including sparsely vegetated or urban land, and therefore will have lower land use impacts than agricultural land use. When discounting weighting factors, the raw land use of the Knallgas bacteria-based system is 0.25 m^2·yr./kg biomass, representing an 11-fold decrease in land use compared to a glucose-fed system. These results are consistent with the solar-to-biomass efficiencies of 9.7% for a *Cupriavidus necator* hydrogen-fed system and ~1% for photosynthetic plants reported by Liu *et al.*[55] Although land use data from databases are generally recognized to be less reliable than greenhouse gas emission data, the land occupation footprint of the EMP systems and of the traditional bioprocess are dominated by the land requirements of solar panels and corn farmland respectively, both of which have well-studied data. Additionally, the calculated land requirements of EMP processes are over an order of magnitude smaller than that of heterotroph-based processes. Therefore, the assessment that EMP processes will have a substantially lower land occupation footprint than current biomanufacturing methods can be reported with high confidence.

LCA as an ecodesign tool: engineering targets for formate electrolysis

The formate-mediated EMP system is associated with a significantly higher GWP than the H_2-mediated system due primarily to differences in electrolyzer performance with currently achievable efficiencies and current densities. Because electrochemical reduction of CO_2 is an active area of research, this technology may improve in coming years, making the formate-mediated system more competitive with the H_2-mediated system. To identify engineering targets that must be met by CO_2 electrolysis systems, the GWP of biomass and lactic acid production as a function of electrolyzer parameters (current density, j; energy efficiency, η), are calculated and compared to the H_2-mediated system operated under intrinsically safer conditions (Fig. 2.8). Intrinsically safer conditions are defined in Supplementary Note A.2, Appendix A.

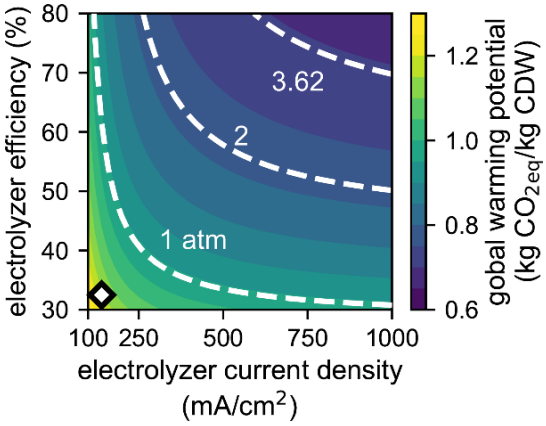

Figure 2.8. Effects of CO_2 electrolysis operating parameters. Global warming potential of biomass production with the formate-mediated system as a function of electrolyzer current density and electrolyzer efficiency. Overlaid white dashed lines correspond to the global warming potential of the intrinsically safer H_2-mediated system (as described in Supplementary Note A.2, Appendix A) operating at different H_2 partial pressures (1 atm, 2 atm, 3.62 atm). Point highlighted by the diamond (white fill, black outline) denotes the base case CO_2 electrolysis operation using current technology.

Base-case electrolysis operation ($j = 140$ mA/cm^2, $\eta = 32.5\%$) results in a significantly higher GWP than the H_2-mediated system (Fig. 2.8). A current density of >~250 mA/cm^2 and η >~40% is necessary to outcompete the H_2-mediated system operating at an H_2 partial pressure of 1 atm, while a current density in excess of ~750 mA/cm^2 with η >75% is necessary to reach parity with

an H_2-mediated system operating at 3.62 atm of H_2 (Fig. 2.8). Despite significant progress towards improving CO_2 electrolysis performance in the past decade,[129] these metrics represent extremely challenging targets that may be infeasible. Hence, H_2-mediated EMP systems based on Knallgas bacteria appear to be better-suited for industrial adoption.

LCA as an ecodesign tool: effect of electric grid and reactor lifetime

The approach taken here of integrating a physics-based bioreactor model with a life cycle impact model can also provide a decision-making tool in designing electromicrobial processes at scale. Alone, the bioreactor model may provide reasonable estimates for productivities, titers, and energy efficiencies that can be achieved in scaled-up electromicrobial production processes, thereby providing a valuable tool in the design of such processes. However, these values alone provide little insight into real-world implications of these systems, particularly in terms of their environmental sustainability. Integrating a bioreactor model with a life cycle assessment framework provides the ability to contextualize the tradeoffs that may occur between efficiency and productivity and provide a single metric (*i.e.*, global warming potential) by which to evaluate the sustainability of a particular EMP design. I highlight this utility by returning to the example of comparing a formatotrophic EMP system (high productivity, low efficiency) with that of a Knallgas-based system operating under inherently safer conditions and atmospheric pressure (low productivity, high efficiency).

All other impact model parameters held constant, the impact model can be reduced to:

$$\mathrm{GWP}_{n,i,j} = \alpha_1 + \frac{\alpha_2}{\eta_{\mathrm{E},n,i,j}} + \frac{\alpha_3}{\dot{m}_{n,i,j}} \tag{2-88}$$

The parameters α_1, α_2, and α_3 are obtained from the life cycle impact model and are dependent on myriad subordinate parameters. These parameters provide a weighting system for comparing the independent effects of energy efficiency and productivity. However, it is important to note that these parameters are not universally set parameters but depend on several specifics of the process design.

For example, α_2 is strongly dependent on the global warming potential of the electric grid from which energy is supplied (which in turn is dependent on the composition of that grid), while α_3 is mostly dependent on the specification of the reactor and plant infrastructure required for the EMP process, and therefore varies with parameters such as the reactor lifetime. Therefore, there is no universal answer for how to weigh the tradeoffs between efficiency and productivity, and therefore no universal solution for comparing the formatotrophic and the (inherently safer) Knallgas EMP systems. This framework, however, provides a tool that considers the parameter landscape of these systems and shows under what conditions efficiency or productivity become dominant factors in minimizing the global warming potential of a system.

Figure 2.9 demonstrates the effect of reactor lifetime and electricity global warming potential (which is in turn dependent on the electricity source) on relative greenhouse gas savings of either the Knallgas system or formatotrophic system. In the base-case scenario, assuming a grid GWP of 9 g/kWh (the GWP associated with wind power) and a reactor lifetime of 8 years, the Knallgas system is preferred (yellow region in Fig. 2.9). This benefit is driven by the higher energy efficiency of this system. However, if the reactor lifetime is reduced, the weighting factor associated with the productivity of the system increases, as the reactor size per functional unit of

product increases. Therefore, if the reactor lifetime becomes sufficiently short, the productivity of the system will become a more important factor in determining the GWP of the system, which will then favor the formatotrophic system (blue-shaded region in Fig. 2.9). Likewise, if the electricity global warming potential is decreased further, the formate-mediated system will be favored as the energy savings of the Knallgas system will become less important. In addition to demonstrating under which conditions either a H_2- or formate-mediated system is superior in terms of minimizing greenhouse gas emissions, Figure 2.9 demonstrates the novel utility of an integrated bioreactor/life cycle model in the eco-design of electromicrobial production systems.

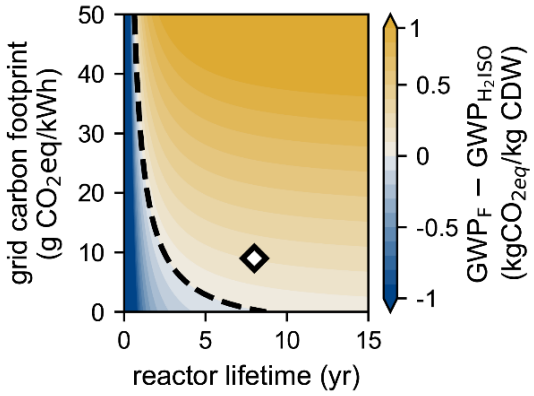

Figure 2.9. Life cycle impact-based break-even analysis. Difference in global warming potential of biomass production between formate-mediated and intrinsically safer H_2-mediated EMP systems as a function of bioreactor lifetime and the electric grid carbon footprint. Base case conditions are highlighted by the diamond (white fill, black outline), and the break-even condition (*i.e.,* no difference between the two systems) is denoted by the black dashed line. Scenarios in which the H_2-mediated system has a lower GWP are shown in yellow and scenarios in which the formate-mediated system has a lower GWP are shown in blue.

Parameter sensitivity analysis

To investigate the impact of uncertainty on the model and conclusions, the 96 individual parameters in the model were subjected to a sensitivity analysis. I identified the most important parameters for biomass production, defined as those for which a 30% change in the parameter value induced a significant change in the results of the analysis as defined in the Methods (Fig. 2.10). Of these, three (global warming potential of glucose, biomass yield on glucose, and global warming potential of wind-produced renewable energy) are outside the scope of reactor models and therefore do not affect the productivities or efficiencies of any of the electromicrobial production systems. These parameters do, however, impact the comparative life cycle assessment of these systems. Of these three parameters, the life cycle global warming potential of glucose production has the greatest potential to affect the assessment indicating the advantages of EMP systems over traditional systems. There is lack of consensus in the literature and databases on this value, which range between 0.75-1.2 kg CO_2-eq./kg glucose, due to variations in corn growth methods, locations, and processing, as well as allocation methods.[130,131] Therefore, the range shown in Figure 2.10a does reasonably depict the uncertainty of this analysis. If EMP systems are to replace traditional bioprocess methods, attention must be paid to the specifics of the heterotrophic feedstock production to ensure an accurate comparison. However, I note that even in the "worst-case" scenario, all three systems do outperform a traditional bioprocess.

The yield of biomass on glucose in the heterotrophic system can also significantly affect the analysis. Although literature yields on glucose do vary slightly,[132,133] a 30% deviation in this value is unlikely, reducing the uncertainty related to this parameter. The global warming production of electricity production (wind power in the base case) does impact the overall life cycle assessment, particularly in the formatotrophic system where the electricity demand is highest. However, due

to the low carbon footprint of wind energy, even a 30% increase of this value would not significantly affect the viability of EMP systems in comparison to heterotrophic systems.

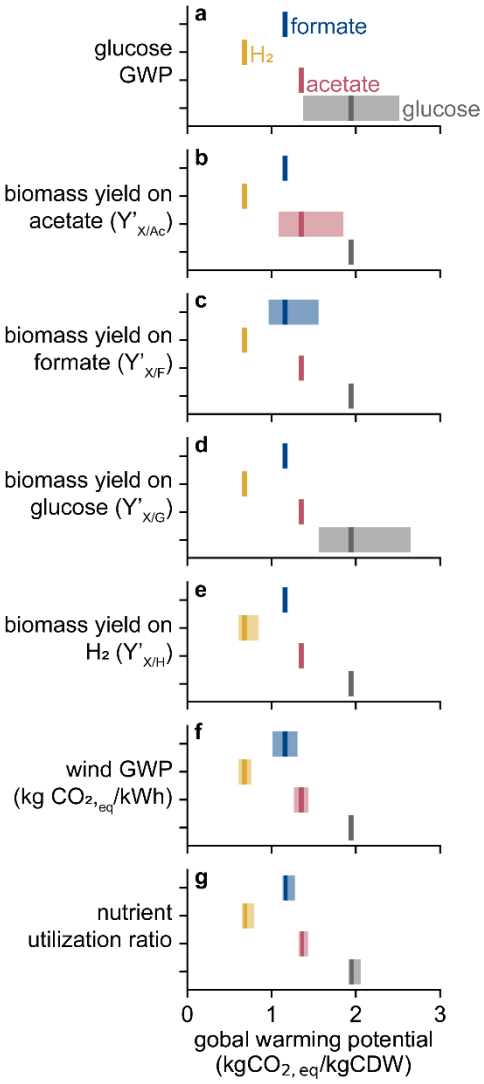

Figure 2.10. Parameter sensitivity analysis. Global warming potential dependence of producing biomass on +/-30% variation in (**a**) glucose production global warming potential, (**b**) biomass yield on acetate, (**c**) biomass yield on formate, (**d**) biomass yield on glucose, (**e**) biomass yield on H_2, (**f**) wind-based energy production global warming potential, and (**g**) the nutrient utilization ratio for each process. Dark bars represent base case values, shaded bars represent range in global warming potential induced by variation.

Biomass yields on acetate, formate, and H_2 can all significantly impact the global warming potential of the relevant processes; however, the Knallgas bacteria system still outperforms the others even if the biomass yield on H_2 is 30% lower than expected while the biomass yields on formate and acetate are 30% higher (Fig. 2.10). Notably, microbial growth rates do not significantly impact global warming potential mainly because gas/liquid mass transfer rates impose an upper bound on productivity (see discussion around Fig. 2.3). Because the electricity demand associated with achieving high k_La values is small compared to energy substrate generation via electrolysis (Table A.2, Appendix A), productivity improvements via increased agitation or other strategies to enhance gas/liquid mass transfer rates are a straightforward strategy to reduce the carbon footprint of a given process. The final significantly impactful parameter is the nutrient utilization ratio, indicating that efforts to recycle unconsumed nutrients (especially ammonia) are also important for the viability of EMP (and traditional) bioprocesses.

The sensitivity analysis demonstrates that neither 30% variability in any single parameter nor any pair of parameters is sufficient to dislodge Knallgas bacteria-based EMP systems as the process with the lowest global warming potential, although variation in some single parameters can result in re-ordering EMP processes: for example, a 30% higher yield on acetate enables the acetate-mediated system to outperform the formate-mediated system. However, all EMP processes outcompete glucose-based bioprocessing given a 30% uncertainty in any single parameter, and concomitant variation in multiple parameters in particular directions is required for glucose-based systems to achieve parity with any of the EMP processes. This analysis indicates that the conclusions are robust to significant uncertainties in parameters used in the reactor, process, and life cycle impact models.

Analysis limitations

This study employed a three-part framework, relying on physics-based bioreactor models, process models, and life cycle assessment, to analyze three proposed electromicrobial production systems. This framework predicted achievable productivity, energy use, life cycle global warming potential, and land use of each of the three EMP systems. General trends regarding system performance, as well as specific engineering targets, were determined in this analysis. However, several limitations and opportunities for future work regarding the analysis of EMP systems remain. First, the three EMP systems considered here do not represent an exhaustive list of proposed or possible EMP systems. Although these three systems are prominent in the literature, several other systems that meet the criteria for electromicrobial production described in the introduction are possible. For example, methanotrophs have also been proposed for the production of bioproducts including PHB.[134,135] Methane and methanol, both potential feedstocks for methanotrophic bacteria, can be produced from CO_2 through a variety of means using renewable electricity.[136–138] Furthermore, in an attempt to obviate the need for an electrochemically-derived mediator molecule, electroautotrophic systems have been proposed in which carbon fixation is driven by direct electron transfer via reversible electron conduit proteins such as those found in *Shewanella oneidensis*.[76,139] The approach taken here could be applied to those systems to evaluate EMP systems more broadly.

Second, the current analysis predicted four key metrics regarding the potential performance of EMP systems (productivity, energy use, life cycle GWP, and land use). These metrics each give valuable insight to the capacities and environmental impacts of EMP processes. However, this is not an exhaustive list of possible social and environmental impacts of such processes. For example, eutrophication effects of unused ammonia in EMP processes, as well as the ecotoxicity of by-products (such as chlorine gas and sodium hypochlorite from the chlor-alkili process) are important environmental considerations. However, such impacts do not affect the energy demand, carbon footprint, or land use of EMP processes and are therefore outside the stated scope of this current life cycle assessment. Targeted analysis of more niche environmental impacts of EMP such as these should be performed prior to large-scale industrial adoption.

2.5 Conclusions

I have developed a tripartite framework for analyzing EMP systems that relies on physics-based bioreactor modelling, process design and modelling, and life cycle assessment. While life cycle assessments are typically done using industrial data of a given process, this three-part framework

allows proactive assessments of the potential environmental impacts of EMP despite its relative immaturity compared to existing industrial biotechnology. Specifically, this methodology predicts vital metrics such as bioreactor productivity, electricity consumption, global warming potential, and land occupation footprint of hypothetical scaled-up EMP technologies based on limited bench-scale empirical data. This analysis not only demonstrates the promise of EMP for industrial application, but also identifies important hurdles that must be addressed for successful and environmentally sustainable implementation.

In brief, bioreactor models predict productivities up to ~0.7 g/L/h with current technology, which are reasonably close to common targets for industrial commodity chemical bioproduction (~1 g/L/h).[140,141] In general, gas-liquid mass transfer is shown to be one of the limiting factors for each system's productivity, indicating that reactor designs that enable high pressure operation and/or high gas-liquid interfacial contact areas can enhance the performance of EMP systems. In some cases, the salinity tolerance of microbes limited the productivity, signaling that efforts to improve halotolerance of industrial strains or employing native halophiles for industrial applications could play an important role in the development of EMP processes. The use of adaptive laboratory evolution to improve the halotolerance of the Knallgas bacterium *Cupriavidus necator* will be described in Chapter 4.

Life cycle impact assessment of biomass production shows that each of the three analyzed EMP (formate-mediated, H_2-mediated, and acetate-mediated) systems can potentially reduce greenhouse gas emissions compared to traditional heterotroph-based processes provided the electric grid is composed of at least ~90% renewable energy sources. The carbon footprint of each EMP process is very sensitive to the composition of the electricity grid, indicating that substantial progress towards decarbonizing the grid must occur before EMP becomes environmentally advantageous. Based on the LCA, assuming current technology, the hydrogen-mediated system has the lowest global warming potential. For the acetate-mediated process to have a carbon footprint comparable to the hydrogen-mediated process, either the need for pH control must be obviated by engineering pH-tolerant strains or operating the anaerobic and aerobic processes in the same reactor (*i.e.*, under microaerobic conditions), or the pH control elements (HCl and NaOH) must be obtained through a more sustainable process than currently exists industrially. This aspect is also an important factor in the economic viability of this EMP strategy, as will be shown in Chapter 3. For the formate-mediated process to have a global warming potential as low as the hydrogen-mediated system, improvements must be made to the energy efficiency and/or current density of formate electrolysis (see Fig. 2.8). Because formate-mediated EMP does have several advantages over hydrogen-mediated (*e.g.*, reduced safety concerns, less challenging transportation and storage), research in the field of electrochemistry to improve the performance of CO_2 reduction to formate has the potential to greatly improve EMP systems. However, in current modelling and analysis, hydrogen-mediated EMP has the lowest global warming potential and is currently most suitable for industrial application.

Sensitivity analysis revealed that the most important biochemical engineering parameter for the global warming potential of the hydrogen-mediated system is the yield of product on hydrogen. Utilization of carbon fixation pathways other than the Calvin cycle with higher thermodynamic efficiency could improve this yield and therefore improve the environmental (and economic) viability of EMP. Efforts to improve the yield through more efficient carbon fixation pathways, as has been done with the reductive glycine pathway in *C. necator*,[142] represent a promising research direction for the field. Likewise, the carbon efficiency (which affects the overall hydrogen-to-

product yield) for commodity chemical products such as lactic acid strongly influences the global warming potential of the process. Therefore, metabolic engineering efforts should prioritize engineering strains capable of maximizing carbon flux towards the product of interest while minimizing the production of unnecessary byproducts. As individual components of EMP systems continue to improve, this framework will be able to contextualize these changes in terms of productivity, energy demand, global warming potential, and land use. This methodology is therefore a useful tool for iteratively evaluating the status of this technology and identifying obstacles to its implementation.

Electromicrobial production has the potential to "electrify" the bioprocessing industry. However, this analysis indicates that, due to the abundance of fossil energy sources in the current electric grid, EMP would lead to higher greenhouse gas emissions compared to traditional bioprocesses if implemented in the United States today. Nonetheless, as the grid is decarbonized in the coming decades, EMP will become an attractive alternative method of bioproduction. Pilot-scale EMP of various value-added products should be thus developed in the near term such that further scaling and distribution can be accomplished in the coming decades as the electricity grid becomes fully decarbonized.

2.6 Acknowledgements

I would like to thank my co-authors on the article that this chapter is adapted from, Anthony J. Abel and Douglas S. Clark. I also thank Dr. Jacob Hilzinger (UC Berkeley) for feedback on the analysis. This work was supported by the Center for the Utilization of Biological Engineering in Space (CUBES, https://cubes.space/), a NASA Space Technology Research Institute (grant number NNX17AJ31G).

Chapter 3: Techno-Economic Assessment of Integrated Direct Air Capture – Electromicrobial Production Process for the Conversion of CO_2 to n-Butanol

3.1 Abstract

Several electromicrobial production (EMP) processes have been proposed and proof-of-concept studies in the literature have garnered significant interest in the prospect of using electrochemically generated substrates as energy sources to drive the biochemical conversion of CO_2 to value-added products. Combining these processes with direct air capture (DAC) has the potential to enable a truly circular carbon economy. While this is an exciting prospect, whether these systems are practical at the necessary scale to enable commodity production remains an open question. In the previous chapter, I used life cycle analysis to examine the claims of environmental benefits that proponents of EMP systems often claim and identified the set of necessary conditions for these systems to have a sufficiently low global warming potential and land occupation footprint. However, if these systems are going to be employed, economic feasibility must also be demonstrated. In this chapter, I take an approach analogous to that in Chapter 2 to perform a techno-economic assessment of an EMP process. Unlike the comparative analysis in Chapter 2, in this chapter I focus on a single EMP process for a single product. Focusing on a single product allows the analysis to be tailored, considering factors that may be unique to a given product (*e.g.*, separations processes and purity requirements) and enables direct comparison to established price targets. The process analyzed here is a hypothetical system that combines solid adsorbent-based direct air capture with an acetate-mediated EMP (as described in the previous chapter) to produce n-butanol, a potential replacement for fossil fuels. First principles-based modeling is used to predict the performance of the direct air capture and bioprocess components. From these results, a process model is developed using mass and energy balances, and finally a techno-economic assessment is performed to determine the minimum fuel selling price for a given set of assumptions. Beyond assessing a specific set of conditions, this analytical framework provides a tool to evaluate multiple different scenarios, which can reveal potential pathways toward the economic viability of this process. While this assessment describes a specific EMP process and product of interest, the approach taken here, combining reactor modeling, process modeling, and techno-economic analysis, can be employed for a variety of the EMP systems for a wide range of products.

3.2 Introduction

The reliance of fossil carbon feedstocks to produce fuels, plastics, and commodity chemicals is a major factor contributing to anthropogenic climate change as a large amount of carbon is emitted during their production, use, or end-of-life.[143] To that end, researchers have sought alternative feedstocks for the production of these critical commodities. Carbon capture and utilization (CCU) seeks to replace fossil carbon feedstocks used in industrial production with carbon dioxide.[144] This CO_2 can be obtained from industrial point sources or directly captured from ambient air. While using carbon dioxide obtained from industrial sources such as flue gases requires less energy compared to direct air capture (DAC), this carbon still ultimately comes from fossil sources; DAC, on the other hand, uses carbon that already exists in the atmosphere. CCU systems that use DAC

therefore have the potential to enable a truly circular carbon economy. Many products of CCU processes, such as biofuels and biodegradable plastics, result in all fixed carbon returning to the atmosphere at the end of the product's life cycle. Therefore, in most circumstances, carbon capture and utilization processes are at best carbon neutral, rather than carbon negative, as is the goal of direct air capture with carbon sequestration.

A multitude of methods for capturing carbon dioxide have been developed, some of which have already been deployed on industrial scales while some are still studied at the laboratory scale. Amine scrubbing has been used for decades to separate CO_2 from flue gas streams.[145] Physical adsorption using sorbents such as activated carbon or zeolites can also be used for purifying CO_2 from industrial sources.[146] For direct air capture applications, physical adsorption is thermodynamically insufficient to overcome the entropic barrier associated with purifying CO_2 from atmospheric concentrations (~400 ppm and rising!) to a relatively pure stream. Chemical reactions with liquid solvents such as aqueous sodium hydroxide can be used due to the favorable thermodynamics of this reaction.[147,148] However, these thermodynamics also lead to large energy demands for CO_2 recovery, as high temperatures (~900 ºC) are required for the regeneration step. Chemisorption is also used for direct air capture, where adsorbent surfaces are functionalized (often with amines or alkali carbonates) to enable binding of CO_2, with these systems requiring lower temperatures (<120 ºC) for regeneration.[149–151]

Metal-organic frameworks (MOFs) are a promising material for solid-phase DAC. MOFs contain metal-based nodes and organic linkers to produce a coordination network that can be functionalized with amines for direct air capture.[152,153] Their high porosity, low heat capacity, and tunability are significant advantages as a class of material for carbon capture applications.[150,153] Covalent organic frameworks (COFs), which are similar porous frameworks that only contain light elements, have many of the same advantages as MOFs.[154,155] Basing the reticular structure of COFs on covalent bonding rather than metal ion coordination can potentially increase the stability of the material.

Similarly, multiple methods of carbon utilization can be used in CCU systems. Electrochemical reduction of carbon dioxide to commodity chemicals and industrial feedstocks such as carbon monoxide, methane, and ethylene have been explored.[54] More traditional thermochemical processes, such as the Sabatier reaction or Fischer-Tropsch process, can be employed by reacting carbon dioxide (or carbon monoxide) with electrolytically-produced hydrogen gas to produce value-added products. Biological carbon utilization provides an alternative to traditional chemical and electrochemical processes. Feeding captured CO_2 to photosynthetic organisms such as algae or cyanobacteria has been explored as a method of producing biofuels. Moreover, cyanobacteria have been metabolically engineered toward producing other molecules of interest, such as sucrose, alcohols, acetaminophen and other molecules.[37,156,157] Unlike chemical/electrochemical systems, biochemical systems excel at producing complex biomolecules such as nucleic acids and proteins, as well as multi-carbon compounds with difficult stereochemistry. Biological systems, however, are often slow relative to chemical processes, and the energy conversion in photosynthetic systems such as algal bioreactors is quite low.

To address the challenges associated with traditional bioprocessing, various researchers have proposed forms of electromicrobial production (EMP), in which a combination of electrochemical and biological processes convert CO_2 to value-added products using electricity as an energy source (see Chapter 1). In one well-studied case of EMP, H_2 derived from the electrolysis of water, as

well as CO_2 and O_2 are converted to value-added products by a Knallgas (aerobic hydrogen-oxidizing) bacterium such as *Cupriavidus necator*.[45,46] Alternatively, carbon dioxide may be electrochemically reduced to formic acid, which can be upgraded by a formatotrophic organism (such as native formatotroph *C. necator* or an engineered formatotrophic strain of *E. coli*)[47,48] to the desired product. A two-microbe method has also been developed in which an acetogenic microbe such as *Sporomusa ovata* converts H_2 and CO_2 to acetate, which is then upgraded to a value-added product by a heterotroph such as *E. coli*.[126] Bioplastics, biofuels, and other commodity products have been produced through these EMP systems at benchtop scales.

Integrated direct air capture with electromicrobial production (DAC-EMP) processes have the potential to convert electricity, water, and air into a seemingly endless array of products, and can shift the paradigm from extractive petrochemical processing to a more circular carbon economy. Process models and analyses have been published to assess material and energy demands for DAC-EMP (note terms may vary in the literature, see nomenclature discussion in Chapter 1), indicating a general interest in understanding how these systems could perform at an industrial scale.[79,96] In Chapter 2, I developed a three-part analytical framework that uses bioreactor modeling, process modeling, and life cycle impact assessment to predict the environmental impacts of scaled-up EMP systems relying on direct air capture as a source of CO_2. While the environmental benefits of DAC-EMP systems for commodity chemical production are promising, thorough techno-economic assessment (TEA) of integrated DAC-EMP systems is still needed to understand the economic viability of such systems at and industrial scale. While multiple techno-economic assessments for direct air capture systems have been performed previously to assess their viability,[158,159] usually in terms of cost per ton of CO_2 sequestered, techno-economic assessments of integrated systems involving direct air and downstream conversion of CO_2 have been less common. To my knowledge, no techno-economic assessments of integrated DAC-EMP systems have been published in the literature.

Here, I study the economics of a hypothetical scaled-up DAC-EMP system for the production of the alternative biofuel n-butanol. As a drop-in replacement for gasoline, the cost targets for n-butanol production are well-established. Moreover, several techno-economic analyses of n-butanol production through traditional bioprocesses have already been performed, allowing a clear basis of comparison.[4,160] I study a hypothetical DAC-EMP process that contains a DAC module based on a solid adsorbent such as a metal-organic framework (MOF), as well as a two-step bioprocess for the conversion of the captured CO_2 to n-butanol. In the first step of the process, CO_2 and H_2 (produced from the electrolysis of water) are converted to acetate by an acetogenic microbe (*e.g.*, *Sporomusa ovata*) in an anaerobic bioreactor. In the second step, acetate is biocatalytically upgraded to n-butanol using a metabolically engineered acetotrophic microbe (*e.g.*, *Escherichia coli*). Downstream separations based on liquid-liquid extraction are then used to purify the butanol.

I first describe the DAC component by developing physics-based model equations that predict the performance of the process based on adsorbent properties (adsorbent capacity, adsorption kinetics, heat capacity, *etc.*). I develop a bioprocess model for the two downstream bioreactors as well, predicting performance metrics such as productivity using biochemical engineering parameters (microbial growth rate, gas-liquid mass transfer rate, product yield, *etc.*). These bioprocess models follow a similar approach to the ones used in Chapter 2, but have been simplified, only accounting for the most prominent model components (*e.g.*, microbial growth, gas-liquid mass transfer, salinity-induced toxicity) while less impactful components (*e.g.*, carbonate equilibrium, acid-base reaction kinetics) are ignored. Process modeling, based on mass and energy balances, links these

subcomponent models to predict the material and energy flows across the entire process. These flows are then translated into capital and operating costs of the process and a techno-economic model determines the minimum selling price of n-butanol. The benefit of this combined multiscale framework is that key system parameters (*e.g.*, capacity of adsorbent, kinetics of adsorption, metabolic efficiency of product, gas-liquid mass transfer) can be varied and their effect on the overall economics of the system can be studied. As a result, the model can predict the metrics of system performance required for economic viability and therefore provide academic researchers working on these systems with key benchmarks.

3.3 Analytical Methods

System description

The process modeled here contains five major components which together effect the end-to-end conversion of air, water, and electricity into n-butanol: a MOF-based direct air capture system, an electrochemical system which uses electricity to produce hydrogen gas from water, an anaerobic bioreactor which converts the purified CO_2 and produced H_2 to acetic acid, an aerobic bioreactor that converts the acetic acid to n-butanol, and a liquid-liquid extraction process that separates the n-butanol from the fermentation broth.

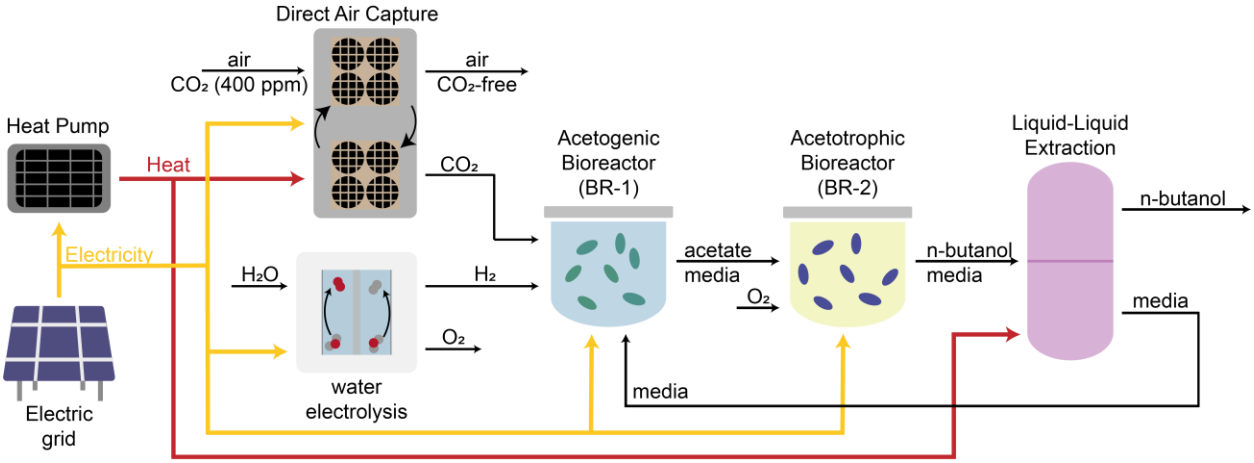

Figure 3.1. Schematic overview of DAC-EMP process. Diagram shows the five major components for conversion of CO_2 in ambient air, water, and electricity to n-butanol, as well as major material (black) and energy (electricity in yellow, heat in red) flows.

The direct air capture module is based on a temperature-vacuum swing adsorption process using a MOF as a solid sorbent. Industrial blowers are used to pass ambient air through a contactor containing the amine-functionalized MOF sorbent onto which CO_2 is selectively chemisorbed. I assume here that a catalytic monolith is used as the sorbent support structure, following the precedent of Sinha *et al.*[159] Following the adsorption phase, CO_2 is desorbed from the MOF, first by evacuating air from the contactor using a vacuum pump, and then using steam produced by a heat pump to bring the sorbent to the desorption temperature, liberating the captured CO_2 where it may then be utilized in downstream processes. The major equipment required for this process consists of the blower, the monolithic support structure, the vacuum pump, and the heat pump.

The major materials and utilities required for the DAC component are the MOF-based sorbent itself, and electricity for the heat pump, vacuum pump, and blower.

The biochemical components of the process rely on the two-step acetate-mediated EMP system described in Chapter 2. The first bioreactor is assumed to operate under anaerobic conditions, with continuous flow of liquid media and gaseous substrates, and contain the acetogen *S. ovata*. The second bioreactor operates under aerobic conditions, with continuous aeration and continuous liquid flow, and contains a genetically engineered strain of *E. coli*. Bubble-column bioreactors used for the bioconversion represent the major equipment demand for the bioprocessing step. An electrolyzer is used to produce the hydrogen for the process on-site. Finally, the butanol is extracted from the media into mesitylene. Following the liquid-liquid extraction, the butanol is then distilled to separate it to a desired purity.

Baseline assumptions and scope of analysis

I assume the process will run 24 hours a day with an uptime of 330 days per year. Furthermore, I assume the project begins in 2022, all equipment is purchased in 2022, and the material/labor costs are based on 2022 prices for the duration of the project (*i.e.*, that future inflation is ignored for the purposes of this TEA). The process is assumed to produce 40 million gallons of butanol per year, comparable in scale to previously reported techno-economic assessments for lignocellulosic ethanol plants.[18]

Direct air capture module model equations

Note the nomenclature used in this chapter may differ from that used in the previous. Due to the extensive models developed in each chapter, maintaining a consistent nomenclature would quickly deplete my available pool of Latin and Greek letters.

Both the adsorption and desorption cycles of the DAC process are explicitly modeled. I assume that adsorption occurs as ambient air flows through a cylindrical contactor containing a packed bed of the MOF-based adsorbent. The adsorption model equations are described here first.

The concentration of adsorbed carbon dioxide, Q, in units of moles of CO_2 per kg of sorbent, as a function of time and length along the DAC contactor, can be described by the following equation:

$$\frac{\partial Q(z,t)}{\partial t} = k(Q^{\mathrm{eq}}(z, T_{\mathrm{ads}}, p_{\mathrm{CO2}}) - Q(z,t)) \tag{3-1}$$

where *k* is the rate constant of the chemisorption reaction in the forward direction and Q^{eq} is the equilibrium concentration of adsorbed CO_2 at a given partial pressure and temperature, which is modeled here as a step isotherm where Langmuir behavior is exhibited before and after the step (See Supplementary Note B.1, Appendix B for validation of the model isotherm against literature data):

$$Q^{\mathrm{eq}} = \begin{cases} \dfrac{Q^{\mathrm{sat1}} K_{\mathrm{eq1}} (\frac{p_{\mathrm{CO2}}}{p^\circ})}{1 + K_{\mathrm{eq1}} (\frac{p_{\mathrm{CO2}}}{p^\circ})} & p_{\mathrm{CO2}} < p_{\mathrm{step}} \\ \dfrac{Q^{\mathrm{sat1}} K_{\mathrm{eq1}} (\frac{p_{\mathrm{step}}}{p^\circ})}{1 + K_{\mathrm{eq1}} (\frac{p_{\mathrm{step}}}{p^\circ})} + \dfrac{Q^{\mathrm{sat2}} K_{\mathrm{eq2}} (\frac{p_{\mathrm{CO2}} - p_{\mathrm{step}}}{p^\circ})}{1 + K_{\mathrm{eq2}} (\frac{p_{\mathrm{CO2}} - p_{\mathrm{step}}}{p^\circ})} & p_{\mathrm{CO2}} \geq p_{\mathrm{step}} \end{cases} \tag{3-2}$$

where Q^{sat1} and Q^{sat2} represent the maximum adsorbed CO_2 concentration (moles CO_2 per kg sorbent) associated with each regime, p_{CO2} is the partial pressure of unadsorbed CO_2 in the contactor, p° is standard pressure (1 bar), p_{step} is the partial pressure of CO_2 at which the step occurs, and K_{eq1} and K_{eq2} are the equilibrium constants of the reversible chemisorption reaction associated with each adsorption regime. K_{eq1}, K_{eq2} and p_{step} are themselves functions of the adsorbent temperature T_{ads} and can be described by a Clausius-Clapeyron relationship as:

$$\begin{aligned} K_{\mathrm{eq1}} &= K_{\mathrm{eq1}}(T_{\mathrm{ref}}) \exp\left[\frac{-\Delta H_{ads}}{R}\left(\frac{1}{T_{\mathrm{ads}}} - \frac{1}{T_{\mathrm{ref}}}\right)\right] \\ K_{\mathrm{eq2}} &= K_{\mathrm{eq2}}(T_{\mathrm{ref}}) \exp\left[\frac{-\Delta H_{ads}}{R}\left(\frac{1}{T_{\mathrm{ads}}} - \frac{1}{T_{\mathrm{ref}}}\right)\right] \\ p_{\mathrm{step}} &= p_{\mathrm{step}}(T_{\mathrm{ref}}) \exp\left[\frac{\Delta H_{ads}}{R}\left(\frac{1}{T_{\mathrm{ads}}} - \frac{1}{T_{\mathrm{ref}}}\right)\right] \end{aligned} \tag{3-3}$$

where ΔH_{ads} is the enthalpy of adsorption and T_{ref} is some reference temperature for which the isotherm parameters are known.

The change in the concentration of unadsorbed carbon dioxide within the contactor space (represented as a partial pressure of CO_2), which can vary in the axial dimension z along the length of the contactor (but is assumed to be constant in the radial dimension), can be written as:

$$\varepsilon \frac{\partial p_{\mathrm{CO2}}}{\partial t} = \frac{L}{\tau} \frac{\partial p_{\mathrm{CO2}}}{\partial z} - kRT_{\mathrm{air}} \rho_{\mathrm{ads}} (1 - \varepsilon)(Q^{\mathrm{eq}} - Q) \tag{3-4}$$

where τ is the space time of the air inside the contactor of length L, R is the gas constant, T_{air} is the temperature of the air inside the contactor, ρ_{ads} is the void-free density of the adsorbent, and ε is the void fraction of the contactor.

During the adsorption phase, the temperature of the adsorbent can change in response to two factors: heat transfer to/from the air blowing into the contactor, and heat generated by the chemisorption process. I assume no spatial temperature gradients form in the contactor. Energy balances yield the following equation for the change in temperature of the adsorbent:

$$c_{\mathrm{p,T}} \frac{dT_{\mathrm{ads}}}{dt} = \frac{2h_{\mathrm{A}}}{r\rho_{\mathrm{ads}}} \frac{T_{\mathrm{air}} - T_{\mathrm{ads}}}{1 - \varepsilon} - \Delta H_{\mathrm{ads}} \frac{1}{L} \int_{z=0}^{z=L} \frac{\partial Q(z,t)}{\partial t} dz \tag{3-5}$$

where h_{A} is the overall heat transfer coefficient between air and the adsorbent/monolithic support and r is the radius of the cylindrical contactor space. I also define a total heat capacity $c_{\mathrm{p,T}}$ as the energy required to raise 1 kg of the sorbent 1 ºC, given that the monolithic structure and adsorbed CO_2 must also be raised by 1 ºC, and is therefore calculated as:

$$c_{\mathrm{p,T}} = c_{\mathrm{p,ads}} + c_{\mathrm{p,mon}} \frac{m_{\mathrm{mon}}}{m_{\mathrm{ads}}} + \hat{c}_{\mathrm{p,CO2}} Q \tag{3-6}$$

where $c_{\mathrm{p,ads}}$, $c_{\mathrm{p,mon}}$, $\hat{c}_{\mathrm{p,CO2}}$ are specific heat capacities of the adsorbent, monolithic support, and CO_2, respectively (note: $\hat{c}_{\mathrm{p,CO2}}$ is on a molar basis), and $\frac{m_{\mathrm{mon}}}{m_{\mathrm{ads}}}$ describes the ratio of the mass of the monolithic support and the mass of the adsorbent.

Similarly, energy balances on the air inside the contactor can be written, again assuming no spatial temperature gradients for air in the contactor emerge, yielding the expression:

$$\frac{dT_{\mathrm{air}}}{dt} = -\frac{2h_A}{r\rho_{\mathrm{air}}} \frac{T_{\mathrm{air}} - T_{\mathrm{ads}}}{c_{\mathrm{p,air}}\varepsilon} + \frac{T_0 - T_{\mathrm{air}}}{\tau\varepsilon} \tag{3-7}$$

where ρ_{air} is the density of air (calculated by the ideal gas law), $c_{\mathrm{p,air}}$ is the constant-pressure heat capacity of air, and T_0 is the temperature of the incoming ambient air.

The desorption model equations can then be written. When considering the desorption process, the same equations used in the adsorption process hold, with minor modifications. First, in Eqn. 3-1 and 3-2, there are no longer spatial gradients to the concentration of CO_2, either adsorbed or in the gas phase. The change in adsorbed concentration in the reactor is therefore modeled as:

$$\frac{dQ(t)}{dt} = k(Q^{\mathrm{eq}}(T_{\mathrm{ads}}, p_{\mathrm{CO2}}) - Q(t)) \tag{3-8}$$

Moreover, in this part of the process, there is no flow of gas into the contactor. However, there is flow of the CO_2 stream out of the contactor due to the applied vacuum. The equation for describing the change of partial pressure of CO_2 inside the contactor is therefore rewritten as:

$$\varepsilon \frac{\partial p_{\mathrm{CO2}}}{\partial t} = -\frac{p_{\mathrm{CO2}}}{L} \sqrt{\frac{2\gamma}{\gamma - 1} \frac{p_{\mathrm{CO2}} - p_{\mathrm{vac}}}{\rho_{\mathrm{CO2}}}} - kRT\rho_{\mathrm{ads}}(1 - \varepsilon)(Q^{\mathrm{eq}} - Q) \tag{3-9}$$

where p_{vac} is the applied vacuum pressure, γ is the ratio of constant-pressure and constant-volume heat capacities of CO_2.

The energy balance on the adsorbent is also adjusted to remove the spatial gradient and is rewritten as:

$$c_{\mathrm{p,T}} \frac{dT_{\mathrm{ads}}}{dt} = \frac{2h_s}{r\rho_{\mathrm{ads}}} \frac{T_{\mathrm{s}} - T_{\mathrm{ads}}}{1 - \varepsilon} - \Delta H_{\mathrm{ads}} \frac{dQ}{dt} \tag{3-10}$$

where h_s is the overall heat transfer coefficient for transferring heat from steam to the contactor and T_{s} is the temperature of steam. It is assumed that the CO_2 will leave the reactor at the temperature of the heating steam.

Bioprocess model equations

The acetogenic bioreactor (labeled as bioreactor 1 or BR-1) is modeled as a chemostat, with a dilution rate of D_1. Assuming a well-mixed reactor environment of constant volume, the concentration of cells in bioreactor 1, X_1 as a function of time is written as:

$$\frac{dX_1}{dt} = (\mu_A - D_1)X_1 \tag{3-11}$$

Biomass concentration is expressed in terms of the molar concentration of carbon that is embodied in the biomass in the reactor. While this is a potentially unintuitive measure of biomass concentration, doing so maintains consistent units of all concentrations. Assuming that hydrogen and carbon dioxide are the major substrates for the acetogen, Monod kinetics are used to predict the growth rate of the bacteria in BR-1. The growth rate of the acetogen, μ_{A}, is therefore described as:

$$\mu_{\mathrm{A}} = \frac{\mu_{\mathrm{A,opt}}\sigma_1(c_{\mathrm{Na,1}})c_{\mathrm{H2,1}}c_{\mathrm{CO2,1}}}{(K_{\mathrm{s,H2}} + c_{\mathrm{H2,1}})(K_{s,\mathrm{CO2}} + c_{\mathrm{CO2,1}})} \tag{3-12}$$

where $c_{\mathrm{H2,1}}$ is the molar concentration of hydrogen dissolved in bioreactor 1, $c_{\mathrm{CO2,1}}$ is the molar concentration of CO_2 dissolved in bioreactor 1, $c_{\mathrm{Na,1}}$ is the molar concentration of sodium in bioreactor 1, $K_{\mathrm{s,H2}}$ is the Monod constant for hydrogen associated with acetogenic growth, $K_{s,\mathrm{CO2}}$ is the Monod constant for CO_2 for the acetogen, and $\mu_{\mathrm{A,opt}}$ is the maximum specific growth rate of the acetogen under optimal conditions. The model also takes into account the effect of salinity, introducing a factor σ_1 adjusts the growth rate and depends on the salinity in bioreactor 1 ($c_{\mathrm{Na,1}}$):

$$\sigma_1 = \begin{cases} 1 & c_{\mathrm{Na,1}} < c_{\mathrm{Na,min,1}} \\ 1 - \dfrac{c_{\mathrm{Na,1}}}{c_{\mathrm{Na,max,1}} - c_{\mathrm{Na,min,1}}} & c_{\mathrm{Na,min,1}} < c_{\mathrm{Na,1}} < c_{\mathrm{Na,max,1}} \\ 0 & c_{\mathrm{Na,1}} > c_{\mathrm{Na,max,1}} \end{cases} \tag{3-13}$$

As NaOH is added to the bioreactor to neutralize the acetic acid generated by the acetogen, the concentration of sodium in BR-1 is equal to the concentration of acetate. I assume acetate is a growth associated product and is produced based on the stoichiometry described in Chapter 2, Eqn. 2-34. Therefore, the concentration of acetate in BR-1 ($c_{\mathrm{Ac,1}}$) is described as:

$$\frac{dc_{\mathrm{Ac,1}}}{dt} = 9.07\mu_A X_1 - D_1 c_{\mathrm{Ac,1}} \tag{3-14}$$

Dissolved hydrogen in BR-1 ($c_{\mathrm{H2,1}}$) is transferred into the liquid phase from the gas phase and is consumed by the acetogen, again following the stoichiometry described in Equation 2-34 in Chapter 2:

$$\frac{dc_{\mathrm{H2,1}}}{dt} = k_{\mathrm{L}}a_{\mathrm{H2}}(H_{\mathrm{H2}}p_{\mathrm{H2,1}} - c_{\mathrm{H2,1}}) - 38.33\mu_{\mathrm{A}}X_1 - D_1 c_{\mathrm{H2,1}} \tag{3-15}$$

where $k_{\mathrm{L}}a_{\mathrm{H2}}$ is the volumetric mass-transfer coefficient of hydrogen into the bioreactor medium, H_{H2} is the Henry's Law constant for hydrogen in water, and $p_{\mathrm{H2,1}}$ is the partial pressure of hydrogen in the head space of BR-1. Assuming a constant volumetric flow of gas into the reactor (written as a gas phase dilution rate $D_{\mathrm{gas,1}}$, which is the volumetric flow rate of gas into the reactor divided by the headspace volume), the partial pressure of hydrogen is written as:

$$\frac{dp_{\mathrm{H2,1}}}{dt} = (p_{\mathrm{H2,1,0}} - p_{\mathrm{H2,1}})D_{\mathrm{gas,1}} - RT_1 k_{\mathrm{L}}a_{\mathrm{H2}}(H_{\mathrm{H2}}p_{\mathrm{H2,1}} - c_{\mathrm{H2,1}})\frac{V_{L,1}}{V_{G,1}} \tag{3-16}$$

where $p_{\mathrm{H2,1,0}}$ is the partial pressure of H_2 in the gaseous feed stream, and T_1 is the temperature in BR-1.

By analogy, the dissolved concentration of CO_2 in BR-1 ($c_{\mathrm{CO2,1}}$) is:

$$\frac{dc_{\mathrm{CO2,1}}}{dt} = k_{\mathrm{L}}a_{\mathrm{CO2}}\left(H_{\mathrm{CO2}}p_{\mathrm{CO2,1}} - c_{\mathrm{CO2,1}}\right) - 19.15\mu_{\mathrm{A}}X_1 - D_1c_{\mathrm{CO2,1}} \tag{3-17}$$

and the partial pressure of CO_2 in the headspace ($p_{\mathrm{CO2,1}}$) is:

$$\frac{dp_{\mathrm{CO2,1}}}{dt} = \left(p_{\mathrm{CO2,1,0}} - p_{\mathrm{CO2,1}}\right)D_{\mathrm{gas,1}} - RT_1k_{\mathrm{L}}a_{\mathrm{CO2}}\left(H_{\mathrm{CO2}}p_{\mathrm{CO2,1}} - c_{\mathrm{CO2,1}}\right)\frac{V_{L,1}}{V_{G,1}} \tag{3-18}$$

where all variables and parameters have the same meaning, except for CO_2 instead of H_2. The relationship between the parameters $k_{\mathrm{L}}a_{\mathrm{H2}}$ and $k_{\mathrm{L}}a_{\mathrm{CO2}}$ is given by Eqn. 2-66.

The second bioreactor (labeled as bioreactor 2 or BR-2), which converts acetate to n-butanol is similarly modeled as a chemostat following an analogous approach as BR-1, with minor adaptations. Unlike in BR-1, where acetate and biomass are assumed to be produced in a fixed stochiometric ratio, the selectivity of biomass production over n-butanol production is a variable in modeling the second bioreactor. The variable ϕ is introduced as the moles of carbon in the produced biomass divided by the total moles of carbon in both biomass and n-butanol. Therefore, the cell production rate is modified by this ratio, such that the concentration of biomass in BR-2 (X_2) as a function of time is described as:

$$\frac{dX_2}{dt} = (\mu_{\mathrm{Ac}}\phi - D_2)X_2 \tag{3-19}$$

where D_2 is the liquid-phase dilution rate of bioreactor 2. The growth rate of the microbe in BR-2 (μ_{Ac}), which consumes acetate and oxygen as primary substrates, is:

$$\mu_{\mathrm{Ac}} = \frac{\mu_{\mathrm{Ac,opt}}\sigma_2\left(c_{\mathrm{Na,2}}\right)c_{\mathrm{Ac,2}}c_{\mathrm{O2,2}}}{(K_{\mathrm{s,Ac}} + c_{\mathrm{Ac,2}} + \frac{{c_{\mathrm{Ac,2}}}^2}{K_{\mathrm{I}}})(K_{\mathrm{s,O2}} + c_{\mathrm{O2,2}})} \tag{3-20}$$

where $\mu_{\mathrm{Ac,opt}}$ is the maximum growth rate of the acetotroph, $c_{\mathrm{Ac,2}}$ and $c_{\mathrm{O2,2}}$ are the concentrations of acetate and oxygen respectively in bioreactor 2, $K_{\mathrm{s,Ac}}$ and $K_{\mathrm{s,O2}}$ are the Monod constants for acetate and oxygen, and K_{I} is a substrate inhibition constant for acetate.

The term $\sigma_2\left(c_{\mathrm{Na,2}}\right)$ is an analogous function of the form described in Eqn. 3-13 (though with potentially different values of $c_{\mathrm{Na,min}}$ and $c_{\mathrm{Na,max}}$). In the second bioreactor, the pH control, to offset the rise in pH when acetate is consumed, is mediated by sulfuric acid. Therefore, this pH control does not increase in concentration of sodium, which is constant in bioreactor 2.

The concentration of n-butanol in the bioreactor ($c_{\mathrm{Bu,2}}$) can then be described by the expression:

$$\frac{dc_{\mathrm{Bu,2}}}{dt} = \mu_{\mathrm{Ac}}\frac{1-\phi}{4}X_2 - D_2c_{\mathrm{Bu,2}} \tag{3-21}$$

The partial pressure of oxygen in the bioreactor headspace ($p_{\mathrm{O2,2}}$), like other gas-phase substrates described in Eqn. 3-16 and 3-18, is described as:

$$\frac{dp_{O2,2}}{dt} = \left(p_{O2,2,i} - p_{O2,2}\right)D_{gas,2} - RTk_L a_{O2}(H_{O2}p_{O2,2} - c_{O2,2})\frac{V_{L,2}}{V_{G,2}} \quad (3\text{-}22)$$

where the nomenclature of those previous equations is maintained.

The concentration of acetate in bioreactor 2, which is fed from the effluent of bioreactor 1 is:

$$\frac{dc_{Ac,2}}{dt} = D_1\left(c_{Ac,1} - c_{Ac,2}\right) - \mu_{Ac}X_2\left(\frac{\phi}{Y_{X/Ac}} + \frac{(1-\phi)}{4Y_{Bu/Ac}}\right) \quad (3\text{-}23)$$

where $Y_{X/Ac}$ and $Y_{Bu/Ac}$ are the molar yields of biomass and butanol on acetate, respectively. The concentration of oxygen in the bioreactor is described by the expression:

$$\frac{dc_{O2,2}}{dt} = k_L a_{O2}\left(H_{O2}p_{O2,2} - c_{O2,2}\right) - \mu_{Ac}X_2\left(\gamma_X\phi + \gamma_{Bu}\frac{(1-\phi)}{4}\right) - D_2 c_{O2,2} \quad (3\text{-}24)$$

where γ_X is the molar consumption of O_2 per moles of biomass produced and γ_{Bu} is the molar consumption of O_2 per moles of n-butanol produced.

Process modeling

The electricity required for the blower (E_{blower}) per mole of CO_2 captured can be calculated as:

$$E_1 = \frac{t_{ads}\Delta P}{\eta_1 \tau\, \Delta q_{cycle}\rho_{ads}(1-\varepsilon)} \quad (3\text{-}25)$$

where η_1 is the efficiency of the blower, t_{ads} is the adsorption time per cycle, and Δq_{cycle} is the amount of CO_2 captured (in moles) per mass of adsorbent each cycle. ΔP is the pressure drop across the contactor, which is a function of the air velocity and is estimated by the Ergun equation:

$$\Delta P = \frac{150\mu_{air}L^2(1-\varepsilon)^2}{{D_p}^2\varepsilon^3\tau} + \frac{1.75L^3\rho_{air}(1-\varepsilon)}{\tau^2 D_p\varepsilon^3} \quad (3\text{-}26)$$

where μ_{air} is the dynamic viscosity of air, and D_p is the equivalent diameter of the packing.

During the desorption cycle, the air inside the contactor is first displaced by nitrogen gas to remove oxygen from the product stream. The contactor is maintained at a pressure of P_{vac} by a vacuum pump, which then pressurizes the captured CO_2 to P_2. This is modeled as an adiabatic compression from P_{vac} to P_2, adjusted by a pump efficiency (η_2), and the energy required per mole of CO_2 captured is:

$$E_2 = \frac{1}{\eta_2 y_{CO2}}\frac{RT_0}{\gamma - 1}\left[\left(\frac{P_2}{P_{vac}}\right)^{(\gamma-1)/\gamma} - 1\right] \quad (3\text{-}27)$$

where γ is the ratio of constant-pressure and constant-volume heat capacities of CO_2. The purity of this CO_2 stream, y_{CO2}, is determined by the relative amounts of CO_2 captured and N_2 in the void space:

$$y_{CO2} = \frac{\Delta q_{cycle}\rho_{ads}(1-\varepsilon)RT_0}{\Delta q_{cycle}\rho_{ads}(1-\varepsilon)RT_0 + \varepsilon P_{vac}} \quad (3\text{-}28)$$

Assuming the energy required for the desorption step is provided by steam generated by a heat pump with a defined coefficient of performance (COP), the electricity required for the temperature swing, per mole of CO_2 captured, is calculated as:

$$E_3 = \frac{1}{\eta_3 \mathrm{COP}}\left(\frac{c_{\mathrm{p,T}}(T_s - T_0)}{\Delta q_{\mathrm{cycle}}} - \Delta H_{\mathrm{ads}}\right) \tag{3-29}$$

where η_3 is an efficiency to account for heat loss to the surroundings.

The electricity required for electrolysis per mole of H_2 is simply calculated as:

$$E_4 = \frac{\Delta H_{\mathrm{comb,H2}}}{\eta_4} \tag{3-30}$$

where $\Delta H_{\mathrm{comb,H2}}$ is the enthalpy of combustion of hydrogen and η_4 is the efficiency of the electrolyzer.

The power required to maintain temperature in both bioreactors is calculated according to Eqn. 2-77, while the power required to maintain a volumetric mass transfer coefficient is calculated according to Eqn. 2-64.

Mass and energy balances, combined with the results of the DAC, BR-1, BR-2, and separations models, are used to determine the material and energy demands for a desired production rate of n-butanol.

Separations modeling

The first step of the separations process is a liquid-liquid extraction step to extract n-butanol from the aqueous fermentation broth in BR-2 into mesitylene. A preliminary distillation column is then used to remove any water that was transferred into the mesitylene-rich fraction during extraction, while a second column distills the n-butanol. CHEMCAD STEADY-STATE (https://www.chemstations.com/) is used to simulate these downstream processes. The UNIFAC LLE model was used to predict thermodynamic parameters, with all other thermodynamics left at the CHEMCAD default values. To simplify the simulation, water, mesitylene, and n-butanol are the only components considered. The flow rate of mesitylene into the extractor relative to the flow of the fermentation medium is set such that 99% of the generated n-butanol is extracted. The first distillation column is defined to remove water such that the remaining weight fraction is 0.5% of that of butanol, and the number of stages and energy requirements are calculated using CHEMCAD. The second distillation column is defined to separate the maximum amount of n-butanol while the mesitylene weight fraction in the product stream remains less than 0.5%. Therefore, the purity of n-butanol in the product stream is >99%. The mesitylene from the bottom fraction of the second distillation column is then recycled for further extraction of butanol. Heat exchangers transfer heat from this hot mesitylene stream to the mesitylene-rich fraction leading to the distillation columns, recycling some of the heat used in the separations process. A minimum temperature difference between hot and cold streams in the heat exchanger of 10 ºC is assumed. The flow rate of mesitylene, consumption of mesitylene, product recovery fraction, energy demands of the distillation columns, and sizes of distillation columns calculated here are then used in the broader process model and techno-economic analysis.

Techno-economic modeling

The capital costs and operating costs for the DAC-EMP process are calculated. The capital cost is calculated based on the cost of installed equipment, with established heuristics used to calculate other factors affecting the capital investment required.

Equipment sizes and number of each equipment required are determined through the process model described in the preceding section. The costs of equipment obtained through established correlations and literature searches may be from years other than 2022. Therefore, C_i, the cost of equipment piece i, is adjusted as necessary from the quoted cost of equipment piece i from year y, by factoring in the cost index (CI) from year y compared to the year 2022:

$$C_i = C_{i,y} \frac{\mathrm{CI}(2022)}{\mathrm{CI(y)}} \tag{3-31}$$

CEPCI is used to determine the cost index. Correlations used to determine the cost of the major pieces of equipment used in this process are described in Table B.2, Appendix B. The installed equipment cost (IEC) then is simply the sum of installed costs for each piece of equipment, or:

$$\mathrm{IEC} = \sum n_i F_i C_i \tag{3-32}$$

where n_i is the number of units required, F_i is the installation factor, and C_i is the unit cost of equipment piece i.

Table 3.1 describes the calculation of capital cost for the DAC-EMP Plant, which is based on similar calculations used in NREL reports describing a plant for lignocellulosic bioethanol production.[18,140]

Table 3.1: Capital cost contributions and their method of calculation

Capital Cost Contributions	**Cost Calculation**
Installed Equipment Cost (IEC)	Equation 3-32
Warehouse Costs	0.04×IEC
Site Development	0.09×IEC
Additional Piping	0.045×IEC
Total Direct Costs (TDC)	Sum of above
Prorateable Costs	0.1×TDC
Field Expenses	0.1×TDC
Home Office and Construction	0.2×TDC
Project Contingency	0.1×TDC
Other Indirect Costs	0.1×TDC
Total Indirect Costs (TIC)	Sum of above
Fixed Capital Investment (FCI)	TDC+TIC
Working Capital (WC)	0.05×FCI
Total Capital Investment (TCI)	FCI+WC

The variable operating costs (VOC) can be calculated from the material and energy flows determined by the process model:

$$\mathrm{VOC} = \sum \dot{m}_j c_j t_{\mathrm{op}} \tag{3-33}$$

where $\dot{m}_j$ refers to the demand of material (or energy) j per unit time, c_j is the unit cost of material (or energy) j, and t_{op} is the time of operation. For the annual variable operating cost, t_{op} is 7920 h (330-day uptime, 24 hours per day). Unit costs of materials used in this process are given in Table B.3, Appendix B. The method of calculating other operating cost contributions is detailed in Table 3.2.

Table 3.2: Operating cost contributions and their method of calculation

Operating Cost Contributions	Cost Calculation
Variable Operating Costs (VOC)	Equation 3-33
Labor Costs (LC)	Sum of annual employee salaries [a]
Labor Burden	0.9×LC
Maintenance Costs	0.03×IEC
Property Insurance	0.007×FCI
Fixed Operating Costs (FOC)	Sum of above
Total Operating Costs (TOC)	VOC+FOC

[a] See Supplementary Note B.2.

Minimum fuel selling price calculations

Table 3.3: Discounted cash flow rate of return analysis parameters

Parameter	Value
Plant Life	30 Years
Discount Rate	10%[161]
Federal Income Tax Rate	21%
Plant Depreciation	200% Declining Balance[162]
Plant Recovery Period	5 Years[162]
Equity Financing	100%
Construction Period	24 months

A Discounted Cash Flow Rate of Return (DCFROR) Analysis is performed to determine the minimum selling price for n-butanol produced in the hypothetical plant described here. A 10% discount rate is assumed, based on the recommendation by the U.S. Department of Energy for renewable energy technologies.[161] The IRS Modified Accelerated Cost Recovery System (MACRS) is used to determine plant depreciation, based on the Asset Class 28.0 "Manufacture of Chemical and Allied Products", which uses a GDS recovery period of 5 years.[162] A construction period of 24 months, with capital expended evenly over the period, followed by a 30-year plant

lifetime, with 100% production capacity beginning immediately following construction, is assumed. A tax rate of 21%, consistent with the federal corporate tax rate in the United States, is assumed. For simplicity, I assume that this project is 100% equity financed. Parameters used in the DCFROR analysis are summarized in Table 3.3.

3.4 Results and Discussion

DAC module performance

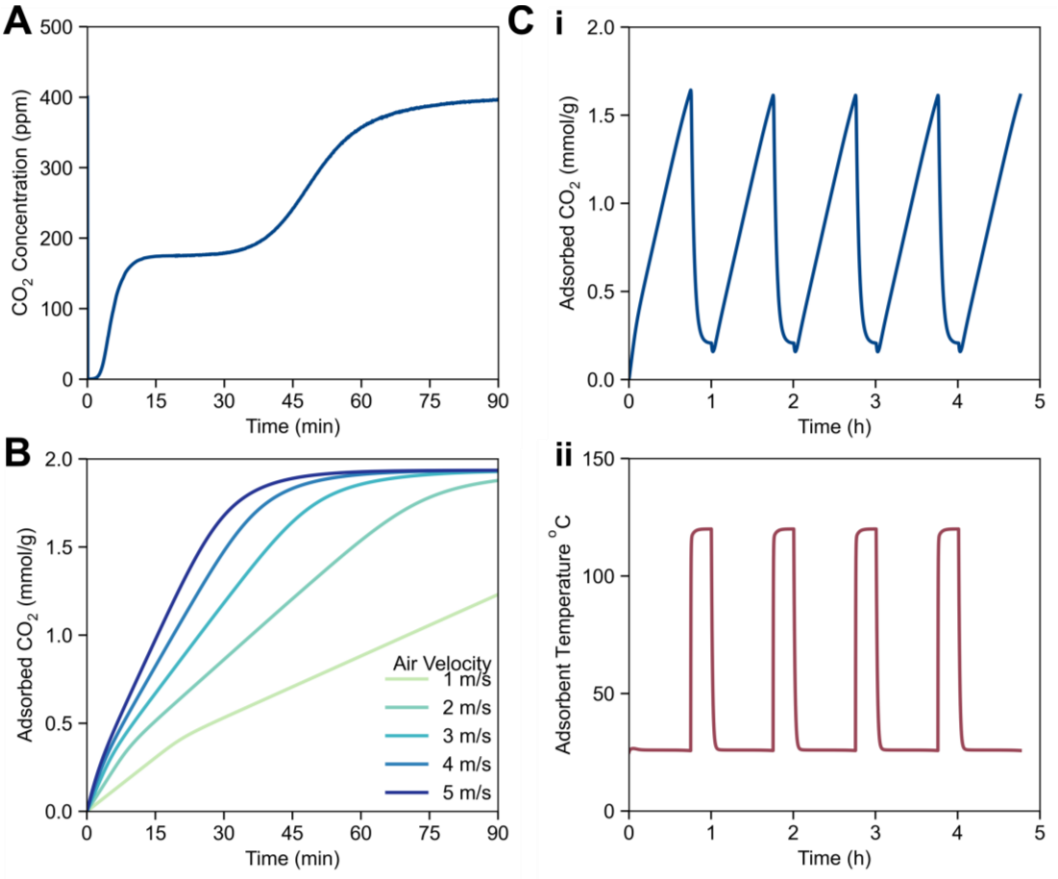

Figure 3.2. Modeled performance of direct air capture process. (A) Breakthrough curve of modeled sorbent operating with base-case parameters and operating conditions. (B) Effect of air flow rate on CO_2 capture rate. (C) Representative adsorption and desorption cycles modeled at base-case parameters and operating conditions, showing adsorbed concentration (i) and temperature of the adsorbent (ii).

I began by modeling the direct air capture component of the DAC-EMP process. The model equations for the DAC system described in the methods are indifferent to the exact type of sorbent used. They could be used to describe MOFs, COFs, or other solid-phase CO_2 adsorbents. However, for the analysis here, I use parameters based on the MOF mmen-Mg_2(dobpdc), first synthesized by McDonald *et al.*[163] Isotherm data (see Supplementary Note B.1, Appendix B), sorbent capacity, density, heat capacity, adsorption kinetics, and adsorption thermodynamics used in the model here match those reported for mmen-Mg_2(dobpdc). In addition to the physical parameters, the behavior of the DAC module is dependent on the geometry of the contactor and other operating conditions. In the base-case scenario, I assume an air-sorbent contactor of length 0.3 m with an air velocity of

3 m/s. All other base-case parameters and operating conditions can be found in Table B.1, Appendix B.

Simulated breakthrough curves were obtained first (Fig. 3.2A). Two distinct adsorption stages are observed in the breakthrough curve, due to step behavior in the isotherm described in the methods. Based on these breakthrough dynamics, adsorption is expected to slow after around 45 min, with the sorbent reaching max capacity around 75 min. This breakthrough curve is similar to the one modeled by Sinha *et al.*[159]

The effect of air velocity on the adsorption kinetics was then examined. As expected, the adsorption process will be sped up with higher air velocities (Fig. 3.2B), as convection is the rate-limiting step in the DAC process. Eventually, further increases in air velocity will not lead to faster adsorption dynamics, as the rate of the chemisorption itself becomes more kinetically relevant. Although the adsorption time decreases with increasing flow rate, higher air velocities will require more energy, introducing a tradeoff.

The desorption process can then be modeled. The final conditions of the adsorption model can serve as the initial conditions of the desorption model described in the methods. Once the desorption dynamics are modeled, those final conditions can serve as the initial conditions for the adsorption model, and DAC cycles can therefore be simulated. For an adsorption time of 45 min, a desorption time of 15 min, and all other parameters at their base-case values, the adsorbed CO_2 concentration and temperature can be simulated for several consecutive cycles (Fig. 3.2C). In this model, the rate of heating the contactor is quite fast, and the dynamics of the desorption process are controlled by the rate of CO_2 desorbing from the adsorbent.

The difference in the adsorbed CO_2 concentration at the end of the adsorption process and at the end of the desorption process is taken to be the captured CO_2 per cycle (Δq_{cycle}), which in this simulation is 1.41 mol/kg adsorbent. The productivity, in moles of CO_2 captured per kg of adsorbent per hour, can then be calculated by dividing this value by the total cycle time (including adsorption step, desorption step, and an assumed dead time of 3 min per cycle), leading to a productivity of 1.34 mol/kg/h.

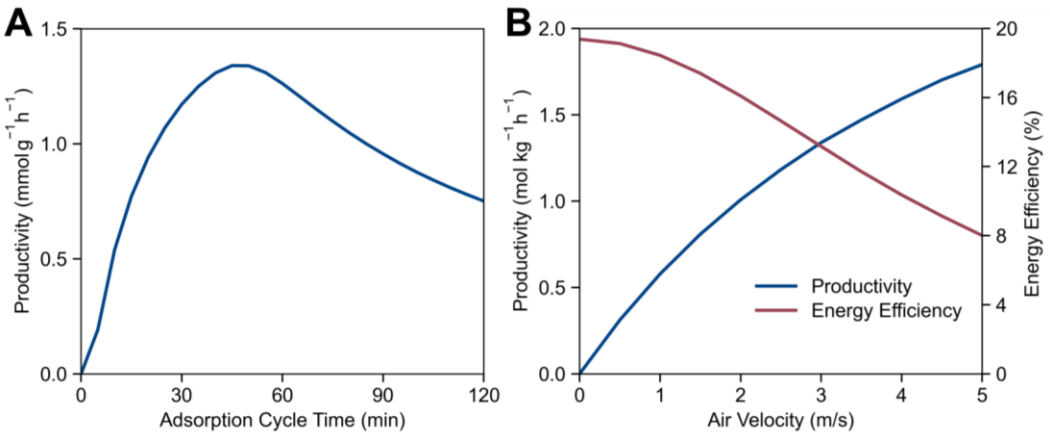

Figure 3.3. Productivity of direct air capture module. (A) Air capture productivity, defined as amount of CO_2 captured per kg of adsorbent per hour as a function of the adsorption time per cycle. (B) Tradeoff between air capture productivity and DAC energy efficiency at various air feed rates.

I then explored the impact of the adsorption cycle time on the productivity of the DAC module. As seen in Fig. 3.2A, it takes nearly an hour and a half for the sorbent to reach its maximum capacity. However, in practice, the sorbent would not become saturated each cycle, as the rate of CO_2 adsorption decreases when nearing its maximum capacity. As shown in Fig. 3.3A, there exists an adsorption cycle time that maximizes productivity, assuming a constant desorption time of 15 minutes (and dead time of 3 minutes per cycle). For the base-case parameters and operating conditions, a maximum productivity of 1.34 mol/kg/h occurs at an adsorption time of 50 min, which corresponds to a Δq_{cycle} of 1.52 mol/kg.

As stated before, there is a tradeoff between productivity and energy demand when running these DAC cycles. At higher air velocities, the productivity will be higher, as less time is needed in the adsorption phase. However, higher air velocities also correspond to higher pressure drops (see Equation 3-26) and higher flow rates, which lead to higher energy demands for the blower. Purifying CO_2 from atmospheric concentrations (400 ppm) to a pure 2 bar stream requires a minimum energy of 21.1 kJ/mol. The energy required to run the DAC cycle, namely the energy required for the blower, vacuum pump, and heat pump, can then be compared to this thermodynamic minimum energy to obtain a value of the energy efficiency of the DAC process. A tradeoff between productivity and energy efficiency can then be observed (Fig. 3.3B).

Bioreactor 1 modeled performance

The first bioreactor, which effects the conversion of the captured carbon dioxide as well as hydrogen gas to acetate, is modeled by the equations described in the methods section. While the equations described are dynamic, the bioreactor operating at a given dilution rate will reach a steady-state, and those steady-state conditions are used to evaluate the system. In this bioreactor, the primary metric to consider is the volumetric acetate productivity. For a given set of parameters and operating conditions, there will be a dilution rate that maximizes the acetate productivity of the bioreactor.

An example is shown in Figure 3.4A, which shows the effect that the liquid dilution rate has on the system, under base-case assumptions. A general trend is seen, in which productivity initially rises with dilution rate, as higher dilution rates enable faster specific growth rates at steady-state and therefore higher acetate production rates. However, as the liquid dilution rate exceeds its optimal value, effects of salinity begin to limit the acetate production. Growth rates that are high enough to avoid cell washout can only occur if the concentration of sodium (which is added in the form of NaOH in stoichiometric proportions to the acetic acid produced to maintain pH neutrality) is sufficiently low. Therefore, as dilution rate continues to increase, the acetate titer becomes lower, leading to a decrease in productivity. Total cell washout occurs when the dilution rate approaches the maximum specific growth rate of the acetogen (0.123 h^{-1}).

For the rest of the chapter, any productivity that is shown will be the productivity at the dilution rate that maximizes productivity for a given set of conditions. Other system parameters and their effect on the acetate productivity can then be examined. There are two major factors that limit the productivity of the system: salt toxicity (which in turn impacts the specific growth rate) and gas-liquid mass transfer. Figure 3.4B shows the impact of the gas-liquid mass transfer coefficient ($k_L a$) on the system productivity, with all other system parameters held constant. The productivity rises roughly linearly with respect to $k_L a$ until the $k_L a$ reaches around 200 h^{-1}, when it begins to plateau. In the linear regime, the system is primarily limited by the rate of gas-liquid mass transfer. For $k_L a$

values above 200 h^{-1}, the effect of toxicity becomes a greater limiting factor to the system. Essentially the same trend is seen for the effect of halotolerance on the bioreactor. As the salt tolerance of inhibition (defined by the parameter $c_{\mathrm{Na,max,1}}$) increases initially, the productivity increases proportionally, as higher acetate titers are achievable. When this parameter increases beyond 1 M, however, productivity begins to plateau, as the production rate is limited by gas-liquid mass-transfer. Thus, for significant improvements in productivity to occur, both the gas-liquid mass transfer rate and the halotolerance of the bacteria would need to increase simultaneously.

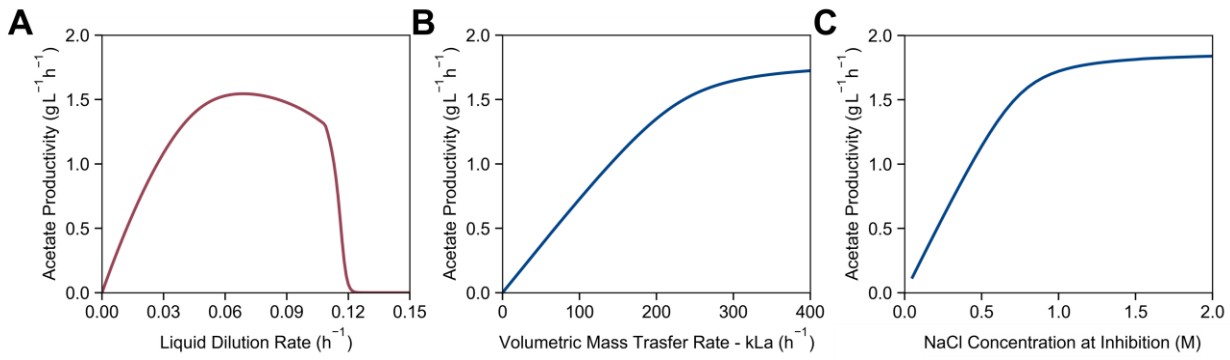

Figure 3.4. Modeled performance of acetogenic bioreactor. (A) Volumetric production rate of acetate in the bioreactor under base-case operating conditions ($k_L a$ = 250 h^{-1}; $c_{\mathrm{Na,max,1}}$ = 0.75 M) as a function of the dilution rate. (B) Productivity of acetate as a function of mass transfer coefficient $k_L a$ ($c_{\mathrm{Na,max,1}}$ = 0.75 M). (C) Productivity of acetate as a function of maximum tolerated sodium concentration $c_{\mathrm{Na,max,1}}$ ($k_L a$ = 250 h^{-1}). Note productivities in (B) and (C) are those at the dilution rate which maximizes the productivity at every point.

The effect of gas recycle was then explored. The gaseous substrates fed to the acetogenic bioreactor are quite costly, and therefore maximizing the utilization of each substrate is critical for an economical bioprocess. Luckily, the substrates are fed in the gas phase, and unused substrates can be recycled with relative ease. However, recycling all gases exhausted from the reactor can pose issues due to the accumulation of inert compounds. In base case DAC simulations (Fig. 3.2C), the purity of the captured CO_2 is calculated to be 98.3%, with the balance being N_2. Whether this impurity will substantially affect the ability to recycle hydrogen and carbon dioxide is studied.

The model is slightly modified such that the feed gas stream is a mixture of fresh gas feed and some fraction of the recycled gas effluent. Assuming that CO_2 is provided from the DAC process with a purity of 98.3%, the effect of the gas recycle fraction, (the fraction of the effluent gas stream that is recycled rather than purged) on the bioprocess performance is then evaluated (Fig. 3.5). As expected, the percent of hydrogen gas utilized approaches 100% as the gas stream is completely recycled. Productivity does decline rapidly, however, when the recycle fraction exceeds 96%, as the inert N_2 is accumulated to such a degree that the feed stream contains too low of H_2 and CO_2 concentrations. Therefore, the recycle fraction is restricted to this value or lower. This still allows significant recycling of the gases, with hydrogen utilization around 97%, indicating that nearly all of the produced hydrogen is reacted. Based on these results, the recyclability and by extension the utilization of the gaseous substrates should not be an issue.

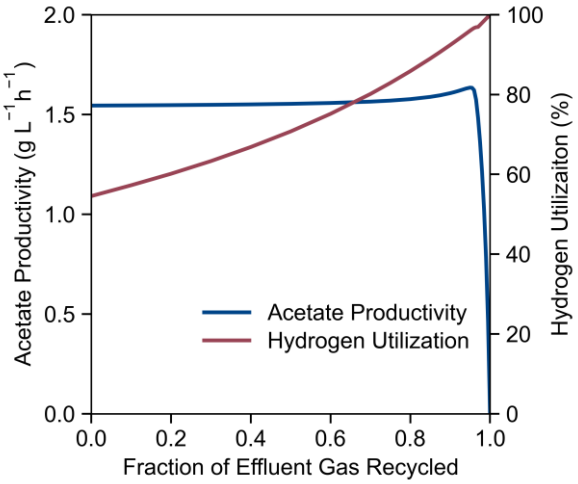

Figure 3.5. Effect of Recycle on the performance of the acetogenic bioreactor

Bioreactor 2 modeled performance

The second bioreactor, in which acetate is converted to n-butanol, is then modeled. The yield of n-butanol on acetate is a critical parameter. As in Chapter 2, I define carbon efficiency to be the fraction of carbon found in the product compared to the total carbon present in the product and biomass (equal to 1- ϕ in the model equations). In this model, at lower carbon efficiencies, the growth rate of the acetotroph will be higher, as a higher fraction of the substrate can be converted to biomass. However, due to the low conversion of acetate to butanol, the butanol titers will be lower, leading to lower productivities. Likewise, at high carbon efficiencies, the butanol titer will be higher, but the dilution rate will be lower, also leading to lower productivities as the carbon efficiency approaches one.

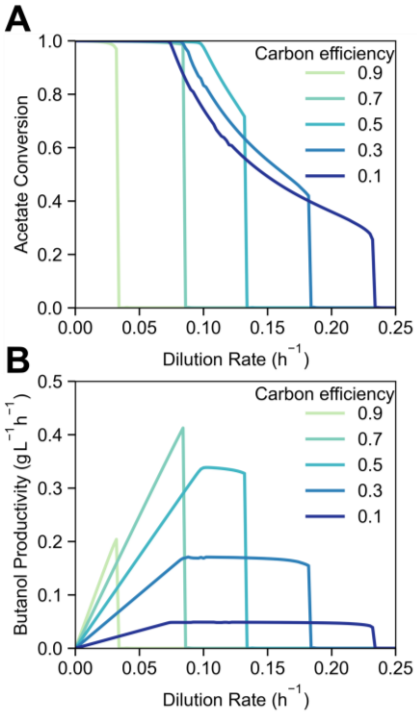

Figure 3.6. Modeled performance of butanol-producing bioreactor. (A) Fractional conversion of acetate (moles of acetate consumed per moles of acetate fed) and (B) butanol productivity as a function of dilution rate for a variety of possible carbon efficiencies. Carbon efficiency is defined as the fraction of carbon found in the product compared to the total carbon present in the product and biomass. Feed acetate concentration is assumed to be 0.4 M.

Unlike in bioreactor 1 where the substrate was fed in the gas phase and would be relatively straightforward to recycle, recovering acetate from the effluent stream of bioreactor 2 to recycle would be technically challenging. Therefore, it would be prudent to also maximize the conversion of acetate in the bioreactor, while also maintaining high productivity. The effect of dilution rate on acetate conversion and acetate productivity for a variety of carbon efficiencies is shown in Figure 3.6.

Carbon efficiencies as high as 0.9 have not been achieved in the conversion of acetate to butanol, although they have been achieved for other substrates (*e.g.*, glycerol, glucose).[86,164] While thermodynamically possible, it is likely that achieving yields this high will require substantial metabolic engineering to achieve. However, a carbon efficiency of 0.9 will be assumed for the rest of this analysis, to demonstrate how the system would perform if such a target is met.

Separations process modeling

The chemical process modeling software CHEMCAD was used to simulate the separation process of purifying n-butanol from the effluent in bioreactor 2, which requires extraction of n-butanol by mesitylene and two distillation steps, first to remove any extracted water and then to purify n-butanol. For a given n-butanol titer, taking into account purity requirements (>99%), the simulation could predict the flow rate of mesitylene required, the amount of mesitylene consumed by the process, the energy demands of the distillation columns, and the fractional recovery of n-butanol. The simulation is also used to size the extractor, distillation columns, and heat exchangers used in the process, which will be factored in during the capital cost calculations. All of these values depend heavily on the butanol concentration on the incoming stream. In particular, the mesitylene demand and energy requirements of the distillation columns appear to be nearly inversely proportional to the starting n-butanol titer (Fig. 3.7).

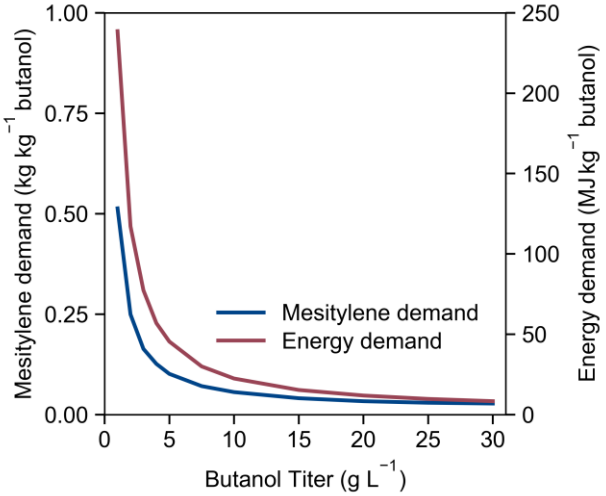

Figure 3.7 Results of CHEMCAD Separation process modeling. Effect of the n-butanol titer in the effluent of bioreactor 2 on the mesitylene (blue) and energy (red) required to purify n-butanol to 99% purity.

The mesitylene demand and energy requirements were simulated for several values of the n-butanol titer. These relationships were then fitted to a power law function. For example, the specific mesitylene demand (kg mesitylene per kg n-butanol purified) can be described as:

$$\frac{m_{\mathrm{Mes}}}{m_{\mathrm{BuOH}}} = 0.4401\left(\frac{c_{\mathrm{Bu,2}}}{\mathrm{g/L}}\right)^{-0.861} \tag{3-34}$$

which fits the results in Fig. 3.7 with an R^2 value of 0.991.

Likewise, the distillation heat requirements per kg of n-butanol purified can be described as:

$$\frac{E_{\mathrm{Dist}}}{m_{\mathrm{BuOH}}} = 229{,}000\,\frac{\mathrm{kJ}}{\mathrm{kg}}\left(\frac{c_{\mathrm{Bu,2}}}{\mathrm{g/L}}\right)^{-0.989} \tag{3-35}$$

This correlation fits the modeled data with an R^2 value of 0.9996.

The relationship between fractional butanol recovery and butanol titer does not lend itself to a simple correlation. Therefore, the fractional recovery for a given butanol titer will be interpolated based on the results of the CHEMCAD simulation.

Whole-process material and energy demands

Now that the direct capture, both the acetogenic and butanol-producing bioreactors, and the separations have been independently modeled, the entire process can then be modeled. The DAC component is simulated first, and the purity of the resulting CO_2 affects the boundary conditions of the first bioreactor model. The concentration of acetate coming out of the first reactor then serves as the concentration of acetate in the feed stream for the second bioreactor. The titer of butanol in the second reactor is used to calculate the material and energy demands for the separations, as described previously. Mass and energy balances can be used to map out the flows in and out of each subprocess based on the desired n-butanol production rate. For a scaled-up 40 million gallons per year process, the material and energy flows for the base-case process are listed in Table 3.4.

Hydrogen production is the most energetically expensive component of the process, accounting for more than two-thirds of the electricity consumed. This is conceptually unsurprising, as hydrogen is the energy carrier driving the conversion of CO_2 to n-butanol. However, it is interesting to note that, despite the high energy costs of separating CO_2 from atmospheric concentrations, the electrolysis component of the process requires roughly five times as much power as the DAC. By employing industrial heat pumps, all energy required by the process can be delivered by electricity. The power demand of the entire process to meet the desired production rate of 40 million gallons butanol per year is over half a gigawatt, slightly lower than the output of the largest photovoltaic power station in the United States at the time of writing (note: this comparison does not consider the time-dependent nature of solar energy generation).

Given the material and energy flows calculated for the process at scale, the variable operating cost can then be calculated (Equation 3-33). An electricity cost of \$0.05/kWh is assumed, based on the levelized cost of solar electricity in a medium resource area[165] (costs of materials used for these calculations are listed in Table B.3, Appendix B). Adding the costs of all material and energy used in the process yields a variable operating cost of \$16.56/gal n-butanol. Even before adding in fixed operating costs and the contribution of the capital costs, this value is too high to currently compete with gasoline fuel or even other biobutanol production processes (*e.g.*, ABE fermentation). However, this is only a snapshot representing the operating costs for a given set of conditions. Differing values of the model parameters as well as economic factors will have a large impact on

this process cost. However, this baseline scenario is instructive to begin to understand where the major economic bottlenecks may be found for this process.

Table 3.4. Material and energy flows in DAC-EMP Process for 40 MM gal/y butanol production

Process Component	Process Demand	Units	Annual Cost ($MM)	Unit Cost (per gal n-BuOH)	Variable Cost Contribution
Energy demands					
DAC Blower	29.4	MW	11.6	$0.29	1.8%
DAC Vacuum	9.0	MW	3.6	$0.09	0.5%
DAC Heat Pump	53.4	MW	21.1	$0.53	3.2%
Electrolyzer	422.4	MW	167.3	$4.18	25.2%
BR-1 energy[a]	20.8	MW	8.2	$0.21	1.2%
BR-2 energy[a]	21.5	MW	8.5	$0.21	1.3%
Separations	63.9	MW	25.3	$0.63	3.8%
Total Electricity	**620.4**	**MW**	**245.7**	**$6.14**	37.1%
Material demands					
Sorbent[b]	0.097	t/h	48.5	$1.21	7.3%
Monolithic support[b]	0.027	t/h	0.9	$0.02	0.1%
Nitrogen gas	0.92	t/h	5.5	$0.14	0.8%
Electrolysis water	76.6	t/h	0.8	$0.02	0.1%
Ammonia	0.84	t/h	7.8	$0.20	1.2%
Phosphoric acid	0.40	t/h	4.1	$0.10	0.6%
Magnesium sulfate	0.62	t/h	1.9	$0.05	0.3%
Sodium hydroxide	37.3	t/h	186.1	$4.65	28.1%
Sulfuric acid	45.8	t/h	94.3	$2.36	14.2%
Mesitylene	1.40	t/h	44.8	$1.12	6.8%
Wastewater treatment	2590	t/h	22.0	$0.55	3.3%
Total Material	-	-	**416.8**	**$10.42**	**62.9%**
Process Total	-	-	**662.5**	**$16.56**	**100%**

[a] Power demand includes agitation and heating for the bioreactors. Heating demand for the bioprocesses is allocated evenly between the two bioreactors.

[b] Both the DAC sorbent and monolithic support are considered as material demands, despite their long lifetime relative to other materials used in the process. The process demand, in t/h, is the amount sorbent required to maintain the given butanol production rate divided by the lifetime of the sorbent (t_{DAC}, 2 years in base case).

One striking element of the variable cost calculation described in Table 3.4 is the large contribution of sodium hydroxide and sulfuric acid, used to control the pH in bioreactor 1 and 2 respectively. These pH control materials alone account for around 42% of the variable operating cost (>$7/gal), more than all the electricity used. The necessity of pH control in both the acetate-producing and acetate-consuming component of the bioprocess is a significant downside of this particular electromicrobial production scheme, a fact noted by the LCA performed in Chapter 2. Addressing

the issue of pH control will likely be a major obstacle in the development of this system, and a discussion of some strategies to obviate this major process cost will be discussed in a later section.

Process economics

Based on the material and energy flows, the major pieces of process equipment may be sized, and their cost may be estimated based on established correlations and other literature data (See Table B.2, Appendix B). The major equipment considered are listed in Table 3.5. While other equipment will be necessary for this process to operate (*e.g.*, pumps), I assume that the equipment listed account for the bulk of the installed equipment cost. At this level of detail (*i.e.*, a conceptual techno-economic assessment) the uncertainty in estimating equipment costs is large enough that the inclusion of minor equipment is not particularly consequential.

Table 3.5: Equipment sizing and estimated costs

Equipment	Unit Size	Unit Cost	Number Of Units	Installed Equipment Cost
DAC Heat Pump	66.7 MW	$22.6MM	2	$45.1 MM
Blower	47.2 m^3/s	$57K	1491	$137.1 MM
Vacuum Pump	0.165 m^3/s	$90K	130	$18.7 MM
DAC Vessel	10,200 m^3	$580K	1	$0.9 MM
Electrolyzer[a]	1 MW	$900K	422	$399 MM
Gas Storage Tanks	11,600 m^3	$1.3MM	20	$41.9 MM
BR-1 Fermenter	1,000 m^3	$2.34MM	36	$193.8 MM
BR-2 Fermenter	1,000 m^3	$2.34MM	80	$430.8 MM
Liquid-Liquid Extractor	177 m^3	$320K	22	$11.2 MM
Distillation Columns	[b]	$870K	13	$21.4 MM
Separations Heat Pump	53.3 MW	$18.5MM	3	$55.4 MM
Heat Exchanger	1090 m^2	$144K	30	$6.9 MM
Total IEC				$1362 MM

[a] An electrolyzer capital cost of $900,000/MW is assumed independent of scale. The effects of the expected reduction in hydrogen production costs will be explored later.
[b] Distillation columns are 5 m in diameter and 11 m high, with 14 stages.

Some key observations can be made from the results described in Table 3.5. The largest component of the installed equipment cost comes from the bioreactors, totaling over $600 million, with the electrolyzer shortly behind, costing around $400 million. The bioreactor cost is quite high, especially in comparison to other techno-economic assessments done for other bioprocesses such as ethanol fermentation.[18] Relative volumetric productivities between this process and other bioprocesses can account for much of this difference. The slow growth of acetogens, the limited substrate concentration fed to the butanol-producing microbe, and the necessity of two separate reactors leads to particularly low overall productivity.

The electrolysis capital cost is also high, significantly adding to the cost of butanol production. The economic argument for hydrogen-mediated EMP rests on hydrogen being a cheaper substrate than sugars such as glucose. With the current high capital costs of electrolyzers, this is currently unlikely. However, capital costs of electrolyzers are expected to fall significantly in coming years, which will improve the feasibility of EMP systems. The Hydrogen Shot Initiative of the U.S. Department of Energy has a goal of achieving $1/kg hydrogen production by the year 2030, which would require reducing the capital cost of electrolysis from $900/kW to $100/kW.[166]

Given the installed equipment cost (IEC) and the variable operating costs (VOC) described in Tables 3.4 and 3.5, following the methodology in Tables 3.1, 3.2, and 3.3, a discounted cash flow rate of return (DCFROR) can be performed to determine the minimum butanol selling price. In the base case scenario, given a discount rate of 10%, the minimum selling price is $26.56/gal (Table 3.6).

Table 3.6: Economic summary of DAC-EMP process under base-case assumptions

Capital Cost Contributions	**Cost Calculation**
Installed Equipment Cost (IEC)	$1.36 BB
Total Capital Investment	**$2.69 BB**
Variable Operating Costs	$662.5 MM/y
Fixed Operating Costs	$72.9 MM/y
Total Operating Costs	**$735.3 MM/y**
Butanol Production	40 MM gal/y
Revenue	$1.06 BB/y
Minimum Selling Price	**$26.56/ gal**

Techno-economic analysis

As mentioned previously, the minimum selling price listed in Table 3.6 is based on many assumptions (see Table B.1, Appendix B). These parameters may change for a variety of reasons. Prices of individual materials may rise or fall, better-performing materials and biocatalysts may be developed, and in many cases the value of a given parameter is subject to uncertainty. Taken together, the models of the individual process components, the process-level mass and energy balances, and the techno-economic model can evaluate the impact of various parameters on the overall economics of the DAC-EMP process described here. Two key examples demonstrating the utility of this approach are shown here: examining the impact of the acetogen's salt tolerance and the manufacturing cost of the DAC sorbent on the overall process economics.

The effect of strain halotolerance is considered first. Several different levels of the variable $c_{\mathrm{Na,max,1}}$, the maximum tolerated sodium concentration in bioreactor 1, are selected and the minimum butanol selling price is recalculated (Fig. 3.8A). In general, the butanol price is lowered at increasing values of this salt tolerance parameter. In Fig. 3.4C, the impact of this parameter on the productivity of bioreactor 1 has already been demonstrated, productivities increasing with increasing halotolerance. In addition, increasing this value also allows higher acetate titers in bioreactor 1, which leads to increased productivity and titer of butanol in bioreactor 2. Therefore, both the capital costs and the cost of separations will decline. However, this only applies to a

certain extent. Once the value of this parameter exceeds 1 M, the overall system becomes limited by salt toxicity effects in bioreactor 2, and therefore the marginal gains become diminished.

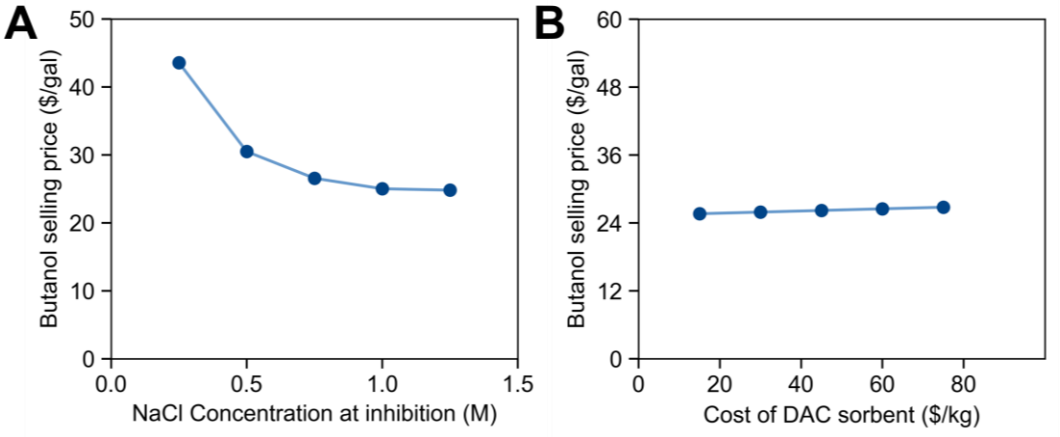

Figure 3.8 Effect of technical parameters on the minimum selling price of n-butanol. Two example parameters, the NaCl concentration at inhibition ($c_{\mathrm{Na,max,1}}$) of the acetogen in bioreactor 1 (A) and the cost of the DAC sorbent per kilogram (B), are varied and the minimum n-butanol selling price is re-calculated with those conditions.

The impact of the cost of the DAC sorbent on the final butanol selling price is also examined (Fig. 3.8B). The cost of butanol does of course increase as this individual cost increases. However, this change is quite small relative to the rest of the process. In the base-case scenario, the cost of DAC contributes only 14% of the overall process cost, and the cost of the sorbent itself is only one factor that affects the cost of air capture. This example highlights the utility of the modeling framework presented here as a tool to determine which parameters, given a set of baseline assumptions, will be the most important factors affecting the economics of production.

Modifying individual parameters is a useful way to determine how sensitive the economic calculations are to different aspects of the process. Changing parameters in parallel, however, allows fully different scenarios to be examined, a process which can allow us to understand various pathways for the DAC-EMP system described to become economically viable. I will now lay out an example of this exercise, by considering successive scenarios that improve the process economics until the minimum selling price of butanol is within the ballpark of being competitive with petroleum-based fuel. The particular pathway I examine here is summarized in Figure 3.9.

We can begin with the original base-case scenario, with a minimum butanol selling price of $26.56 per gallon. From here, other scenarios can be considered. The first modification assumes that the need for pH control can be removed from the system. I will discuss practical strategies to achieve this later, but in this scenario, pH control is eliminated from the model. In addition to eliminating the demand and therefore the cost of NaOH and H_2SO_4, the elimination of salinity-induced toxicity also leads to an increase in productivity of the bioreactors, which in turn reduces the capital cost of the process. Higher butanol titers are also achievable in this scenario, reducing the cost of separations. Eliminating the need for pH control alone decreases the minimum selling price of butanol fuel by $9.50/gal.

The next change examines the impact of the expected decline in hydrogen production costs. If the goal of the Hydrogen Shot Initiative ($1/kg H_2) mentioned previously is met by 2030, declines of

electrolzyer capital costs from $900/kW to $100/kW, along with electricity available at $0.02/kWh, are required. Lowering the cost of hydrogen, the primary microbial energy source utilized in the bioprocess, would lead to a further reduction in butanol cost of $6/gal.

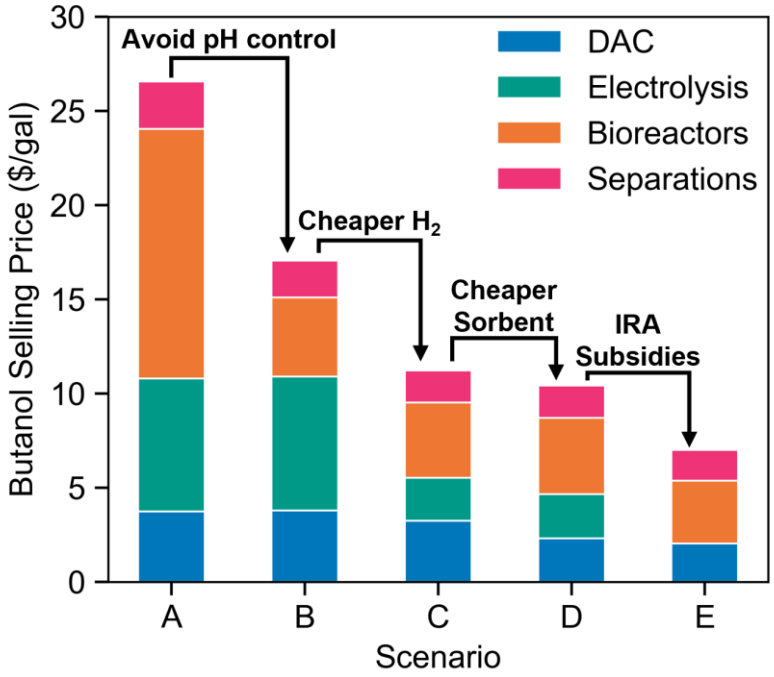

Figure 3.9 Potential pathway to economic viability of acetate-mediated DAC-EMP system for n-butanol production. Demonstration of how different scenarios will progressively lead to decreased butanol costs, starting from the base-case scenario (A). Scenario B describes a scenario in which pH control is no longer necessary. Scenario C describes a scenario in which the electrolysis capital cost falls to $100/kW and the electricity price falls to $0.02/kWh, consistent with the goals of the U.S. Department of Energy's Hydrogen Shot Initiative. Scenario D describes a process with the DAC sorbent decreasing in cost by two-thirds compared to the base-case cost. Scenario E factors in the 10-year tax credit for hydrogen production in the United States provided by the Inflation Reduction Act of 2022.

At this point, the cost of direct air capture becomes a meaningful contributor to the process economics. The next scenario envisions a three-fold reduction in synthesis cost of the adsorbent used in the DAC subprocess. This lowers the cost of direct air capture from $130/ton to $85/ton, which would be roughly in line with optimistic projections of DAC systems operating at a large scale.[150] This would decrease the cost of butanol per gallon by around a dollar, to $10.40/gal.

I finally consider the impact of the subsidies for hydrogen production that are currently available in the United States following passage of the Inflation Reduction Act of 2022, which allows for a tax credit of up to $3 per kg H_2 produced for a period of ten years. This final consideration brings the butanol selling price to $7/gallon. Considering the significant uncertainty that is likely present in this value, I would consider the cost of butanol fuel in this scenario to be *comparable* to that of gasoline, within the level of error that would be expected in any techno-economic assessment. Without a more exhaustive techno-economic assessment based on a more detailed process design, the exact cost of butanol produced in this method is subject to significant uncertainty. However, given a certain optimistic set of assumptions, this process is in the realm of economic viability.

I also wish to emphasize that these scenarios represent only one possible pathway to economic viability of the DAC-EMP process described here. Other paths (*e.g.,* through more productive bioreactors or different financialization schemes) may also lead to low enough butanol costs. Demonstrating the effect of these specific scenarios illustrates the utility of the modeling approach taken here. This framework is a useful tool to evaluate several different scenarios to understand multiple possible paths to economic viability of a DAC-EMP system, which can aid in driving research directions toward addressing the roadblocks identified.

3.5 Conclusion

In this chapter I developed a multipart framework to analyze the techno-economics of a hypothetical scaled-up DAC-EMP butanol production process. The approach taken here mirrors the approach taken in Chapter 2 to analyze the environmental impacts of similar systems, substituting environmental impact metrics such as global warming potential for economic impacts (*i.e.,* minimum fuel selling price). I began by developing physics-based models for the constitutive components that make up the process: a solid adsorbent-based direct air capture process, an acetogen-containing bioreactor, and a bioreactor containing a butanol-producing acetotroph. These models can predict subsystem performance metrics such as energy efficiency, productivity, and titer based on limited empirical data. A process model based on mass and energy balances can be used to calculate the material and energy demands, as well as equipment sizes, for the process at a given scale. Techno-economic assessment then calculated the operating costs, capital costs, and a minimum n-butanol selling price based on the process model results. Importantly, I then showed how this tool can be used to assess the impact of certain parameters on the overall process economics and determine potential pathways for economic viability.

This techno-economic assessment is still quite conceptual in nature, given the fact that it evaluated a proposed DAC-EMP system that has not been yet developed but is instead modeled from first principles. The final value of a minimum selling price is calculated primarily as a means of contextualizing various metrics (*e.g.,* productivity, titer, energy efficiency, material demands) to understand how they impact the viability of the system as a whole. Given the fact that this value is based on numerous models, each of which alone are subjected to significant uncertainty (and which together compound that uncertainty) there is limited confidence in the exact dollar value. Moreover, I've demonstrated the sensitivity of the final selling price to a number of process parameters and assumptions, which makes a declarative statement on the economic viability of this specific EMP process, either now or in the future, contingent. In short, the purpose of this TEA is neither to prove nor disprove the economic viability of this specific EMP process or EMP in general. Rather, this analysis seeks to identify the factors that would most contribute to the economic viability (or perhaps lack thereof) of DAC-EMP systems. With this goal in mind, the following takeaways regarding the combination of direct air capture and electromicrobial production for biofuel generation can be made.

First, capital costs in this analysis were quite high compared to other bioprocesses, mainly due to the costs of the bioreactors (and electrolyzers, which will be addressed soon). The cost of bioreactors will be inversely proportional to the volumetric productivity of the system, and therefore the particularly high bioreactor costs calculated here are a result of the low productivity predicted by the model. Improving the overall system productivity beyond the base-case estimates

described earlier will likely be critical for a cost-effective acetate-mediated EMP process. Improving the volumetric butanol productivity from 0.13 g/L/h in the base-case scenario to 1 g/L/h would, only by considering the contribution of the bioreactor capital cost, decrease the price of n-butanol by over $3/gal. One strategy to achieve this lies in innovative bioreactor designs that move beyond the simple chemostats described by this model. Kantzow *et. al* for example used a submerged membrane bioreactor in an acetogenic process to achieve productivities four times higher than those modeled here.[72] Researchers should continue innovating to develop clever bioreactor schemes to improve productivity in EMP processes.

Similarly, the butanol titer was an important factor in determining the production cost, as the cost of separations was heavily dependent on titer, especially below 20 g/L n-butanol. One of the major factors limiting the titer is the concentration of acetate in the feed stream of bioreactor 2. Therefore, many of the same strategies for improving productivity mentioned would likely improve the titer. One factor not captured in the model is product inhibition, which could prevent the high titers necessary for affordable separations. Strategies to overcome this limitation should be developed by researchers. I will address this point specifically in Chapter 5.

Other products generated in this EMP strategy will have different separations, which would need to be independently considered. The economic penalty of lower product titers in this specific EMP system may not be present for other applications. Separation processes for intracellular products, for example, are much less dependent on titer, as low-cost methods can be used to concentrate cells prior to separation. However, these processes require cell lysis, which adds an extra component to the separations, an issue that I will address in the following chapter.

A perhaps underappreciated aspect of this type of EMP system is the need for pH control. Unless the acids and bases used for pH control become significantly less expensive, the economic viability of acetate-mediated EMP systems will likely require substantial reduction or elimination of pH control. In Chapter 2 I noted that the need for pH control can be avoided if the two bioprocesses can be localized in a single reactor. The net reaction converting hydrogen and carbon dioxide to butanol involves no net consumption or production of protons. If acetate production and consumption occurred in the same reactor with similar rates, the environment can remain neutral with little or no addition of acid or base. This would require an acetogen that is not strictly anaerobic as acetate consumption requires oxygen (or an equivalent electron acceptor). As noted previously, adaptive laboratory evolution has been used to develop an oxygen-tolerant strain of the acetogen *Sporomusa ovata*.[125] Therefore, this may be the most promising strategy to avoid issues of pH control with the EMP strategy examined here, and would be an interesting area of further research.

Knallgas bacteria-based EMP systems do not have this challenge, as the conversion of H_2, CO_2, and O_2 to n-butanol occurs with no net generation or consumption of protons. In systems where pH control is unavoidable and becomes an important economic factor, using Knallgas bacteria may be a better option than the two-step acetogen/acetotroph system analyzed here. However, this claim would need to be evaluated with a techno-economic model focusing on the Knallgas bacteria-based system. Moreover, as shown in Chapter 2, Knallgas bacteria-based systems can achieve higher titers and productivities than two-step acetate-mediated systems. This should be considered when selecting an EMP strategy for a given product.

The cost of hydrogen, unsurprisingly, is a critical cost component of the process. The assessment here indicates that the current cost of renewable hydrogen is too high for this process to be

economical. However, assuming the projections of lower hydrogen costs (reaching $1/kg by the end of the present decade) are realized, the system will not be limited by the cost of electrolysis. The decreases in electrolysis capital costs in the previous decades,[167] and the rapidly declining cost of solar electricity production,[168] give reason to be optimistic about this aspect.

This analysis suggests that the pathway to economic viability for this DAC-EMP butanol production process may be challenging. Fuels are particularly difficult products as their production costs must be very low to displace fossil-based analogs. Other products, especially those with higher value, may have more favorable economics. However, this analysis also suggests that a road to economic viability is possible. None of the barriers I've mentioned are inherent to the system. The thermodynamics and underlying metabolisms suggest indeed that biological conversion of hydrogen and carbon dioxide to alcohols such as n-butanol may be a cost-effective and environmentally sustainable method of liquid fuel production. The major limitations of productivity, titer, and pH control can all be conceivably addressed. Therefore, researchers working on these systems should continue their efforts, and focus on creating innovative strategies to address these problems.

Finally, the approach described here, combining first principles modeling and techno-economic assessment, provides a straightforward method to analyze other EMP strategies and applications. Only minor modifications to the bioreactor models would be required to analyze Knallgas bacteria- and formatotroph-based systems, such as was done in Chapter 2. Moreover, other products can easily be examined by varying the stoichiometry and yields described in the model (Eqn. 3-23 and 3-24). While understanding the limitations on the final value of the minimum selling price, the work in this chapter details the development of a useful tool in understanding the economics of large-scale commodity chemical production through EMP that can in turn guide research directions.

3.6 Acknowledgements

I would like to thank Anthony Abel for helpful discussions regarding the model development in this chapter. This work was supported by the ARPA-E OPEN 2021 Award No. DE-AR0001555.

Chapter 4: Engineering Osmolysis Susceptibility in *Cupriavidus necator* and *Escherichia coli* for Recovery of Intracellular Products[**]

4.1 Abstract

Intracellular biomacromolecules, such as industrial enzymes and biopolymers, represent an important class of bio-derived products obtained from bacterial hosts. A common key step in the downstream separation of these biomolecules is lysis of the bacterial cell wall to effect release of cytoplasmic contents. Cell lysis is typically achieved either through mechanical disruption or reagent-based methods, which introduce issues of energy demand, material needs, high costs, and scaling problems. Osmolysis, a cell lysis method that relies on hypoosmotic downshock upon resuspension of cells in distilled water, has been applied for bioseparations such as the purification of polyhydroxybutyrate (PHB) from extreme halophiles and protein products from mammalian cells. However, most industrial bacterial strains are non-halotolerant and relatively resistant to hypoosmotic cell lysis. To overcome this limitation, I developed two strategies to increase the susceptibility of non-halotolerant hosts to osmolysis using *Cupriavidus necator*, a strain often used in electromicrobial production, as a prototypical strain. In one strategy, *C. necator* was evolved to increase its halotolerance from 1.5% to 3.25% (w/v) NaCl through adaptive laboratory evolution, and genes potentially responsible for this phenotypic change were identified by whole genome sequencing. The evolved halotolerant strain experienced an osmolytic efficiency of 47% in distilled water following growth in 3% (w/v) NaCl. In a second strategy, the cells were made susceptible to osmolysis by knocking out the large-conductance mechanosensitive channel (*mscL*) gene in *C. necator*. When these strategies were combined by knocking out the *mscL* gene from the evolved halotolerant strain, greater than 90% osmolytic efficiency was observed upon osmotic downshock. A modified version of this strategy was applied to *E. coli* BL21 by deleting the *mscL* and *mscS* (small-conductance mechanosensitive channel) genes. When grown in medium with 4% NaCl and subsequently resuspended in distilled water, this engineered strain experienced 75% cell lysis, although decreases in cell growth rate due to higher salt concentrations were observed. This strategy is shown to be a simple and effective way to lyse cells for the purification of intracellular biomacromolecules and may be applicable in many bacteria used for bioproduction.

4.2 Introduction

Whole-cell biocatalysis encompasses a wide range of existing and potential processes in which microbes convert low-value feedstocks to higher-value products. Biochemical processes can produce biomolecules such as proteins that cannot be produced by traditional chemical processes, as well as fuels, commodity chemicals, and bioplastics that would otherwise be produced in petrochemical processes that contribute to anthropogenic climate change.[21,24,86,87] Downstream separations of the desired product are an important and costly component of any bioprocess.[169] Intracellular macromolecular bioproducts produced in bacteria can be especially challenging as

[**] This chapter has been adapted from an article that was originally published in *Microbial Cell Factories* and has been included with the permission from the co-authors.[232]

these molecules cannot easily diffuse through the cell membrane, and therefore require cellular disruption to recover the product.

Yet, intracellular macromolecules represent an important class of bioproducts. For example, recombinant proteins (industrial enzymes and biopharmaceuticals, in particular) are widely used intracellular products.[89] Moreover, the demand for high-quality plasmid DNA, generally produced as an intracellular product in bacteria such as *E. coli*, has greatly increased as more cell and gene therapies have been developed.[170] Certain bioplastics such as polyhydroxyalkanoates (PHAs) are produced as full-length polymers in many bacteria.[21] PHAs, most notably polyhydroxybutyrate (PHB), are native products in many bacteria that use them as a store of carbon and energy.[171,172] Non-native PHB producers, such as *E. coli*, have also been engineered for PHB production.[10,173]

Traditional bioseparations of biomacromolecules first require cell lysis prior to downstream purification of the desired product.[98] Mechanical methods such as ultrasonication and high-pressure homogenization can efficiently lyse cells, though these require expensive equipment, are energy-intensive, and may damage sensitive biomolecules.[98,174] Chemical and enzymatic methods of cell lysis can also be used to liberate intracellular products, though the cost of the materials make these techniques difficult to scale.[175] Certain industrial microbial hosts, for example *Bacillus subtilis* and *Bacillus licheniformis*, secrete enzymes such as proteases with high yields, obviating the need for cell lysis.[176] However, these strains are usually used only for a select group of native enzymes, limiting this approach to specific products. Strategies relying on native or engineered secretion systems in *E. coli* and other bacterial hosts have been developed, though this approach requires modification of the protein with a signal peptide and can be dependent on the structure of the secreted protein.[177–179] Therefore, in most applications, cell wall disruption is required to recover intracellular products from bacterial hosts.

Osmolysis is a simple, low-cost method of cell lysis that relies on osmotic pressure to swell cells and burst membranes following the resuspension of cells in a hypotonic solution (Fig. 4.1A). Osmolysis as a cell lysis technique in downstream separations has traditionally been restricted to mammalian cell culture, where the weaker cell membrane is fairly labile to osmotic pressure changes.[175] The more robust bacterial cell wall, as well as stress-response survival mechanisms, allow most bacteria to survive moderate fluctuations of osmolarity.[175,180] More recently, extremely halophilic bacteria have been explored as microbial PHB producers.[181,182] Extreme halophiles can grow in salinities from 15-30% NaCl (w/v),[183] and therefore resuspension of these microbes in distilled water will cause a much higher osmotic pressure shock than can be achieved with bacteria grown in conventional media. For example, Rathi *et al.* demonstrated a PHB recovery of 98% from pre-dried *Halomonas* sp. SK5 biomass using this technique, and showed that the addition of sodium dodecyl sulfate at low concentrations could improve the purity of the biopolymer.[181] Osmolysis is therefore a promising technique to reduce the energy demand, material use, and cost of bioseparations. However, extremely halophilic bacteria are rarely, if at all, used in industrial bioprocesses, and many applications call for specific bacterial strains that are likely not halophilic.

Electromicrobial production (EMP), for example, relies on bacteria which utilize electricity or electrochemically-generated mediator molecules such as hydrogen gas and formic acid as energy sources to produce various bioproducts.[43] Traditional biochemical systems use crop-derived sugars as microbial substrates and therefore cause social and environmental impacts such as carbon emissions from fertilizer production, nitrous oxide emissions from fertilizer application, land use effects, and competition with the food supply.[28,31] EMP systems, however, do not rely on the

agricultural system, and, if using a clean electricity source, can lead to a decreased global warming potential and land occupation footprint (see Chapter 2).

A particularly promising microbe studied for EMP systems is *Cupriavidus necator*, a soil bacterium capable of growth on various substrates, including H_2/CO_2, formate, and organic molecules.[184] Electrolysis of water to produce hydrogen or electrochemical reduction of carbon dioxide to formic acid can therefore be used to generate substrates that Knallgas or formatotrophic bacteria (both of which describe *C. necator*) can convert to desired products.[47,185] *C. necator* naturally produces the polyester PHB, and is often regarded as a model organism for PHA production due to its ability to accumulate high levels of the polymer intracellularly (up to 90% of total cell mass) and its potential in producing many PHA variants.[186,187] In addition, expression systems have been developed for *C. necator* that allow production of recombinant proteins,[55,57] and metabolic engineering has been applied to produce various fuels and commodity chemicals such as isopropanol, acetoin, and various alkanes.[63,65]

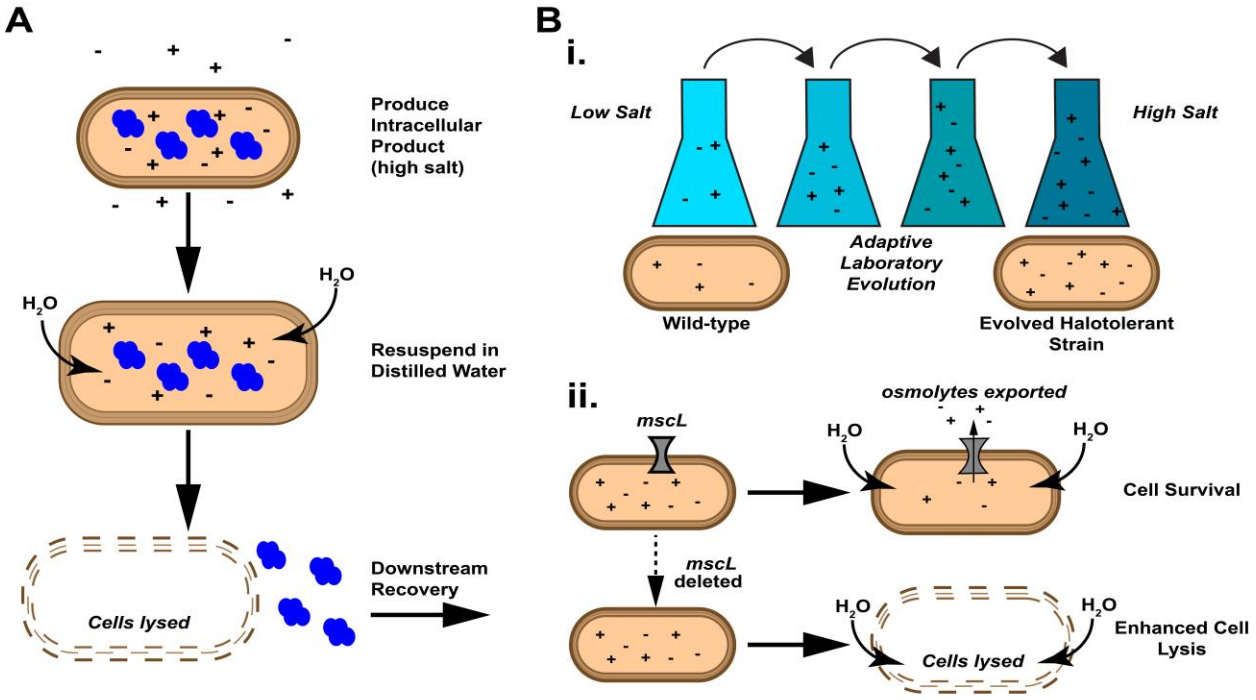

Figure 4.1. Overview of approach taken in this chapter. (A) Schematic representation of osmolysis-based recovery of intracellular biomacromolecules. The product is first produced by a microbial host under elevated salt concentrations. Cells are then resuspended in distilled water, causing an increase of turgor pressure due to osmotic shock, which lyses the cell membrane and enables downstream recovery of the product. (B) Two orthogonal strategies employed here to increase the sensitivity of microbial hosts to osmotic downshock. In one strategy (i) ALE is used to increase the halotolerance of the microbe, enabling cell growth at higher salt concentrations and therefore a greater magnitude of osmotic downshock when cells are resuspended in distilled water. In the other strategy (ii) the large-conductance mechanosensitive channel (*mscL*) or a related gene is deleted from the microbial host, which limits the ability of cells to export osmolytes in hypotonic solutions, increasing their susceptibility to osmotic lysis.

While EMP addresses the environmental impacts of substrate generation in bioprocessing, a sustainable bioproduction system must also minimize energy and resource demand during separations. Adapting the osmolysis cell disruption method to work with EMP-relevant microbes

could address the resource-intensive separations process for intracellular macromolecular products produced through EMP. However, to my knowledge, no EMP systems have used halophilic or halotolerant bacteria. I address this issue by developing a two-part strategy to render non-halophilic bacteria susceptible to lysis by osmotic downshock, using *C. necator* as a model host (Fig. 4.1B). I demonstrate that intracellular biomolecule products can then be separated from the cells, using recombinant red fluorescent protein (RFP) as a useful example product due to its ease of measurement.

I first use adaptive laboratory evolution (ALE) to improve the halotolerance of *C. necator*, which enables a greater magnitude of osmolarity change and therefore greater osmotic pressure when the cells are resuspended in distilled water. In parallel, I rationally engineer *C. necator* by knocking out the large-conductance mechanosensitive channel (*mscL*) gene, a membrane protein that facilitates cell survival during hypotonic shock that is found in a wide range of bacteria.[188,189] While either method individually can improve the susceptibility of the bacteria to osmolysis, I then show that combining these two methods in a single strain (*i.e.*, one that is both halotolerant and lacks the *mscL* gene) enables significantly higher osmolytic efficiency than either method individually. To measure the osmolytic efficiency of cells lysed upon osmotic downshock, I develop an RFP-based assay to determine the fraction of intracellular contents released to the media. I finally demonstrate that this approach can be expanded to other bacteria by adapting the approach to *E. coli* BL21, a strain routinely used in the production of recombinant proteins. Both the *mscL* gene, and the related small-conductance mechanosensitive channel (*mscS*) gene are knocked out of BL21 to make it susceptible to osmolysis.

4.3 Materials and Methods

Microbial media and culturing methods

All *E. coli* strains were grown at 37 ºC and all *C. necator* strains were grown at 30 ºC unless otherwise stated. Luria Broth (LB) was used as media for all cultures unless otherwise stated. Media were supplemented with kanamycin (50 μg/mL *E. coli*, 200 μg/mL *C. necator*) and/or carbenicillin (100 μg/mL) as appropriate. All liquid cultures were shaken at 200 RPM.

Adaptive laboratory evolution

The halotolerance of *Cupriavidus necator* was improved by adaptive laboratory evolution (ALE) in 10-mL batch cultures. Wild-type *C. necator* H16 was grown in 50-mL tubes with 10 mL LB medium with NaCl starting at 15 g/L (final concentration). After 24 hours of growth, cells were passaged into 10 mL fresh LB media in 50-mL tubes at an initial optical density of A_{600}=0.001. At the end of each passage, the average growth rate was calculated from the initial and final culture densities, assuming constant exponential growth. When the average growth rate either plateaued or exceeded 0.3 hr^{-1}, the salt concentration of the culture was increased by 0.25% (w/v) NaCl. This was repeated for 30 passages. Cells were plated every several passages on LB agar plates to ensure the cultures were free of contamination. The final passage was plated on LB agar with 3% NaCl (w/v, final concentration) and a single colony was selected for further experiments, with the strain named *C. necator* ht030b.

The growth rate of strain ht030b was compared to that of wild-type *C. necator* H16 at elevated salt concentrations. Overnight cultures of each respective strain were inoculated into four 1-mL

volumes of LB supplemented with 3.25% NaCl (w/v, final concentration) in a 24-well plate at a cell density of A_{600}=0.01 and grown overnight at 30 ºC. Absorbance measurements (600 nm) were taken every hour.

Table 4.1: Strains and plasmids used in this chapter

Strain/Plasmid	Description	Source
Strains		
C. necator H16	Wild-type *Cupriavidus necator* strain	DSM 428
C. necator H16 *ΔmscL*	*C. necator* strain deficient in gene encoding large-conductance mechanosensitive channel	This work
C. necator ht030b	*C. necator* strain with improved halotolerance following 250 generations of adaptive laboratory evolution	This work
C. necator ht030b *ΔmscL*	Adapted halotolerant *C. necator* strain deficient in gene encoding large-conductance mechanosensitive channel	This work
E. coli WM3064	DAP-auxotrophic *E. coli* donor strain used for conjugation of *C. necator*	William Metcalf (UIUC)
E. coli BL21	*E. coli* B strain deficient in Lon and OmpT proteases widely used in protein expression	New England Biolabs
E. coli BL21 *ΔmscL*	*E. coli* BL21-derived strain deficient in gene encoding large-conductance mechanosensitive channel	This work
E. coli BL21 *ΔmscL ΔmscS*	*E. coli* BL21-derived strain deficient in genes encoding large-conductance mechanosensitive channel and small-conductance mechanosensitive channel	This work
Plasmids		
pBADTrfp	araBAD promoter, T7-stem loop, Kan^R, mRFP1 expression gene. Addgene #99382	[55]
pMQ30k	pMQ-30 derivative with Kan^R marker; SacB sucrose sensitivity gene; integrating plasmid used for gene deletion in *C. necator*	[190]
pMQ30k-ΔmscL	pMQ30k plasmid derivative containing 500 nt upstream and 500 nt downstream of *mscL* gene	This work
pSIJ8	Temperature-sensitive plasmid expressing lambda Red recombinase and flippase recombinase genes; Amp^R; for gene deletion in *E. coli*; Addgene #68122	[191]

Genomic methods

The final strain from the adaptive laboratory evolution, ht030b, was streaked on an LB plate containing 3% (w/v) NaCl. Two colonies were grown overnight in liquid LB containing 3% (w/v) NaCl, and the genome was purified from each sample using a Monarch® Genomic Purification Kit (New England Biolabs). A single colony of wild-type H16 was grown, and the genome was likewise purified as a control. Extracted genomic DNA was provided to the Vincent J. Coates Genomics Sequencing Lab at the University of California, Berkeley (QB3 Genomics, UC Berkeley, Berkeley, CA, RRID:SCR_022170), which prepared 150 bp paired-end Illumina sequencing libraries. These libraries were then sequenced using a NovaSeq 6000 S4 Sequencing System. Single nucleotide polymorphisms and other genomic variants were determined using requisite applications within the Geneious Prime software (version 2022.2.2, https://www.geneious.com). SNP's/variants were called from mapped reads originating from three different samples: one sample of the unevolved, wildtype *C. necator* H16 strain, which served as input to the adaptive laboratory evolution, and two different samples of the evolved strain exhibiting elevated halotolerance.

Paired reads were first trimmed to remove low quality bases, filter out and remove short reads (<10 bp), remove sequencing adapter content, and trim/remove low complexity regions using the 'Trim using BBDuk' application within the software. The 'minimum quality' setting was set to 30 and all other parameters were left at their default values. Reads were then mapped to a *C. necator* H16 reference genome composed of GenBank accession numbers CP039287, CP039288, and CP039289.[192] The application 'Map to Reference' was used for this process with the Sensitivity set to 'Medium-Low Sensitivity-Fast' and all other parameters set to their default values. The application 'Find Variations/SNP's' was then used to identify variations within the mapped assemblies with all parameters set to their default values. Identified variants were then manually filtered to remove those that were not represented with at least 27X coverage, variant frequencies < 90% among mapped reads covering the candidate variant position, and those exhibiting a strand bias <25% or >75%. Tandem repeat variants > 5bp were also filtered out and not considered further.

Variants were first called from reads originating from the unevolved *C. necator* H16 sample in order to identify differences between this assembly and the reference genome. Variations found to be unique to either of the evolved populations and not present in the unevolved *C. necator* H16 sample assembly, and meeting aforementioned criteria, were considered. Also considered were variations that were found in the *C. necator* H16 unevolved samples but not found in the evolved populations.

Transformation of plasmids to Cupriavidus necator

C. necator strains were transformed with plasmids in a two-step method in which the plasmids were first transformed to chemically competent *E. coli* WM3064 cells by heat shock, followed by conjugation of the plasmid from the WM3064 donor strain to *C. necator*. Strain WM3064 was a gift from William Metcalf (University of Illinois). Chemically competent WM3064 cells were made as follows. WM3064 cells were cultured in LB containing diaminopimelic acid (DAP, 0.3 μM) to an optical density of A_{600}=0.4. Cells were chilled on ice for 20 min before being pelleted via centrifugation at 4,000 g for 10 min. Cells were resuspended in ice cold 100 mM $CaCl_2$ solution and incubated on ice for one hour. Cells were then centrifuged at 4,000 g and resuspended in 100

mM $CaCl_2$ solution with 10% glycerol at 50x the original cell concentration. Cells were stored in 50 µL aliquots at -80 ºC until needed.

All *C. necator* strains listed in Table 4.1 were transformed with the red fluorescent protein (RFP) expression plasmid pBADTrfp via conjugation using *E. coli* WM3064 as a donor, following the protocol from Windhorst *et al.*[65] pBADTrfp was a gift from Nathan Hillson (Addgene plasmid # 99382; http://n2t.net/addgene:99382; RRID:Addgene_99382).[55] pBADTrfp was transformed into chemically competent WM3064 cells using heat shock and positive clones were selected for on LB agar plates containing DAP and kanamycin (50 µg/mL) following a 1-hour outgrowth in SOC medium. The *C. necator* strain and the transformed WM3064 strain were both grown overnight in LB and LB with DAP and kanamycin, respectively. The following day, the two cultures were inoculated into a fresh culture of the same media and were allowed to grow until the optical density of each culture reached A_{600}~0.5. The WM3064 culture was washed twice with LB DAP, and 0.75 mL of each culture was mixed. This mixture was pelleted by centrifugation at 8,000 g for 10 min, resuspended in 100 µL of LB-DAP, plated on a nitrocellulose membrane on an LB DAP plate, and incubated at 30 ºC for 18 hours. The filter was then resuspended in 2 mL of LB with kanamycin (200 µg/mL) and 50 µL was plated on an LB agar plate with kanamycin (200 µg/mL). The conjugation plate was incubated at 30 ºC for two days. Proper transformation of the plasmid was confirmed via colony PCR.

Gene deletion in Cupriavidus necator

Strains lacking the *mscL* gene were generated following a method relying on integrative plasmids and sucrose counterselection adapted from Windhorst *et al.*[65] A gene fragment containing a 500 nucleotide region matching the region upstream of the *mscL* gene in *C. necator* H16 followed by a 500 nucleotide matching the region downstream was synthesized by IDT DNA Technologies. Overhang regions matching 20 nucleotide-long regions upstream and downstream of EcoRI and BamHI cut sites, respectively, were added by PCR, and the fragment was assembled with the linearized pMQ30k vector by Gibson Assembly,[193] yielding the plasmid pMQ30k-ΔmscL. This plasmid was transformed into *C. necator* H16 and ht030b via conjugation with WM3064 as described above, and cells were selected on an LB agar plate with kanamycin (200 µg/mL). Kanamycin-resistant colonies were then grown overnight in liquid LB supplemented with kanamycin (200 µg/mL). This culture was then passaged in a 1000-fold dilution into LB without antibiotics and cultured for 24 hours. The cells were plated on an LB agar plate supplemented with 15% (w/v) sucrose for counterselection. Proper gene deletion was confirmed by colony PCR and Sanger Sequencing.

Gene deletion in E. coli BL21

The *mscL* gene was deleted from *E. coli* BL21 using a lambda Red recombination system as has been established previously.[191] A gene cassette, containing a kanamycin resistance gene flanked by a flippase recognition target (FRT) site on each end, and with homology arms matching 120 bp upstream and downstream of the *E. coli* BL21 *mscL* gene on the 5'- and 3'- termini, was synthesized by Integrated DNA Technologies. Chemically competent BL21 cells (New England Biolabs) were transformed with pSIJ8, a temperature-sensitive plasmid that contains an arabinose-inducible λ-Red recombinase gene and a rhamnose-inducible flippase recombinase gene. pSIJ8 was a gift from Alex Nielsen (Addgene plasmid # 68122 ; http://n2t.net/addgene:68122 ; RRID:Addgene_68122).[191] Strains containing the pSIJ8 plasmid were grown at 30 ºC to maintain plasmid stability. BL21 pSIJ8 was grown in 15 mL of Terrific Broth (TB) medium (supplemented

with carbenicillin) until reaching a cell density of A_{600}=0.35, followed by a 45-minute induction with arabinose (2 mg/mL, final concentration). Cells were then made electrocompetent by four consecutive wash steps in chilled 10% (v/v) glycerol solution, which concentrated cells ~100-fold.

On ice, 5 μL (250 ng) of the synthetic DNA cassette were added to 50 μL of electrocompetent cells and cells were electroporated (1.8 kV, 1 mm gap, BTX Gemini X2). Cells were recovered with 950 μL TB for 3 hours. Cells from outgrowth were pelleted and resuspended in 200 μL TB, and cells were plated on an LB agar plate with kanamycin and carbenicillin and grown for 36 hours. A single colony was selected and grown in LB with kanamycin and carbenicillin overnight. The following day, the culture was washed in LB, diluted to a cell density of A_{600}=0.1, and flippase expression was induced for 4 hours with 50 mM L-rhamnose, which removed the integrated kanamycin gene from the BL21 genome. Serial dilutions were performed and cells were plated on LB agar with carbenicillin and grown overnight. Correct gene deletions were verified by colony PCR. This strain was saved for further experiments.

The *mscS* gene was then deleted from the BL21 *ΔmscL* strain using a similar DNA cassette with homology arms matching 120 bp upstream and downstream of the *E. coli* BL21 *mscS* gene, following the same protocol. The plasmid pSIJ8 was then cured from both BL21 *ΔmscL ΔmscS* and BL21 *ΔmscL* by growing them overnight in LB at 37 ºC without antibiotics.

RFP-based lysis assay for C. necator cells

An RFP-based lysis assay was developed to measure the osmolysis efficiency, or the fraction of cells that lysed upon resuspension in distilled water. The *C. necator* strain of interest was first transformed with the expression vector pBADTrfp, which contains an arabinose-inducible RFP gene, by conjugation. The *C. necator* strain carrying pBADTrfp was grown overnight in LB (final NaCl concentration 1.5% for the non-halotolerant strain and 3.0% for the evolved strain). For experiments relying on heterotrophic growth, cells from the overnight culture were inoculated into LB (at appropriate salt concentrations). In mid-exponential phase (A_{600}~0.5), cells were induced with arabinose (final concentration 1 mg/mL) and RFP was expressed overnight at room temperature. For experiments relying on organoautotrophic growth, cells from the overnight culture (grown in LB) were inoculated into M9 minimal salts medium supplemented with 4 g/L sodium formate and either 6 g/L NaCl (for the non-halotolerant strain) or 16 g/L NaCl (for the halotolerant strain). Cells were grown overnight, pelleted, and resuspended in fresh medium containing arabinose (final concentration 1 mg/mL). RFP was expressed overnight at room temperature.

For both heterotrophic and organoautotrophic experiments, following overnight expression, the cells were washed once in their respective growth media and the cell concentration was adjusted to A_{600}=1.0. Cells were aliquoted in 1-mL volumes and centrifuged at 4,000 g for 10 minutes. Cells were resupended in an aqueous solution containing various NaCl concentrations representing either an isotonic or hypotonic solution, and were shaken at 30 ºC for 30 minutes. Two 150-μL samples were taken from the well-mixed cell solution and the fluorescence intensity was measured by a Tecan Spark® 10M microplate reader (Ex. 585 nm/ Em. 620 nm). Samples were diluted as needed to ensure measurements fell within the linear range (see Fig. C.4, Appendix C). The rest of the cell solution was centrifuged at 4,000 g for 10 minutes and two 150-μL samples of the supernatant were collected and their fluorescent signal was measured as before in order to quantify

the amount of RFP released to the extracellular space. The ratio of fluorescent signal in the supernatant and cell solutions was taken to be the fraction of cells lysed.

RFP-based lysis assay for E. coli BL21 cells

E. coli strains BL21 *ΔmscL* and BL21 *ΔmscL ΔmscS* were made chemically competent following the same protocol as for WM3064, except for the omission of DAP. Chemically competent BL21 *ΔmscL ΔmscS*, BL21 *ΔmscL*, and wild-type BL21 cells were transformed with pBADTrfp via heat shock and selected for on LB agar plates with kanamycin (50 μg/mL). Osmolysis experiments were performed following the same protocol as for *C. necator*, with minor adjustments. Overnight cultures were regrown at 37 ºC in LB supplemented with the appropriate NaCl concentration. In mid-exponential phase (A_{600nm}~0.5), cells were induced with arabinose (final concentration 1 mg/mL) and RFP was expressed for 3 hours at 30 ºC. The rest of the osmolysis assay follows the exact protocol as for *C. necator*. Samples from the total cell fraction, post-lysis supernatant, and cell pellet were saved for SDS-PAGE.

4.4 Results and Discussion

Adaptive laboratory evolution of C. necator improves halotolerance

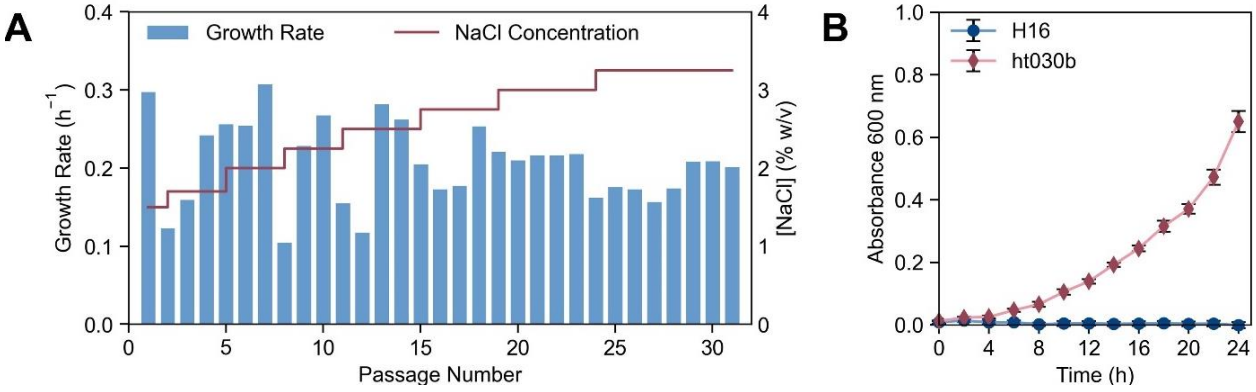

Figure 4.2. Adaptive laboratory evolution yields halotolerant strain of *C. necator*. (A) Results of ALE experiment showing the growth rate (blue bars) and NaCl concentration (red line) at each passage. (B) Growth curve of wild-type *C. necator* strain H16 and evolved strain ht030b in LB containing 3% NaCl (w/v, final concentration). For each data point in (B), mean ± s.d. is displayed (n=4).

Through 30 passages of ALE, accounting for roughly 250 generations of growth, the tolerance of *C. necator* to NaCl was improved from 1.5% to 3.25% (Fig. 4.2A). Microbial behavior during the ALE process was typical compared to studies performed previously. Sharp decreases in growth rate following addition of the stress (in this case NaCl) were regularly observed. Similar to other ALE experiments,[194,195] the steepest increases in cell fitness were observed in early passages, with growth rate mostly plateauing in later passages. For example, the NaCl tolerance of *C. necator* improved by 1.25% (from 1.5% to 2.75%) in the first fifteen passages, while only improving an additional 0.5% in the later fifteen passages. The osmolarity of 3.25% (w/v) NaCl, where the ALE began to plateau, is nearly identical to that of seawater. Given the existence of extremely halophilic proteobacteria such as *Halomonas* sp., it is plausible that the halotolerance of *C. necator* could improve with further rounds of ALE. However, it is likely these adaptations would occur significantly more slowly than the initial improvements observed here.

The growth of evolved strain ht030b, in comparison to the wild-type H16 strain, was tested in LB containing a (final) concentration of 3.25% NaCl (Fig. 4.2B). Under the conditions tested, the wild-type H16 did not display measurable growth over a 24-hour period while strain ht030b grew with a growth rate of 0.16 h^{-1}. I do note that when seeded with a high enough starting cell concentration, *C. necator* H16 displays some growth in LB with 3.25% NaCl, albeit at a significantly lower rate as compared to ht030b (Fig. C.1, Appendix C). In any case, the strain generated through the ALE displays a clear phenotypic difference from the wild-type strain. This growth rate is significantly lower than the growth rate of wild-type *C. necator* in LB containing the standard 0.5% NaCl (0.45 h^{-1}). Therefore, despite the improved fitness compared to the wild-type, strain ht030b grows more slowly as salt concentration is increased, introducing a tradeoff between higher media salinity and growth rate.

Genomic analysis of ht030b

Genomic sequencing and the subsequent variant analysis identified five mutations (meeting the filtering criteria applied) that were acquired by strain ht030b throughout the course of the ALE (Table 4.2). Four mutations were present only in the ht030b genome, but not in either the reference H16 genome used for mapping or in the unevolved H16 genome sequenced. Each caused substitutions of a single amino acid in a different protein: a PAS domain-containing sensor histidine kinase *NtrY*, a peptidoglycan D,D-transpeptidase *mrdA*, an acetolactate synthase gene, and an IS66 family transposase gene. One SNP, causing a point substitution in a *YgcG* family protein, was surprisingly found only in the H16 genome, but not in the evolved strain ht030b or in the reference genome. This indicates that this mutation was present in the starting H16 strain but reverted to the original sequence as found in the reference genome throughout the course of the ALE. Unfortunately, the function of this gene family is unknown (although it is predicted to have transmembrane domains), limiting the understanding of the mechanism by which this could affect halotolerance.

The *mrdA* gene encodes an enzyme in the penicillin-binding protein 2 (PBP2) family, and is involved in the synthesis of the peptidoglycan cell wall in bacteria, particularly in cell elongation.[196] Penicillin-binding proteins have been shown to be important to cell survival under conditions of high salt stress, perhaps in response to the morphological changes (*i.e.* cell plasmolysis) that occur during osmotic upshifts.[197,198] Hocking *et al.* demonstrated recruitment of an *mrdA* homolog to the cell division site in *Caulobacter crescentus* in response to increases in salinity,[199] suggesting the regulation of this gene is indeed involved in the osmotic stress-response mechanism. Therefore, it is conceivable that a change in either expression level or activity due to the detected mutation in the *mrdA* gene causes structural changes of the cell wall in *C. necator* ht030b, leading to enhanced survival in high-salt conditions. Interestingly, mutations of this type seem to be highly conserved in bacterial species. Strain ht030b displays a T563I mutation, substituting the polar amino acid threonine with a branched chain nonpolar amino acid isoleucine in that position. Notably, 63 out of the 72 diverse bacterial species represented in the *mrdA* protein family model in the TIGRFAM database (TIGR03423) contain a branched chain amino acid (I, L, or V) at that position, while only three contain a polar residue.[200] Although elucidating the precise mechanism would require further investigation, it is plausible that this mutation is a major contributor to the enhanced halotolerance of strain ht030b.

Table 4.2: Mutations detected in H16 and ht030b strains [a]

Chromosome (NCBI Accession No.)	Genome Coordinates	Gene/ Encoded Protein	Mutation (CDS position)	Effect	SNP Present In [b]
1 (CP039287)	3982709	PAS domain-containing sensor histidine kinase	G→A (1606)	Substitution (R→C)	ht030b
1 (CP039287)	131230	*mrdA* Peptidoglycan D,D-transpeptidase	C→T (1688)	Substitution (T→I)	ht030b
1 (CP039287)	791503	*YgcG* family protein	C→A (757)	Substitution (G→W)	H16
2 (CP039288)	829590	Acetolactate synthase	C→T (1490)	Substitution (T→I)	ht030b
pHG-1 (CP039289)	138984	IS66 family transposase	T→A (206)	Substitution (E→V)	ht030b

[a] The genomic datasets generated and analyzed in this chapter are available in the Sequence Read Archive (https://www.ncbi.nlm.nih.gov/bioproject/906984).

[b] Whole genome sequences of both the parent strain H16 and the evolved strain ht030b were obtained to identify the mutations that arose throughout the ALE. Both genomes were first mapped to the reference *C. necator* H16 genome obtained by Little *et al*,[192] and differences between each of the two genomes sequenced and the reference genomes were identified. Several of these variations were found in both the parent strain and evolved strain, indicating these mutations were not acquired throughout the ALE. Five variations (meeting quality control criteria described in the Methods) were unique to either the parent or evolved strain. Four variations (relative to the reference genome) were found in ht030b, while one was found in the unevolved H16 strain. This is denoted by the column labeled "SNP Present In".

A thiamine pyrophosphate-binding protein with putative acetolactate synthase activity was found with a mutation in ht030b. Acetolactate synthase catalyzes the first step in the synthesis of branched-chain amino acids.[201] A study of cells from diverse origins carried out by Sévin *et al.* found a negative correlation between halotolerance and the intracellular concentration of branched-chain amino acids.[202] Amino acids and amino acid derivatives can be accumulated as compatible solutes as a mechanism of halotolerance.[203,204] Therefore, changes to enzymes involved in the synthesis of amino acids could divert metabolic fluxes leading to the synthesis of these compatible solutes, although the exact mechanism of this is difficult to predict.

The histidine kinase gene (*NtrY*) mutated in the ALE is predicted to regulate nitrogen metabolism and the assimilation of nitrate.[205,206] The NtrXY system and the related NtrBC system have been shown in other species to regulate the production and degradation of nitrogen-containing compounds such as arginine and ectoine,[207,208] which again may affect osmotolerance due to the regulation of compatible solutes. The final gene determined to have been altered through the ALE was a transposase of the IS66 family. However, no significant transposition was determined in the variant analysis. In short, several of the unique mutations accumulated by strain ht030b through ALE could conceivably impart halotolerance, although the precise mechanisms are unclear and outside the scope of the present study.

Deletion of mscL gene from C. necator enhances cell lysis

A putative *mscL* gene was identified in the *C. necator* genome by a protein BLAST search of the homologous gene found in *E. coli*. The entire gene was deleted from *C. necator* H16 and successful *ΔmscL* mutants were screened by colony PCR and verified by Sanger Sequencing. Deletion of the *mscL* gene led to no obvious deleterious effects on the microbe, besides the desired sensitivity to osmotic downshock. Growth curves of both wild-type and mutant strains were obtained under identical conditions (Fig. C.2, Appendix C). The growth rate of the mutant H16 *ΔmscL* (0.43 ± 0.01 h^{-1}) was not statistically different from the growth rate of wild-type H16 (0.45 ± 0.01 h^{-1}), indicating that the genome deletion did not impact overall cellular fitness.

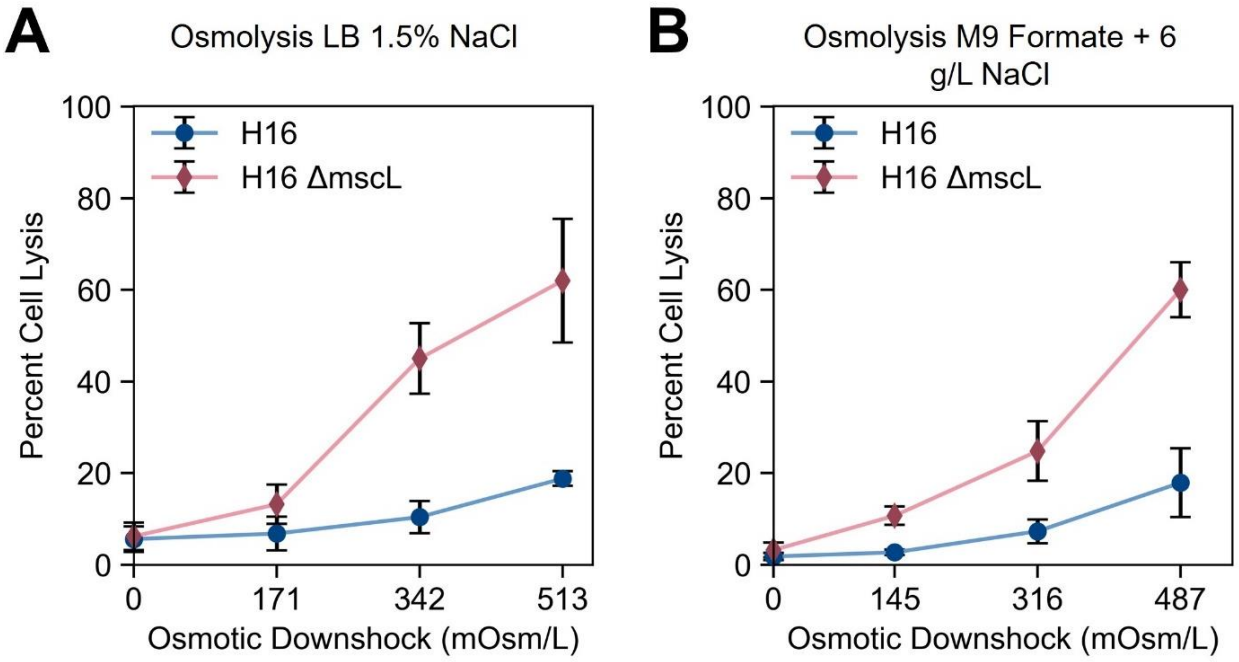

Figure 4.3. Osmolysis efficiency, calculated as a fraction of RFP recovered in supernatant compared to total RFP content following osmotic shock (see methods), as a function of osmotic downshock magnitude for wild-type *C. necator* H16 (blue circles) and mutant *C. necator* H16 *ΔmscL* (red diamonds) following growth in (A) LB with 1.5% (w/v) NaCl (final concentration) and (B) M9 sodium formate (4 g/L) medium supplemented with 6 g/L NaCl. Differences in values on the x-axis of the two graphs reflect slight differences in starting osmolarities of the two media tested. For each data point, the mean ± s.d. is displayed (n=6).

Both wild-type H16 and the mutant H16 *ΔmscL* were transformed with pBADT-rfp, containing the RFP gene under an inducible arabinose promoter, and the effect of the *mscL* gene deletion on the fraction of cells lysed upon osmotic downshock was tested. LB was supplemented with NaCl such that the final concentration of NaCl in the medium was 1.5% (w/v). This was the highest salt concentration at which the wild-type *C. necator* H16 strain still displayed measurable overnight growth (Fig. C.3, Appendix C), maximizing the possible magnitude of osmotic downshock while still enabling functional cell growth. As described in the methods section in detail, RFP was expressed in both strains overnight, and washed cells were resuspended either in distilled water or an aqueous solution of 0.5%, 1%, or 1.5% (w/v) NaCl. After 30-minute incubations, cells were pelleted and the ratio of red fluorescence intensity found in the supernatant to the fluorescence

intensity of the whole solution was taken to be the osmolysis efficiency, or the fraction of cells lysed due to osmotic downshock.

For both wild-type and knockout strains, the highest osmolysis efficiency was observed when cells were resuspended in distilled water, as this caused the highest magnitude of osmotic downshock (0.51 OsM) and therefore the highest osmotic pressure (1.3 MPa). However, significantly greater cell lysis efficiencies were achieved with the *mscL* knockout strain (62%) compared to the wild-type (19%). This demonstrates that the native function of the putative *mscL* gene in *C. necator* is involved in the cell survival response following osmolarity changes, as it is in other bacteria. Following downshock, most of the cells in the wild-type *C. necator* sample remain intact, whereas a majority of cells are lysed when the gene is deleted. Deletion of this gene, therefore, is a simple strategy to increase the osmolysis susceptibility of microbial hosts and aid in the recovery of intracellular biomolecules.

Similar levels of background cell lysis, which I define as cell lysis observed when resuspended in an isotonic solution, are observed in both the *mscL*$^{+}$ and *ΔmscL* strains (<5%). Therefore, the *mscL* gene knockout does not make *C. necator* significantly more fragile under normal conditions. The increase in cell lysis only occurs upon osmotic downshock. This, along with the lack of change in the growth rate in H16 *ΔmscL* mentioned previously, suggests that the *mscL* gene is not critical to *C. necator* survival under normal conditions.

This experiment was repeated in defined medium using sodium formate as a sole carbon and energy source to evaluate osmolysis following autotrophic growth. Although there is interest in using *C. necator* for bioproduction under heterotrophic conditions,[171,209] autotrophic production of biomolecules using molecules such as formic acid or hydrogen gas as energy sources enables electromicrobial production. *C. necator* was grown in M9 mineral medium with 4 g/L sodium formate as a carbon source with variable concentrations of added sodium chloride. The maximum amount of NaCl that could be added to M9 medium was determined to be 6 g/L (Fig. C.3, Appendix C). The osmolarity of the medium with this much added salt (0.49 OsM) is close to the osmolarity of LB with 1.5% NaCl (0.51 OsM). Nearly identical trends were seen in experiments with LB and M9 formate, with both H16 and H16 *ΔmscL* experiencing greater osmolytic efficiencies as the magnitude of osmotic downshock increased. The mutant strain lysed significantly more than the wild-type strain (60% vs 18%) when resuspended in distilled water, similar to the LB experiment. While not surprising, as the *mscL* gene is not known to affect cellular metabolism and therefore the effect of its absence should be indifferent towards the carbon metabolism used, this does demonstrate that this strategy can be used to aid downstream recovery for both heterotrophic and autotrophic processes.

Osmolysis efficiency of C. necator ht030b and ht030b ΔmscL

The evolved halotolerant strain of *C. necator* was transformed with the plasmid pBADTrfp and osmolysis was tested following growth in LB supplemented with 3% NaCl (w/v, final concentration). Cells were resuspended in aqueous solutions ranging from 0% (distilled water) to 3% NaCl in 0.5% increments and lysis efficiency was measured as before (Fig. 4.4A). As expected, the maximum cell lysis (47%) was observed after resuspension in distilled water, corresponding to an osmotic pressure change of 1.03 OsM. This is more than double the lysis efficiency observed when resuspending wild-type *C. necator* H16 in distilled water (19%, Fig. 4.3A), indicating that adapting bacteria for growth in higher salinities allows for higher levels of osmolysis. Therefore,

both strategies described in Figure 4.1, adapting the microbial host to greater halotolerance and deleting the large-conductance mechanosensitive channel gene, led to enhanced cell lysis in *C. necator*.

These two strategies were then combined in a single strain by deleting the *mscL* gene from the evolved ht030b strain. Successful gene deletion was confirmed by colony PCR and the resultant strain was transformed with the RFP-expressing plasmid. The experiment performed on ht030b was then performed on this new strain. As with the unevolved *C. necator*, deletion of the *mscL* gene significantly enhanced the fraction of cells lysed, with over 90% osmolysis efficiency observed when ht030b *ΔmscL* was resuspended in distilled water (Fig. 4.4A). The combination of the two strategies described led to a greater osmolysis efficiency than either strategy independently. While the osmolysis efficiency of wild-type *C. necator* was only 19% at its maximum, nearly complete lysis of ht030b *ΔmscL* was achieved (compare Fig. 4.3A and Fig. 4.4A). The combination of ALE to increase halotolerance and gene deletion of mechanosensitive channels is clearly an effective method for engineering osmolytic susceptibility in a microbial host, which can greatly simplify downstream bioprocessing.

Interestingly, the magnitude of osmotic downshock, and therefore the magnitude of osmotic pressure, does not alone determine the cell lysis efficiency. For both *mscL*$^+$ and *ΔmscL* strains, significantly greater cell lysis occurred upon moving cells from 1.5% $NaCl_{(aq)}$ to distilled water (19% for *mscL*$^+$ and 62% for *ΔmscL*) than from 3.0% to 1.5% $NaCl_{(aq)}$ (8% for *mscL*$^+$ and 13% for *ΔmscL*), despite equivalent osmotic pressure changes in each scenario. Similar observations can be made in the experiments with formate media. The salinity of the resuspension solution also plays a role in determining the efficiency of cell lysis. It's possible that certain membrane proteins take on different conformations in deionized water than they do under normal salt concentrations. Therefore, the cells would experience greater cell lysis in distilled water despite the same osmotic pressure change.

While *C. necator* ht030b grew moderately well in 3% NaCl under heterotrophic conditions (*i.e.*, in LB), it did not grow as well at equivalent salinities during organoautotrophic growth. When M9 formate was supplemented with various concentrations of NaCl, *C. necator* ht030b did not significantly grow when the added NaCl concentration exceeded 16 g/L (Fig. C.3, Appendix C). The total osmolarity of this medium was 830 mOsm/L, which is equivalent in ionic strength to a roughly 2.4% (w/v) NaCl solution. Moderate halotolerance is usually effected by the accumulation of compatible solutes, including sugars and amino acids (and their derivatives), inside the cell to balance osmotic pressure.[204] Rich media such as LB contain an abundance of amino acids, which can easily be imported by the cell and used as compatible solutes directly or converted to compatible solutes. Therefore, it is not particularly surprising to see slight differences in halotolerance in the two media tested.

Strains ht030b and ht030b *ΔmscL* were grown in M9 formate supplemented with 16 g/L NaCl, and the RFP lysis assay was performed. Various solutions ranging from distilled water to 2.4% NaCl were tested to measure cell lysis in response to various magnitudes of osmotic downshock. As in all other experiments, the deletion of the *mscL* gene leads to significantly greater osmolysis efficiencies, reaching 98% of ht030b *ΔmscL* cells compared to 49% of ht030b cells. These strategies for engineering susceptibility to lysis by osmotic downshock are thus useful not only for heterotroph-based bioprocesses, but autotrophic processes as well.

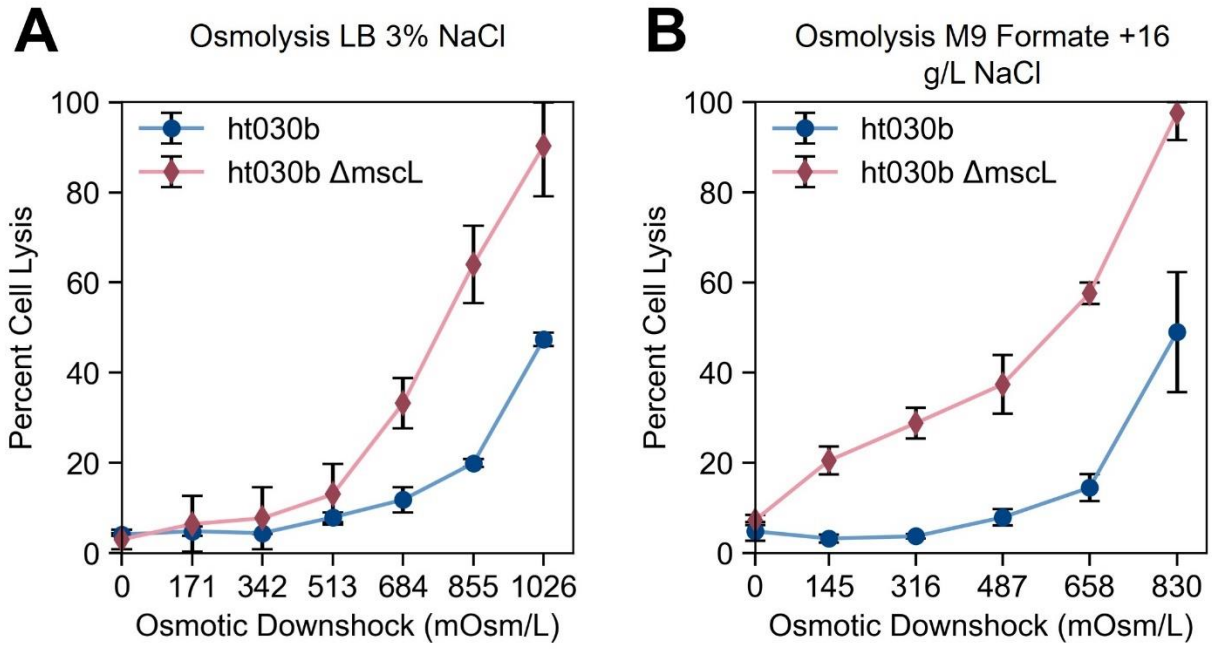

Figure 4.4. Effect of combined *mscL* gene knockout and improved halotolerance on osmolysis in *C. necator*. Osmolysis efficiency as a function of osmotic downshock magnitude for ht030b (blue circles) and ht030b *ΔmscL* (red diamonds) following growth in (A) LB with 3.0% NaCl (w/v, final concentration) and (B) M9 sodium formate (4 g/L) medium supplemented with 16 g/L NaCl. Differences in values on the x-axis of the two graphs reflect differences in starting osmolarities of the two media tested. For each data point, mean ± s.d. is displayed (n=6).

Knockout of mscL and mscS genes in E. coli BL21 enables significant protein release

Due to the success of the osmolysis strategy in *C. necator*, I explored whether this technique could be broadly applied to other microbial hosts. *E. coli* BL21, a derivative of *E. coli* B strain deficient in Lon and OmpT proteases routinely used for production of recombinant proteins, was chosen as a second model system to evaluate this strategy. Because *E. coli* BL21 could already grow in elevated NaCl concentrations, maintaining around half of its maximum growth rate even in 4% NaCl (Fig. C.5, Appendix C), further adaptation of the strain was unnecessary. Therefore, only the effect of the mechanosensitive channel gene deletions was tested.

The *mscL* gene was successfully knocked out of *E. coli* BL21, as confirmed by colony PCR, and the resultant strain was transformed with the RFP-expressing plasmid pBADTrfp. The RFP-based osmolysis assay was then performed as it was for *C. necator* (with minor variations, see methods for details) comparing the engineered and wild-type strains. Cultures of these strains were grown in LB containing 4% (w/v) NaCl and cell lysis was tested following resuspension in distilled water, a 4% NaCl isotonic aqueous solution, or B-PER™, a commercial bacterial lysis reagent (ThermoFisher Scientific) used as a positive control. As it did in *C. necator*, deleting the *mscL* gene from *E. coli* BL21 significantly increased the lysis efficiency in distilled water (41% vs. 15%). Although this is encouraging evidence that this strategy is broadly applicable in many bacterial hosts, ~40% recovery of a given macromolecule product is likely too low in most practical applications. To improve the lysis efficiency, a second gene in the mechanosensitive channel family, the small-conductance mechanosensitive channel (*mscS*) gene, was also deleted

from BL21. The double knockout demonstrated increased sensitivity to osmotic shock, reaching an average cell lysis efficiency of 75% (and efficiency as high as 81% in individual trials) following growth in LB with 4% NaCl (Fig. 4.5A). While a majority of the biomolecule product RFP is separated from the cell biomass through osmolysis, the fractional recovery of the product will be moderately lower than when using detergent-based lysis reagents such as B-PER, which consistently demonstrated near 100% efficiency.

Following the RFP-based assay, SDS-PAGE was performed on the whole-cell, supernatant, and cell pellet fractions post-osmolysis (Fig. 4.5C). Although more difficult to quantify exactly, the results of the gel are roughly consistent with the results of the RFP assay. Almost no protein is observed in the supernatant for the wild-type BL21 cells following resuspension in distilled water, while a significant fraction is for BL21 *ΔmscL ΔmscS* cells. It appears that a greater fraction of the total protein content is present in the supernatant fraction compared to the cell pellet fraction in the double knockout cells, consistent with the results of the RFP assay. Taken with the RFP assay results, this demonstrates that the BL21 *ΔmscL ΔmscS* strain can be used to greatly simplify the recovery of expressed proteins, while maintaining a high protein recovery.

This osmolysis efficiency is slightly lower than the >90% cell death rate observed by Levina *et al.* in a double knockout *ΔmscL ΔmscS* strain of *E. coli* K-12 derivative Frag1 following similar osmotic downshock.[189] This difference could be due to the different assays used to measure the effects of osmotic downshock. Levina *et al.* measured cell viability by counting colony-forming units on agar plates while release of intracellular protein is measured here. It is possible that more than 75% of cells become non-viable following downshock, yet their membranes remain intact enough to retain the cytosolic contents.

To test the effect of media salt concentration on osmolysis efficiency, this experiment was repeated in LB with NaCl concentrations of 0.5%, 1%, 2%, and 3% (w/v, Fig. 4.5B). I note that 0.5% and 1% NaCl concentration are the two salt concentrations found in most LB formulations. Even in the double knockout strain, little more than background levels of cell lysis were observed for NaCl concentrations of 2% or less. Low (18%), but statistically significant ($p<0.013$), levels of cell lysis were observed for BL21 *ΔmscL ΔmscS* beginning at a media NaCl concentration of 3%. A sharp increase in the cell lysis efficiency occurred with an increase from 3% to 4% NaCl, suggesting the critical osmotic pressure required for cell lysis for most cells in the population falls within that range. As expected, the mutant *E. coli* strain experienced the greatest degree of cell lysis upon osmotic downshock following growth in the media with the highest osmolarity tested (4% NaCl). However, under these conditions, the growth rate of *E. coli* BL21 was significantly affected. A roughly linear decrease in specific growth rate of BL21 with increasing NaCl concentrations is observed, a trend demonstrated previously.[103] Increasing the salt concentration in the media from 0.5% to 4% w/v NaCl coincided with a growth rate decrease from 1.6 h^{-1} to 0.88 h^{-1}.

In practical applications, a tradeoff would be encountered in which greater product recovery via osmolysis would come at the cost of a slower microbial growth rate. However, for many applications, a decreased growth rate may be worthwhile. The specific growth rate of 0.88 h^{-1} corresponds to a doubling time of roughly 45 min, which is still significantly faster than many microbial hosts. Routine lab-scale protein expression and purification protocols could still be performed in a single day, even at this diminished growth rate, as a seed culture inoculated to an optical density of A_{600}=0.05 could reach mid-log phase (A_{600}=0.5) in around 3 hours. In continuous industrial-scale reactors, productivity is often limited by oxygenation rate rather than specific

growth rate.[210] Therefore, continuous bioreactor systems can likely operate at higher salt concentrations with a similar productivity despite the decrease in growth rate.

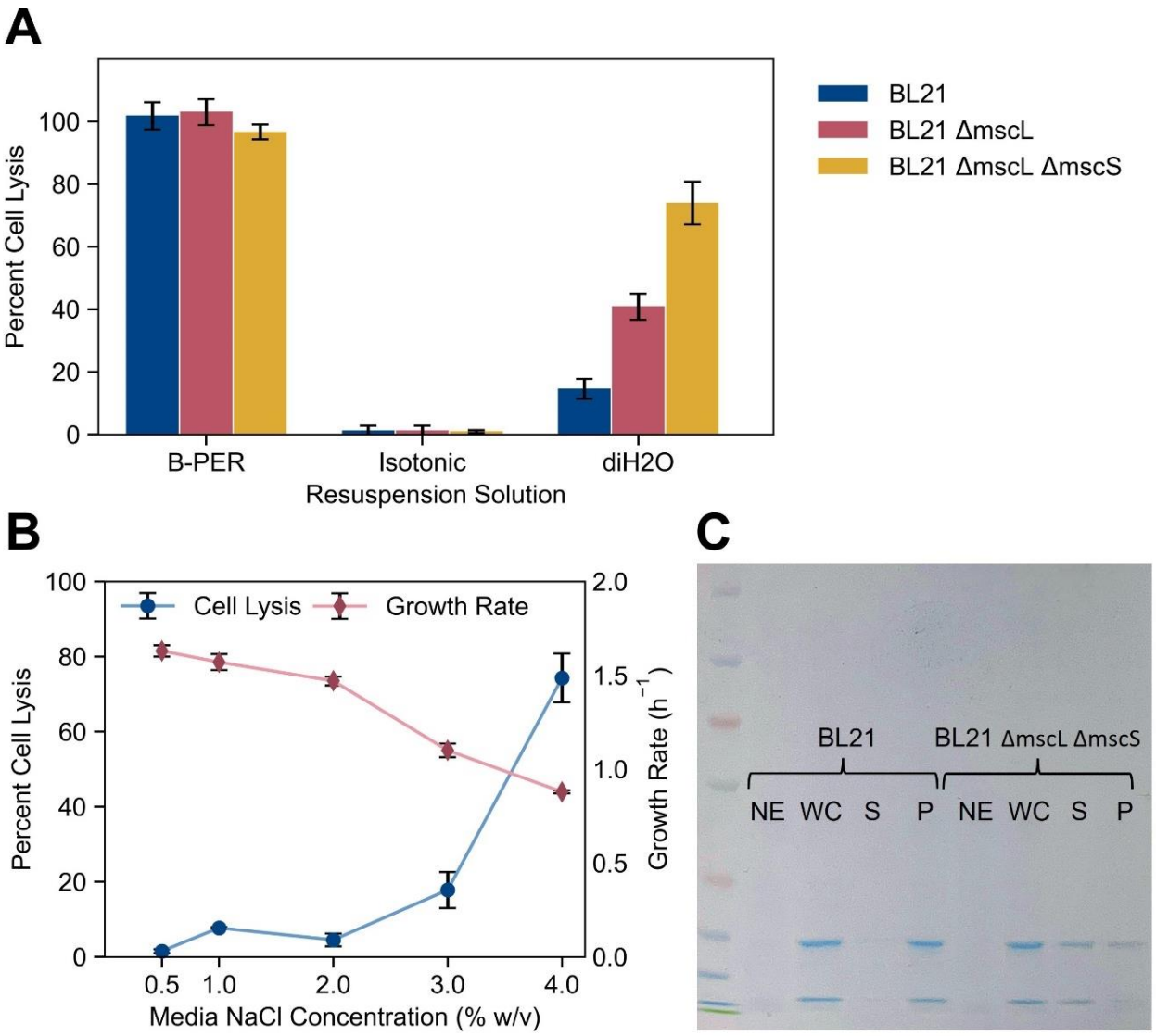

Figure 4.5. Application of mechanosensitive knockout for osmolysis in *E. coli* BL21. (A) Percent cell lysis following growth in LB with 4% NaCl of BL21 (blue), BL21 *ΔmscL* (red), and BL21 *ΔmscL ΔmscS* (yellow) in three different solutions: commercial B-PER™ Bacterial Protein Extraction Reagent; a 4% $NaCl_{(aq)}$ isotonic solution; and distilled water (diH2O); n=6. (B) Growth rate (red diamonds) and osmolysis efficiency (blue circles) of BL21 *ΔmscL ΔmscS* in LB with various (final) NaCl concentrations (n=3). (C) SDS-PAGE gel of various fractions of RFP-expressing BL21 and BL21 *ΔmscL ΔmscS.* NE: cells not expressing RFP, WC: whole-cell fraction, S: post-osmolysis supernatant fraction, P: post-osmolysis cell pellet. For each data point in (A) and (B), the mean ± s.d. is displayed.

Although only a 75% cell lysis efficiency (on average) was attained in these experiments, this efficiency could likely be improved. Slightly higher NaCl concentrations in the media would likely be tolerated by BL21, and if the trend in Figure 4.5B continues, one would expect near complete cell lysis could be achieved. Furthermore, this strain could also be used in conjunction with other cell lysis methods. For example, adding a single freeze-thaw step to the process increased the osmolysis efficiency of BL21 *ΔmscL ΔmscS* grown in LB with 2% NaCl from 4.5% to 22% (Fig.

C.6, Appendix C), while such an increase was not observed for BL21 without the gene deletions. In summary, the engineered BL21 variant becomes more susceptible to cell lysis in distilled water than the original BL21 strain, which can be exploited for simplified protein purification.

4.5 Conclusion

Although downstream bioseparations represent a critical (and costly) component of any biochemical process, most genetic engineering and strain development has been performed to aid in the generation of a product rather than its purification. Focusing on cell lysis as an important step in purification of intracellular bioproducts, I present strategies that utilize adaptive laboratory evolution and rational genome engineering to produce strains that are sensitive to osmotic downshock, and therefore may be used for simplified, osmolysis-based downstream recovery. First, I have shown that *Cupriavidus necator* can be made slightly halotolerant relatively quickly through adaptive laboratory evolution. The evolved strain ht030b was the result of 30 passages of ALE, which improved its halotolerance from 15 to 32.5 g/L NaCl. This adaptation alone improved the maximum efficiency of osmolysis from 19% to 47%. A halotolerant strain of *C. necator* also provides benefits in other areas of electromicrobial production. For example, reactor modeling in Chapters 2 and 3 showed that, in certain EMP applications, effects of salinity-induced toxicity can limit productivity. Therefore, the halotolerant strain of *C. necator* evolved here could be useful in improving productivity of bioprocesses limited by salinity effects.

In parallel, a strain of *C. necator* was engineered by deleting the *mscL* gene, which increased the cell lysis efficiency following osmotic downshock from 19% to 62%. While the putative function of this gene in *C. necator* was inferred by homology to be a large-conductance mechanosensitive channel, I provide the first experimental evidence of its function. I then combined the two strategies in a single strain, *C. necator* ht030b *ΔmscL*, which exhibited the highest cell lysis efficiency of over 90% when grown in LB medium and 99% when grown in M9 formate, demonstrating for the first time the efficacy of combining adaptive laboratory evolution with rational mechanosensitive channel knockouts to enhance cell lysis efficiency.

I then adapted these techniques to develop a strain of *E. coli* BL21, a common strain for protein expression, that is susceptible to osmolysis. Two gene knockouts (*mscL* and *mscS*) were required for significant (75%) protein release, though adaptive laboratory was unnecessary. Previous experiments focusing on the *mscL* and *mscS* genes, which have included knockouts, were done primarily to study the function of these genes. Therefore, phenomena such as cell viability have been studied rather than biomacromolecule release. I provide, to my knowledge, the first study of mechanosensitive channel knockouts to aid the recovery of intracellular macromolecules.

I have demonstrated significant cell lysis in both *E. coli* and *C. necator*. As many (especially non-marine) bacteria contain the *mscL* gene[188], and adaptive laboratory evolution is suitable for most bacterial strains, either of the strategies described here for increasing osmolysis should be broadly applicable. Whether this method is also applicable to gram-positive bacteria or archaea given their different cell membrane structures[211] remains an interesting avenue for future exploration, although previous research suggests *mscL* deletions in gram-positive *B. subtilis* causes increased cell death upon osmotic downshock.[212] I have also shown that *C. necator* is much more sensitive to osmotic downshock compared to *E. coli*. This is interesting as *C. necator* and *E. coli* are both gram-negative proteobacteria and therefore have similar membrane structures. Under similar

osmotic downshocks (equivalent to 3% NaCl) the wild-type *C. necator* strain had a lysis efficiency of 47% compared to only about 3% for *E. coli* cells. This large disparity was also seen among the *ΔmscL* versions of each species, with *C. necator* experiencing 90% cell lysis and *E. coli* experiencing only 14% cell lysis following a 3% (w/v) NaCl osmotic downshock (Fig. C.7, Appendix C). Therefore, although this work has shown that knocking out mechanosensitive channel genes does increase osmolytic sensitivity in both strains, the cell lysis efficiencies can vary from strain to strain. This strategy must therefore be tested in individual strains to assess the viability of the osmolysis technique.

While the cell lysis efficiencies obtained through osmolysis were quite high (90% for *C. necator* and 75% for *E. coli* BL21), other established methods of cell lysis can achieve higher values. For example, this work demonstrated that detergent-based methods routinely achieve near total cell lysis (Fig. 4.5A), while Sauer *et al.* showed that high-pressure homogenization leads to similarly high (95-98%) cell lysis efficiencies.[213] However, some methods of cell lysis, such as repeated freeze-thaw cycles are less effective (~50% protein recovery).[214] I also note that all of the values mentioned will depend on the bacterial strain, scale of operation, and other conditions, making direct comparison to other methods in the literature subject to some uncertainty.

Whether the high cell lysis fractions obtained through osmolysis are sufficiently high for a given bioprocess will depend on a number of factors, including the product. It is likely that low-value products such as biopolymers would be more suitable for osmolysis compared to high-value products such as therapeutic proteins. If the product of interest is very valuable, then the cost savings of the simplified cell lysis method will likely not outweigh the marginal gain of value from using more expensive but more effective cell lysis methods. Therefore, the efficacy of osmolysis will depend on the specific application, including the strain used and biomolecule produced. Economic and environmental impact concerns should also be taken into consideration in determining whether osmolysis or a traditional cell lysis method is used prior to downstream product recovery. However, this chapter has conclusively demonstrated two broadly applicable strategies to improving the susceptibility of bacteria to osmolysis that are both independently effective and compatible with each other in a single strain. These results serve as a foundation for potentially simpler and cheaper downstream biomolecule processing, an area often overlooked in fundamental research.

4.6 Acknowledgements

I would like to thank my co-authors on the article that this chapter is adapted from: Kyle B. Sander, Craig S. Criddle, Adam P. Arkin, and Douglas S. Clark. I also thank Dr. Jacob Hilzinger (UC Berkeley), Dr. Anthony Abel (UC Berkeley), and Dr. Sung-Geun Woo (Stanford University) for helpful discussions on experimental design and analysis. This work was supported by the Center for the Utilization of Biological Engineering in Space (CUBES, https://cubes.space/), a NASA Space Technology Research Institute (grant number NNX17AJ31G).

Chapter 5: Metabolic engineering for n-butanol production in *Cupriavidus necator*

5.1 Abstract

In Chapter 3, I developed a techno-economic model for a large-scale EMP process that generates n-butanol as a biofuel. The assessment was predicated on the existence of a bacterial strain capable of converting non-conventional EMP-relevant substrates to n-butanol with high (>90% of theoretical maximum) yields. Moreover, I found in the TEA that high titers are needed for economically feasible separation processes. The hypothetical strain capable of achieving high yield and titers of n-butanol from substrates such as H_2/CO_2, formate, and acetate, however, does not yet exist. To that end, in this chapter I detail efforts toward engineering a strain of *Cupriavidus necator* that can accomplish those goals. I engineered *C. necator* strains with two different n-butanol production pathways and tested butanol biosynthesis using fructose as a carbon source. The better performing pathway led to n-butanol titers as high as 1.12 g/L. This strain can serve as a platform for further optimization to improve the n-butanol yield. I also address limitations on titers by developing a strain of *C. necator* tolerant to n-butanol. Through 30 passages of ALE, which translates to around 275 generations of growth, three strains of *C. necator* exhibiting improved butanol tolerance were produced. The strain with the greatest tolerance to n-butanol, labeled *C. necator* bt530, grew reasonably well in media containing 6 g/L n-butanol, while the wild-type strain H16 could only grow comparably well in 3 g/L n-butanol.

5.2 Introduction

The use of fossil fuels in transportation, accounting for 27% of U.S. greenhouse gas emissions, contributes significantly to the ongoing climate crisis.[215] While fully electric vehicles have become more economically viable in recent years, they still represent less than 1% of vehicles on the road in the U.S. Moreover, some forms of transportation, such as air travel, are difficult to electrify. Therefore, there is an unmet need for carbon-neutral substitutes for liquid fossil fuels, which would substantially reduce the carbon footprint of the transportation sector without requiring significant changes to transportation infrastructure. The U.S. alone consumes ~130 billion gallons of gasoline per year,[216] so a successful replacement fuel must be produced in a process that has low carbon emissions over its life cycle while demonstrating both scalability and economic competitiveness.

Biofuels provide an opportunity to replace fossil fuels used in transportation with liquid fuels that can, in theory, be carbon neutral over their life cycle. Ethanol fuel, produced by fermentation of sugars derived from crops such as corn and sugarcane, is still the predominant biofuel commercially available. Metabolic engineering efforts have been employed to produce biofuels with superior energy density and lower water miscibility compared to ethanol, such as higher-chain alcohols, fatty acids, and isoprenoids.[86] However, as noted previously in this dissertation, these bioprocesses have mostly relied on crop-derived sugars as substrates, and therefore introduce challenges such as the high carbon footprint of feedstock crop production, concerns over land use changes, and fears over competition with the food supply.[29,30] As noted in Chapter 1, fermentation of lignocellulosic biomass and algal-based bioprocesses ($2^{nd}/3^{rd}$ generation bioprocesses) have

been proposed as alternatives to traditional biofuel production, yet the economic viability of these strategies is questionable.[34]

Electromicrobial production can address some of these challenges that face biofuel production. As demonstrated in Chapter 2, chemicals produced through EMP can have lower carbon footprints (provided that the electricity comes from a clean source) and land use over their life cycle compared to those produced in traditional glucose-based processes. To realize this vision, the bacterium *Cupriavidus necator*, which can metabolize multiple EMP-relevant substrates (*e.g.*, H_2/CO_2, formic acid, acetate) has been engineered to produce various biofuels (see Table 1.1 in Chapter 1 for examples). Despite the excitement generated at the prospect of these biochemically produced "electrofuels", several challenges must be addressed prior to the industrial adoption of these processes.

As I showed in Chapter 2, EMP processes producing low-value products will only be environmentally viable if the yield of the product is very high (around 90% of the theoretical maximum or higher, depending on the specific product and substrate). Similarly, the results of Chapter 3 demonstrated that similarly high yields as well as high titers are required to maintain acceptably low costs of substrate generation and separations. High yields (>85% compared to their theoretical value) have been achieved in engineered *E. coli* strains using glucose as a substrate for products such as ethanol, n-butanol, and isobutanol.[217–219] While various alcohols and alkanes have been produced in metabolically engineered *C. necator* as possible fuels from non-conventional substrates, the titers and yields reported remain lower than those achieved in *E. coli* grown on sugars.[63,64,66] Moreover, *C. necator*, the model Knallgas bacteria, is relatively sensitive to alcohol toxicity compared to other industrially relevant strains, which poses a limitation in developing high-titer bioprocesses.[220]

In this Chapter, I seek to develop and evaluate broad strategies to maximize the performance of *C. necator* in biofuel production, using the biofuel n-butanol as an example target product. While n-butanol formation in metabolically engineered *C. necator* has been demonstrated,[221] this was done primarily as an intermediate engineering step toward developing a novel pathway for isobutanol production. Therefore, further work in developing *C. necator* as a chassis for n-butanol production is required. I begin by metabolically engineering *C. necator* with a n-butanol production pathway, diverting carbon flux from PHB production. Variations of the butanol synthesis pathway are tested in *C. necator* to evaluate the impact of factors such as enzyme identity and codon optimization on the yield of butanol. Fructose is used as a carbon source for these studies to examine the n-butanol synthesis pathway specifically. However, this work establishes a basis for which further pathway optimization can occur for a particular substrate of interest.

I also address the issue of product inhibition mentioned previously. Given the success in adapting *C. necator* for greater halotolerance in Chapter 4, I use adaptive laboratory evolution (ALE) to improve the tolerance of *C. necator* to n-butanol and characterize the resultant strain. I finally discuss how the results obtained in this chapter provide insight into strategies that can be used to improve the performance of *C. necator* for n-butanol production in particular and in biochemical processes broadly.

5.3 Materials and Methods

Microbial media and culturing

Table 5.1: Strains and plasmids used in Chapter 5

Strain/Plasmid	Description	Source
Strains		
C. necator H16	Wild-type *Cupriavidus necator* strain	DSM 428
C. necator H16 *ΔphaC1*	*C. necator* strain deficient in gene encoding PHB synthase	[65]
C. necator bt430	*C. necator* strain with improved tolerance to n-butanol following 250 generations of adaptive laboratory evolution (replicate experiment #1)	This work
C. necator bt530	*C. necator* strain with improved tolerance to n-butanol following 250 generations of adaptive laboratory evolution (replicate experiment #2)	This work
C. necator bt630	*C. necator* strain with improved tolerance to n-butanol following 250 generations of adaptive laboratory evolution (replicate experiment #3)	This work
E. coli WM3064	DAP-auxotrophic *E. coli* donor strain used for conjugation of *C. necator*	William Metcalf (UIUC)
Plasmids		
pBADTrfp	araBAD promoter, T7-stem loop, Kan^R, mRFP1 expression gene. Addgene #99382	[55]
pBADT-Bu-A	araBAD promoter, T7-stem loop, Kan^R, expresses *adhe2* (*Clostridium acetobutylicum*), *ccr* (*Streptomyces collinus*), *crt* (*Clostridium acetobutylicum*)	This work
pBADT-Bu-B	araBAD promoter, T7-stem loop, Kan^R, expresses *adhe2* (*Clostridium acetobutylicum*), *ter* (*Treponema denticola*), *phaJ* (*Aeromonas caviae*)	This work
pBADT-Bu-B2	araBAD promoter, T7-stem loop, Kan^R, expresses *adhe2* (*Clostridium acetobutylicum*), *ter* (*Treponema denticola*), *phaJ* (*Aeromonas caviae*); *C. necator* codon optimized	This work

All bacterial strains and plasmids used in this chapter are listed in Table 5.1. Luria Broth (LB) was used as media for routine culturing, M9 acetate medium (for composition, see Supplementary Note D.1, Appendix D) was used in certain butanol toxicity experiments and Terrific Broth (TB) was used for butanol production experiments. All *C. necator* strains were grown at 30 ºC while all *E.*

coli strains were grown at 37 ºC; all liquid cultures were shaken at 200 RPM. Media were supplemented with kanamycin (50 μg/mL *E. coli*, 200 μg/mL *C. necator*) when culturing strains containing Kan^R plasmids. All bacterial strains used in the study were stored at -80 ºC in 25% glycerol until needed. To reactivate the strains, cells were first streaked onto agar plates (with appropriate antibiotic as needed), incubated, and then a liquid LB culture was started from a single colony.

Plasmid Construction

Plasmids containing the three-gene butanol synthesis operon were constructed using standard techniques. DNA fragments encoding the *adhe2* (bifunctional aldehyde/alcohol dehydrogenase, *Clostridium acetobutylicum*), *ccr* (crotonyl-CoA reductase, *Streptomyces collinus*), *ter* (trans-2-enoyl-CoA reductase, *Treponema denticola*), *crt* (3-hydroxybutyryl-CoA dehydratase, *Clostridium acetobutylicum*), and *phaJ* ((R)-specific enoyl-CoA hydratase, *Aeromonas caviae*) were synthesized by IDT DNA Technologies, and were designed to contain overhang regions allowing the fragments to be assembled. The red fluorescent protein gene in the plasmid pBADTrfp was removed by digestion with the NdeI and BamHI restriction enzymes. pBADTrfp was a gift from Nathan Hillson (Addgene plasmid # 99382; http://n2t.net/addgene:99382; RRID:Addgene_99382).[55] The appropriate synthetic DNA fragments were assembled with this linearized plasmid using Gibson Assembly to create the butanol synthesis plasmids listed in Table 5.1. The proper DNA sequence was confirmed by whole-plasmid nanopore sequencing.

Transformation of C. necator

The transformation of *C. necator* strains with plasmids follows the same conjugation protocol used in Chapter 4. The protocol will be briefly restated here. Plasmids were first transformed by heat shock into *E. coli* WM3064 cells, which were made chemically competent following the method in the previous chapter and selected for on LB agar plates containing DAP and kanamycin. *E. coli* WM3064 was a gift from William Metcalf (University of Illinois). Plasmids were then transformed into *C. necator* H16 *ΔphaC1* by conjugation of the plasmid from the WM3064 donor strain, following the conjugation protocol described in Chapter 4. *C. necator* H16 *ΔphaC1* was a gift from Johannes Gescher (Karlsruhe Institute of Technology). The conjugated strains were selected on an LB agar plate with kanamycin (200 μg/mL), and proper transformation was confirmed by PCR.

Butanol production in engineered C. necator strains

Cultures of the engineered strains were first grown overnight in LB. The cells were then inoculated into a 30-mL culture of Terrific Broth medium supplemented with 15 g/L fructose to a starting cell density of A_{600}=0.2. For culturing under aerobic conditions, cells were grown in 300-mL flasks, while cells cultured in microaerobic conditions were grown in 50-mL falcon tubes with caps sealed. L-arabinose was added to a final concentration of 0.2% (w/v) to induce expression of the butanol synthesis genes. Cultures were grown at 30 ºC, shaking, for six days. Every two days, 1-mL samples of each culture were taken, centrifuged for 10 min at 4,000 g, and the supernatant was removed and saved for further analysis. At each sampling time, additional fructose was added such that the final concentration of fructose in the media was raised by 10 g/L.

Measurement of butanol titers

Butanol concentrations were measured following a protocol adapted from the methods described by Bond-Watts *et al.*[222] Any residual cell mass from the samples taken from the cultures was removed by centrifuging at 15,000 g for 5 min. Cleared supernatants were mixed in a 1:1 ratio

with toluene containing an internal standard of 1-hexanol (1000 mg/L), and mixtures were vortexed for 2 min. Mixtures were centrifuged for 5 min at 4,000 g and a 40-uL sample was removed from the organic layer and quantified using gas chromatography-mass spectrometry. Aqueous n-butanol standards were prepared for each GC-MS run and were extracted into toluene (with the hexanol internal standard) following the same protocol.

Adaptive laboratory evolution

The tolerance of *Cupriavidus necator* to n-butanol was improved by adaptive laboratory evolution similar to the procedure described in Section 4.3 with minor modifications. Wild-type *C. necator* H16 was first streaked onto an LB agar plate, and a single colony was subsequently grown to saturation in liquid LB medium overnight. Three 10-mL cultures in LB were inoculated from this overnight culture with a starting optical density of A_{600}=0.001, and n-butanol was added to each culture to a final concentration of 3 g/L. After 24 hours, each of the three cultures was passaged into a new 10-mL culture of LB containing 3 g/L n-butanol, again with a starting optical density of A_{600}=0.001. As in the ALE for increased halotolerance described in Chapter 4, this was repeated for 30 passages, with the n-butanol concentration of the culture increasing in 0.5 g/L increments throughout the course of the ALE. Cultures were plated every several passages to ensure they were free of contamination. The final passage of each ALE replicate was plated on LB agar and a single colony was selected from each, with the evolved strains designated as *C. necator* bt430, bt530, and bt630. Colony PCR was performed to ensure contamination had not occurred throughout the ALE.

Butanol tolerance assays

The tolerance of evolved strain bt530 compared to wild-type H16 was tested. The overnight growth of the two strains in the presence of variable butanol concentrations was evaluated. Each strain was first cultured overnight in LB containing no butanol. These overnight cultures were used to inoculate a 10-mL culture (in a 50-mL falcon tube with its cap loose to allow air exchange) of either LB or M9 acetate medium. Cultures in LB were inoculated at a starting A_{600} of 0.001 while cultures in M9 acetate media were inoculated at a starting A_{600} of 0.02. Variable amounts of n-butanol were added to each culture at the time of inoculation. The optical density of each culture was measured 24 hours post-inoculation.

Growth curves under butanol stress

The behavior of each of the evolved strains, as well as wild-type *C. necator* H16, under butanol stress was evaluated. Cultures of each strain were grown overnight in LB. The next day, strains were inoculated into a 300-mL flask containing 50mL of LB with a starting cell density of A_{600}=0.05, and n-butanol was added to a final concentration of 6 g/L. Cells were cultured and optical densities were measured every 90 minutes for 12 hours.

5.4 Results and Discussion

Metabolic engineering in C. necator for n-butanol production

Two potential pathways of producing n-butanol from intermediates theoretically present in *C. necator* (based on expected metabolites according to the Kyoto Encyclopedia of Genes and Genomes)[223] were identified (Fig. 5.1). Each pathway requires three heterologous genes. In one pathway, (R)-3-hydroxybutyryl-CoA, the penultimate molecule in the PHB synthesis pathway, is

converted to crotonyl-CoA by an (R)-specific enoyl-CoA hydratase (*phaJ*). In the other pathway, (S)-3-hyxroybutyryl-CoA is converted to crotonyl-CoA by a 3-hydroxybutyryl-CoA dehydratase (*crt*). In both pathways, crotonyl-CoA is then converted to butyryl-CoA by a trans-2-enoyl-CoA reductase (*ccr* or *ter*). Finally, butyryl-CoA is converted to n-butanol (through a butyraldehyde intermediate) by a bifunctional aldehyde/alcohol dehydrogenase (*adhe2*). Both pathways were tested in *C. necator* to identify which leads to higher butanol yields. Two plasmids were constructed, each containing a version of this pathway: one containing *adhe2*, *ccr*, and *crt* genes and one containing *adhe2*, *ter*, and *phaJ* genes. Species from which the gene sequences used to construct these plasmids were obtained are listed in Table 5.1.

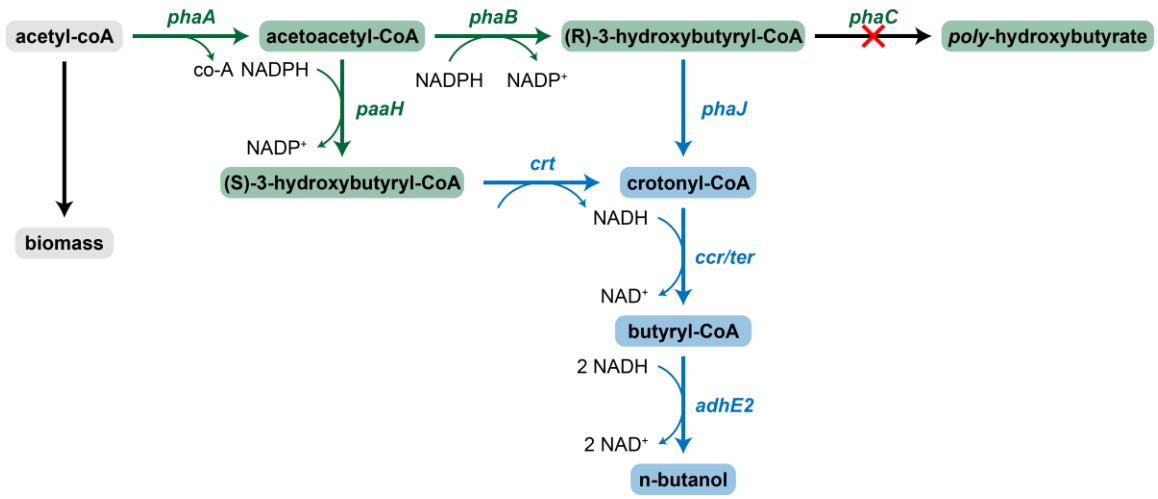

Figure. 5.1. Metabolic pathway for n-butanol production in *C. necator*. Two possible engineered pathways for n-butanol production in *C. necator*, starting from (R)-3-hyroxybutyryl-CoA and (S)-3-hydroxybutyryl-CoA, are tested in this chapter.

The two plasmids containing the butanol synthesis operons (Fig. 5.2A) were successfully constructed, with correct sequences confirmed by full-plasmid nanopore sequencing. These plasmids were transformed into a *C. necator* H16 strain lacking the *phaC1* gene, to remove a potential competing carbon sink. The Δ*phaC1* gene deletion was performed previously by Windhorst and Gescher, who generously provided this strain.[65] Both of these strains were then tested for butanol production to identify the optimal pathway.

Production of n-butanol from fructose in C. necator

The two engineered *C. necator* strains, each with a distinct potential butanol production pathway, were evaluated. Strains were cultured in rich media (TB) containing fructose as a carbon source. 35 g/L of fructose were fed to these cultures over a six-day period (see Methods). While the primary interest in engineering *C. necator* rests on its ability to metabolize non-conventional substrates (*e.g.*, H_2/CO_2, formic acid, acetate), using a rich medium with fructose as a carbon source enables studying the butanol production pathway in isolation.

The two strains, designated as Bu-A and Bu-B, produced significantly different levels of n-butanol. Strain Bu-B produced butanol to a final titer of 1.12 g/L following six days of growth in microaerobic conditions, while butanol in the Bu-A culture was barely detectable, over an order of magnitude lower in concentration (Fig. 5.2B). There are two primary differences between the

two pathways evaluated, each of which could contribute to the stark differences in butanol titers between the strains. Strain Bu-B contains the trans-2-enoyl-CoA reductase gene (*ter*) from *Treponema denticola* which catalyzes the reduction of crotonyl-CoA to butyryl-CoA, while in Bu-A, this step is catalyzed by the crotonyl-CoA reductase gene (*ccr*) from *Streptomyces collinus*. The use of the *ter* gene has previously led to higher butanol titers in *E. coli*,[217] so higher enzymatic activity in this step may be part of reason for high butanol production in Bu-B.

The other difference in the pathways tested is the enzyme used in the first heterologous step in butanol production, the formation of crotonyl-CoA. Based on the known substrate specificities of the two enzymes tested,[222] Bu-A utilizes (S)-3-hydroxybutyryl-CoA as an intermediate in butanol synthesis while Bu-B uses the stereoisomer (R)-3-hydroxybutyryl-CoA. As mentioned previously, both of these intermediates are predicted to occur in *C. necator*. However, (R)-3-hydroxybutyryl-CoA directly participates in the PHB synthesis pathway, as the final molecule prior to PHB polymerization. The gene which catalyzes PHB polymerization is knocked out of the *C. necator* strain used for butanol production (H16 *ΔphaC1*) which could lead to an accumulation of (R)-3-hydroxybutyryl-CoA. For this reason, the starting intermediate in the pathway in Bu-B likely plays a significant role in achieving greater butanol synthesis. Elucidating the relative contribution of each of these factors to the disparity in butanol production would require engineering more strains such that the effects of each can be examined in isolation. This remains an area of further exploration. However, I succeeded in developing a strain of *C. necator* capable of butanol production, which can serve as a foundation to further develop strategies for achieving high butanol yields in this organism.

The 1.12 g/L titer is around 8% of the theoretical n-butanol concentration that can be produced from the concentration of fructose available, given the metabolic pathway of butanol fermentation. However, this value does not take into account the available carbon in the rich media and should not be taken as the actual yield of butanol on fructose in this strain. This comparison is merely for illustrative purposes. However, it does indicate that there is significant room for improvement in butanol production. Possible strategies for improving this yield will be discussed in the conclusion.

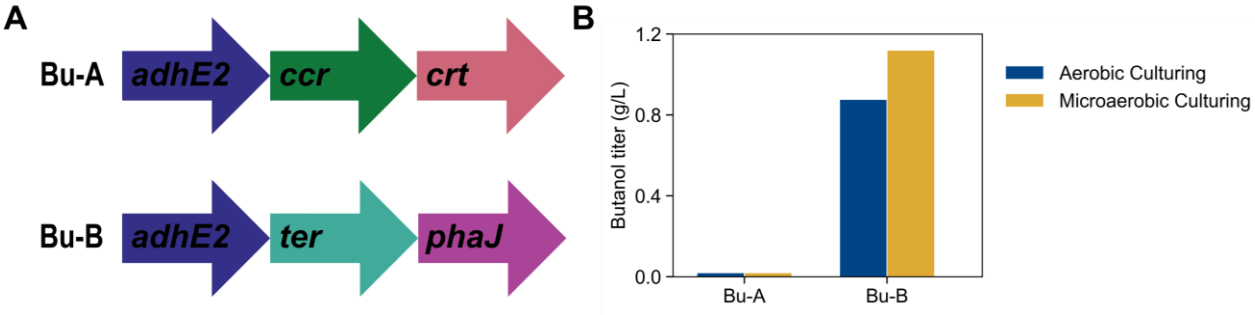

Figure 5.2. Butanol production in *C. necator*. (A) Heterologous butanol synthesis operons tested in this chapter. (B) Butanol titers achieved by the two metabolically produced strains under aerobic (blue) and microaerobic (yellow) culturing conditions.

The experiment was repeated under aerobic culturing conditions. As expected, as butanol fermentation requires the reduction of acetoacetyl-CoA, higher butanol titers were found under microaerobic conditions. However, the difference was marginal, suggesting the culturing conditions are not particularly impactful.

Codon optimization was also tested. The plasmid pBADT-Bu-B was reconstructed such that the coding sequences of the expressed heterologous enzymes matched the native codon bias of *C. necator*. Codon optimization was performed using the helpful online tool OPTIMIZER.[224] This plasmid was transformed into *C. necator* and the strain, designated Bu-B2, was tested for butanol production following the same protocol as before. The total butanol titer achieved by this strain was roughly the same as for the unoptimized strain (see Fig. D.1, Appendix D), with a titer of 1.07 g/L achieved following six days of fermentation. At least for this pathway, codon optimization did not significantly affect butanol yields, and was therefore taken to be unnecessary in the metabolic engineering of *C. necator* for n-butanol production.

This result does not strongly impact the achievable butanol production, but it does have some significance for metabolic engineering of *C. necator* in general. Previous studies have demonstrated that codon optimization for the metabolically engineered host being used often leads to improved protein expression and product yields.[225] As such, when synthesizing gene fragments for heterologous protein expression, optimizing the codon bias specifically for the microbial host is a common practice. This poses some challenges for *C. necator*, however, which has a natural codon bias with a high (66%) GC content.[192] High GC content leads to difficulty with DNA synthesis and assembly, with errors in DNA sequence likely as a result. Fortunately, the result here suggests that codon optimization does not affect product yield in *C. necator*. Genes can be synthesized with codon biases containing moderate GC contents, such as the codon usage found in *E. coli* (which was used to synthesize genes for pBADT-Bu-A and pBADT-Bu-B). This result should inform future metabolic engineering efforts in *C. necator*, which will facilitate easier construction of engineered strains in the laboratory.

Adaptive laboratory evolution improves butanol tolerance in C. necator

The adaptive laboratory evolution experiment successfully yielded three strains of *C. necator* that evolved butanol tolerance in parallel. Prior to the ALE, it was determined that the growth rate of *C. necator* was substantially reduced for n-butanol concentrations greater than 3 g/L. Therefore, the butanol concentration during the first passage of the ALE was 3 g/L, and the concentration was raised in 0.5 g/L increments throughout the course of the experiment. Similar behavior compared to the ALE performed in Chapter 4 was observed. Increases in butanol concentration often led to sharp decreases in the growth rate of the strains, with gradual recovery of the growth rate as the concentration was held constant (Fig. 5.3A). The thirty passages performed for each strain throughout the course of the ALE accounted for around 275 generations of growth.

The concentration of n-butanol present in the ALE reached 7 g/L during the final passages. However, the growth rate of the strains under this butanol concentration remained substantially lower than the growth rate of the wild-type strain under 3 g/L. The growth rate of the evolved strains in the presence of 6 g/L butanol was (on average) roughly equal to the growth rate of the wild-type strain in the presence of 3 g/L. Therefore, it is more appropriate to say the ALE improved the butanol tolerance of *C. necator* from 3 g/L (0.37% v/v) to 6 g/L (0.74% v/v) throughout the course of the ALE.

Unlike the experiment in Chapter 4, this ALE was performed in triplicate. At different points in the ALE, some of the replicates tolerated the higher butanol concentration better than others. Divergence between these replicates is reflected by the error bars in Figure 5.3A. Of the three final strains, labelled bt430, bt530, and bt630, bt530 consistently displayed better growth in response to the increasing butanol concentrations (see Fig. D.2, Appendix D). To verify this was the best strain,

growth curves were obtained for all three evolved strains growing in LB with 6 g/L n-butanol. As expected, strain bt530 grew faster than the other two evolved strains under these conditions (Fig. 5.3B). The calculated specific growth rate of bt530 was around 0.18 h^{-1}, while those of bt430 and bt630 were both around 0.13 h^{-1} (Table 5.2). Therefore, *C. necator* bt530 was chosen as the best evolved strain and further characterized.

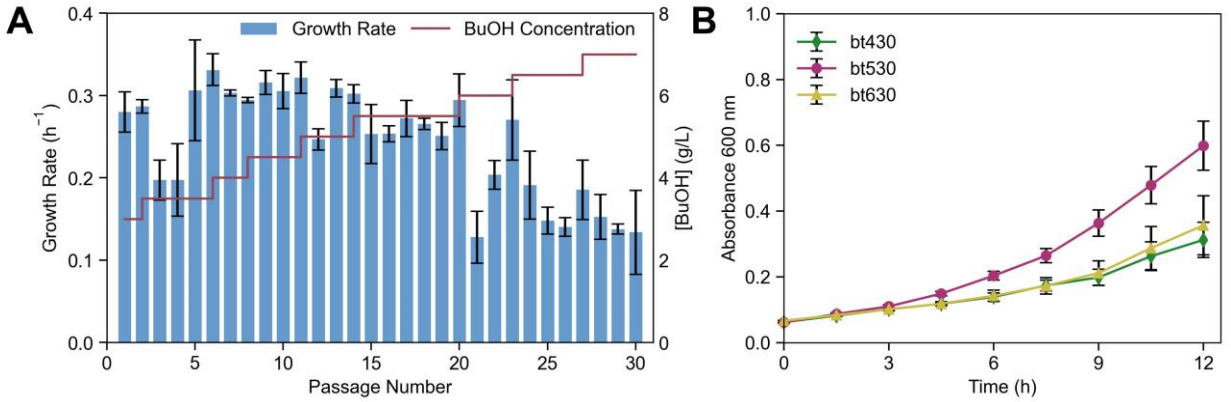

Figure 5.3. Adaptive laboratory evolution of *Cupriavidus necator* for enhanced butanol tolerance. (A) Results of ALE experiment showing the average growth rate (blue bars) and n-butanol concentration (red line) at each passage. The mean of the growth rates of the three ALE strains is plotted, with error bars representing the standard deviation. Therefore, larger error bars occur when divergence between the strains' behavior during the ALE occurs. (B) Growth curves of the three strains obtained through the ALE experiment in LB media containing 6 g/L n-butanol. For each data point in (B), the mean ± s.e.m. is plotted (n=6).

Comparison of wildtype C. necator H16 and adapted strain bt530

The evolved strain with the highest growth rate under butanol stress, *C. necator* bt530, was compared to the wild-type strain, *C. necator* H16, under a variety of butanol concentrations. The two strains were inoculated to an optical density of 0.001 in LB medium with variable n-butanol concentrations, and the change in cell density after 24 hours was recorded. While the two strains behaved similarly at low butanol concentrations, a clear difference between their growths is apparent at butanol concentrations 3 g/L and higher (Fig. 5.4Ai). The strain bt530 is clearly more tolerant to n-butanol stress compared to the wild-type strain H16. The starkest difference between the two strains could be seen when growing in LB containing 6 g/L n-butanol; at this concentration strain bt530 grew ~250-fold over a 24-hour period while strain H16 grew a negligible amount. The growth that bt530 experienced under 6 g/L butanol was about the same that H16 experienced under 3 g/L butanol. By this metric, therefore, the ALE roughly doubled the butanol tolerance of *C. necator*.

This experiment was repeated in defined acetate medium (M9-acetate, see Table D.1 in Appendix D for composition) to determine whether the carbon source impacts the butanol tolerance of the strain. The primary benefit of using *C. necator* as a microbial catalyst is its ability to metabolize non-conventional substrates, and therefore in a practical application the bacteria would be cultured in a defined medium with a single carbon source. Systems in which *Cupriavidus* strains convert acetate (first produced from H_2/CO_2 by an acetogen) to a product of interest have been demonstrated previously.[69] Due to the slower growth rate of *C. necator* in defined acetate medium, the optical density at inoculation was increased from 0.001 to 0.02 in this experiment, and the change in cell density over a 24-hour period was measured. Similar trends were observed in the

defined acetate medium as were seen in LB, with strain bt530 demonstrating superior growth compared to H16 in the presence of n-butanol. The magnitude of growth over the 24-hour period for both strains in defined media was less than in LB, as expected. In media containing 5 g/L n-butanol, the evolved strain grew 18-fold while the wild-type strain only tripled in optical density. The adaptation acquired during the ALE is therefore observed in both rich and defined media with different sources of carbon.

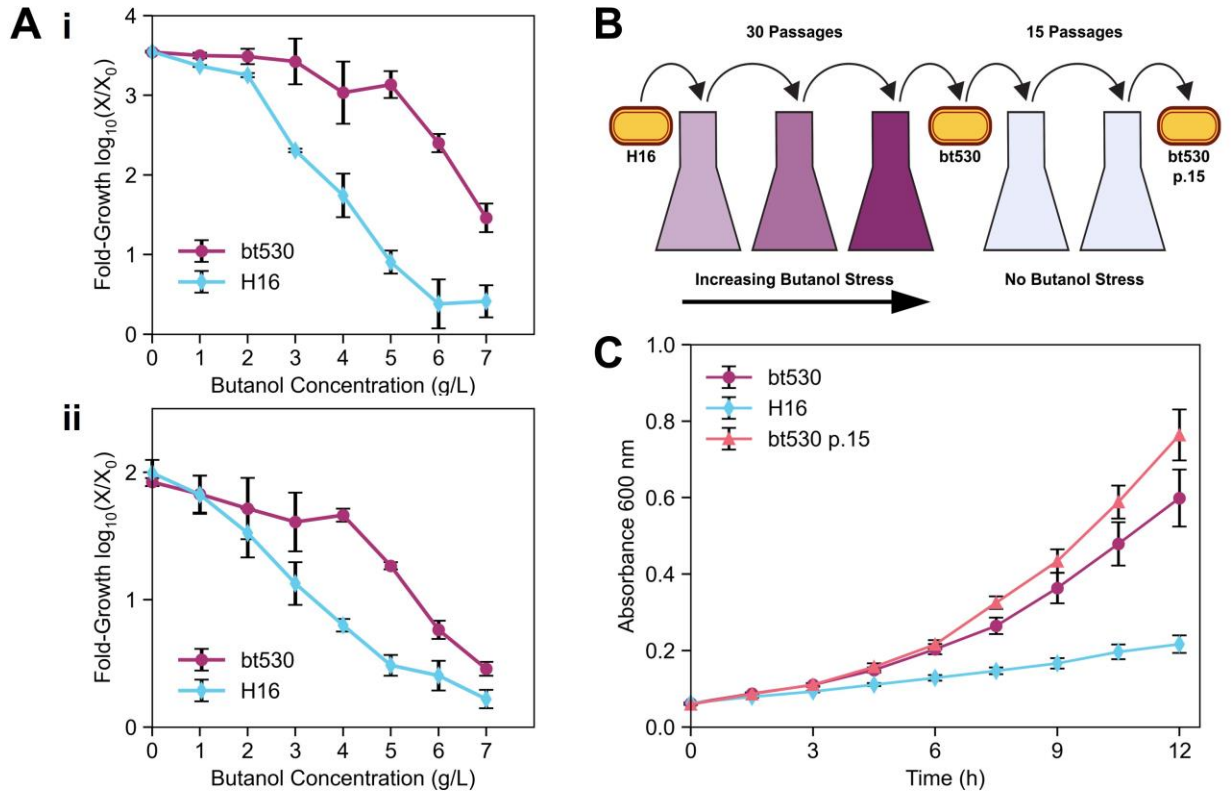

Figure. 5.4. Characterization of evolved butanol-tolerant strain *C. necator* bt530. (A) Change in cell concentration of *C. neactor* strains H16 (light blue) and bt530 (magenta) in (i) LB or (ii) M9 acetate following 24 hours of growth in the presence of various concentrations of n-butanol. Geometric means (n=6) are plotted with log-transformed s.e.m. displayed as error bars. (B) Procedure to obtain strains bt530 and bt530 p.15 from wild-type *C. necator* H16. Butanol-tolerant strain bt530 was obtained from wild-type *C. necator* H16 by growing it in the presence of n-butanol for thirty passages, while fifteen further passages of growth without the presence of n-butanol yielded strain bt530 p.15. (C) Growth curves of strains H16, bt530, and bt530 p.15 in LB containing 6 g/L n-butanol. For each data point in (C), the mean ± s.e.m. is plotted (n=6).

Evolved butanol-tolerant C. necator bt530 retains adapted phenotype even in prolonged absence of stress

After the clear phenotypic difference between wild-type *C. necator* H16 and the butanol-tolerant strain bt530 was demonstrated (Fig. 5.4A), the stability of the adaptation in strain bt530 was evaluated. To that end, the strain was grown in LB without any butanol for fifteen consecutive passages (Fig. 5.4B). Following this, the growth of the wild-type strain H16, the adapted strain bt530, and the strain obtained from the fifteen passages of stress-free growth (designated bt530 p.15) was tested in the presence of butanol. All strains were grown in LB with 6 g/L n-butanol, and growth curves were obtained.

Despite growing without butanol for fifteen passages, which accounted for >175 generations of cell growth, bt530 retained the phenotype it gained through the ALE. The growth curves of bt530 and bt530 p.15 were similar, and both strains grew significantly faster than the wild-type H16 in the presence of 6 g/L n-butanol (Fig. 5.4C). The specific growth rates of bt530 (.18 ± 0.02) and bt530 p.15 (0.21 ± 0.01) were roughly double that of wild-type H16 (0.10 ± 0.01) under these conditions (Table 5.2). Therefore, strain bt530 does not need to be cultured under constant butanol stress in order to maintain its beneficial adaptation.

Table 5.2: Growth rate of *C. necator* strains studied in this chapter in the presence of 6 g/L

Strain	Specific Growth Rate (h^{-1})
H16	0.10 ± 0.01
bt430	0.13 ± 0.02
bt530	0.18 ± 0.02
bt630	0.13 ± 0.03
bt530 p.15	0.21 ± 0.01

This result is significant when considering the practical application of the evolved strain. Even if this strain is used for butanol production (having been appropriately engineered with the n-butanol synthesis pathway), it would likely not be under the presence of constant butanol stress. During the process of engineering the strain, as well as in culturing the seed train prior to butanol production, the strain would not be in the presence of n-butanol. It's possible that the butanol tolerance trait of bt530 would eventually diminish with continued culturing in a butanol-free environment. Therefore, it is vital to have a strain that does not lose its butanol tolerance even when grown in the absence of butanol for prolonged periods of time. The persistence of this phenotype for at least fifteen stress-free overnight passages suggests that this will not be a major problem for strain bt530. I do note that adaptation is dependent on stochastic genome mutations, and therefore the result obtained here, that *C. necator* bt530 retains its improved butanol tolerance for at least fifteen consecutive overnight cultures, is not necessarily guaranteed. However, this result does indicate that the adaptation acquired through the ALE is not particularly energetically costly to the cell, as there was no apparent driving force to lose the mutation. Therefore, in practical applications, one can be reasonably confident that the strain would not lose its adaptation through normal day-to-day culturing.

5.5 Conclusion

Electromicrobial production of liquid fuels is a promising pathway for the decarbonization of the transportation industry. Multiple examples of metabolically engineered *C. necator* converting CO_2 and H_2 (or formic acid) into alcohols have been reported in the literature.[63,66] However, systems demonstrating sufficient productivity, titer, and yield at scale will need to be developed. In this chapter, I presented work toward developing a strain of *C. necator* that can efficiently produce n-butanol.

Two different n-butanol production pathways were tested in genetically engineered *C. necator* strains and the pathway that led to the highest butanol titer (1.12 g/L) when using fructose as a carbon source was identified. I also determined that codon optimization does not impact the production of n-butanol in this pathway. Therefore, in further engineering of this strain, complications due to the GC-rich *C. necator* genome can be avoided by simply applying the codon bias found in *E. coli* to synthesized genes. The engineering done here only represents a first pass in the metabolic engineering of *C. necator* for butanol production. Further improvement may come from knocking out competing carbon sinks and upregulating genes involved in intermediate synthesis.

Given the native gene regulation in *C. necator*, other methods such as nitrogen starvation can be tested to improve the butanol yield. In wild-type *C. necator*, in the absence of sufficient available nitrogen concentrations, carbon is diverted routed through the PHB synthesis pathway as a store of carbon and energy. Because the PHB synthesis pathway and butanol synthesis pathway share several enzymatic steps in common, and the final PHB synthesis gene *phaC1* is knocked out in the engineered strain, it's possible that nitrogen starvation would lead to improved butanol concentrations as the production of (R)-3-hydroxybutyryl-CoA is upregulated. Therefore, a combination of genetic engineering and simple cell culturing techniques should be studied to maximize the butanol yield. Additionally, further engineering and optimization may be required when using substrates such as formate or acetate.

In parallel, I developed a strain of *C. necator* with improved tolerance to n-butanol. Through 30 passages of adaptive laboratory evolution, I obtained a strain (bt530) that can grow in media containing two-fold higher butanol concentrations compared to the wild-type strain. The butanol tolerance adaptation was found to be stable, with that phenotype persisting even after growing without butanol stress for fifteen additional days. In principle, this strain should be better-suited for n-butanol production compared to the wild-type strain, as higher titers would be possible. As shown in Chapter 3, achieving high n-butanol titers in an EMP process is critical to lowering the cost of separations. Testing whether the improved butanol tolerance of this strain, if engineered with the butanol synthesis pathway, leads to higher possible n-butanol titers remains an interesting area of further study. In brief, in this chapter I demonstrated the use of two broad techniques, rational genetic engineering and adaptive laboratory evolution, toward developing a strain of *C. necator* suitable as a biocatalyst for the electromicrobial production of n-butanol.

5.6 Acknowledgements

I would like to thank Hye Jin Jo, Chloe Li, Ryan Liang, Peidong Yang, and Douglas S. Clark for their contributions to the work in this chapter. This work was supported by the ARPA-E OPEN 2021 Award No. DE-AR0001555.

Chapter 6: Conclusion and Outlook

6.1 Summary of Key Results and Conclusions

This dissertation describes several advances in the field of electromicrobial production through both process modeling/analysis and microbial engineering. Broadly, the analytical portion of the thesis provides a top-level view of the role that EMP can play in bioproduction, interacting with both the environment and the economy. This provides an insight into how well EMP technologies might perform, what technical and non-technical factors are required for them to be successful, and how this might be affected by the use of different substrates, strains, and products. Meanwhile, the experimental section focused primarily on developing microbial biocatalysts that are suited for specific applications in electromicrobial production. These chapters were much more focused on the details of biocatalyst development for specific bioprocesses, although some insights that can be applied to EMP more broadly were attained.

I began in Chapter 1 by placing electromicrobial production in the context of previously developed bioprocessing approaches and technologies, describing the shortcomings of previous approaches that EMP holds potential in addressing. Here, I summarized the current state of the field, describing the various areas of research and development that have advanced EMP in recent years and highlighting some achievements in the literature to date.

In Chapter 2, I systematically evaluated the claims that EMP systems are more environmentally friendly than traditional bioprocesses. To do so, I developed a tripartite analysis framework that combines physics-based reactor modeling, process modeling, and life cycle assessment to predict the productivity, energy demand, life cycle greenhouse gas emissions, and land occupation footprint of three possible EMP systems for three example products. Of the three systems examined, a Knallgas bacteria-based system, a formatotroph-based system, and a two-step acetogen/acetotroph-based system, the Knallgas bacteria consistently had the lowest global warming potential and land use for the range of situations considered. I showed that EMP systems can have lower global warming potential compared to traditional bioprocesses provided that the electricity used is clean and the yield for a given product is sufficiently high. I also showed that EMP systems can lead to a reduction in land use as high as 95% compared to traditional crop-based processes. This work is the first use of life cycle analysis to compare EMP strategies to each other, as well as one of the most exhaustive analyses of the potential of EMP systems to date.

In Chapter 3, I studied the economics of EMP processes. I focused on one specific hypothetical system, where CO_2 (obtained through direct air capture) is converted to acetate by an acetogen using H_2 as an energy source, with the acetate then converted to n-butanol by a second engineered microorganism. I used a similar approach as in Chapter 2, beginning with reactor and process modeling, but then used techno-economic assessment to predict a minimum fuel selling price for butanol produced in this process. I found that even for a process with a high yield of butanol from acetate, the requirement of pH control, high capital costs for bioreactors (due to the system's relatively low productivity), and high cost of hydrogen production would currently prevent this system from being economically viable. However, I showed that by removing the need for pH control and by reducing the cost of H_2 production, a pathway to economic viability may be possible. The framework for economic analysis of EMP developed in this chapter provides a useful

tool to evaluate EMP systems and understand what factors contribute to the overall economics of the process.

In Chapter 4, I began detailing my experiment work toward the development of EMP systems. In this chapter I addressed the issue of cell lysis for the recovery of intracellular bioproducts. As Chapter 3 underscored, separations processes are a costly component of bioprocesses in general and can affect the economic feasibility of EMP systems. The use of osmolysis, cell lysis through osmotic pressure changes, had previously been used to recover products from mammalian cells or extreme halophiles, but had not been demonstrated in mesophilic bacteria such as *C. necator*, one of the primary microbes suitable for EMP. By using adaptive laboratory evolution to improve the halotolerance of *C. necator,* and by knocking out the large conductance mechanosensitive channel gene, I developed a strain of *C. necator* that lyses when resuspended in distilled water. Using this strain, I demonstrated an intracellular product recovery of around 90% when cells were grown under heterotrophic conditions and around 99% when cells were grown using formate as a sole carbon source. I used recombinant red fluorescent protein as an example molecule in this study, but this technique in principle may be used for the recovery of multiple intracellular products, including other recombinant proteins and intracellularly produced polyester granules (*e.g.*, polyhydroxyalkanoates). While the motivation of this work was specifically for EMP systems using *C. necator*, I demonstrated that this strategy is broadly applicable, showing its application to *E. coli*. Therefore, this strategy holds promise in simplifying separations for a range of bioprocesses beyond EMP.

In Chapter 5, I described efforts to develop a strain of *C. necator* capable of producing n-butanol from non-conventional substrates with high yield and titers, two factors that were found to be critical in the process economics studied in Chapter 3. Through metabolic engineering, I created two *C. necator* strains with different biosynthetic pathways that produce n-butanol from available intermediates and determined which of the tested pathways leads to the highest n-butanol production. The best strain led to butanol titers as high as 1.12 g/L. I further examined the effect of codon optimization on butanol production. In parallel, I used adaptive laboratory evolution to improve the butanol tolerance of *C. necator*, which is relatively sensitive to solvents like n-butanol making high titers difficult to achieve. The laboratory evolution roughly doubled the tolerance of *C. necator* to n-butanol from 3 g/L to 6 g/L and showed that the adaptation was stable even when grown without butanol stress. Taken together, in this chapter I demonstrated two parallel approaches that can independently be employed to improve n-butanol yields and possible titers in bioprocesses using *C. necator*. This work serves as a foundation on which further efforts in strain development for this application can be pursued.

Overall, this work represents a significant advancement in the understanding of EMP systems and in the development of biocatalysts used in EMP systems. The use of modeling, life cycle analysis and techno-economic assessment described here evaluated the feasibility of using EMP systems for large-scale commodity chemical production, identified specific bottlenecks to their adoption, and created an analytical framework by which various EMP strategies may be compared to each other for a specific application. The experimental work showed how two techniques, rational genetic engineering and adaptive laboratory evolution, can be used to develop strains of *C. necator* with specific properties needed in two different example applications. Rather than seeing the analytical and experimental work in isolation, the greatest benefit is achieved when these two components are placed in conversation with each other, such that the analytical work can direct specific laboratory research directions and evaluate the impact of their advancements.

I now provide some concluding thoughts on the prospects of electromicrobial production in attaining some degree of industrial relevance. I will speculate on what work is required by academic researchers prior to large-scale adoption of the technology, what non-technical preconditions must be met for EMP to be effective as a sustainable production scheme, and what paths may be pursued in implementing scalable systems.

6.2 Electromicrobial Production: Where do we go from here?

EMP and the academic laboratory

Electromicrobial production provides an opportunity to produce a seemingly endless array of molecules from carbon dioxide, using only electricity to drive the biochemical process. However, these systems are still technologically immature relative to other generations of bioprocesses and have not yet been deployed to a significant degree. A number of non-technical factors will be required such that EMP makes environmental and economic sense, which will be touched on later. However, several outstanding technical issues must be addressed to improve the technological readiness of EMP. While some of this innovation may come from companies that work on EMP or related technologies (*e.g.,* LanzaTech), many of these advances will likely originate in the academic lab.

Much of this work will involve microbial engineering. A number of strains have already been engineered that can convert substrates such as formic acid or H_2/CO_2 to certain products of interest, a few of which have been developed in this dissertation and many more of which have been reported in previous literature described in the introduction. However, the breadth of engineered strains capable of utilizing these novel substrates still pales in comparison to that of more traditional strains such as *E. coli* that metabolize substrates such as sugar.

For the product spectrum of EMP to reach that of traditional bioprocesses, there are, in my view, two major strategies. In one strategy, which I call the "catch-up" strategy, strains like *C. necator* can simply be engineered with the pathways that have been demonstrated in *E. coli* and other more conventional strains. This would involve significant time and effort, and pathway optimization in *C. necator* may look different than in *E. coli*, but this strategy is fairly straightforward. The other strategy, which I call the "co-opt" strategy, involves engineering *E. coli* to contain heterologous primary metabolisms so that it can utilize substrates such as CO_2 and formate as carbon sources. The work done by Kim *et al.,* on engineering the reductive glycine pathway into *E. coli* provides an exciting example of this strategy.[48,60] This work may be challenging upfront, but once *E. coli* is optimized to efficiently use electrochemically produced substrates, the plethora of work in the metabolic engineering of *E. coli* may be co-opted for use in electromicrobial production. Both strategies may be useful, and work to compare the resulting strains developed in both efforts should be pursued.

The initial phase of EMP research involved proof-of-principle studies demonstrating that strains like *C. necator* can be engineered to produce compounds of interest from H_2/CO_2 or formic acid. That point has been successfully demonstrated. Further academic research must now develop new tools and techniques to maximize yields in EMP systems. Studies that aim to improve the energy efficiency of carbon fixation as well as maximize the selectivity of the fixed carbon to the product of interest will greatly advance the appeal of EMP.

EMP systems must also operate at sufficiently high productivities to be practical for large-scale commodity chemical production. This may be challenging as EMP systems often rely on substrates with low solubility (H_2) or are toxic (formate) or use microbes that are notoriously slow growing (acetogens). Researchers should continue developing bioreactor engineering strategies that can improve productivity in these systems. In the analytical chapters of this dissertation, the models assume conventional chemostat bioreactors would be used for EMP at scale. Advances in bioreactor design for other applications may be applied to EMP. For example, the work of Kantzow *et al.* highlighted how submerged membrane reactors, originally used in wastewater treatment processes, could be used to increase the productivity of an acetogenic reactor 8-fold.[72]

Engineering integrated systems where electrochemical and biochemical reactions occur in the same co-localized module is an interesting endeavor and will likely lead to important insights regarding extracellular electron transfer and other important areas of microbiology and biochemistry. However, given the starkly different environments that lead to optimal performance in electrochemical and biochemical processes, I suspect that these systems do not reflect the types of systems that will enable large-scale industrial EMP. While this should not dissuade this type of academic research from being pursued, the question of how academic research relates to the eventual application should be considered.

Modeling and analysis of EMP systems is another area of academic research that should be actively pursued. The analytical frameworks used in Chapters 2 and 3 to assess process performance, environmental impacts, and economics of EMP processes are a good step in this direction. However, there are still outstanding questions that may be addressed by similar modeling and analysis. Process modeling, life cycle analysis, and techno-economic assessment should continue to be applied to EMP systems and be used to compare various EMP schemes to each other (as was done in Chapter 2). This approach should also be used to compare EMP systems to alternative CO_2-to-X processes, including biochemical systems, electrochemical systems, thermochemical systems, and systems created through a hybrid of these types of processes.

In theory, a single product may be made from CO_2 through multiple possible paths. Some products made from CO_2, such as methane, will likely be easier through traditional thermochemical processes (using electrolytically produced hydrogen) rather than through EMP. Others, such as enzymes, will only be effectively produced through systems with a biological component. Frameworks to systematically compare these various strategies to each other should be developed to understand the tradeoffs with each approach. A single answer of what is the best approach to take is impossible from an objective viewpoint, as there is no correct way to weigh economic costs, resource demands, environmental impacts, carbon footprint, labor requirements, and other factors, even if they can be accurately predicted through modeling. However, modeling may be used to inform these more complex decisions.

Societal factors, or It's not all about the science

The analyses in Chapters 2 and 3 illuminate the fact that the success of electromicrobial production depends as much as exogenous factors as it does on technological progress. Some factors such as carbon efficiency are important to both the environmental and economic viability of EMP and can be addressed by the synthetic biologists and biochemical engineers working in the lab. However, other factors, such as the fraction of renewables in the electricity grid and the overall cost of electricity are major determinants of whether EMP can be environmentally advantageous and cost-competitive.

As noted in Chapter 3, electricity (which due to the constraints described in Chapter 2 must be from a decarbonized source) must be cheap enough for EMP to be economically viable. The exact breakeven price will depend on the value of the product, efficiency of the process, *etc*. However, in any case, the price of electricity will likely need to fall to make the economic argument for EMP. The U.S. Department of Energy Sunshot 2030 initiative seeks to reduce the average price of solar to $0.03/kWh by 2030.[168] In sunnier areas of the world, solar energy may be even cheaper, which would make the prospects of EMP even better depending on the location. The price of solar power in the coming decades will be set by a combination of technological development, market factors, and public policy.

The analysis in Chapter 2 suggests that EMP systems can effectively reduce the negative environmental impacts of the biotechnology industry assuming clean electricity is used. Currently, however, electromicrobial systems are not environmentally viable due to the high carbon footprint of electricity generation. However, the climate crisis does necessitate a transition to a fully decarbonized grid in the coming decade. Absent an energy grid dominated by renewables, the carbon emissions due to electromicrobial production would likely be significantly higher than conventional petroleum-based manufacturing.

As of April 2023, it is the position of the present U.S. administration that the U.S. electricity grid will be composed of at least 80% renewable energy sources by 2030, with a fully decarbonized grid by 2035. While technically and economically feasible, meeting these ambitious yet necessary targets will require strong public policies, according to an analysis by Abhyankar *et al.*,[226] including the passage of a Clean Electricity Standard (CES) by the U.S. Congress. Despite a large majority (63% of U.S. voters) supporting a Clean Electricity Standard, the character of the political system in the United States (both structurally and in its current makeup) makes the future of such a policy uncertain.[227] Policy concerns, in addition to technological hurdles, will play a large role in the feasibility of electromicrobial production.

The public policy aspects affecting EMP deployment goes beyond reaching economic and environmental viability. If EMP systems are deployed, policies must be enacted such that they are deployed responsibly. The incentives of for-profit companies controlling these systems may, by their position in society, be significantly misaligned with the public good. EMP requires vast amounts of electricity to function, and if the electricity does not come from a clean energy source, these systems will lead to increased carbon emissions. Regulations to prevent this should therefore be developed.

For sensible policy debates to occur, the role that EMP can play in a carbon-neutral economy must be clearly understood. The concept of carbon utilization in managing ongoing CO_2 emissions has been used in corporate greenwashing, especially by the fossil fuel industry, as a way of justifying continued use of fossil fuels.[228] Nearly any product of interest in an EMP system will eventually be converted back into CO_2, either through combustion (as in the case of fuels) or degradation (as in the case of bioplastics). A possible exception to this general rule would be using EMP to produce materials that do not biodegrade, such as bio-PET or similar long-lasting plastics; however, the sequestration of carbon in the form of giant patch of garbage floating in the ocean is hardly a cause for celebration in my opinion.

Therefore, EMP can at best be carbon neutral, and therefore does not reduce carbon emissions or atmospheric carbon concentrations, regardless of whether the CO_2 required for the process comes from industrial point-sources or direct air capture. EMP, from a simple mass balance observation,

does little to directly abate atmospheric carbon emissions, and any benefit comes from its ability to *replace* fossil-based chemical processes. Claims that EMP, or any other carbon utilization technology, can be used to manage existing fossil processes must therefore be soundly rejected. EMP as a technology cannot be used to abate carbon emissions and "buy time" for a clean energy transition to occur; by contrast, as I have shown in Chapter 2, EMP will only be sustainable at scale following the necessary clean energy transition.

Pathways for implementations

As I stated previously, my advocacy for the field of EMP does not lead me to discount other forms of bioproduction. EMP will not be suitable for every situation. However, EMP may play a role in developing a truly circular carbon economy to finally replace the existentially destructive and extractive fossil carbon economy. Even if the technologies enabling this shift are fully developed, there will almost certainly be a large "activation energy" to achieving such a fully circular economy. I see two distinct (but not incompatible) paths to achieving this.

EMP will have the greatest environmental impact if it can produce low value, high volume products, such as fuels or plastics, especially if the alternative is a petroleum-based product. One strategy would be to focus efforts on optimizing an EMP process for one (or perhaps a few) of these products. Research efforts could be devoted to optimizing strains for this product. Rather than engineering Knallgas bacteria to produce umpteen different small molecule products, labs could focus on marginal improvements to the yield of, say, butanol from H_2/CO_2. Pilot-scale plants could emerge from these efforts, and eventually be commercialized. This strategy would be risky, as competing with existing production technologies would be enormously challenging. Not only would EMP have to outcompete other forms of bioprocessing but would need to outcompete petroleum-based processing as well. However, the potential benefit would be significant.

Another path would be less risky, but less immediately impactful. This would be to target products of higher value produced on smaller scales, at least in the early phase of EMP deployment. At this stage, focusing on biomolecules that cannot be created in abiotic processes, such as industrial enzymes, would reduce the level of competition and therefore relax the requirements for economic performance. While the impact of these early ventures would be smaller, they would serve as an early success story for the technology. EMP would get its proverbial foot in the metaphorical door. Successful commercialization of these systems would lead to "experience curve effects", and therefore the costs of EMP processes as a whole would decrease over time. As this occurs, products of lower value may be targeted, and EMP could eventually expand to the applications described in the previous paragraph. The major environmental benefits would be more marginal during the early adoption phase, but the reduced risk may justify this strategy.

Of course, both strategies can, and likely will, be attempted in parallel, as there are many actors involved in academia, industry, and government and a single consensus approach will not be reached by the field. However, considering these possible outcomes is a useful exercise that should inform decision-making by those involved in developing and implementing electromicrobial production systems.

Closing thoughts

With those final thoughts suggesting important areas of future research as well as speculating on the future of EMP, thoughts which have accumulated over the course of four years dedicated to

studying this technology, I can now bring this dissertation to a close. The combination of electrochemical and biochemical processes for chemical production is not only intellectually fascinating, but the carbon-neutral nature of these processes provides a possible avenue for decarbonizing the chemical industry. The integration of metabolic pathways developed in nature over millions of years with the electrochemical innovations of the modern era creates a synergy that enables possibilities that could not exist through either independently. Hopefully the work and discussion contained here will lead to greater advances in the field, and to science and engineering broadly.

References

1. Rasmussen, S. C. From Honey Wine to the Cultivation of the Grape: An Early History of Fermented Beverages. in *Chemical Technology in Antiquity* (American Chemical Society, 2015).
2. Barnett, J. A. Beginnings of microbiology and biochemistry: The contribution of yeast research. *Microbiology* **149**, 557–567 (2003).
3. Jones, D. T. & Woods, D. R. Acetone-butanol fermentation revisited. *Microbiol. Rev.* **50**, 484–524 (1986).
4. Ozturk, A. B. *et al.* Techno-economic analysis of a two-step fermentation process for bio-butanol production from cooked rice. *Sustain. Energy Fuels* **5**, 3705–3718 (2021).
5. Mohr, K. I. History of antibiotics research. *Curr. Top. Microbiol. Immunol.* **398**, 237–272 (2016).
6. Cohen, S. N., Chang, A. C. Y., Boyer, H. W. & Helling, R. B. Construction of biologically functional bacterial plasmids in vitro. *Proc. Natl. Acad. Sci. U. S. A.* **70**, 3240–3244 (1973).
7. Riggs, A. D. Bacterial Production of Human Insulin. *Diabetes Care* **4**, 64–68 (1981).
8. Cruz-Morales, P. *et al.* Biosynthesis of polycyclopropanated high energy biofuels. *Joule* **6**, 1590–1605 (2022).
9. Ro, D.-K. *et al.* Production of the antimalarial drug precursor artemisinic acid in engineered yeast. *Nature* **440**, 940–943 (2006).
10. Jung, Y. K., Kim, T. Y., Park, S. J. & Lee, S. Y. Metabolic engineering of *Escherichia coli* for the production of polylactic acid and its copolymers. *Biotechnol. Bioeng.* **105**, 161–171 (2010).
11. Grewal, P. S., Modavi, C., Russ, Z. N., Harris, N. C. & Dueber, J. E. Bioproduction of a betalain color palette in *Saccharomyces cerevisiae*. *Metab. Eng.* **45**, 180–188 (2018).
12. Ko, Y.-S. *et al.* Tools and strategies of systems metabolic engineering for the development of microbial cell factories for chemical production. *Chem. Soc. Rev.* **49**, 4615–4636 (2020).
13. Zhang, J. *et al.* A microbial supply chain for production of the anti-cancer drug vinblastine. *Nature* **609**, 341–347 (2022).
14. Rossino, G. *et al.* Biocatalysis: A smart and green tool for the preparation of chiral drugs. *Chirality* **34**, 1403–1418 (2022).
15. Agouridas, V., El Mahdi, O. & Melnyk, O. Chemical Protein Synthesis in Medicinal Chemistry. *J. Med. Chem.* **63**, 15140–15152 (2020).
16. Tan, Y., Wu, H., Wei, T. & Li, X. Chemical Protein Synthesis: Advances, Challenges, and Outlooks. *J. Am. Chem. Soc.* **142**, 20288–20298 (2020).
17. Chum, H. *et al.* Bioenergy. in *IPCC Special Report on Renewable Energy Sources and Climate Change Mitigation*. 209–332 (Cambridge University Press, 2012).
18. Davis, R. *et al.* Process Design and Economics for the Conversion of Lignocellulosic

Biomass to Hydrocarbon Fuels and Coproducts: 2018 Biochemical Design Case Update. *Renew. Energy* 147 (2018).

19. Amiri, H. Recent innovations for reviving the ABE fermentation for production of butanol as a drop-in liquid biofuel. *Biofuel Res. J.* **7**, 1256–1266 (2020).

20. Peralta-Yahya, P. P., Zhang, F., Del Cardayre, S. B. & Keasling, J. D. Microbial engineering for the production of advanced biofuels. *Nature* **488**, 320–328 (2012).

21. Brandon, A. M. & Criddle, C. S. Can biotechnology turn the tide on plastics? *Curr. Opin. Biotechnol.* **57**, 160–166 (2019).

22. Boussie, T. R., Diamond, G. M., Dias, E. & Murphy, V. Synthesis of Adipic Acid Starting from Renewable Raw Materials. in *Chemicals and Fuels from Bio-Based Building Blocks* 151–172 (Wiley, 2016).

23. Cheng, J., Li, J. & Zheng, L. Achievements and Perspectives in 1,4-Butanediol Production from Engineered Microorganisms. *J. Agric. Food Chem.* **69**, 10480–10485 (2021).

24. Werpy, T. & Petersen, G. *Top Value Added Chemicals from Biomass Volume I-Results of Screening for Potential Candidates from Sugars and Synthesis Gas*. (NREL, 2004).

25. Lee, R. A. & Lavoie, J.-M. From first- to third-generation biofuels: Challenges of producing a commodity from a biomass of increasing complexity. *Anim. Front.* **3**, 6–11 (2013).

26. Vink, E. T. H. & Davies, S. Life Cycle Inventory and Impact Assessment Data for 2014 Ingeo^{TM} Polylactide Production. *Ind. Biotechnol.* **11**, 167–180 (2015).

27. Gustavsson, M. & Lee, S. Y. Prospects of microbial cell factories developed through systems metabolic engineering. *Microb. Biotechnol.* **9**, 610–617 (2016).

28. McKone, T. E. *et al.* Grand challenges for life-cycle assessment of biofuels. *Environ. Sci. Technol.* **45**, 1751–1756 (2011).

29. Fargione, J., Hill, J., Tilman, D., Polasky, S. & Hawthorne, P. Land Clearing and the Biofuel Carbon Debt. *Science.* **319**, 1235–1238 (2008).

30. Crutzen, P. J., Mosier, A. R., Smith, K. A. & Winiwarter, W. N_2O release from agro-biofuel production negates global warming reduction by replacing fossil fuels. *Atmos. Chem. Phys.* **8**, 389–395 (2008).

31. Rathmann, R., Szklo, A. & Schaeffer, R. Land use competition for production of food and liquid biofuels: An analysis of the arguments in the current debate. *Renew. Energy* **35**, 14–22 (2010).

32. Roche, C. M., Glass, N. L., Blanch, H. W. & Clark, D. S. Engineering the filamentous fungus *Neurospora crassa* for lipid production from lignocellulosic biomass. *Biotechnol. Bioeng.* **111**, 1097–1107 (2014).

33. Shill, K. *et al.* Ionic liquid pretreatment of cellulosic biomass: Enzymatic hydrolysis and ionic liquid recycle. *Biotechnol. Bioeng.* **108**, 511–520 (2011).

34. Liu, Y. *et al.* Biofuels for a sustainable future. *Cell* **184**, 1636–1647 (2021).

35. Leite, G. B., Abdelaziz, A. E. M. & Hallenbeck, P. C. Algal biofuels: Challenges and opportunities. *Bioresour. Technol.* **145**, 134–141 (2013).

36. López Barreiro, D., Prins, W., Ronsse, F. & Brilman, W. Hydrothermal liquefaction (HTL) of microalgae for biofuel production: State of the art review and future prospects. *Biomass and Bioenergy* **53**, 113–127 (2013).

37. Hilzinger, J. M. *et al.* Acetaminophen production in the edible, filamentous cyanobacterium *Arthrospira platensis*. *bioRxiv* 2022.06.30.498297 (2022) doi:10.1101/2022.06.30.498297.

38. Varman, A. M., Yu, Y., You, L. & Tang, Y. J. Photoautotrophic production of D-lactic acid in an engineered cyanobacterium. *Microb. Cell Fact.* **12**, 1–8 (2013).

39. Blankenship, R. E. *et al.* Comparing Photosynthetic and Photovoltaic Efficiencies and Recognizing the Potential for Improvement. *Science.* **332**, 805–809 (2011).

40. Chen, H., Li, T. & Wang, Q. Ten years of algal biofuel and bioproducts: gains and pains. *Planta* **249**, 195–219 (2019).

41. Aro, E.-M. From first generation biofuels to advanced solar biofuels. *Ambio* **45** Suppl 1, 24–31 (2016).

42. Straathof, A. J. J. *et al.* Grand Research Challenges for Sustainable Industrial Biotechnology. *Trends Biotechnol.* **37**, 1042–1050 (2019).

43. Claassens, N. J., Cotton, C. A. R., Kopljar, D. & Bar-Even, A. Making quantitative sense of electromicrobial production. *Nat. Catal.* **2**, 437–447 (2019).

44. Rabaey, K. & Rozendal, R. A. Microbial electrosynthesis — revisiting the electrical route for microbial production. *Nat. Rev. Microbiol.* **8**, 706–716 (2010).

45. Tanaka, K. & Ishizaki, A. Production of poly-d-3-hydroxybutyric acid from carbon dioxide by a two-stage culture method employing *Alcaligenes eutrophus* ATCC 17697T. *J. Ferment. Bioeng.* **77**, 425–427 (1994).

46. Kunasundari, B., Murugaiyah, V., Kaur, G., Maurer, F. H. J. & Sudesh, K. Revisiting the Single Cell Protein Application of *Cupriavidus necator* H16 and Recovering Bioplastic Granules Simultaneously. *PLoS One* **8**, 78528 (2013).

47. Grunwald, S. *et al.* Kinetic and stoichiometric characterization of organoautotrophic growth of *Ralstonia eutropha* on formic acid in fed-batch and continuous cultures. *Microb. Biotechnol.* **8**, 155–163 (2015).

48. Kim, S. *et al.* Growth of *E. coli* on formate and methanol via the reductive glycine pathway. *Nat. Chem. Biol.* **16**, 538–545 (2020).

49. Nybo, S. E., Khan, N. E., Woolston, B. M. & Curtis, W. R. Metabolic engineering in chemolithoautotrophic hosts for the production of fuels and chemicals. *Metab. Eng.* **30**, 105–120 (2015).

50. Moon, J. *et al.* Formate metabolism in the acetogenic bacterium *Acetobacterium woodii*. *Environ. Microbiol.* **23**, 4214–4227 (2021).

51. Liu, C. *et al.* Nanowire-bacteria hybrids for unassisted solar carbon dioxide fixation to value-added chemicals. *Nano Lett.* **15**, 3634–3639 (2015).

52. Hu, P. *et al.* Integrated bioprocess for conversion of gaseous substrates to liquids. *Proc. Natl. Acad. Sci.* **113**, 3773–3778 (2016).

53. Meraz, J. L., Abel, A. J., Clark, D. S. & Criddle, C. S. Biological conversion of methane to bioplastics: Kinetics, stoichiometry, and thermodynamic considerations for process optimization. *Chem. Eng. J.* **454**, 140166 (2023).

54. Jouny, M., Luc, W. & Jiao, F. General Techno-Economic Analysis of CO_2 Electrolysis Systems. *Ind. Eng. Chem. Res.* **57**, 2165–2177 (2018).

55. Bi, C. *et al.* Development of a broad-host synthetic biology toolbox for *Ralstonia eutropha* and its application to engineering hydrocarbon biofuel production. *Microb. Cell Fact.* **12**, 107 (2013).

56. Köpke, M. *et al. Clostridium ljungdahlii* represents a microbial production platform based on syngas. *Proc. Natl. Acad. Sci.* **107**, 13087–13092 (2010).

57. Johnson, A. O., Gonzalez-villanueva, M., Tee, K. L. & Wong, T. S. An Engineered Constitutive Promoter Set with Broad Activity Range for *Cupriavidus necator* H16. *ACS Synth. Biol.* **7**, 1918–1928 (2018).

58. Xiong, B. *et al.* Genome editing of *Ralstonia eutropha* using an electroporation-based CRISPR-Cas9 technique. *Biotechnol. Biofuels* **11**, 172 (2018).

59. Nagaraju, S., Davies, N. K., Walker, D. J. F., Köpke, M. & Simpson, S. D. Genome editing of *Clostridium autoethanogenum* using CRISPR/Cas9. *Biotechnol. Biofuels* **9**, 219 (2016).

60. Kim, S. *et al.* Optimizing *E. coli* as a formatotrophic platform for bioproduction via the reductive glycine pathway. *Frontiers in Bioengineering and Biotechnology*. **11** (2023).

61. Garcia-Gonzalez, L., Mozumder, M. S. I., Dubreuil, M., Volcke, E. I. P. & De Wever, H. Sustainable autotrophic production of polyhydroxybutyrate (PHB) from CO_2 using a two-stage cultivation system. *Catal. Today* **257**, 237–245 (2015).

62. Nangle, S. N. *et al.* Valorization of CO_2 through lithoautotrophic production of sustainable chemicals in *Cupriavidus necator*. *Metab. Eng.* **62**, 207–220 (2020).

63. Liu, C., Colón, B. C., Ziesack, M., Silver, P. A. & Nocera, D. G. Water splitting–biosynthetic system with CO_2 reduction efficiencies exceeding photosynthesis. *Science.* **352**, 1210–1213 (2016).

64. Crépin, L., Lombard, E. & Guillouet, S. E. Metabolic engineering of *Cupriavidus necator* for heterotrophic and autotrophic alka(e)ne production. *Metab. Eng.* **37**, 92–101 (2016).

65. Windhorst, C. & Gescher, J. Efficient biochemical production of acetoin from carbon dioxide using *Cupriavidus necator* H16. *Biotechnol. Biofuels* **12**, 163 (2019).

66. Li, H. *et al.* Integrated Electromicrobial Conversion of CO_2 to Higher Alcohols. *Science.* **335**, 1596 (2012).

67. Groher, A. & Weuster-Botz, D. Comparative reaction engineering analysis of different acetogenic bacteria for gas fermentation. *J. Biotechnol.* **228**, 82–94 (2016).

68. Liew, F. E. *et al.* Carbon-negative production of acetone and isopropanol by gas fermentation at industrial pilot scale. *Nat. Biotechnol.* **40**, 335–344 (2022).

69. Cestellos-Blanco, S. *et al.* Production of PHB From CO_2-Derived Acetate With Minimal Processing Assessed for Space Biomanufacturing. *Front. Microbiol.* **12**, 1–12 (2021).

70. Ishizaki, A. & Tanaka, K. Batch culture of *Alcaligenes eutrophus* ATCC 17697^T using recycled gas closed circuit culture system. *J. Ferment. Bioeng.* **69**, 170–174 (1990).

71. Tanaka, K., Ishizaki, A., Kanamaru, T. & Kawano, T. Production of poly(D-3-hydroxybutyrate) from CO_2, H_2, and O_2 by high cell density autotrophic cultivation of *Alcaligenes eutrophus*. *Biotechnol. Bioeng.* **45**, 268–275 (1995).

72. Kantzow, C., Mayer, A. & Weuster-Botz, D. Continuous gas fermentation by *Acetobacterium woodii* in a submerged membrane reactor with full cell retention. *J. Biotechnol.* **212**, 11–18 (2015).

73. Islam Mozumder, M. S., Garcia-Gonzalez, L., Wever, H. De & Volcke, E. I. P. Poly(3-hydroxybutyrate) (PHB) production from CO_2: Model development and process optimization. *Biochem. Eng. J.* **98**, 107–116 (2015).

74. Chen, J., Gomez, J. A., Höffner, K., Barton, P. I. & Henson, M. A. Metabolic modeling of synthesis gas fermentation in bubble column reactors. *Biotechnol. Biofuels* **8**, 1–12 (2015).

75. Abel, A. J. & Clark, D. S. A Comprehensive Modeling Analysis of Formate-Mediated Microbial Electrosynthesis. *ChemSusChem* **14**, 344–355 (2021).

76. Abel, A. J., Hilzinger, J. M., Arkin, A. P. & Clark, D. S. Systems-informed genome mining for electroautotrophic microbial production. *Bioelectrochemistry* 108054 (2022).

77. Abel, A. J., Adams, J. D., Hilzinger, J. M. & Arkin, A. P. Charting a narrow course for direct electron uptake-facilitated electromicrobial production. *bioRxiv* 2022.05.28.493842 (2022) doi:10.1101/2022.05.28.493842.

78. Salimijazi, F. *et al.* Constraints on the Efficiency of Engineered Electromicrobial Production. *Joule* **4**, 2101–2130 (2020).

79. Leger, D. *et al.* Photovoltaic-driven microbial protein production can use land and sunlight more efficiently than conventional crops. *Proc. Natl. Acad. Sci.* **118**, e2015025118 (2021).

80. Holmström, S. & Pitkänen, J.-P. Strains and processes for single cell protein or biomass production. (2021).

81. Air Protein. Making Air Meat. https://www.airprotein.com/making-air-meat.

82. Circe Biosciences. Decarbonizing food production. https://www.circebioscience.com/.

83. Lanzatech. Carbon Recycling Technology for the Future. https://lanzatech.com/.

84. Ou, X., Zhang, X., Zhang, Q. & Zhang, X. Life-cycle analysis of energy use and greenhouse gas emissions of gas-to-liquid fuel pathway from steel mill off-gas in China by the LanzaTech process. *Front. Energy* **7**, 263–270 (2013).

85. LanzaJet. Jet Fuel Derived from Ethanol Now Eligible for Commercial Flights. https://www.lanzajet.com/900-2/ (2018).

86. Huffer, S., Roche, C. M., Blanch, H. W. & Clark, D. S. *Escherichia coli* for biofuel production: bridging the gap from promise to practice. *Trends Biotechnol.* **30**, 538–545 (2012).

87. Singh, R., Kumar, M., Mittal, A. & Mehta, P. K. Microbial enzymes: industrial progress in 21st century. *3 Biotech* **6**, 174 (2016).

88. Adams, J. D., Røise, J. J., Lee, D. S. & Murthy, N. The methionase chain reaction: An enzyme-based autocatalytic amplification system for the detection of thiols. *Chem. Commun.* **56**, 3175–3178 (2020).

89. Puetz, J. & Wurm, F. M. Recombinant Proteins for Industrial versus Pharmaceutical Purposes: A Review of Process and Pricing. *Processes*. **7**, 476 (2019).

90. Laurens, L. M. L. *et al.* Development of algae biorefinery concepts for biofuels and bioproducts; a perspective on process-compatible products and their impact on cost-reduction. *Energy Environ. Sci.* **10**, 1716–1738 (2017).

91. Grousseau, E., Lu, J., Gorret, N., Guillouet, S. E. & Sinskey, A. J. Isopropanol production with engineered *Cupriavidus necator* as bioproduction platform. *Appl. Microbiol. Biotechnol.* **98**, 4277–4290 (2014).

92. Yishai, O., Lindner, S. N., Gonzalez de la Cruz, J., Tenenboim, H. & Bar-Even, A. The formate bio-economy. *Curr. Opin. Chem. Biol.* **35**, 1–9 (2016).

93. International Organization for Standardization (ISO). International Standard ISO 14044 Environmental management — Life cycle assessment — Requirements and guidelines Management. *ISO 14044* (2006).

94. International Organization for Standarization. Environmental Management - Life Cycle Assessment - Principles and Framework. *ISO 14040* (2006).

95. Izursa, J., Hanlon, E. A., Amponsah, N. Y. & Capece, J. C. *Carbon Footprint of Biofuel Sugarcane Produced in Mineral and Organic Soils in Florida*. U.S. Dept. of Energy. (2013).

96. Sillman, J. *et al.* Bacterial protein for food and feed generated via renewable energy and direct air capture of CO_2: Can it reduce land and water use? *Glob. Food Sec.* **22**, 25–32 (2019).

97. Cumberlege, T., Blenkinsopp, T. & Clark, J. *Assessment of environmental impact of FeedKind protein*. (2016).

98. Blanch, H. W. & Clark, D. S. *Biochemical Engineering*. (CRC Press, 1997).

99. Xiao, Y. *et al.* Kinetic modeling and isotopic investigation of isobutanol fermentation by two engineered *Escherichia coli* strains. *Ind. Eng. Chem. Res.* **51**, 15855–15863 (2012).

100. Fast, A. G. & Papoutsakis, E. T. Stoichiometric and energetic analyses of non-photosynthetic CO_2-fixation pathways to support synthetic biology strategies for production of fuels and chemicals. *Curr. Opin. Chem. Eng.* **1**, 380–395 (2012).

101. Schuchmann, K. & Müller, V. Autotrophy at the thermodynamic limit of life: A model for energy conservation in acetogenic bacteria. *Nat. Rev. Microbiol.* **12**, 809–821 (2014).

102. Rosso, L., Lobry, J. R., Bajard, S. & Flandrois, J. P. Convenient model to describe the combined effects of temperature and pH on microbial growth. *Appl. Environ. Microbiol.* **61**, 610–616 (1995).

103. Wu, X., Altman, R., Eiteman, M. A. & Altman, E. Adaptation of *Escherichia coli* to Elevated Sodium Concentrations Increases Cation Tolerance and Enables Greater Lactic Acid Production. *Appl. Environ. Microbiol.* **80**, 2880–2888 (2014).

104. Mook, W. G. *Environmental isotopes in the hydrological cycle: Principles and*

applications. (UNESCO, 2000).

105. Meraz, J. L., Dubrawski, K. L., El Abbadi, S. H., Choo, K. H. & Criddle, C. S. Membrane and Fluid Contactors for Safe and Efficient Methane Delivery in Methanotrophic Bioreactors. *J. Environ. Eng.* **146**, (2020).

106. Ciroth, A. ICT for environment in life cycle applications openLCA — A new open source software for life cycle assessment. *Int. J. Life Cycle Assess.* **12**, 209 (2007).

107. Manfredi, S., Allacker, K., Chomkhamsri, K., Pelletier, N., de Souza, D. M. *Product Environmental Footprint (PEF) Guide*. (European Commision Joint Research Centre, 2012).

108. Subramanian, M. R., Talluri, S. & Christopher, L. P. Production of lactic acid using a new homofermentative *Enterococcus faecalis* isolate. *Microb. Biotechnol.* **8**, 221–229 (2015).

109. Heldal, M., Norland, S. & Tumyr, O. X-ray microanalytic method for measurement of dry matter and elemental content of individual bacteria. *Appl. Environ. Microbiol.* **50**, 1251 LP – 1257 (1985).

110. Deutz, S. & Bardow, A. Life-cycle assessment of an industrial direct air capture process based on temperature–vacuum swing adsorption. *Nat. Energy* **6**, 203–213 (2021).

111. Singh, V., Dincer, I. & Rosen, M. A. Life Cycle Assessment of Ammonia Production Methods. in *Energetic and Environmental Dimensions* (eds. Dincer, I., Colpan, C. O. & Kizilkan, O.) 935–959 (Academic Press, 2018).

112. Garcia-Herrero, I., Margallo, M., Onandía, R., Aldaco, R. & Irabien, A. Environmental challenges of the chlor-alkali production: Seeking answers from a life cycle approach. *Sci. Total Environ.* **580**, 147–157 (2017).

113. Buttler, A. & Spliethoff, H. Current status of water electrolysis for energy storage, grid balancing and sector coupling via power-to-gas and power-to-liquids: A review. *Renew. Sustain. Energy Rev.* **82**, 2440–2454 (2018).

114. Xu, J., Liu, G., Li, J. & Wang, X. The electrocatalytic properties of an IrO_2/SnO_2 catalyst using SnO_2 as a support and an assisting reagent for the oxygen evolution reaction. *Electrochim. Acta* **59**, 105–112 (2012).

115. Yang, H., Kaczur, J. J., Sajjad, S. D. & Masel, R. I. Electrochemical conversion of CO_2 to formic acid utilizing Sustainion™ membranes. *J. CO_2 Util.* **20**, 208–217 (2017).

116. Hábová, V., Melzoch, K., Rychtera, M. & Sekavová, B. Electrodialysis as a useful technique for lactic acid separation from a model solution and a fermentation broth. *Desalination* **162**, 361–372 (2004).

117. Stropnik, R., Lotrič, A., Bernad Montenegro, A., Sekavčnik, M. & Mori, M. Critical materials in PEMFC systems and a LCA analysis for the potential reduction of environmental impacts with EoL strategies. *Energy Sci. Eng.* **7**, 2519–2539 (2019).

118. Stadel, A., Gursel, P. & Masanet, E. *Life-Cycle Evaluation of Concrete Building Construction as a Strategy for Sustainable Cities*. (2012) doi:10.2172/1223003.

119. Ma, B. L., Liang, B. C., Biswas, D. K., Morrison, M. J. & McLaughlin, N. B. The carbon footprint of maize production as affected by nitrogen fertilizer and maize-legume rotations.

Nutr. Cycl. Agroecosystems **94**, 15–31 (2012).

120. Huang, J. *et al.* Anthropogenic and natural radiative forcing. in *Climate Change 2013: The Physical Science Basis: Working Group I Contribution to the Fifth Assessment Report of the Intergovernmental Panel on Climate Change*. (Cambride University Press, 2013).

121. Huijbregts, M. *et al. ReCiPe 2016 - A harmonized life cycle impact assessment method at midpoint and endpoint level. Report I: Characterization*. (National Institute for Public Health and the Environment, 2016).

122. Terpstra, M. A. Flammability Limits of Hydrogen-Diluent Mixtures in Air. (University of Calgary, 2012).

123. Möller, B., Oßmer, R., Howard, B. H., Gottschalk, G. & Hippe, H. *Sporomusa*, a new genus of gram-negative anaerobic bacteria including *Sporomusa sphaeroides* spec. nov. and *Sporomusa ovata* spec. nov. *Arch. Microbiol.* **139**, 388–396 (1984).

124. Kutscha, R. & Pflügl, S. Microbial upgrading of acetate into value-added products—examining microbial diversity, bioenergetic constraints and metabolic engineering approaches. *Int. J. Mol. Sci.* **21**, 1–30 (2020).

125. Shi, X.-C. C., Tremblay, P.-L. L., Wan, L. & Zhang, T. Improved robustness of microbial electrosynthesis by adaptation of a strict anaerobic microbial catalyst to molecular oxygen. *Sci. Total Environ.* **754**, 142440 (2021).

126. Nichols, E. M. *et al.* Hybrid bioinorganic approach to solar-to-chemical conversion. *Proc. Natl. Acad. Sci.* **112**, 201508075 (2015).

127. Upadhyaya, B. P., DeVeaux, L. C. & Christopher, L. P. Metabolic engineering as a tool for enhanced lactic acid production. *Trends Biotechnol.* **32**, 637–644 (2014).

128. de Chalendar, J. A., Taggart, J. & Benson, S. M. Tracking emissions in the US electricity system. *Proc. Natl. Acad. Sci. U. S. A.* **116**, 25497–25502 (2019).

129. Lee, M. Y. *et al.* Current achievements and the future direction of electrochemical CO_2 reduction: A short review. *Crit. Rev. Environ. Sci. Technol.* **50**, 769–815 (2020).

130. Tsiropoulos, I., Cok, B. & Patel, M. K. Energy and greenhouse gas assessment of European glucose production from corn – a multiple allocation approach for a key ingredient of the bio-based economy. *J. Clean. Prod.* **43**, 182–190 (2013).

131. Vercalsteren, A. & Boonen, K. *Life Cycle Assessment study of starch products for the European starch industry association (Starch Europe): sector study*. (Starch of Europe, 2015).

132. Link, H., Anselment, B. & Weuster-Botz, D. Leakage of adenylates during cold methanol/glycerol quenching of *Escherichia coli*. *Metabolomics* **4**, 240–247 (2008).

133. Shiloach, J. & Fass, R. Growing *E. coli* to high cell density—A historical perspective on method development. *Biotechnol. Adv.* **23**, 345–357 (2005).

134. Sundstrom, E. R. & Criddle, C. S. Optimization of Methanotrophic Growth and Production of Poly(3-Hydroxybutyrate) in a High-Throughput Microbioreactor System. *Appl. Environ. Microbiol.* **81**, 4767 – 4773 (2015).

135. Nangle, S. N. *et al.* The case for biotech on Mars. *Nat. Biotechnol.* **38**, 401–407 (2020).

136. Götz, M. *et al.* Renewable Power-to-Gas: A technological and economic review. *Renew. Energy* **85**, 1371–1390 (2016).

137. Fornaciari, J. C. *et al.* A Perspective on the Electrochemical Oxidation of Methane to Methanol in Membrane Electrode Assemblies. *ACS Energy Lett.* **5**, 2954–2963 (2020).

138. Umeda, M., Niitsuma, Y., Horikawa, T., Matsuda, S. & Osawa, M. Electrochemical Reduction of CO_2 to Methane on Platinum Catalysts without Overpotentials: Strategies for Improving Conversion Efficiency. *ACS Appl. Energy Mater.* **3**, 1119–1127 (2020).

139. Prévoteau, A., Carvajal-Arroyo, J. M., Ganigué, R. & Rabaey, K. Microbial electrosynthesis from CO_2: forever a promise? *Curr. Opin. Biotechnol.* **62**, 48–57 (2020).

140. Davis, R. *et al.* Process Design and Economics for the Conversion of Lignocellulosic Biomass to Hydrocarbons: Dilute-Acid and Enzymatic Deconstruction of Biomass to Sugars and Biological Conversion of Sugars to Hydrocarbons. *Natl. Renew. Energy Lab.* 147 (2013).

141. Li, Y. *et al.* Sustainable Lactic Acid Production from Lignocellulosic Biomass. *ACS Sustain. Chem. Eng.* **9**, 1341–1351 (2021).

142. Claassens, N. J. *et al.* Replacing the Calvin cycle with the reductive glycine pathway in *Cupriavidus necator*. *Metab. Eng.* **62**, 30–41 (2020).

143. IEA, The future of petrochemicals – Towards more sustainable plastics and fertilizers. 1–130 (IEA, 2018).

144. Kätelhön, A., Meys, R., Deutz, S., Suh, S. & Bardow, A. Climate change mitigation potential of carbon capture and utilization in the chemical industry. *Proc. Natl. Acad. Sci.* **116**, 11187–11194 (2019).

145. Rochelle, G. T. Amine Scrubbing for CO_2 Capture. *Science.* **325**, 1652–1654 (2009).

146. Abd, A. A., Naji, S. Z., Hashim, A. S. & Othman, M. R. Carbon dioxide removal through physical adsorption using carbonaceous and non-carbonaceous adsorbents: A review. *J. Environ. Chem. Eng.* **8**, 104142 (2020).

147. Baciocchi, R., Storti, G. & Mazzotti, M. Process design and energy requirements for the capture of carbon dioxide from air. *Chem. Eng. Process. Process Intensif.* **45**, 1047–1058 (2006).

148. Keith, D. W., Holmes, G., St. Angelo, D. & Heidel, K. A Process for Capturing CO_2 from the Atmosphere. *Joule* **2**, 1573–1594 (2018).

149. Choi, S., Drese, J. H., Eisenberger, P. M. & Jones, C. W. Application of Amine-Tethered Solid Sorbents for Direct CO_2 Capture from the Ambient Air. *Environ. Sci. Technol.* **45**, 2420–2427 (2011).

150. McQueen, N. *et al.* A review of direct air capture (DAC): Scaling up commercial technologies and innovating for the future. *Prog. Energy* **3**, (2021).

151. Beuttler, C., Charles, L. & Wurzbacher, J. The Role of Direct Air Capture in Mitigation of Anthropogenic Greenhouse Gas Emissions. *Front. Clim.* **1**, 1–7 (2019).

152. Piscopo, C. G. & Loebbecke, S. Strategies to Enhance Carbon Dioxide Capture in Metal-Organic Frameworks. *Chempluschem* **85**, 538–547 (2020).

153. Sumida, K. *et al.* Carbon Dioxide Capture in Metal–Organic Frameworks. *Chem. Rev.* **112**, 724–781 (2012).

154. Côté, A. P. *et al.* Porous, Crystalline, Covalent Organic Frameworks. *Science.* **310**, 1166 – 1170 (2005).

155. Lyu, H., Li, H., Hanikel, N., Wang, K. & Yaghi, O. M. Covalent Organic Frameworks for Carbon Dioxide Capture from Air. *J. Am. Chem. Soc.* **144**, 12989–12995 (2022).

156. Ducat, D. C., Avelar-rivas, J. A., Way, J. C. & Silver, P. A. Rerouting Carbon Flux To Enhance Photosynthetic Productivity. *Appl. Environ. Microbiol.* **78**, 2660–2668 (2012).

157. M., V. A., Yi, X., B., P. H. & J., T. Y. Metabolic Engineering of *Synechocystis* sp. Strain PCC 6803 for Isobutanol Production. *Appl. Environ. Microbiol.* **79**, 908–914 (2013).

158. Fasihi, M., Efimova, O. & Breyer, C. Techno-economic assessment of CO_2 direct air capture plants. *J. Clean. Prod.* **224**, 957–980 (2019).

159. Sinha, A., Darunte, L. A., Jones, C. W., Realff, M. J. & Kawajiri, Y. Systems Design and Economic Analysis of Direct Air Capture of CO_2 through Temperature Vacuum Swing Adsorption Using MIL-101(Cr)-PEI-800 and mmen-Mg_2(dobpdc) MOF Adsorbents. *Ind. Eng. Chem. Res.* **56**, 750–764 (2017).

160. Grisales Díaz, V. H. & Olivar Tost, G. Techno-economic analysis of extraction-based separation systems for acetone, butanol, and ethanol recovery and purification. *Bioresour. Bioprocess.* **4**, (2017).

161. Short, W., Packey, D. & Holt, T. A manual for the economic evaluation of energy efficiency and renewable energy technologies. *Renew. Energy* **95**, 73–81 (1995).

162. Internal Revenue Service. *How To Depreciate Property*. (IRS, 2022).

163. McDonald, T. M. *et al.* Capture of Carbon Dioxide from Air and Flue Gas in the Alkylamine-Appended Metal–Organic Framework mmen-Mg_2(dobpdc). *J. Am. Chem. Soc.* **134**, 7056–7065 (2012).

164. Saini, M., Wang, Z. W., Chiang, C.-J. & Chao, Y.-P. Metabolic engineering of *Escherichia coli* for production of n-butanol from crude glycerol. *Biotechnol. Biofuels* **10**, 173 (2017).

165. Feldman, D. *et al.* U.S. Solar Photovoltaic System and Energy Storage Cost Benchmark: Q1 2021. *Natl. Renew. Energy Lab.* 1–120 (2021).

166. Pivovar, B. S., Ruth, M. F., Myers, D. J. & Dinh, H. N. Hydrogen: Targeting $1/kg in 1 Decade. *Electrochem. Soc. Interface* **30**, 61–65 (2021).

167. U.S. Department of Energy. *Department of Energy Hydrogen Program Plan*. (U.S. DOE, 2020).

168. U.S. Department of Energy. *The SunShot 2030 Goals: 3¢ per Kilowatt Hour for PV and 5 ¢ per Killowatt Hour for Dispatchable CSP*. (U.S. DOE, 2017).

169. Wang, Y., Ling, C., Chen, Y., Jiang, X., Chen, G.-Q. Microbial engineering for easy downstream processing. *Biotechnol Adv*. **37**, 107365 (2019).

170. Ohlson, J. Plasmid manufacture is the bottleneck of the genetic medicine revolution. *Drug discovery today*. **25**, 1891–1893 (2020).

171. Arikawa, H. Polyhydroxyalkanoate production from sucrose by *Cupriavidus necator* strains harboring csc genes from *Escherichia coli* W. **16**, 7497–7507 (2017).

172. Mozumder, M. S. I., De Wever, H., Volcke, E. I. P. & Garcia-Gonzalez, L. A robust fed-batch feeding strategy independent of the carbon source for optimal polyhydroxybutyrate production. *Process Biochem.* **49**, 365–373 (2014).

173. Nikel, P. I., De Almeida, A., Melillo, E. C., Galvagno, M. A. & Pettinari, M. J. New recombinant *Escherichia coli* strain tailored for the production of poly(3-hydroxybutyrate) from agroindustrial by-products. *Appl. Environ. Microbiol.* **72**, 3949–3954 (2006).

174. Jacquel, N., Lo, C.-W., Wei, Y.-H., Wu, H.-S. & Wang, S. S. Isolation and purification of bacterial poly(3-hydroxyalkanoates). *Biochem. Eng. J.* **39**, 15–27 (2008).

175. Harrison, R. G., Todd, P. W., Rudge, S. R. & Petrides, D. P. *Bioseparations Science and Engineering*. *Topics in Chemical Engineering* (Oxford University Press, 2015). doi:10.1093/oso/9780195391817.001.0001.

176. Schallmey, M., Singh, A. & Ward, O. P. Developments in the use of Bacillus species for industrial production. *Can. J. Microbiol.* **50**, 1–17 (2004).

177. Azam, A., Li, C., Metcalf, K. J. & Tullman-ercek, D. Type III Secretion as a Generalizable Strategy for the Production of Full-Length Biopolymer-Forming Proteins. *Biotechnol. Bioeng.* **113**, 2313-20 (2016).

178. Linton, E., Walsh, M. K., Sims, R. C. & Miller, C. D. Translocation of green fluorescent protein by comparative analysis with multiple signal peptides. *Biotechnol J.* **7**, 667–676 (2012).

179. Bakkes, P. J., Jenewein, S., Smits, S. H. J., Holland, I. B. & Schmitt, L. The Rate of Folding Dictates Substrate Secretion by the *Escherichia coli* Hemolysin Type 1 Secretion System. *J. Biol. Chem.* **285**, 40573–40580 (2010).

180. Bialecka-Fornal, M., Lee, H. J. & Phillips, R. The rate of osmotic downshock determines the survival probability of bacterial mechanosensitive channel mutants. *J. Bacteriol.* **197**, 231–237 (2015).

181. Rathi, D. *et al.* Polyhydroxyalkanoate biosynthesis and simplified polymer recovery by a novel moderately halophilic bacterium isolated from hypersaline microbial mats. *J. Appl. Microbiol.* **114**, 384-95 (2012).

182. Tan, D., Xue, Y.-S., Aibaidula, G. & Chen, G.-Q. Unsterile and continuous production of polyhydroxybutyrate by *Halomonas* TD01. *Bioresour. Technol.* **102**, 8130–8136 (2011).

183. de Lourdes Moreno, M., García, M. T., Ventosa, A. & Mellado, E. Characterization of *Salicola* sp. IC10, a lipase- and protease-producing extreme halophile. *FEMS Microbiol. Ecol.* **68**, 59–71 (2009).

184. Panich, J., Fong, B. & Singer, S. W. Metabolic Engineering of *Cupriavidus necator* H16 for Sustainable Biofuels from CO_2. *Trends Biotechnol.* **39**, 412–424 (2021).

185. Yu, J. Fixation of carbon dioxide by a hydrogen-oxidizing bacterium for value-added products. *World J. Microbiol. Biotechnol.* **34**, 1–7 (2018).

186. Bellini, S., Tommasi, T. & Fino, D. Poly(3-hydroxybutyrate) biosynthesis by *Cupriavidus*

necator: A review on waste substrates utilization for a circular economy approach. *Bioresour. Technol. Reports* **17**, 100985 (2022).

187. Nygaard, D., Yashchuk, O. & Hermida, É. B. Polyhydroxyalkanoates (PHAs) Production from Residual Glycerol by Wild Type *Cupriavidus necator*. *Waste Biomass Valor.* (2022) doi:10.1007/s12649-022-01979-4.

188. Booth, I. R., Miller, S., Müller, A. & Lehtovirta-Morley, L. The evolution of bacterial mechanosensitive channels. *Cell Calcium* **57**, 140–150 (2015).

189. Levina, N. *et al.* Protection of *Escherichia coli* cells against extreme turgor by activation of MscS and MscL mechanosensitive channels: identification of genes required for MscS activity. *EMBO J.* **18**, 1730–1737 (1999).

190. Sander, K. *et al.* Eliminating Genes for a Two Component System Increases PHB Productivity in *Cupriavidus basilensis* 4G11 Under PHB Suppressing, Non-Stress Conditions. *bioRxiv* 2022.09.19.508597 (2022) doi:10.1101/2022.09.19.508597.

191. Jensen, S. I., Lennen, R. M., Herrgård, M. J. & Nielsen, A. T. Seven gene deletions in seven days: Fast generation of *Escherichia coli* strains tolerant to acetate and osmotic stress. *Sci. Rep.* **5**, 17874 (2015).

192. T., L. G. *et al.* Complete Genome Sequence of *Cupriavidus necator* H16 (DSM 428). *Microbiol. Resour. Announc.* **8**, e00814-19 (2019).

193. Gibson, D. G. *et al.* Enzymatic assembly of DNA molecules up to several hundred kilobases. *Nat. Methods* **6**, 343–345 (2009).

194. Barrick, J. E. *et al.* Genome evolution and adaptation in a long-term experiment with *Escherichia coli*. *Nature* **461**, 1243–1247 (2009).

195. Dragosits, M. & Mattanovich, D. Adaptive laboratory evolution – principles and applications for biotechnology. *Microb. Cell Fact.* **12**, 64 (2013).

196. Matsuzawa, H. *et al.* Nucleotide sequence of the rodA gene, responsible for the rod shape of *Escherichia coli*: rodA and the pbpA gene, encoding penicillin-binding protein 2, constitute the rodA operon. *J. Bacteriol.* **171**, 558–560 (1989).

197. Möll, A. *et al.* A D, D-carboxypeptidase is required for *Vibrio cholerae* halotolerance. *Environ. Microbiol.* **17**, 527–540 (2015).

198. Palomino, M. M., Sanchez-Rivas, C. & Ruzal, S. M. High salt stress in *Bacillus subtilis*: involvement of PBP4* as a peptidoglycan hydrolase. *Res. Microbiol.* **160**, 117–124 (2009).

199. Jason, H. *et al.* Osmolality-Dependent Relocation of Penicillin-Binding Protein PBP2 to the Division Site in *Caulobacter crescentus*. *J. Bacteriol.* **194**, 3116–3127 (2012).

200. Li, W. *et al.* RefSeq: expanding the Prokaryotic Genome Annotation Pipeline reach with protein family model curation. *Nucleic Acids Res.* **49**, D1020–D1028 (2021).

201. Singh, V., Chandra, D., Srivastava, B. S. & Srivastava, R. Biochemical and transcription analysis of acetohydroxyacid synthase isoforms in *Mycobacterium tuberculosis* identifies these enzymes as potential targets for drug development. *Microbiology* **157**, 29–37 (2011).

202. Sévin, D. C., Stählin, J. N., Pollak, G. R., Kuehne, A. & Sauer, U. Global metabolic responses to salt stress in fifteen species. *PLoS One* **11**, 1–21 (2016).

203. Wood, J. M. *et al.* Osmosensing and osmoregulatory compatible solute accumulation by bacteria. *Comp. Biochem. Physiol. Part A Mol. Integr. Physiol.* **130**, 437–460 (2001).

204. Roberts, M. F. Organic compatible solutes of halotolerant and halophilic microorganisms. *Saline Systems* **1**, 1–30 (2005).

205. Dong, W. *et al.* The *Sinorhizobium meliloti* ntrX Gene Is Involved in Succinoglycan Production, Motility, and Symbiotic Nodulation on Alfalfa. *Appl. Environ. Microbiol.* **79**, 7150–7159 (2013).

206. Lu, S. *et al.* CDD/SPARCLE: The conserved domain database in 2020. *Nucleic Acids Res.* **48**, D265–D268 (2020).

207. K., K. A. & Larry, R. ArgR-Independent Induction and ArgR-Dependent Superinduction of the astCADBE Operon in *Escherichia coli*. *J. Bacteriol.* **184**, 2940–2950 (2002).

208. Schulz, A. *et al.* Transcriptional regulation of ectoine catabolism in response to multiple metabolic and environmental cues. *Environ. Microbiol.* **19**, 4599–4619 (2017).

209. Domingos, J. M. B. *et al.* Cheese whey integrated valorisation: Production, concentration and exploitation of carboxylic acids for the production of polyhydroxyalkanoates by a fed-batch culture. *Chem. Eng. J.* **336**, 47–53 (2018).

210. Garcia-Ochoa, F. & Gomez, E. Bioreactor scale-up and oxygen transfer rate in microbial processes: An overview. *Biotechnol. Adv.* **27**, 153–176 (2009).

211. Beveridge, T. J. & Schultze-Lam, S. The response of selected members of the archaea to the Gram stain. *Microbiology* **142**, 2887–2895 (1996).

212. Hoffmann, T., Boiangiu, C., Moses, S. & Bremer, E. Responses of *Bacillus subtilis* to hypotonic challenges: Physiological contributions of mechanosensitive channels to cellular survival. *Appl. Environ. Microbiol.* **74**, 2454–2460 (2008).

213. Sauer, T., Robinson, C. W. & Glick, B. R. Disruption of native and recombinant *Escherichia coli* in a high-pressure homogenizer. *Biotechnol. Bioeng.* **33**, 1330–1342 (1989).

214. Johnson, B. H. & Hecht, M. H. Recombinant Proteins Can Be Isolated from *E. coli* Cells by Repeated Cycles of Freezing and Thawing. *Bio/Technology* **12**, 1357–1360 (1994).

215. EPA. *Inventory of U.S. Greenhouse Gas Emissions and Sinks: 1990-2019*. (United States Environmental Protection Agency, 2021).

216. EIA. *Annual Energy Outlook*. (U.S. Energy Information Administration, 2023).

217. R., S. C. *et al.* Driving Forces Enable High-Titer Anaerobic 1-Butanol Synthesis in *Escherichia coli*. *Appl. Environ. Microbiol.* **77**, 2905–2915 (2011).

218. Atsumi, S., Hanai, T. & Liao, J. C. Non-fermentative pathways for synthesis of branched-chain higher alcohols as biofuels. *Nature* **451**, 86–89 (2008).

219. Ohta, K., Beall, D. S., Mejia, J. P., Shanmugam, K. T. & Ingram, L. O. Genetic improvement of *Escherichia coli* for ethanol production: chromosomal integration of *Zymomonas mobilis* genes encoding pyruvate decarboxylase and alcohol dehydrogenase II. *Appl. Environ. Microbiol.* **57**, 893–900 (1991).

220. Lu, J., Brigham, C. J., Gai, C. S. & Sinskey, A. J. Studies on the production of branched-

chain alcohols in engineered *Ralstonia eutropha*. *Appl. Microbiol. Biotechnol.* **96**, 283–297 (2012).

221. Black, W. B., Zhang, L., Kamoku, C., Liao, J. C. & Li, H. Rearrangement of Coenzyme A-Acylated Carbon Chain Enables Synthesis of Isobutanol via a Novel Pathway in *Ralstonia eutropha*. *ACS Synth. Biol.* **7**, 794–800 (2018).

222. Bond-Watts, B. B., Bellerose, R. J. & Chang, M. C. Y. Enzyme mechanism as a kinetic control element for designing synthetic biofuel pathways. *Nat. Chem. Biol.* **7**, 222–227 (2011).

223. Kanehisa, M. & Goto, S. KEGG: Kyoto Encyclopedia of Genes and Genomes. *Nucleic Acids Res.* **28**, 27–30 (2000).

224. Puigbò, P., Guzmán, E., Romeu, A. & Garcia-Vallvé, S. OPTIMIZER: a web server for optimizing the codon usage of DNA sequences. *Nucleic Acids Res.* **35**, W126–W131 (2007).

225. Wang, Y. *et al.* Stepwise increase of resveratrol biosynthesis in yeast *Saccharomyces cerevisiae* by metabolic engineering. *Metab. Eng.* **13**, 455–463 (2011).

226. Abhyankar, N., Paliwal, U., McNair, T., Wooley, D., O'Boyle, M., & Phadke, A. *2030 Report: Powering America's Clean Economy*. (Goldman School of Public Policy, 2021).

227. Stokes, L. C., Ricketts, S., Quinn, O. & Subramanian, N. A Roadmap to 100% Clean Electricity by 2035. (Data for Progress, 2021).

228. Malm, A. & Carton, W. Seize the Means of Carbon Removal: The Political Economy of Direct Air Capture. *Hist. Mater.* **29**, 3–48 (2021).

229. Malm, A. *Fossil Capital: The Rise of Steam Power and the Roots of Global Warming*. (Verso, 2016).

230. Lü, J., Sheahan, C. & Fu, P. Metabolic engineering of algae for fourth generation biofuels production. *Energy Environ. Sci.* **4**, 2451–2466 (2011).

231. Abel, A. J., Adams, J. D. & Clark, D. S. A comparative life cycle analysis of electromicrobial production systems. *Energy Environ. Sci.* **15**, 3062–3085 (2022).

232. Adams, J. D., Sander, K. B., Criddle, C. S., Arkin, A. P. & Clark, D. S. Engineering osmolysis susceptibility in *Cupriavidus necator* and *Escherichia coli* for recovery of intracellular products. *Microb. Cell Fact.* **22**, 69 (2023).

APPENDIX A: Supplementary Information for Chapter 2

Table A.1: Base case modeling parameters in Chapter 2

Parameter	Value	Units	References
Operating conditions			
P_{CO_2}	0.2	atm	--
D_{gas}	100	hr^{-1}	--
T	30 (*C. necator*)	°C	DSMZ
	35 (*S. ovata*)		DSMZ
	37 (*E. coli*)		DSMZ
Microbial growth			
C. necator (formatotrophy)			
$\mu_{max,opt}$	0.18	hr^{-1}	[1]
$Y'_{X/F,maz}$	0.169	mol mol^{-1}	[1]
$Y'_{L/F,maz}$	0.11	mol mol^{-1}	calculated
θ_F	75.11	mM	[1]
$K_{S,F}$	10	μM	[2]
K_{S,O_2}	2.5	μM	[3]
pH_{opt}	7	--	[1]
pH_{min}	4	--	[4]
pH_{max}	9	--	[4]
$c_{Na,min}$	0.2	M	[5]
$c_{Na,max}$	1.05	M	[5]
C. necator (hydrogenotrophy)			
$\mu_{max,opt}$	0.18	hr^{-1}	[6]
Y'_{X/H_2}	0.19	mol mol^{-1}	[6]
Y'_{L/H_2}	0.11	mol mol^{-1}	calculated
K_{S,H_2}	20.4	μM	[7]
K_{S,O_2}	2.5	μM	[3]
K_{S,CO_2}	9.38	μM	[7]
pH_{opt}	7	--	[1]
pH_{min}	4	--	[4]
pH_{max}	9	--	[4]
$c_{Na,min}$	0.2	M	[5]
$c_{Na,max}$	1.05	M	[5]

Parameter	Value	Units	References
S. ovata (acetogenesis)			
$\mu_{\max,\mathrm{opt}}$	0.044	hr^{-1}	[8]
$K_{\mathrm{S,H_2}}$	20	μM	[9]
$K_{\mathrm{S,CO_2}}$	20	μM	[9]
n	0.47	--	[10]
$\mathrm{pH_{opt}}$	7	--	[8]
$\mathrm{pH_{min}}$	4	--	assumed
$\mathrm{pH_{max}}$	9	--	assumed
$c_{\mathrm{Na,min}}$	0.2	M	[5]
$c_{\mathrm{Na,max}}$	1.05	M	[5]
E. coli (acetotrophy)			
$\mu_{\max,\mathrm{opt}}$	0.3	hr^{-1}	[11]
$Y'_{\mathrm{X/Ac}}$	0.936	mol mol^{-1}	[11]
$Y'_{\mathrm{L/Ac}}$	0.5	mol mol^{-1}	calculated
$K_{\mathrm{S,O_2}}$	2.5	μM	[3]
$K_{\mathrm{S,Ac}}$	10	μM	assumed
$K_{\mathrm{I,Ac}}$	0.83	M	[12]
$\mathrm{pH_{opt}}$	7	--	[11]
$\mathrm{pH_{min}}$	4	--	[13–15]
$\mathrm{pH_{max}}$	9.5	--	[13–15]
$c_{\mathrm{Na,min}}$	0.2	M	[5]
$c_{\mathrm{Na,max}}$	1.05	M	[5]
Acid/base reactions			
S_5	-71.0	J mol^{-1} K^{-1}	[16]
S_6	-92.4	J mol^{-1} K^{-1}	[16]
S_{w}	-80.66	J mol^{-1} K^{-1}	[16]
H_5	-0.12	kJ mol^{-1}	[16]
H_6	-0.4	kJ mol^{-1}	[16]
H_{w}	55.84	kJ mol^{-1}	[16]
K_7	1.38×10^{-4}	mol L^{-1}	[16]
k_{+1}	$\exp\left(1246.98\text{-}\frac{6\times10^4}{\mathrm{T}}\text{-}183\ln(\mathrm{T})\right)$	s^{-1}	[17]
k_{+2}	59.44	s^{-1}	[17]
k_{+3}	2.23×10^3	L mol^{-1} s^{-1}	[17]
k_{+4}	6.0×10^9	L mol^{-1} s^{-1}	[17]
k_{+5}	10	s^{-1}	assumed

Parameter	Value	Units	References
k_{+6}	10	s^{-1}	assumed
k_{+7}	10	s^{-1}	assumed
k_{+w}	2.4×10^{-5}	L mol^{-1} s^{-1}	[18]
Gas/liquid mass transfer			
$k_L a_{O_2}$	200	hr^{-1}	assumed
A_S	0.56	m^{-1}	assumed
Diffusion coefficients			
D_{CO_2}	$14.68 \times 10^{-9}\left(\frac{T}{217.206}-1\right)^{1.997}$	m^2 s^{-1}	[19]
D_{H_2}	$\frac{2.290\times10^{-11}}{\mu^{0.819}}T$	m^2 s^{-1}	[2]
D_{O_2}	$10\text{^}\left[-8.410+\frac{773.8}{T}-\left(\frac{506.4}{T}\right)^2\right]$	m^2 s^{-1}	[20]
Bunsen coefficients			
A_{1,CO_2}	-60.2409	--	[21]
A_{2,CO_2}	93.4517	--	[21]
A_{3,CO_2}	23.3585	--	[21]
B_{1,CO_2}	2.3517×10^{-2}	--	[21]
B_{2,CO_2}	-2.3656×10^{-2}	--	[21]
B_{3,CO_2}	4.7036×10^{-3}	--	[21]
A_{1,O_2}	-58.3877	--	[22]
A_{2,O_2}	85.8079	--	[22]
A_{3,O_2}	23.8439	--	[22]
B_{1,O_2}	3.4892×10^{-2}	--	[22]
B_{2,O_2}	1.5568×10^{-2}	--	[22]
B_{3,O_2}	-1.9387×10^{-3}	--	[22]
A_{1,H_2}	-39.9611	--	[23]
A_{2,H_2}	53.9381	--	[23]
A_{3,H_2}	16.3135	--	[23]
B_{1,H_2}	2.3517×10^{-2}	--	[23]
B_{2,H_2}	1.7566×10^{-2}	--	[23]
B_{3,H_2}	-2.3010×10^{-3}	--	[23]
pH controller			
K_C	0.1	hr^{-1}	--
τ	60	s	--

Parameter	Value	Units	References
Combustion energy			
$\Delta_r G^0_{\mathrm{X}}$	-479	kJ mol^{-1}	Note A.4
$\Delta_r G^0_{\mathrm{E}}$	-479	kJ mol^{-1}	Note A.4
$\Delta_r G^0_{\mathrm{H_2}}$	-260	kJ mol^{-1}	Note A.4
$\Delta_r G^0_{\mathrm{FFA}}$	-240	kJ mol^{-1}	Note A.4
$\Delta_r G^0_{\mathrm{LLA}}$	-1370	kJ mol^{-1}	Note A.4
$\Delta_r G^0_{\mathrm{AAA}}$	-870	kJ mol^{-1}	Note A.4
CO_2 electrolyzer			
j	140	mA cm^{-2}	[24]
η_{F}	94	%	[24]
V_{e}	3.5	V	[24]
$c_{\mathrm{FFA,eff}}$	2.08	M	[24]
H_2 electrolyzer			
j	1000	mA cm^{-2}	[25]
η_{F}	99	%	[25]
V_{e}	2.0	V	[25]
Electrodialysis – lactic acid			
a_{ED}	0.5154	kWh kg^{-1}	Note A.5
b_{ED}	3.7×10^{-2}	Wh L^{-1}	Note A.5
Γ_{max}	7.56	kg m^2 h^{-1}	Note A.5
κ_{M}	51.5	g L^{-1}	Note A.5
Electrodialysis – formic acid			
$\eta_{\mathrm{ED,F}}$	3	%	Note A.5
Γ_{max}	6.42	kg m^2 h^{-1}	Note A.5
κ_{M}	26.3	g L^{-1}	Note A.5

Table A.2: Power breakdown for subprocesses

Process power (kWh/kg CDW)	**Value**			
	Formatotrophic	*Knallgas*	*Acetogenic*	*Theoretical*
Substrate generation	47.26	22.61	19.55	5.32
Gas-liquid mass transfer and fluid mixing	0.48	0.43	1.38	0
Liquid heating	0.26	0.13	0.91	0
Direct air capture of CO_2	4.22	3.56	4.2	0.22
Haber-Bosch ammonia production	1.68	1.68	1.89	0.88
Chlor-alkali process (pH control)	0.38	0	4.01	0

Supplementary Note A.1: Optimizing lactic acid productivity in the formate-mediated system

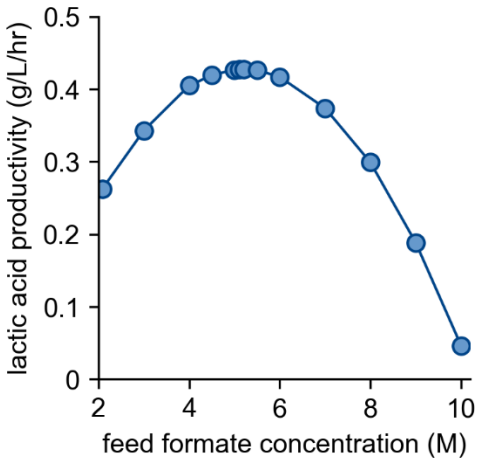

Figure A.1. Optimal formate feed concentration for lactic acid productivity. Maximum lactic acid productivity as a function of the formate feed concentration. Maximum value of ~0.42 g/L/h is achieved at a feed concentration of ~5.1 M.

The productivity of lactic acid (and any generic product) is given by $D_{\mathrm{liq}}c_{\mathrm{LLA}}$. The titer, c_{LLA}, is proportional to the product of the lactic acid yield on formate ($Y'_{\mathrm{L/F}}$) and the feed concentration of formate ($c_{\mathrm{FFA,f}}$), that is, $c_{\mathrm{LLA}} \propto Y'_{\mathrm{L/F}}c_{\mathrm{FFA,f}}$. The dilution rate, D_{liq}, is typically thought of as independently controllable. However, the dilution rate is bounded by the maximum specific growth rate, μ_{max}. The maximum specific growth rate is a function of the sodium concentration, specifically, $\mu_{\mathrm{max}} \propto -c_{\mathrm{Na}}$ (Eqn. 2-47 in the main text). The sodium concentration, in turn, is a function of the lactic acid titer (specifically, $c_{\mathrm{Na}} \propto c_{\mathrm{LLA}}$) because sodium hydroxide is added to neutralize the proton liberated by lactic acid production. Hence, because c_{LLA} is proportional to $c_{\mathrm{FFA,f}}$, the maximum specific growth rate is negatively proportional to the feed concentration of formate/ic acid (that is, $\mu_{\mathrm{max}} \propto -c_{\mathrm{FFA,f}}$). This also means that the maximum dilution rate is negatively proportional to the feed concentration because the dilution rate is bounded by the specific growth rate ($D_{\mathrm{liq}} \propto -c_{\mathrm{FFA,f}}$). Together, this means the productivity of lactic acid in the formate mediated system ($\dot{m}_{\mathrm{LLA,F}}$) is negatively proportional to the squared feed concentration of

formate/ic acid, that is, $\dot{m}_{\mathrm{LLA,F}} \propto -\left(c_{\mathrm{FFA,f}}\right)^2$. Hence, we should expect to see a feed formate/ic acid concentration that maximizes the lactic acid productivity. Figure A.1 shows the maximum lactic acid productivity as a function of the feed concentration of formic acid and demonstrates a maximum productivity at ~5.1 M formate/ic acid. A 5.1 M feed stream for formatotrophic production of lactic acid was chosen and the life cycle impact of an electrodialysis process to concentrate the effluent from the CO_2 electrolysis reactor was calculated.

Supplementary Note A.2: Intrinsically safer operation of the H_2-mediated system

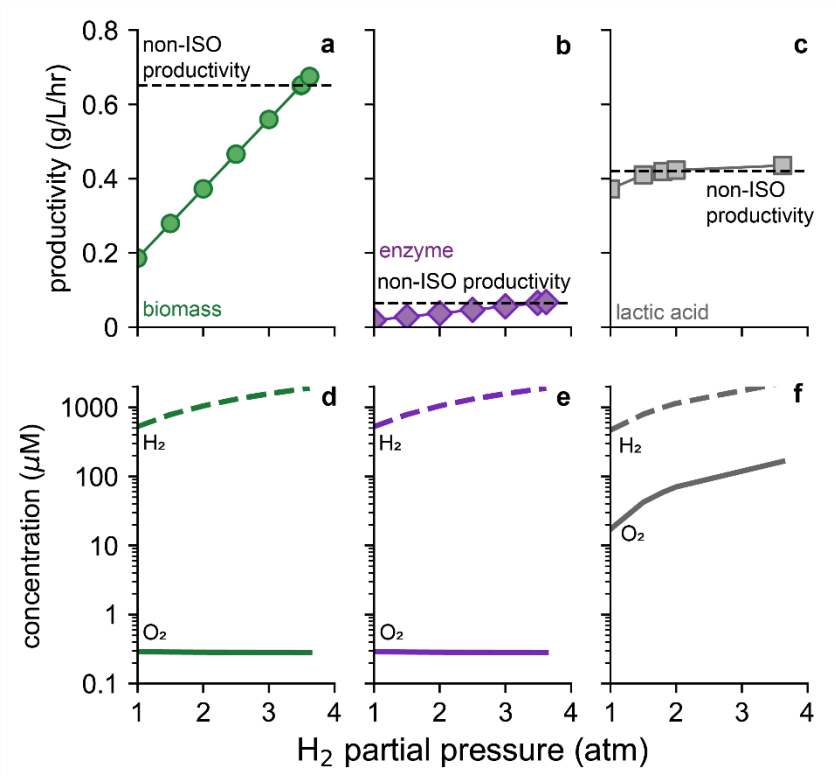

Figure A.2. Intrinsically safer operation of the H_2-mediated system. Productivity (**a**, **b**, **c**) and liquid-phase concentration of H_2 and O_2 (**d**, **e**, **f**) for the H_2-mediated EMP system under intrinsically safer operation (ISO, p_{H2}:p_{O2} = 10:1) producing biomass (**a**, **d**), enzyme (**b**, **e**), and lactic acid (**c**, **f**). Horizontal black dashed lines in (**a**, **b**, **c**) correspond to the non-ISO (p_{H2}:p_{O2} = 1:0.21) base-case productivity for each of the three products. Low (<10 μM) O_2 concentration (solid lines in **d**, **e**, **f**) indicate O_2 gas-liquid mass transfer limitation on the productivity.

Despite the lower GWP associated with the H_2-mediated system, the flammable gas mixture fed to the reactor under base-case operating conditions (1 atm H_2 and 0.21 atm O_2) may pose a significant barrier to adoption of this EMP strategy. Intrinsically safer operation (ISO) of the H_2-mediated system was evaluated by adjusting the H_2:O_2 ratio in the gas phase such that the gas mixture was inherently non-flammable (defined as comprising an H_2:O_2 ratio of >10:1).[26] Under these conditions, O_2 gas/liquid mass transfer limits the productivity for each product, biomass, enzymes, and lactic acid (Fig. A.2). However, reactor productivities equivalent to that of the base case scenario can be achieved simply by increasing the total gas pressure while maintaining the inherently non-flammable gas ratio, so the GWP of the H_2-mediated EMP process is not negatively impacted by ensuring intrinsically safer operating conditions (Fig. A.2). For biomass, enzymes,

and lactic acid, the partial pressure of H_2 must be 3.62 atm, 3.62 atm, and ~1.8 atm, respectively, to match the GWP of the base case scenario, pressures that are readily achievable with existing water electrolysis and bioreactor technology.[27,28]

Supplementary Note A.3: Polylactic acid production life cycle impacts

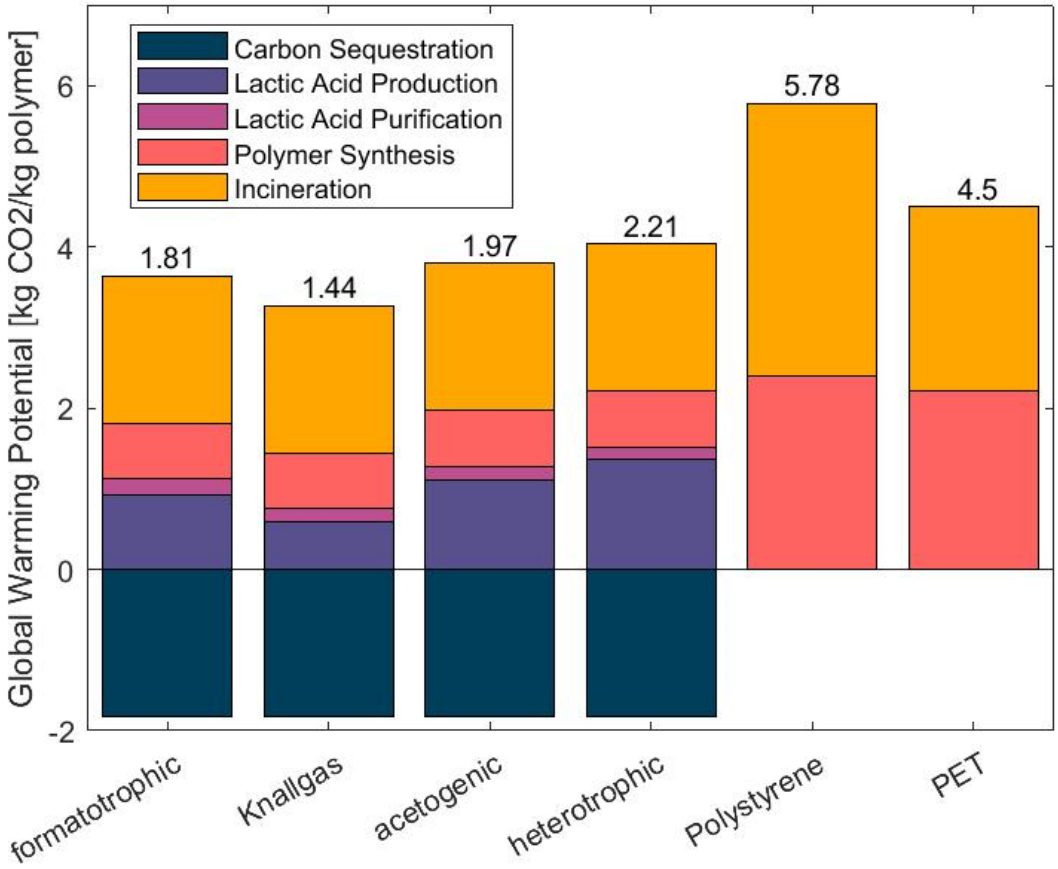

Figure A.3: Life cycle global warming potential of EMP-based and traditional plastics. Life cycle (cradle-to-grave) global warming potential of polymer production of polylactic acid (PLA) in the three EMP systems and traditional bioprocesses compared to those of fossil-fuel based plastics polyethylene terephthalate (PET) and polystyrene (PS). EMP production assumes a 90% carbon efficiency (as defined in main text) and grid composed solely of wind power.

I analyzed the cradle-to-grave life cycle impact of polylactic acid (PLA) production. I split the PLA production process into five categories: carbon sequestration, lactic acid production, lactic acid purification, polymer synthesis, and end of life. The global warming potentials for the lactic acid production are identical to the results in Fig. 2.5c in the main text. Purification of lactic acid relies on acidifying the lactate anion produced in the bioreactor and therefore requires a stoichiometric proportion of sulfuric acid, the carbon footprint of which is obtained from the PEF dataset. Data for the carbon footprint of polylactic acid polymer production was obtained from Morão and de Bie.[29] I further compared the global warming footprints to those of two major fossil-fuel based polymers: polyethylene terephthalate (PET) and polystyrene (PS). Carbon footprints for the production of these two polymers were obtained from the PEF dataset. I assume all plastics are incinerated at the end of their life and assume the carbon footprint is equal to the stoichiometric amount of carbon dioxide that would be produced by complete combustion of the polymer.

The global warming potentials of the cradle-to-grave PLA production of the three EMP systems and the traditional bioprocess reflect the same trends as for lactic acid production because the lactic acid purification and polymer synthesis steps are identical for each system. Therefore, the Knallgas bacteria-based system outcompetes the other bioprocesses in PLA production as it does in lactic acid production. All lactic acid production systems outperform the two fossil-based polymers, PET and PS, in terms of life cycle global warming potential, in the scenario shown. The acetogenic system and heterotrophic system both have comparable carbon footprints to the fossil-based plastics if the plastics are not incinerated, which is a plausible scenario given that burial is a common practice for plastic disposal. However, a true like-to-like comparison will involve incinerating these plastics to leave no waste, as PLA will ultimately biodegrade in the environment. In the scenario, all methods of PLA production have smaller carbon footprints when compared to PET and PS.

These results are for a carbon conversion efficiency of 90%, similar to current glucose-based lactic acid fermentation. As noted in the main text, an efficiency this high may be difficult in EMP processes. Lower carbon efficiencies in the lactic acid production step will therefore increase the total carbon footprint of PLA production. As shown in Fig. 2.6b in the main text, this change in GWP is also dependent on the electricity source/grid composition. As with lactic acid production, for H_2-mediated electromicrobial production of PLA to outcompete heterotroph-based processes, the process must rely on renewable electricity and must achieve a carbon efficiency of around 50%.

Supplementary Note A.4: calculating combustion energies

Combustion energies were calculated by adopting the strategy of Claassens *et al.*[30] Briefly, eQuilibrator[31] was used to calculate the $\Delta_r G'^0$ of the combustion reaction at a pH of 7.0 and ionic strength of 0.1 M. The biomass combustion energy was adopted from previous calculations.[32,33]

Supplementary Note A.5: calculating parameters for electrodialysis-based separations

Data from Hábová *et al.*[34] were used to determine parameters for membrane electrodialysis. Energy consumption as a function of lactic acid feed concentration was determined according to a linear model, Eqn. 2-87 in the main text. The linear model fit well to reported data ($R^2 = 0.73$), as shown in Fig. A.4a. Lactic acid flux parameters were determined similarly and fit well to the proposed model ($R^2 = 0.85$), as shown in Fig. A.4b.

The same dataset was used for formic acid concentration by estimating an average energy efficiency ($\eta_{ED,F}$) of 3% and using the same fitting parameters, modified to account for the different molar masses and diffusivities of lactic acid and formic acid.

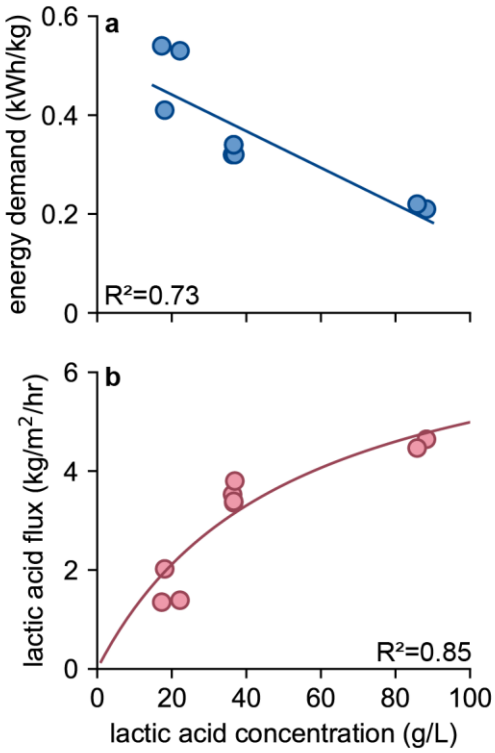

Figure A.4. Fitting parameters for membrane electrodialysis. (**a**) energy demand and (**b**) through-membrane lactic acid flux for membrane electrodialysis as a function of the fed lactic acid concentration. Circles represent data from Hábová *et al.* and solid lines are fitted equations.

Supplementary Note A.6: Theoretical energy and material demands of EMP process

Table 2.2 in the main text displays the predicted material and energy demands for EMP processes through the three studied schemes. Also included are theoretical minimum values for each of the material and energy demands listed.

Grosz and Stephanopolous give the Gibbs Free Energy of Formation for *E. coli* as -46.0 kJ/mol C [32]:

$$C_{(s)} + 0.885H_{2(g)} + 0.12N_{2(g)} + 0.245O_{2(g)} \rightarrow CH_{1.77}O_{0.49}N_{0.24(s)} \qquad \Delta G_X^0 = -46.0\ \text{kJ/mol}$$

To determine Gibbs free energies for reactions relevant to the EMP systems, however, manipulations can be made. As CO_2, rather than solid carbon, and ammonia rather than nitrogen gas are fed into the EMP system, the chemical equation above may be linearly combined with the equation for formation of CO_2:

$$CO_{2(g)} \rightarrow C_{(s)} + O_{2(g)} \qquad \Delta G^0 = +394.4\ \text{kJ/mol}$$

as well as the equation for the formation of ammonia:

$$NH_{3(l)} \rightarrow \frac{1}{2}N_{2(g)} + \frac{3}{2}H_{2(g)} \quad \Delta G^0 = +26.5\ \text{kJ/mol}$$

The free energy of biomass from CO_2, H_2, and NH_3, as it occurs in an electromicrobial system, is therefore:

$$CO_2 + 0.525H_2 + 0.24NH_3 \rightarrow CH_{1.77}O_{0.49}N_{0.24} + 0.755O_2\ \Delta G^0 = 354.8\ \text{kJ/mol}$$

When considering water, rather than hydrogen gas, as a reactant for the EMP system:

$$H_2O_{(l)} \rightarrow \frac{1}{2}O_{2(g)} + H_{2(g)}\ \ \Delta G^0 = +274.1\ \text{kJ/mol}$$

the equation becomes:

$$CO_2 + 0.525H_2O + 0.24NH_3 \rightarrow CH_{1.77}O_{0.49}N_{0.24} + 1.02O_2\ \Delta G^0 = +479\ \text{kJ/mol}$$

Therefore, the theoretical energy input required to produce biomass is 479 kJ/mol C of biomass. Using a biomass molar mass of 25 g/mol C, and converting the energy to kWh, this energy requirement on a mass basis is 5.32 kWh/kg biomass.

Carbon Demand

The carbon demand to produce biomass is simply determined by stoichiometry. As one mole of CO_2 is fixed per carbon mole of biomass (MW=25.0 g/mol), 1.76 kg CO_2 are required per mole of biomass.

Assuming CO_2 is fed to the EMP reactor at 1 atm, and is fixed from atmospheric CO_2, the minimum energy required to produce this CO_2 is equal to the Gibbs Free Energy required to concentrate from 400 pm to pure CO_2. Assuming CO_2 behaves as an ideal gas, this free energy at standard temperature is:

$$\Delta G^0 = -RT\ln\left(\frac{1\ \text{atm}}{0.0004\ \text{atm}}\right) = 19.4\frac{\text{kJ}}{\text{mol}} = 0.12\frac{\text{kWh}}{\text{kg}\ CO_2} = 0.22\ \frac{\text{kWh}}{\text{kg Biomass}}$$

Nitrogen Demand

The theoretical ammonia demand is obtained by stoichiometry, assuming one mole of ammonia is required per mole of nitrogen fixed in biomass, using the biomass equation $CH_{1.77}O_{0.49}N_{0.24}$. Therefore, 0.24 mol of ammonia per carbon mole of biomass, or 0.163 kg NH_3 per kg biomass, is required.

The minimum energy required to produce this ammonia using nitrogen gas (from air) and water (as is the case in green ammonia production) can be determined from the Gibbs Free Energy of the following reaction:

$$\frac{1}{2}N_{2(g)} + \frac{3}{2}H_2O_{(l)} \rightarrow NH_{3(l)} + \frac{3}{4}O_{2(g)} \qquad \Delta G^0 = 329.1\ \text{kJ/mol}$$

Using the ammonia to biomass ratio determined above, the energy required in nitrogen fixation for 1 kg of biomass is 0.88 kWh.

Total NaOH and HCl

As the net equation for the formation of biomass (see above) involves no net consumption/generation of protons, the theoretical required mass of NaOH and HCl is 0. The theoretical energy required to produce these pH-control agents is therefore also 0.

Total Process Electricity

The theoretical total process electricity is equal to the sum of the theoretical energy requirements of the constitutive subprocesses (electrolysis/bioreactor electricity, NH_3 generation electricity, CO_2 generation electricity, and NaOH/HCl generation electricity).

APPENDIX B: Supplementary Information for Chapter 3

Supplementary Note B.1: Validation of model isotherm against literature data

Many of the DAC model parameters are based on that of the MOF mmen-Mg_2(dobpdc), originally synthesized by McDonald *et al.*[35] The isotherms of this MOF exhibit step-behavior, and the authors fit experimental data to a multi-site Langmuir-Freuidlich model, which was valid across a wide range of temperatures and pressures.

To simplify the DAC model used in Chapter 3, I described the sorbent isotherm as two successive Langmuir isotherms with a transition at a certain partial pressure of CO_2 (see Eqn. 3-2). To obtain the parameters used in the model, I fit this equation to the isotherm data for mmen-Mg_2(dobpdc) reported by McDonald *et al.* The adsorbed CO_2 concentration in a direct air capture process would not exceed the equilibrium adsorbed concentration with a partial pressure of 0.4 mbar at 298 K; therefore, the parameter fitting was restricted for data below this threshold. As shown in Figure B.1, this simplified model fit the data of interest fairly well (R^2 =0.964). Relevant parameters were obtained from this fit, the values of which are listed in Table B.1.

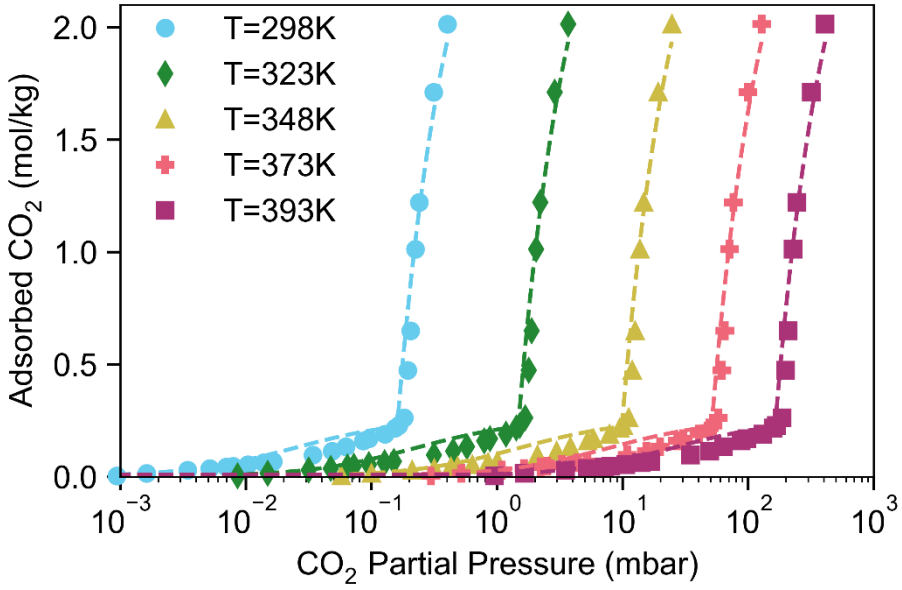

Figure B.1 Validation of isotherm model used in this analysis (dotted lines) against literature data (solid markers).

Supplementary Note B.2: Estimation of total labor costs

Due to the higher complexity of the processing components involved, I assume that the process described here would require roughly double the total labor costs of a cellulosic ethanol plant operating at the same scale described in the TEA by Humbird *et al.*[36] This value is also adjusted for inflation and regional variation (BLS Employment Cost Index), leading to an annual employee salaries cost of $7.4 million per year.

Table B.1: Base-case parameters used in DAC and bioreactor models described in Chapter 3

Parameter	Value	Unit	Source
DAC Model			
k	0.007	s^{-1}	[37]
Q^{sat1}	0.258	mol/kg	See Note B.1
Q^{sat2}	2.791	mol/kg	See Note B.1
$p_{\mathrm{step}}(298\mathrm{K})$	0.16	mbar	See Note B.1
$K_{\mathrm{eq1}}(298\mathrm{K})$	4.065×10^4	-	See Note B.1
$K_{\mathrm{eq2}}(298\mathrm{K})$	6.6107×10^3	-	See Note B.1
$p_{\mathrm{CO2}}(z=0)$	0.4	mbar	Assumed
ΔH_{ads}	-71	kJ/mol	[35]
ε	0.95	-	Assumed
L	0.3	m	Assumed
ρ_{ads}	3220	kg/m^3	[35]
τ	0.1	s^{-1}	Assumed
h_{A}	8.8	$W/m^2 \cdot K$	[38]
r	1	mm	Assumed
T_{s}	120	ºC	Assumed
$c_{\mathrm{p,ads}}$	892.5	$J\ kg^{-1}\ K^{-1}$	[39]
$c_{\mathrm{p,mon}}$	897	$J\ kg^{-1}\ K^{-1}$	www.catalystdpf.com
$m_{\mathrm{mon}}/m_{\mathrm{ads}}$	1.4	-	Assumed
$\hat{c}_{\mathrm{p,CO2}}$	37.2	$J\ mol^{-1}\ K^{-1}$	[40]
p_{vac}	0.1	bar	Assumed
γ	1.3	-	[40]
h_s	18	$W/m^2 \cdot K$	[41]
Bioreactor 1 Model			
$\mu_{\mathrm{A,opt}}$	0.123	h^{-1}	[42]
$K_{\mathrm{s,H2}}$	20	µM	[9]
$K_{s,\mathrm{CO2}}$	20	µM	[9]
$c_{\mathrm{Na,min,1}}$	0.2	M	[5]
$c_{\mathrm{Na,max,1}}$	0.75	M	[43]
$k_{\mathrm{L}}a_{\mathrm{H2}}$	250	h^{-1}	Assumed
H_{H2}	0.00078	$mol\ kg^{-1}\ bar^{-1}$	[40]
$p_{\mathrm{H2,1,0}}$	0.67	atm	Assumed
T_1	35	ºC	DSMZ
$D_{\mathrm{gas,1}}$	30	h^{-1}	Assumed
$V_{L,1}/V_{G,1}$	4	-	Assumed
H_{CO2}	0.0013	$mol\ kg^{-1}\ bar^{-1}$	[40]
$p_{\mathrm{CO2,1,0}}$	0.33	atm	Assumed

Model variable	Value	Unit	Source
Bioreactor 2 Model			
$\mu_{\mathrm{A,opt}}$	0.46	h^{-1}	[44]
$K_{\mathrm{s,Ac}}$	1.3	mM	Assumed
$K_{s,\mathrm{O2}}$	2.5	μM	[3]
K_{I}	0.83	M	[12]
$c_{\mathrm{Na,min,2}}$	0.2	M	[5]
$c_{\mathrm{Na,max,2}}$	1.05	M	[5]
$p_{\mathrm{O2},2,i}$	0.21	atm	Assumed
$V_{L,2}/V_{G,2}$	4	-	Assumed
$D_{\mathrm{gas,2}}$	30	h^{-1}	Assumed
$Y_{\mathrm{X/Ac}}$	0.936	mol/mol	[11]
$Y_{\mathrm{Bu/Ac}}$	0.27	mol/mol	Calculated
H_{O2}	0.0012	mol kg^{-1} bar^{-1}	[40]
γ_{X}	1.12	mol/mol	Calculated
γ_{Bu}	1.5	mol/mol	Calculated
Process Model			
η_1	0.8	-	Assumed
μ_{air}	1.85	kg m^{-1} s^{-1}	[45]
D_p	1	mm	Assumed
η_2	0.8	-	Assumed
P_2	2	atm	Assumed
η_3	0.9	-	Assumed
$\Delta H_{\mathrm{comb,H2}}$	286	kJ/mol	[40]
η_4	0.8	-	[46]
t_{DAC}	2	years	[39]

Table B.2: Cost correlations for equipment used in technoeconomic assessment

Equipment	Sizing Variable (Unit)	Correlation Used	Maximum Size	Source
Heat Pump	Heat ouput power – P (kW_{th})	$C_{p,HP} = \$1{,}186P^{0.887}$	70,000 kW_{th}	[47]
Blower	Air Flow Rate – Q (m^3/s)	$C_{p,bloiwer}/\$ = \exp[7.864 + 0.364 \ln Q + 0.1139(\ln Q)^2]$	47.2 m^3/s	[48]
Vacuum Pump	Suction Rate – Q (m^3/s)	$C_{p,vac} = \$169{,}357Q^{0.35}$	0.165 m^3/s	[48]
DAC Vessel	Volume – V (m^3)	$C_{p,vessel}/\$ = \exp[8.0715 + 0.5102 \ln V + 0.00582(\ln V)^2]$	12,000 m^3	[48]
Electrolyzer	Power draw – P (kW)	$C_{p,Elec} = \$900P$	n/a	[49]
Gas Storage	Volume – V (m^3)	$C_{p,GS} = \$23{,}421V^{0.43}$	12,000 m^3	[48]
Bioreactors	n/a	$C_{p,BR} = \$2{,}341{,}000$	1000 m^3	[50]
Liquid-Liquid Extractor	Volume – V (m^3)	$C_{p,LLE} = \$8523V^{0.7}$	177 m^3	[48]
Heat Exchanger	Surface Area – A (m^2)	$C_{p,HX}/\$ = \exp[10.26 - 0.453 \ln A + 0.0979(\ln A)^2]$	1100 m^2	[48]
Distillation Column		Multiple correlations (following method described by Seider)		[48]

Table B.3: Material costs used in technoeconomic assessment

Material	Unit	Cost/Unit	Source
Sorbent	kg	$63	[39]
Monolithic support	kg	$4.25	www.catalystdpf.com
Nitrogen gas	kg	$0.76	www.chemanalyst.com
Process water	1000 gal	$4.70	[51]
Ammonia	kg	$1.18	www.chemanalyst.com
Phosphoric acid	kg	$1.30	www.chemanalyst.com
Magnesium sulfate	kg	$0.38	www.chemanalyst.com
Sodium hydroxide	kg	$0.63	www.chemanalyst.com
Sulfuric acid	kg	$0.26	www.chemanalyst.com
Mesitylene	kg	$4.04	[52]
Wastewater treatment	1000 gal	$4.07	[53]

APPENDIX C: Supplementary Information for Chapter 4

Supplementary Note C.1: Growth of H16 and ht030b in high salt media

Figure 4.2B in the main text compares the growth of wild-type *C. necator* H16 with the adapted halotolerant strain ht030b. In that experiment, 4 replicate cultures each of H16 and ht030b were grown in a 24-well plate and grown overnight at 30 °C, with starting optical densities (A_{600}) of 0.01. H16 demonstrated no visible growth, whereas ht030b exhibited exponential growth with a specific growth rate of 0.16 h^{-1}. However, I have found that growth of H16 in high salt conditions appears dependent on the starting optical density of the culture and other culturing conditions. A similar experiment was therefore performed in 50-mL volumes in 250 mL baffled shake flasks. Both H16 and ht030b were seeded to starting optical densities of ~0.05.

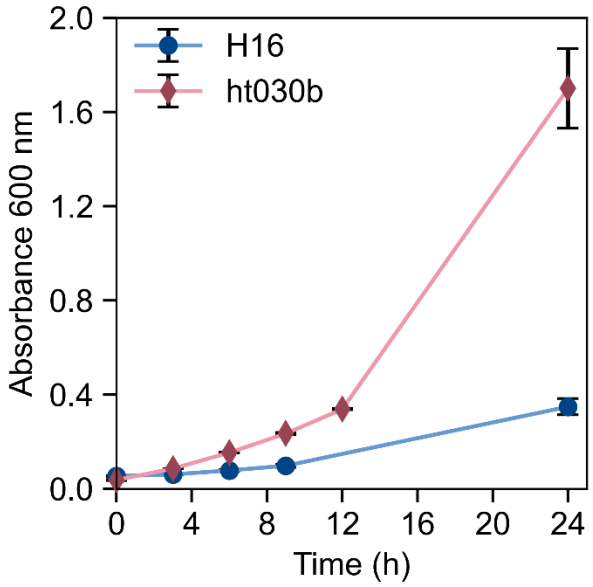

Figure C.1 Growth curve of H16 (blue circles) and ht030b (red diamonds) in LB containing 3.25% NaCl in 50-mL cultures in shake flasks, seeded at an optical density of A_{600}=0.05.

Although wild-type H16 did grow slightly in LB containing 32.5 g/L NaCl (final concentration) in this experiment, the evolved strain still grew significantly faster. Calculated specific growth rates were 0.18 h^{-1} for ht030b and 0.08 h^{-1} for H16. In addition to the higher starting cell concentration, it is likely that greater oxygen mass transfer was achieved in flasks compared to that in 24-well plates. The growth of H16 is somewhat dependent on the culturing conditions when growing in LB at elevated salt concentrations. However, in all cases, the evolved strain ht030b grew significantly better than the wild-type strain in high salt concentrations.

Supplementary Note C.2: Growth of wild-type and mscL knockout Cupriavidus necator

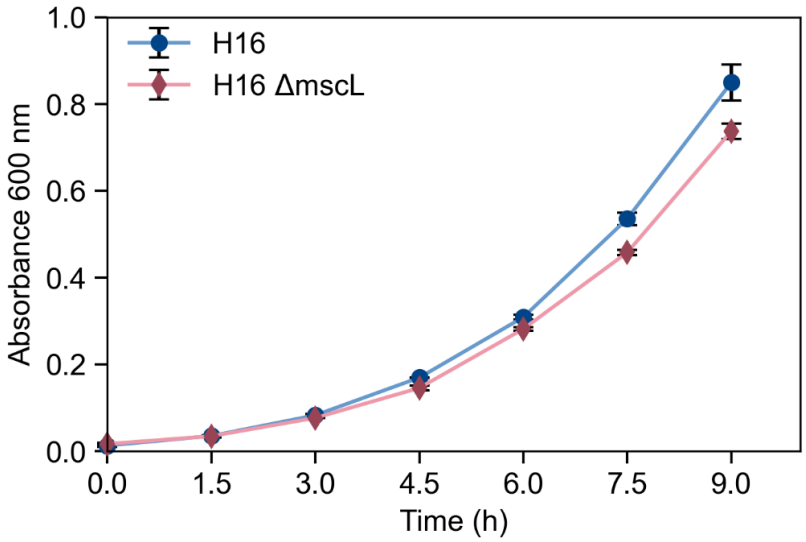

Figure C.2 Growth curve of *C. necator* H16 (blue circles) and H16 *ΔmscL* (red diamonds).

Growth curves were measured for both wild-type *Cupriavidus necator* H16 and *C. necator ΔmscL* in LB medium. Overnight cultures of both strains were inoculated to an initial cell density with A_{600}=0.015 in 50-mL cultures in shake flasks. Cultures were grown at 30 ºC shaking at 200 rpm for 9 hours, with absorbance measurements (600 nm) taken every 90 minutes.

The growth curves of the two strains in LB were not significantly different. The measured growth rate of the wild-type strain (0.45 ± 0.01 h^{-1}) was just slightly higher than the growth rate of the *ΔmscL* strain (0.43 ± 0.01 h^{-1}). Although there was an observable difference between the growth of the two strains, this result was not statistically significant ($p>0.07$). Therefore, the absence of the *mscL* gene does not significantly affect the growth rate of *C. necator*, and that the *mscL* gene is not required for normal functioning of the cell.

Supplementary Note C.3: Effect of salt concentration on growth of C. necator H16 and C. necator ht030b in LB and M9 Formate

The maximum salt concentration tolerated by both wild-type *C. necator* H16 and evolved strain ht030b was determined for both heterotrophic growth (LB) and organoautotrophic growth (M9 formate). To test salt tolerance for heterotrophic growth, both strains were inoculated in 50-mL tubes containing 10 mL LB with variable salt concentrations to a starting OD of 0.001. As the measured average growth rate of *C. necator* H16 was 0.45 h^{-1}, I defined the salt tolerance as the maximum salt concentration for which the average growth rate over a 24-hour period exceeded 0.225 h^{-1} (half of normal growth rate). This corresponded to an optical density of over 0.22 after a 24-hour period. The NaCl concentrations tolerated by H16 and ht030b were 16.3 and 29.4 g/L, respectively. For convenience, NaCl concentrations of 15 g/L and 30 g/L were used for H16 and ht030b respectively for osmolysis experiments of those two strains.

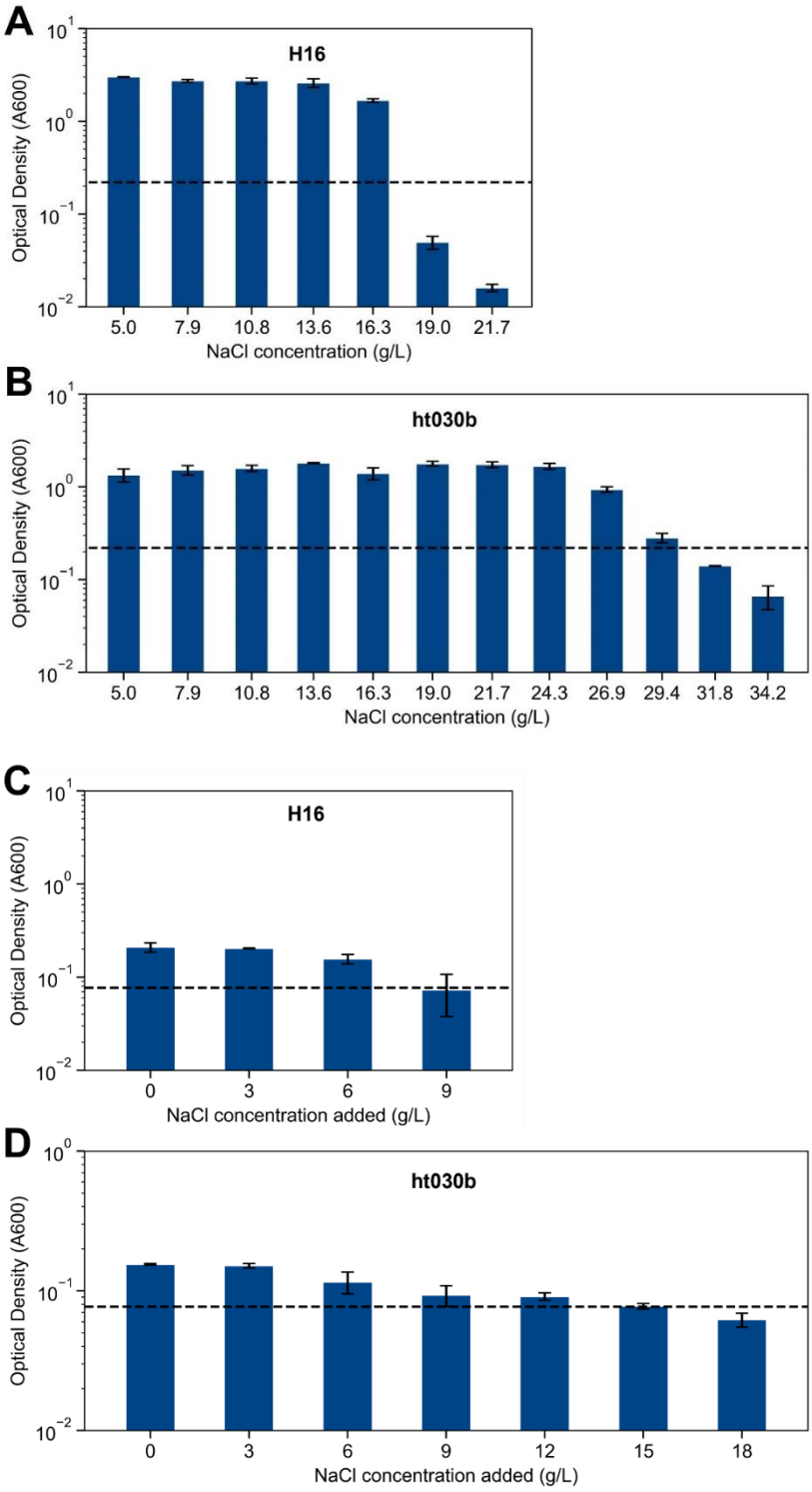

Figure C.3. Measured optical densities of *C. necator* H16 (A) and *C. necator* ht030b (B) following 24 hours of growth in LB at various salt (final) concentrations as well as H16 (C) and ht030b (D) following 48 hours of growth in M9 formate with various (added) salt concentrations. Black dashed line represents cutoff OD of 0.22 (LB growth) and 0.077 (M9 growth) which defines thresholds of salt tolerance in the respective media.

To test NaCl tolerance under formatotrophic growth, various salt concentrations were added to M9 formate (note: these represent the amount of salt *added* to M9 medium, which already contains various amounts of certain salts, rather than the final salt concentration; final osmolarities are taken into account in the data shown in Figures 4.3B and 4.4B). Both strains (H16 and ht030b) were then inoculated in 50-mL tubes containing 10 mL of formate media to a starting OD of 0.02. Formatotrophic growth in defined medium was significantly slower than heterotrophic growth in rich medium. Optical densities were measured after 48 hours. The optical density threshold for maximum tolerated salt concentration was 0.077, which is half of the measured OD of ht030b after 48 hours in M9 formate with no added salt.

The added NaCl concentrations tolerated by H16 and ht030b in M9 formate were 6 g/L and 15 g/L respectively. Therefore, M9 formate with 6 g/L added was used as the growth medium for the experiments described in Figure 4.3B. For the experiments described in Figure 4.4B, M9 formate with 16 g/L was used. As shown in Fig. S3D, the drop in cell growth when the added salt concentration is raised from 15 g/L to 18 g/L is fairly small. M9 formate with 16 g/L NaCl added has an osmolarity of 0.834 OsM, which is roughly equivalent to that of a 2.5% NaCl solution. Because osmolysis experiments were performed with salt solutions in 0.5% (w/v) increments, this was a more convenient starting solution from a practical standpoint.

Supplementary Note C.4: RFP-based cell lysis assay diagram and measurement notes

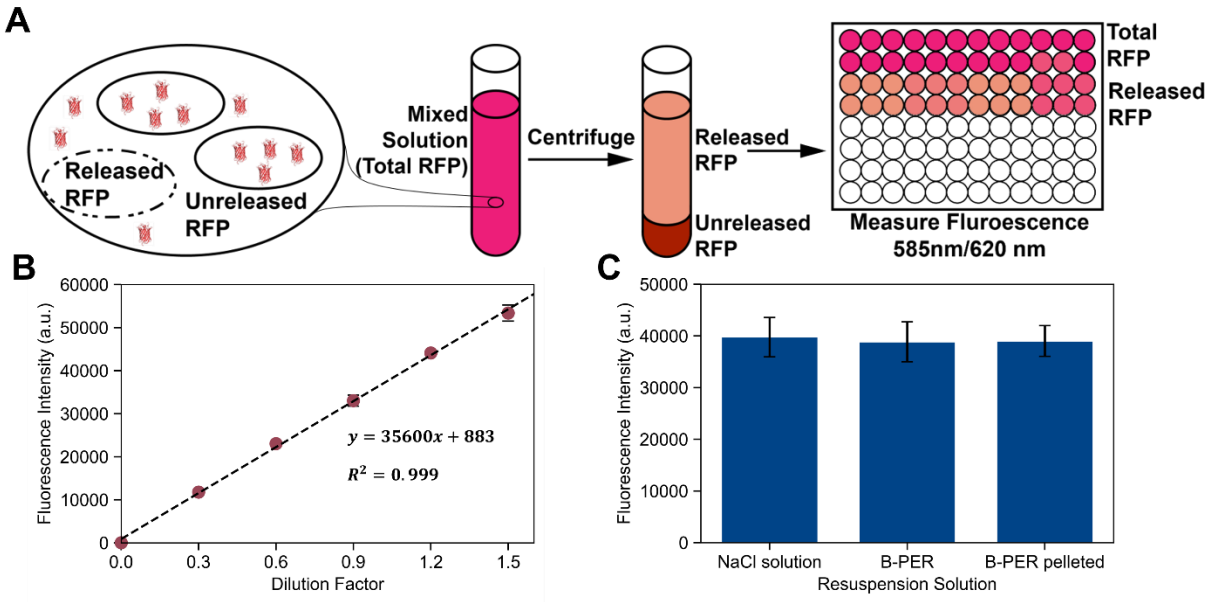

Figure C.4. Overview of RFP-based cell lysis assay developed. (A) Schematic overview of RFP assay as described in methods. Well-mixed red fluorescence measurements (585 nm excitation/ 620 nm emission) were performed on the well-mixed sample, representing the total RFP content, and from the supernatant following centrifugation, representing the released RFP content. Cell lysis fraction was taken to be the ratio of released RFP to total RFP. (B) Representative linear range validation that was replicated in each experiment to verify that the RFP concentration was proportional to fluorescence intensity. (C) Fluorescence intensity measurements of identical RFP-expressing cell samples in various solutions, demonstrating that the fluorescence intensity is not sensitive to the various environments encountered in the assay.

In each osmolysis experiment relying on the RFP-based cell lysis assay described in the main text, samples were verified to ensure they fell within the linear range. Cells expressing RFP following the wash step in the osmolysis protocol were concentrated or diluted such that they were 30%, 60%, 90%, 120%, or 150% of the original cell density. Volumes equivalent to the volume measured in the experiment (usually 150 μL for experiments using *C. necator* and 50 μL for experiments using *E. coli*) were aliquoted into a 96-well plate and red fluorescence was measured (same excitation/emission values as described in main text methods). If the standard curve was linear, and all samples measured fell within the linear range, then the osmolysis measurements were considered valid. A representative standard curve is shown in Figure C.4B. If needed, samples were further diluted in water such that they did fall within this linear range.

The assay relies on the assumption that the fluorescence signal is a function only of the concentration of RFP in the sample (*i.e.*, that neither the solvent nor the presence/absence of cells significantly affects the fluorescence measurement). To verify this was always the case, fluorescence measurements were taken on three types of samples encountered throughout the experiments. All samples were prepared from equal volumes of the same culture, and therefore began with same amount of RFP. One sample was resuspended in an aqueous salt solution, and therefore nearly all of the RFP remained within the cell. One sample was resuspended in B-PER™ (a commercial bacterial lysis reagent) and therefore cell membranes were lysed and nearly all the RFP was in solution. In the final sample, cells were resuspended in B-PER™ but were then centrifuged, such that RFP was present in a supernatant free of cell debris. As seen in Fig. C.4C, all three samples have nearly identical fluorescence values, within 3% of each other. Therefore, neither the solvent nor the location of RFP with respect to cell biomass significantly impacts fluorescence measurement, and the assay is valid in comparing RFP concentration in the various fractions.

Supplementary Note C.5: Growth of BL21 ΔmscL ΔmscS in various salt concentrations

As described in the main text, the growth rate of *E. coli* BL21 *ΔmscL ΔmscS* was measured to demonstrate a tradeoff between the microbial growth rate and osmolysis efficiency. Growth curves were determined for this strain in LB supplemented with NaCl (if necessary) to final concentrations of 0.5%, 1%, 2%, 3%, and 4% (w/v). Cultures were grown in 50-mL volumes in 250-mL baffled shake flasks at 37 ºC, starting at an optical density of 0.01. Absorbance measurements were taken every half hour for cultures grown in 0.5%, 1%, and 2% salt and every hour for cultures grown in 3% and 4% salt. Specific growth rates were calculated from the slope of the line of a semilog plot for the range in which the log of absorbance was linear with respect to time.

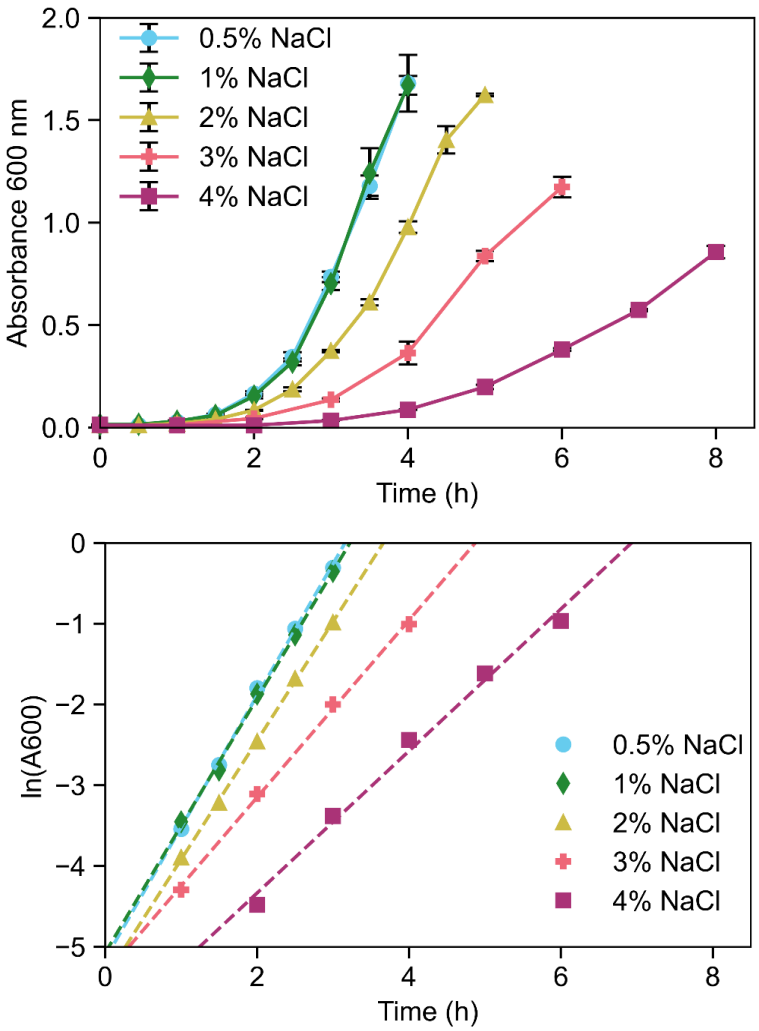

Figure C.5: (A) Growth of *E. coli* BL21 at various salt concentrations as a function of time. (B) Semilog of cell density as a function of time during logarithmic growth phase.

Supplementary Note C.6: Cell lysis combined with freeze-thaw enhances cell lysis

The effect the adding a freeze-thaw step to osmolysis was determined for BL21 cells grown in LB with 2% NaCl (w/v). The procedure was the same as for other osmolysis experiments with minor modifications. Cells were grown, RFP was expressed, and cells were washed as they were in other BL21 osmolysis experiments. For trials labelled "No Freeze-Thaw" samples were resuspended in distilled water and incubated for 30 min at 30 ºC as was normally done. For samples treated with a freeze-thaw step, however, cells were resuspended in distilled water, placed in a freezer set at −20 ºC for twenty minutes, and then thawed in a heat block set at 37 ºC for ten minutes. Samples from the well-mixed culture and supernatant were taken and measured as they were in previous experiments.

Adding a freeze-thaw step significantly enhances the cell lysis efficiency in BL21 *ΔmscL ΔmscS* cells. The highest cell lysis (22%) is observed for BL21 *ΔmscL ΔmscS* cells that are subjected to freeze-thaw, which is roughly 5-fold higher than lysis of BL21 *ΔmscL ΔmscS* without a freeze-thaw step and 15-fold higher than lysis of BL21 with a freeze-thaw. This improvement indicates

that even higher cell lysis efficiencies may be obtained by combining osmolysis with other methods of cell lysis.

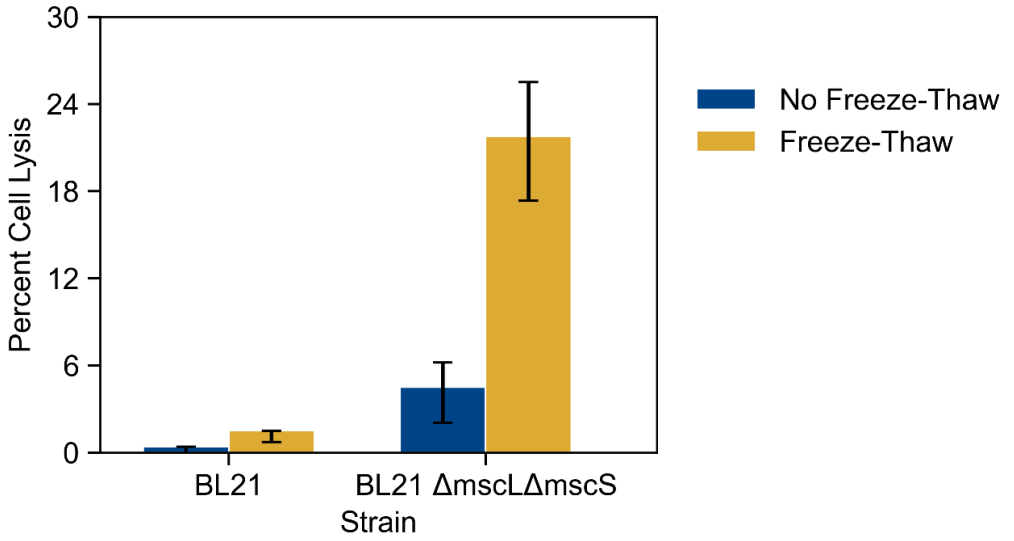

Figure C.6 Effect of addition of freeze-thaw step (yellow) with osmolysis for BL21 and BL21 *ΔmscL ΔmscS* compared to cells only subjected to osmotic downshock (blue).

Supplementary Note C.7: Osmolysis of BL21 after growth in 3% NaCl

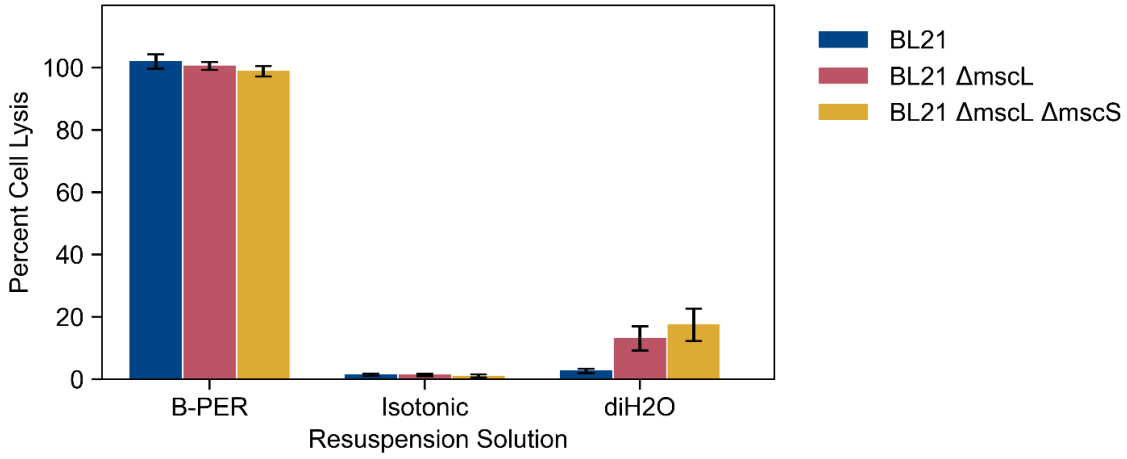

Figure C.7. Percent cell lysis of *E. coli* BL21 (blue), BL21 *ΔmscL* (red), and BL21 *ΔmscL ΔmscS* (yellow) in three different media: commercial B-PER™ Bacterial Protein Extraction Reagent, a 3% $NaCl_{(aq)}$ isotonic solution, and distilled water. (n=3).

Experiments described in Fig. 5A of the main text were repeated exactly, except with cells grown in LB containing 3% NaCl. Note the considerable difference between osmolytic efficiencies of cells grown in 3% and 4% NaCl. This also allows direct comparison of osmolysis between *C. necator* ht030b and BL21 (as well as their *ΔmscL* variants), as they were both grown in 3% NaCl. The percent cell lysis in distilled water following growth in 3% NaCl LB was >90% for ht030b *ΔmscL* and 14% for BL21 *ΔmscL*.

APPENDIX D: Supplementary Information for Chapter 5

Supplementary Note D.1 Defined media recipes used in Chapter 4

Table D.1 M9-acetate recipe

Component	Concentration
Sodium acetate	48.8 mM
Ammonium chloride	18.7 mM
Sodium phosphate dibasic	42.3 mM
Potassium phosphate dibasic	22.0 mM
Sodium chloride	8.6 mM
Magnesium sulfate	1.0 mM
Calcium chloride	0.1 mM

Supplementary Note D.2 Effect of codon optimization on butanol production

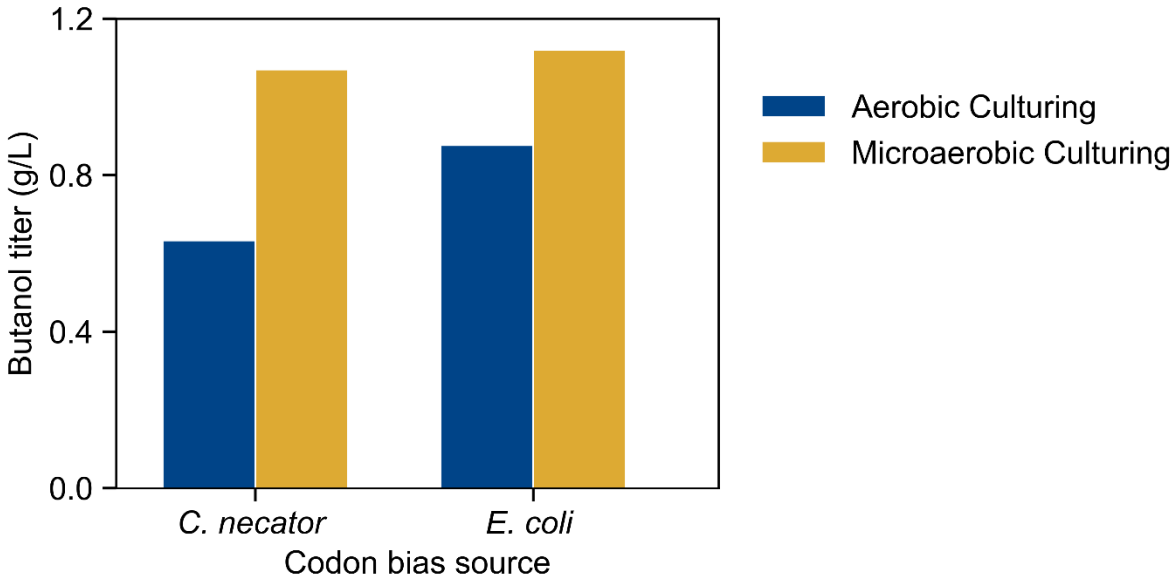

Figure D.1 Effect of codon bias on butanol production in *C. necator*. Identical enzymes sequences were encoded with a codon bias matching that of *C. necator* and *E. coli* and plasmids containing each variation were transformed into *C. necator*, and the concentration of n-butanol produced by each strain after culturing 6 days in TB with 35 g/L fructose was measured.

Supplementary Note D.3 Individual strains' adaptive laboratory evolution data

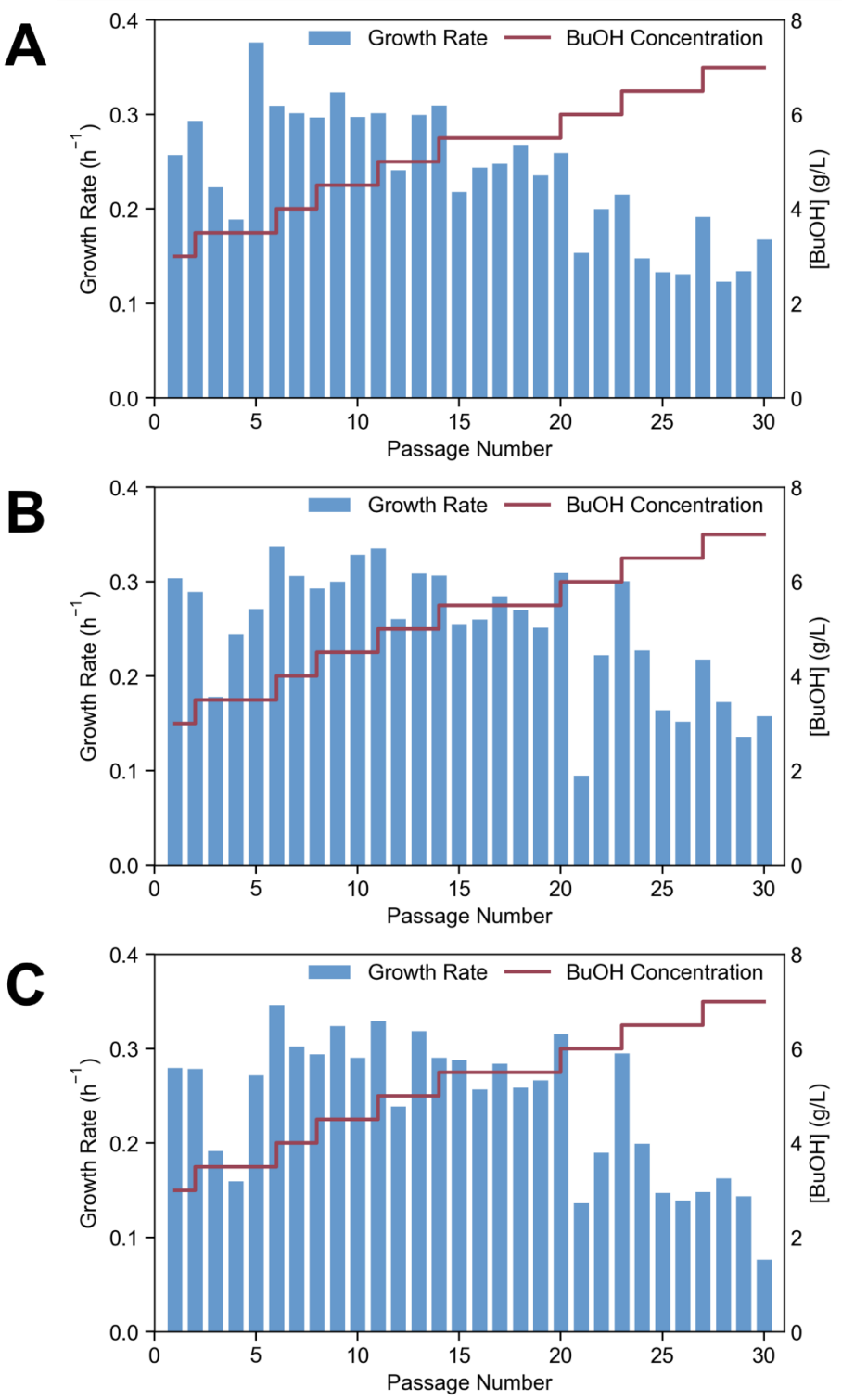

Figure D.2 Data from individual ALE replicates. Average growth rate (blue bars) and n-butanol concentration for each passage during the adaptive laboratory evolution, leading to (A) bt430, (B) bt5300, and (C) bt630 evolved *C. necator* strains.

Appendix References:

1. Grunwald, S. *et al.* Kinetic and stoichiometric characterization of organoautotrophic growth of *Ralstonia eutropha* on formic acid in fed-batch and continuous cultures. *Microb. Biotechnol.* **8**, 155–163 (2015).
2. Abel, A. J. & Clark, D. S. A Comprehensive Modeling Analysis of Formate-Mediated Microbial Electrosynthesis. *ChemSusChem* **14**, 344–355 (2021).
3. Stolpera, D. A., Revsbech, N. P. & Canfield, D. E. Aerobic growth at nanomolar oxygen concentrations. *Proc. Natl. Acad. Sci. U. S. A.* **107**, 18755–18760 (2010).
4. Dursun, A. Y. & Tepe, O. Internal mass transfer effect on biodegradation of phenol by Ca-alginate immobilized *Ralstonia eutropha*. *J. Hazard. Mater.* **126**, 105–111 (2005).
5. Wu, X., Altman, R., Eiteman, M. A. & Altman, E. Adaptation of *Escherichia coli* to Elevated Sodium Concentrations Increases Cation Tolerance and Enables Greater Lactic Acid Production. *Appl. Environ. Microbiol.* **80**, 2880–2888 (2014).
6. Ishizaki, A. & Tanaka, K. Batch culture of *Alcaligenes eutrophus* ATCC 17697T using recycled gas closed circuit culture system. *J. Ferment. Bioeng.* **69**, 170–174 (1990).
7. Takeshita, T. & Ishizaki, A. Influence of Hydrogen Limitation on Gaseous Substrate Utilization in Autotrophic Culture of *Alcaligenes eutrophus* ATCC 17697T. *J. Ferment. Bioeng.* **81**, 83–86 (1996).
8. Shi, X.-C. C., Tremblay, P.-L. L., Wan, L. & Zhang, T. Improved robustness of microbial electrosynthesis by adaptation of a strict anaerobic microbial catalyst to molecular oxygen. *Sci. Total Environ.* **754**, 142440 (2021).
9. Chen, J., Gomez, J. A., Höffner, K., Barton, P. I. & Henson, M. A. Metabolic modeling of synthesis gas fermentation in bubble column reactors. *Biotechnol. Biofuels* **8**, 1–12 (2015).
10. Fast, A. G. & Papoutsakis, E. T. Stoichiometric and energetic analyses of non-photosynthetic CO_2-fixation pathways to support synthetic biology strategies for production of fuels and chemicals. *Curr. Opin. Chem. Eng.* **1**, 380–395 (2012).
11. Andersen, K. B. & Von Meyenburg, K. Are Growth Rates of *Escherichia coli* in Batch Cultures Limited by Respiration? *J. Bacteriol.* **144**, 114–123 (1980).
12. Xiao, Y. *et al.* Kinetic modeling and isotopic investigation of isobutanol fermentation by two engineered *Escherichia coli* strains. *Ind. Eng. Chem. Res.* **51**, 15855–15863 (2012).
13. Gale, E. F. & Epps, H. M. R. The effect of the pH of the medium during growth on the enzymic activities of bacteria (*Escherichia coli* and *Micrococcus lysodeikticus*) and the biological significance of the changes produced. *Biochem. J.* **36**, 600–618 (1942).
14. Blankenhorn, D., Phillips, J. & Slonczewski, J. L. Acid- and base-induced proteins during aerobic and anaerobic growth of *Escherichia coli* revealed by two-dimensional gel electrophoresis. *J. Bacteriol.* **181**, 2209–2216 (1999).
15. Presser, K. A., Ross, T. & Ratkowsky, D. A. Modelling the growth limits (growth/no growth interface) of *Escherichia coli* as a function of temperature, pH, lactic acid concentration, and water activity. *Appl. Environ. Microbiol.* **64**, 1773–1779 (1998).

16. *CRC Handbook of Chemistry and Physics, 84th edition*. (CRC Press, 2004).

17. Schulz, K. G., Riebesell, U., Rost, B., Thoms, S. & Zeebe, R. E. Determination of the rate constants for the carbon dioxide to bicarbonate inter-conversion in pH-buffered seawater systems. *Mar. Chem.* **100**, 53–65 (2006).

18. Atkins, P. W. *Physical Chemistry*. (Oxford University Press, 1990).

19. Zeebe, R. E. On the molecular diffusion coefficients of dissolved CO_2, HCO_3^-, and CO_3^{2-} and their dependence on isotopic mass. *Geochim. Cosmochim. Acta* **75**, 2483–2498 (2011).

20. Han, P. & Bartels, D. M. Temperature Dependence of Oxygen Diffusion in H_2O and D_2O. *J. Phys. Chem.* **100**, 5597–5602 (1996).

21. Riebesell, U., Fabry, V.J., Hansson, L & Gattuso, J.-P. *Guide to best practices for ocean acidification research and data reporting*. (2011).

22. Weiss, R. F. The solubility of nitrogen, oxygen and argon in water and seawater. *Deep. Res. Oceanogr. Abstr.* **17**, 721–735 (1970).

23. Crozier, T. E. & Yamamoto, S. Solubility of Hydrogen in Water, Seawater, and NaCI Solutions. *J. Chem Eng. Data*. **19**, 242-244 (1974).

24. Yang, H., Kaczur, J. J., Sajjad, S. D. & Masel, R. I. Electrochemical conversion of CO_2 to formic acid utilizing Sustainion™ membranes. *J. CO_2 Util.* **20**, 208–217 (2017).

25. Buttler, A. & Spliethoff, H. Current status of water electrolysis for energy storage, grid balancing and sector coupling via power-to-gas and power-to-liquids: A review. *Renew. Sustain. Energy Rev.* **82**, 2440–2454 (2018).

26. Terpstra, M. A. Flammability Limits of Hydrogen-Diluent Mixtures in Air. (University of Calgary, 2012).

27. Carmo, M., Fritz, D. L., Mergel, J. & Stolten, D. A comprehensive review on PEM water electrolysis. *Int. J. Hydrogen Energy* **38**, 4901–4934 (2013).

28. Van Hecke, W., Bockrath, R. & De Wever, H. Effects of moderately elevated pressure on gas fermentation processes. *Bioresour. Technol.* **293**, 122129 (2019).

29. Morão, A. & de Bie, F. Life Cycle Impact Assessment of Polylactic Acid (PLA) Produced from Sugarcane in Thailand. *J. Polym. Environ.* **27**, 2523–2539 (2019).

30. Claassens, N. J., Cotton, C. A. R., Kopljar, D. & Bar-Even, A. Making quantitative sense of electromicrobial production. *Nat. Catal.* **2**, 437–447 (2019).

31. Flamholz, A., Noor, E., Bar-Even, A. & Milo, R. eQuilibrator - the biochemical thermodynamics calculator. *Nucleic Acids Res.* **40**, (2012).

32. Grosz, R. O. N. & Stephanopoulos, G. Statistical Mechanical Estimation of the Free Energy of Formation of *E. coli* Biomass for Use with Macroscopic Bioreactor Balances. *Biotechnol. Bioeng.* **25**, 2149–2163 (1983).

33. Liu, C., Colón, B. C., Ziesack, M., Silver, P. A. & Nocera, D. G. Water splitting–biosynthetic system with CO_2 reduction efficiencies exceeding photosynthesis. *Science.* **352**, 1210–1213 (2016).

34. Hábová, V., Melzoch, K., Rychtera, M. & Sekavová, B. Electrodialysis as a useful technique

for lactic acid separation from a model solution and a fermentation broth. *Desalination* **162**, 361–372 (2004).

35. McDonald, T. M. *et al.* Capture of Carbon Dioxide from Air and Flue Gas in the Alkylamine-Appended Metal–Organic Framework mmen-Mg2(dobpdc). *J. Am. Chem. Soc.* **134**, 7056–7065 (2012).

36. Davis, R. *et al.* Process Design and Economics for the Conversion of Lignocellulosic Biomass to Hydrocarbon Fuels and Coproducts: 2018 Biochemical Design Case Update. *Renew. Energy* 147 (2018).

37. Darunte, L. A. *et al.* Moving Beyond Adsorption Capacity in Design of Adsorbents for CO_2 Capture from Ultradilute Feeds: Kinetics of CO_2 Adsorption in Materials with Stepped Isotherms. *Ind. Eng. Chem. Res.* **58**, 366–377 (2019).

38. Casas, N., Schell, J., Pini, R. & Mazzotti, M. Fixed bed adsorption of CO_2/H_2 mixtures on activated carbon: experiments and modeling. *Adsorption* **18**, 143–161 (2012).

39. Sinha, A., Darunte, L. A., Jones, C. W., Realff, M. J. & Kawajiri, Y. Systems Design and Economic Analysis of Direct Air Capture of CO_2 through Temperature Vacuum Swing Adsorption Using MIL-101(Cr)-PEI-800 and mmen-Mg2(dobpdc) MOF Adsorbents. *Ind. Eng. Chem. Res.* **56**, 750–764 (2017).

40. Linstrom, P. J. & Mallard, W. G. *NIST Chemistry WebBook, NIST Standard Reference Database Number 69*. (National Institute of Standards and Technology).

41. Engineering ToolBox. Heat Exchangers - Heat Transfer Coefficients. https://www.engineeringtoolbox.com/heat-transfer-coefficients-exchangers-d_450.html (2003).

42. Groher, A. & Weuster-Botz, D. Comparative reaction engineering analysis of different acetogenic bacteria for gas fermentation. *J. Biotechnol.* **228**, 82–94 (2016).

43. Kantzow, C., Mayer, A. & Weuster-Botz, D. Continuous gas fermentation by *Acetobacterium woodii* in a submerged membrane reactor with full cell retention. *J. Biotechnol.* **212**, 11–18 (2015).

44. Noh, M. H., Lim, H. G., Woo, S. H., Song, J. & Jung, G. Y. Production of itaconic acid from acetate by engineering acid-tolerant *Escherichia coli* W. *Biotechnol. Bioeng.* **115**, 729–738 (2018).

45. Perry, R. H. & Green, D. W. *Perry's chemical engineers' handbook.* (McGraw-Hill, 2008).

46. Shiva Kumar, S. & Himabindu, V. Hydrogen production by PEM water electrolysis – A review. *Mater. Sci. Energy Technol.* **2**, 442–454 (2019).

47. Zuberi, M. J. S., Hasanbeigi, A. & Morrow, W. Techno-economic evaluation of industrial heat pump applications in US pulp and paper, textile, and automotive industries. *Energy Effic.* **16**, 19 (2023).

48. Seider, W. D. *et al. Product and process design principles : synthesis, analysis, and evaluation* . (John Wiley & Sons Inc., 2017).

49. Pivovar, B. S., Ruth, M. F., Myers, D. J. & Dinh, H. N. Hydrogen: Targeting $1/kg in 1 Decade. *Electrochem. Soc. Interface* **30**, 61–65 (2021).

50. Humbird, D., Davis, R. & McMillan, J. D. Aeration costs in stirred-tank and bubble column bioreactors. *Biochem. Eng. J.* **127**, 161–166 (2017).

51. U.S. Department of Energy. *Water and Wastewater Annual Price Escalation Rates for Selected Cities across the United States*. (2017).

52. Grisales Díaz, V. H. & Olivar Tost, G. Techno-economic analysis of extraction-based separation systems for acetone, butanol, and ethanol recovery and purification. *Bioresour. Bioprocess.* **4**, (2017).

53. Ulrich, G. D. & Vasudevan, P. T. How to estimate utility costs. *Chem. Eng.* **113**, 66–69 (2006).